THE CRITICAL ROLE OF CHEMICAL AND BIOLOGICAL COMPOSITION AND SOURCES IN $PM_{2.5}$ TOXICITY IN CHINESE MEGACITIES

WANG YIHUA

PhD

The Hong Kong Polytechnic University

2025

The Hong Kong Polytechnic University

Department of Civil and Environmental Engineering

The Critical Role of Chemical and Biological Composition and Sources in $PM_{2.5}$ Toxicity in Chinese megacities

WANG Yihua

A thesis submitted in partial fulfilment of the requirements for the degree of Doctor of Philosophy

Aug 2025

Citation of Originality

I hereby declare that this thesis is my own work and that, to the best of my knowledge and belief, it reproduces no material previously published or written, nor material that has been accepted for the award of any other degree or diploma, except where due acknowledgement has been made in the text.

_____(Signed)

____WANG Yihua_____Name of student

Abstract

Fine particulate matter ($PM_{2.5}$) has become a significant public health concern in China, where rapid urbanization and industrialization have led to severe air pollution. While previous studies have primarily focused on $PM_{2.5}$ mass concentration and chemical composition, limited attention has been given to the specific chemical and biological components responsible for its toxicity, as well as the emission sources contributing to the toxicity. This study addresses these gaps by conducting an integrated assessment of $PM_{2.5}$ in two Chinese megacities, Nanjing and Guangzhou, across six sites representing different land-use types. Through comprehensive chemical and biological characterization, *in vitro* toxicological assays, and source apportionment, this study quantifies the component- and source-specific contributions to $PM_{2.5}$-induced toxicity.

First, it investigates $PM_{2.5}$ concentration, chemical composition, and metal-induced and PAH-induced health risks in six sampling sites in Nanjing and Guangzhou from June 2019 to May 2020, along with long-term trends from 2013 to 2020. During 2019–2020, $PM_{2.5}$ levels mostly exceeded the World Health Organization (WHO) 24 h guideline (25 μg m^{-3}), especially in autumn and winter. Urban and suburban-industrial sites in Nanjing exhibited higher $PM_{2.5}$ concentrations than the rural site, while spatial differences of three sites in Guangzhou were less distinct. Chemical composition varied regionally: $PM_{2.5}$ in Nanjing was dominated by water-soluble ions (WSI), while Guangzhou showed higher levels of carbonaceous matter. Despite the low mass concentration, trace metals posed considerable carcinogenic risk (CR), with Cr being the dominant contributor while Mn accounting for most non-carcinogenic risk (NCR). PAHs concentration was significantly higher in Nanjing, particularly at the suburban-industrial site, and was primarily from pyrogenic sources. Over the 7-year period from 2013 to 2020, both cities experienced significant reductions in $PM_{2.5}$ and metal-induced health risks, reflecting the effectiveness of air pollution control policies, though risks from certain metals persisted.

Second, the investigation shifts focus to biological components, specifically endotoxins and bacterial communities. $PM_{2.5}$-bound endotoxins concentration in Guangzhou was nearly double those in Nanjing and varied significantly within Guangzhou, with urban sites exhibiting the highest levels. As an important toxic biological component, endotoxins were more abundant on cleaner days, indicating that $PM_{2.5}$ mass does not adequately represent toxicity. Bacterial load was similar between cities, but the diversity was higher in Guangzhou. Gram-negative bacteria dominated compared to Gram-positive bacteria, and were positively associated with endotoxins levels, indicating their involvement in $PM_{2.5}$-induced toxicity. In addition, there are associations between chemical and biological components in $PM_{2.5}$. The concentrations of endotoxins were positively correlated with Al, Mg^{2+}, and Ca^{2+}, likely due to shared sources such as dust. Most Gram-negative bacteria also showed positive correlations with WSI, which may provide nutrients for bacteria and enhance their attachment.

Following these findings, this study further evaluates the toxicological effects of $PM_{2.5}$ using *in vitro* assays with BEAS-2B cells, focusing on intracellular oxidative stress as a toxicity endpoint. Endotoxins, trace metals, and PAHs together accounted for 35.9–56.9% of $PM_{2.5}$-induced oxidative stress, despite contributing a small share (1.01–2.23%) to total $PM_{2.5}$ mass. Metals (31.6–46.7%), particularly Fe and Mn, were the largest contributors, followed by endotoxins (4.24–12.2%) and PAHs (0.0218–0.135%). The toxic contribution of these components far exceeded their mass contributions, emphasizing the need for component-specific toxicity assessments.

Source apportionment revealed that mass and toxicity were driven by different sources. In Nanjing, secondary aerosols and combustion dominated $PM_{2.5}$ mass, but fugitive dust and combustion contributed more to toxicity. In Guangzhou, vehicle emissions were the dominant source of $PM_{2.5}$ mass in the urban site, and combustion dominated in the semirural-industrial and suburban sites. In contrast, the major contributors to $PM_{2.5}$-induced toxicity in Guangzhou were vehicle emissions, industrial emissions,

combustion, and biological emissions. Notably, biological emissions contributed significantly to both $PM_{2.5}$ mass and $PM_{2.5}$-induced toxicity across six sites.

In conclusion, this study provides an integrated assessment of $PM_{2.5}$ chemical and biological composition, toxicity, and sources in two megacities in China. The findings highlight that $PM_{2.5}$-induced toxicity were primarily driven by specific toxic components, particularly trace metals, endotoxins, and PAHs, rather than total mass. Moreover, emission sources contributing most to mass are not always those driving toxicity, highlighting the need for more targeted control strategies. Importantly, biological components such as endotoxins were shown to have a significant and previously underestimated role in $PM_{2.5}$-induced toxicity. The integration of chemical, biological, and toxicological evidence presented in this study offers new insights for air quality regulation and public health protection.

Acknowledgement

Pursuing a PhD has been not only a significant step toward my research career but also a meaningful journey in perseverance. Throughout this process, I have been fortunate to receive support and encouragement from many individuals. Their assistance, in various forms, has been invaluable, and without their help, the completion of this thesis would not have been possible.

First, I wish to convey my sincere appreciation to my chief supervisor Prof. Xiangdong Li for his invaluable mentorship and consistent support during my doctoral studies. His profound passion for research and commitment to excellence have been a constant source of inspiration and motivation for me. I would also like to thank my co-supervisor, Prof. Sonata Suk-Yu Yau, for her kind assistance and invaluable support throughout my academic journey.

I am grateful to Dr. Jiawen Xie, Dr. Xiaohao Sun, Dr. Lu Zhang, Dr. Haotian Zheng, Dr. Ling Jin, Ms. Qian Yang and Mr. Zehua Yan for providing insightful comments and guidance regarding both the development of my research project and the preparation of related manuscripts. My thanks also go to other members and alumni of Prof. Li's research group, including Dr. Tangtian He, Dr. Jue Zhao, Dr. Lili Ming, Dr. Ke Chen, Dr. Fang Guo, Dr. Shangchao Xiong, Dr. Yao Lu, Dr. Yangyang Wu, Dr. Danyang Tao, Dr. Xiaohua Zhang, Mr. Hongyu Shi, Ms. Yichen Xu, Ms. Yunzhe Chen, and Ms. Yiran Zhang for their support during my study. I would like to give my thanks to our technicians, Mr. W. S. Lam, Ms. Carman Ip, Mr. Jonathan Chan, Mr. Bosco Tam, and Ms. Kate Tam for their assistance with my laboratory work. In addition, I am grateful to Prof. Xiaosan Luo from Nanjing University of Information Science and Technology, Prof. Jun Li from Guangzhou Institute of Geochemistry, Chinese Academy of Sciences, for assisting in sample collection. I also thank Prof. Jianzhen Yu and Dr. Wing Sze Chow from The Hong Kong University of Science and Technology for their kind help in analyzing the PAHs data. I am thankful to my friends for their companionship and encouragement.

I want to express my appreciation to the Research Grant Council of Hong Kong for providing financial support for my research project.

Last but not least, I want to thank my family for their support—my parents, Ms. Guoping Shi and Mr. Xiong Wang, my grandparents, and my cats. I also would like to express my gratitude to myself for persevering through the PhD journey.

Table of Contents

Abbreviations

Abbreviations	Full names
ANOVA	Analysis of Variance
ANT	Anthracene
ATCC	American Type Culture Collection
BaA	Benz[a]anthracene
BaP	Benzo[a]pyrene
BbF	Benzo[b]fluoranthene
BEQs	Bioanalytical equivalent concentrations
BghiP	Benzo[g,h,i]perylene
BkF	Benzo[k]fluoranthene
CA	Concentration addition
CalEPA	California Environmental Protection Agency
CH	Conghua
Chr	Chrysene
CI	Confidence interval
COVID-19	Coronavirus Disease 2019
CR	Carcinogenic risk
DahA	Dibenz[a,h]anthracene
DBaeP	Dibenzo[a,e]pyrene
DBalP	Dibenzo[a,l]pyrene
DCFH-DA	2,7-dichlorofluorescein diacetate
DMEM	Dulbecco's Modified Eagle's Medium
DNA	Deoxyribonucleic acid
DTT	Dithiothreitol
EC	Elemental carbon
ECR	Excessive cancer risk
EF	Enrichment factors
ELF	Epithelial lining fluid

EU	Endotoxin unit
FLA	Fluoranthene
GC-MS	Gas chromatography-mass spectrometry
HMW	High-molecular-weight
HQ	Hazard Quotients
HS	Heshan
IA	Independent action
IcdP	Indeno[1,2,3-cd]pyrene
ICP-OES	Inductively coupled plasma optical emission spectrometer
IL	Interleukin
IPQ	Index on prediction quality
IR	Induction ratio
LDA	Linear Discriminant Analysis
LEfSe	Linear discriminant analysis Effect Size
LMW	Low-molecular-weight
LS	Lishui
MMW	Moderate-molecular-weight
MV	Minute ventilation
NAAQS	National Ambient Air Quality Standard
NCR	Non-carcinogenic risk
Nrf2	Nuclear factor erythroid-2-related factor 2
OC	Organic carbon
OD	Optical density
OEHHA	Office of Environmental Health Hazard Assessment
OM	Organic matter
OTU	Operational taxonomic unit
PBS	Phosphate-buffered saline
PCA	Principal component analysis
PCoA	Principal Coordinates Analysis

PERMANOVA	Permutational multivariate analysis of variance
PES	Polyether sulfone
PHE	Phenanthrene
PK	Pukou
PM	Particulate matter
$PM_{2.5}$	Atmospheric particulate matter with an aerodynamic diameter of or less than 2.5 μm
PMF	Positive matrix factorization
PYR	Pyrene
QA/QC	Quality assurance and quality control
qPCR	Quantitative polymerase chain reaction
RDE	Realistic daily exposure
RDP	Ribosomal Database Project
REP	Relative effect potency
ROS	Reactive oxygen species
RPF	Relative potency factor
rRNA	Ribosomal ribonucleic acid
SD	Standard deviation
TBHP	Tert-butyl hydroperoxide
TH	Tianhe
TOR	Thermal optical reflectance
UR	Unit risk
USEPA	United States Environmental Protection Agency
WHO	World Health Organization
WSI	Water-soluble ions
XW	Xuanwu

List of Figures

List of Tables

Chapter 1 Introduction

1.1 Background

Air pollution is a serious global environmental and public health challenge, with fine particulate matter ($PM_{2.5}$, aerodynamic diameter ≤ 2.5 μm) as a key contributor to morbidity and mortality worldwide (Health Effects Institute, 2024). Due to its small size, $PM_{2.5}$ can penetrate deep into the human respiratory tract, reaching the alveolar regions and even entering the bloodstream (Hao et al., 2020; Shen et al., 2019; Xie et al., 2020), causing adverse health effects, including respiratory, cardiovascular, and neurological diseases (Gangwar et al., 2020; Thangavel et al., 2022). In China, rapid urbanization and industrialization have caused frequent and severe $PM_{2.5}$ pollution, particularly in megacities such as Nanjing and Guangzhou. These regions have various emission sources and diverse land-use patterns, making effective $PM_{2.5}$ control especially important for protecting public health.

The toxicity of $PM_{2.5}$ is closely associated with its composition, rather than its mass concentration (Perrone et al., 2010). While $PM_{2.5}$-bound major chemical constituents, such as trace metals and polycyclic aromatic hydrocarbons (PAHs), have been widely investigated (Gualtieri et al., 2009; Pavagadhi et al., 2013; Sun et al., 2021; Zhou et al., 2022), biological components have been underexplored in toxicological evaluations (Degobbi et al., 2011; Samake et al., 2017). In China, $PM_{2.5}$ pollution demonstrates significant spatial and temporal variations driven by regional differences in land use, emission sources, and atmospheric processes (Liu et al., 2025; Zheng et al., 2019). Among $PM_{2.5}$ components, trace metals represent a small mass fraction but contribute significantly to health risks. In both human and animal studies, metals such as Fe, Mn, Cr, and Cu have been identified as key drivers of oxidative stress and inflammation (Dergham et al., 2012; Huang et al., 2014a; Maciejczyk et al., 2010; Torres-Ramos et al., 2011). Organic compounds are also potential toxicants which can elevate intracellular ROS levels (Gualtieri et al., 2012; Kouassi et al., 2010; Longhin et al., 2013; Torres-Ramos et al., 2011). In addition to chemical components, $PM_{2.5}$ also contains a wide range of biological constituents, including bacteria, fungi, viruses, and

endotoxins. These bioaerosols comprise up to 25% of atmospheric aerosol and can transmit infectious components and cause respiratory diseases (Douwes et al., 2003; Jaenicke, 2005). Endotoxins, in particular, a type of pyrogen produced by Gram-negative bacteria, are heat-resistant, chemically stable and difficult to remove or inactivate (Ruiz et al., 2009). They exist across a wide particle size range and have been detected in various environments such as school campuses, industrial and agricultural workplaces (Basinas et al., 2013; Gioffrè et al., 2012; Thilsing et al., 2015; Visser et al., 2006). Studies showed that even low concentrations of airborne endotoxins (*e.g.*, 0.05 endotoxin unit (EU) m^{-3}) are associated with exacerbation of asthma symptoms, particularly in children (Rabinovitch et al., 2005; Ryan et al., 2009). In addition, endotoxins have significant correlations with the production of ROS, apoptosis, inflammatory damage, and DNA damage (Yan et al., 2023), which are major mechanisms of endotoxins-induced toxicity. However, endotoxins and bioaerosols remain largely excluded from $PM_{2.5}$ risk assessments. Quantitative evaluations of their toxic contributions in comparison with well-studied chemical components like metals and PAHs are limited. This research gap limits a full understanding of $PM_{2.5}$'s health impacts and makes it harder to develop targeted regulatory strategies.

In vitro toxicological assessments provide feasible and effective methods for examining cellular responses to $PM_{2.5}$ exposure. Oxidative stress has been widely adopted as a key endpoint in driving PM-related health effects (Abbas et al., 2019; Bo et al., 2016; Hou et al., 2024; Liu et al., 2022; Traina et al., 2022). To support component-based health risk assessments, source apportionment has been used as a critical tool for identifying emission sources contributing to $PM_{2.5}$ mass and health risks (Xie et al., 2020; Yan et al., 2022). Previous research found that the major sources of $PM_{2.5}$ mass are not always the same as those causing health risks (Yan et al., 2022). Few have linked *in vitro* toxicity endpoints to specific emission sources. Filling this knowledge gap is crucial for developing effective mitigation strategies that prioritize reducing the most harmful emission sources.

Collectively, these insights highlight the need for an integrated toxicological approach that incorporates both chemical and biological components of $PM_{2.5}$, evaluates their individual and joint contributions to cellular toxicity, and connects these findings to emission sources across different land-use types. This comprehensive study conducted in two megacities in China, Nanjing and Guangzhou, is important for guiding air quality management efforts, adjusting risk assessment frameworks, and protecting public health impacted by $PM_{2.5}$ pollution.

1.2 Research objectives

This study involves both chemical and biological analyses, and *in vitro* experiments on $PM_{2.5}$ samples from Nanjing and Guangzhou based on objectives listed below:

(1) To identify the spatial and temporal variations (between cities and within each city) in the chemical composition profile of $PM_{2.5}$ (trace metals, OC, EC, WSI, and PAHs).

(2) To evaluate the health risks posed by chemical components – metals and PAHs in $PM_{2.5}$.

(3) To characterize and compare the regional features of key biological components in $PM_{2.5}$ – endotoxins and bacteria, including their concentrations and community structures, and to investigate the associations between Gram-negative bacteria and endotoxins, and between chemical and biological components.

(4) To compare the spatial variation in $PM_{2.5}$-induced toxicity, and to quantify the toxic potency of individual chemical and biological components and their contributions to $PM_{2.5}$-induced toxicity.

(5) To quantify the contributions of emission sources to $PM_{2.5}$-induced toxicity.

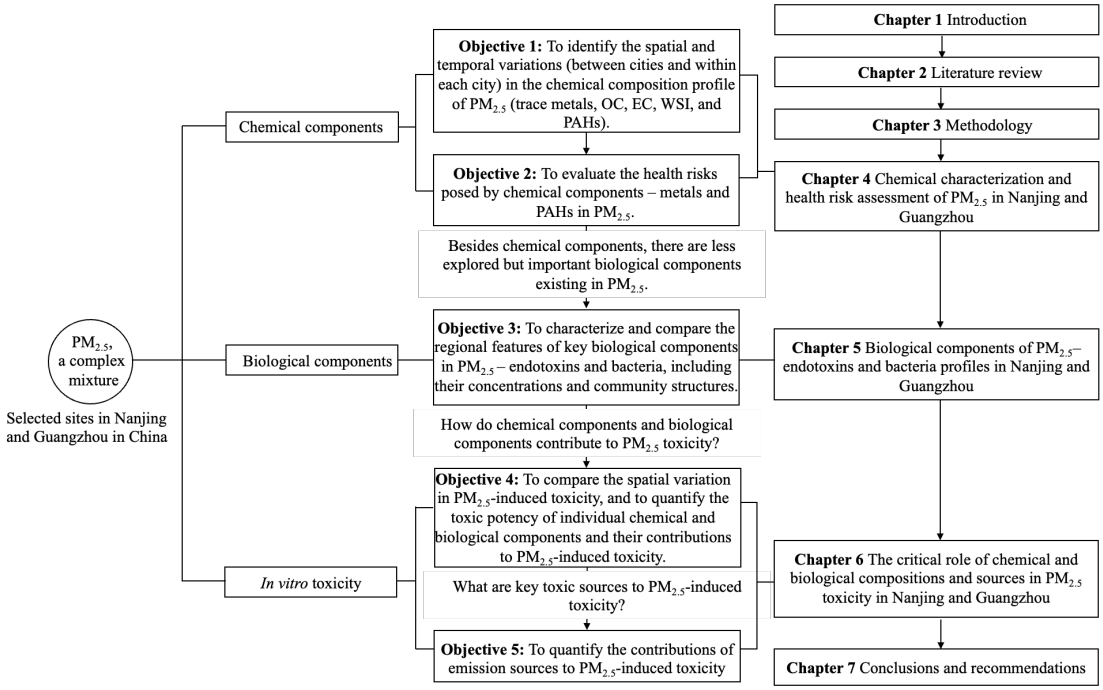

Figure 1-1. A flowchart of the objectives and structure of the thesis.

1.3 Organization

This thesis contains 7 chapters (Figure **1-1**), including "Introduction", "Literature review", "Methodology", three chapters about results and discussions, and the last chapter about "Conclusions and recommendations".

Chapter 1– Introduction provides background information on the study and explains objectives and organization of this study.

Chapter 2– Literature Review provides an overview of $PM_{2.5}$ pollution, summarizing previous and current research on the chemical and biological components of $PM_{2.5}$ and their associated health risks. It also discusses the sources of $PM_{2.5}$ and its biotoxicity. Furthermore, this chapter identifies existing research gaps and clearly states the objectives of this study, offering readers a comprehensive understanding of the research background and framework.

Chapter 3– Methodology describes the sampling procedures, chemical and biological analysis techniques, *in vitro* experimental designs, mixture-toxicity modeling and source apportionment modeling employed in this study. In addition, it outlines the sequencing, data processing steps, and statistical analyses applied in this thesis.

Chapter 4 evaluates the health risks posed by chemical components–metals and PAHs in $PM_{2.5}$, and investigates long-term trends of $PM_{2.5}$ and its chemical composition, especially the health risk caused by these components.

Chapter 5 characterizes and compares the regional profiles of key biological components in $PM_{2.5}$ — endotoxins and bacteria — by examining their concentrations and community structures. In addition, this chapter explores the relationship between endotoxin abundance and individual bacterial taxa, as well as the associations between $PM_{2.5}$-bound chemical and biological components.

Chapter 6 compares the spatial variation in $PM_{2.5}$-induced toxicity, quantifies the toxic potency of individual chemical and biological components, and assesses their contributions to $PM_{2.5}$-induced toxicity. It also evaluates and compares the contributions of different emission sources to both $PM_{2.5}$ mass and $PM_{2.5}$-induced toxicity.

Chapter 7 highlights the key findings of the study and stresses its originality and scientific significance. It also offers recommendations for future research.

Chapter 2 Literature Review

$PM_{2.5}$ is a complex mixture comprising various chemical and biological components such as bacterial communities and endotoxins. This chapter reviews the composition, sources, and toxicity of $PM_{2.5}$ under different climatic, seasonal, and regional conditions. Special emphasis is placed on the *in vitro* toxicity induced by $PM_{2.5}$ and its specific components, particularly endotoxins. In addition, this review introduces source apportionment methods, approaches to mixture-toxicity modeling, and compares different *in vitro* methods used to assess $PM_{2.5}$ toxicity.

2.1 $PM_{2.5}$ pollution, an environmental concern with serious health implications

As the second leading global risk factor for mortality, ambient air pollution contributed to 8.1 million premature deaths in 2021, with $PM_{2.5}$ (particulate matter in the air with an aerodynamic diameter less than 2.5 μm) being the largest driver of disease burden, causing 7.8 million deaths globally due to its association with illness and early death from chronic exposure (Health Effects Institute, 2024). According to country-level data on average $PM_{2.5}$ exposure (Figure **2-1**), China falls within the "unhealthy for sensitive groups" category, with an annual concentration of 39.1 μg m^{-3}. Notably, there were 48 Chinese cities featuring among the top 100 most polluted cities worldwide (IQAir, 2019). Exposure to high levels of $PM_{2.5}$ can cause health problems and shorten human life spans by months, even years. With more than 18% of the world's population, China's air quality affects the most people in any single country, with the average 1.25 years' loss of life span (Apte et al., 2018) (Figure **2-2**). The diameter of $PM_{2.5}$ is about 1/24 that of a human hair, which gives it a high surface area-to-volume ratio (Chang et al., 2021) and facilitates the adsorption and transport of a variety of toxic and harmful substances. Furthermore, due to the small particle size, it can reach the deepest regions of the lungs, depositing in the terminal bronchioles and alveoli during respiration, and even cross the air-blood barrier and subsequently enter the circulatory system (Hao et al., 2020; Shen et al., 2019; Xie et al., 2020) (Figure **2-3**). It was observed that 96% of the particles deposited at human lung parenchyma are $PM_{2.5}$ (Churg and Brauer, 1997). Upon inhalation, toxic substances can deposit on the upper respiratory tract and lungs

together with $PM_{2.5}$, triggering oxidative stress and inflammation, resulting in respiratory diseases, cardiovascular diseases, and other health issues (Gangwar et al., 2020; Thangavel et al., 2022). Ambient air pollution, especially fine particles, is a threat to human health. It is necessary to study its sources, components and toxic mechanisms to provide information for air pollution control and understanding of health effects.

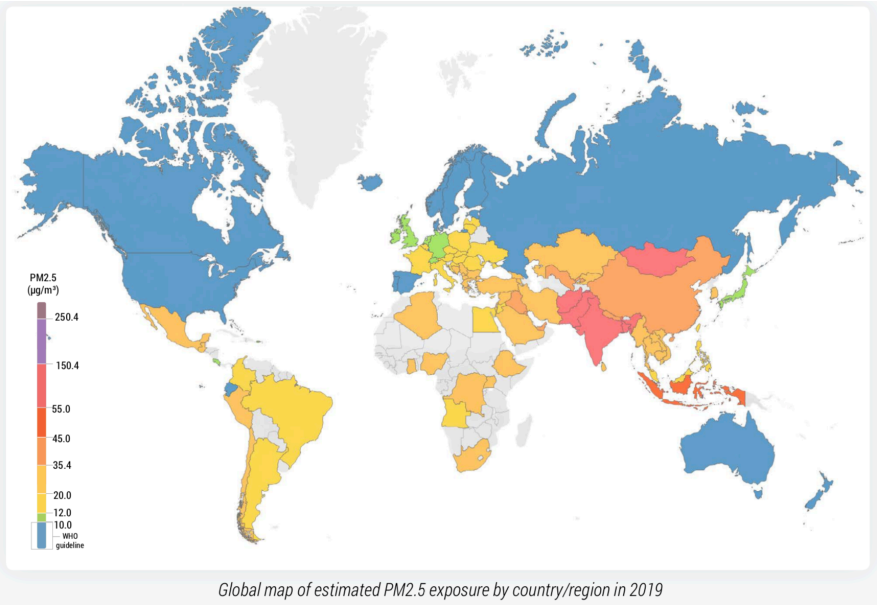

Figure 2-1. Global map of estimated $PM_{2.5}$ exposure by country/region (IQAir, 2019).

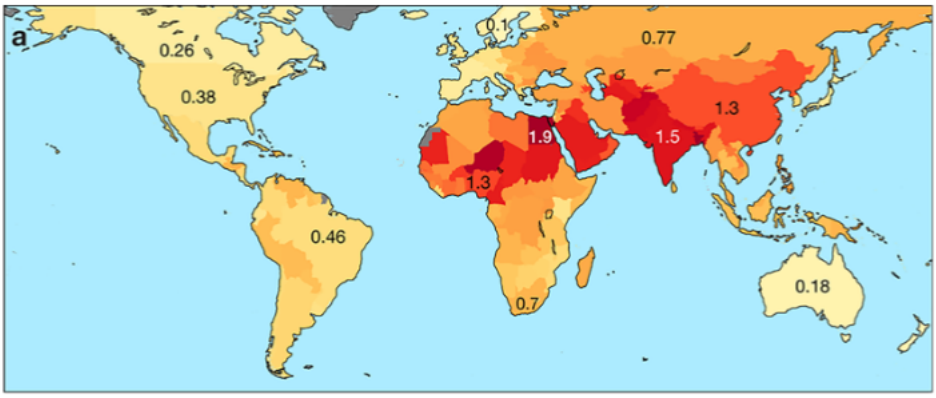

Figure 2-2. Global maps of the life expectancy decrement (ΔLE) from $PM_{2.5}$ in year 2016 concentrations (Apte et al., 2018).

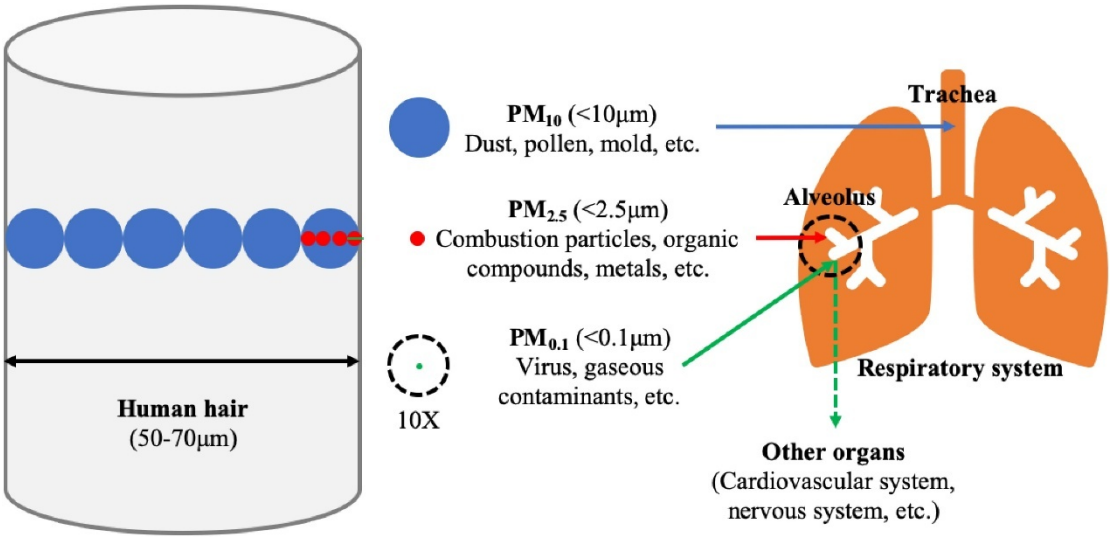

Figure 2-3. The size, main composition, and deposition site in the lung of the particulate matter (PM) (Yang et al., 2020).

2.2 Chemical composition of $PM_{2.5}$

2.2.1 Major chemical components in $PM_{2.5}$ and their sources

$PM_{2.5}$ is a mixture of various chemical components, including EC, OC, heavy metals (*e.g.*, Al, Cd, Cr, Co, Mn, Fe, Cu, Ca, Mg, Ni, Pb, V, and Zn) and WSI (*e.g.*, SO_4^{2-}, NO_3^-, NH_4^+, Na^+, K^+, and Cl^-) (Hao et al., 2020; Shen et al., 2019; Xie et al., 2020). $PM_{2.5}$ concentration and sources can differ greatly between locations as a result of varying climatic conditions, emission sources, and dispersion mechanisms. Depending on the area, $PM_{2.5}$ may originate from both natural and anthropogenic activities, with the relative contribution of each source varying by region (Almeida et al., 2020). $PM_{2.5}$ can be released from natural sources, such as dust storms, forest fires, volcanoes, and human activities, including transportation, fuel burning, and industrial processes (Ryou et al., 2018). Secondary aerosol and sea salts are also significant sources of $PM_{2.5}$ (Xie et al., 2020). $PM_{2.5}$ concentration varies depending on the surrounding activities, including those in rural areas (Hu et al., 2012), urban environments (Zhang and Cao, 2015), industrial zones such as mining sites (Hu and Jiang, 2013; Hu et al., 2014; Zhang and Cao, 2015), and regions influenced by marine activities (Wang et al., 2006). The dominant sources of $PM_{2.5}$ exhibit regional characteristics. For instance, according to a study conducted in China which includes eight anthropogenic emission sectors (Zheng

et al., 2019), from 2005 to 2015, the major sources of $PM_{2.5}$ in China were industrial processes, domestic combustion, and open burning. The decreasing rate of $PM_{2.5}$ was 39% from 2005 to 2015, and the decrease was primarily due to reductions from power plants, industry, and domestic combustion. Our previous study also showed that $PM_{2.5}$ samples collected from the Pearl River Delta and the Yangtze River Delta during 2016–2017 in China were mainly from traffic emissions, non-traffic combustion, and industrial emissions (Xie et al., 2020). Identifying the sources and impacts of $PM_{2.5}$ concentration is crucial for formulating effective control measures and protecting public health (Hopke et al., 2020; Manousakas et al., 2017).

Various source apportionment approaches have been developed to identify $PM_{2.5}$ sources and their contributions, including analysis of monitoring data, use of emission inventories combined with dispersion models to simulate aerosol emission, formation, transport, and deposition, and statistical analysis of PM chemical composition at receptor sites, known as receptor models (Viana et al., 2008). The enrichment factor (EF) of trace metals provides an effective way to distinguish anthropogenic contributions from those of natural origins (Chen et al., 2008). For water soluble ions, their sources can be identified by principal component analysis (PCA) (Chen et al., 2019c). EC derives from incomplete combustion of fossil fuels or biomass. OC can be directly emitted as primary OC or secondary OC from anthropogenic and natural sources (Fuzzi et al., 2006). Radiocarbon (^{14}C) analysis is a powerful tool to unambiguously distinguish fossil and non-fossil sources of carbonaceous particles (Currie, 2000). The PAHs molecular diagnostic ratios can also be used to trace the sources of $PM_{2.5}$-bound PAHs (Katsoyiannis et al., 2011). The USEPA's Positive Matrix Factorization (PMF) approach is utilized to identify and characterize the distinct sources of $PM_{2.5}$ (Norris, 2014).

2.2.2 Seasonal and geographic variations in $PM_{2.5}$ concentration and components

The concentration and chemical composition of $PM_{2.5}$ exhibit considerable diversity across different geographic regions and seasons. As illustrated in Figure **2-4**, which

presents the seasonal variation in $PM_{2.5}$ concentration throughout 2018, highlighting that cities in eastern China typically experienced higher levels than those in the west. Furthermore, $PM_{2.5}$ concentrations were typically greater in northern cities compared to southern cities. Pollution was more widespread and severe during the spring and winter seasons in these regions (Liu et al., 2025). Another study (Wang et al., 2021b) also found that $PM_{2.5}$ concentrations in Chinese cities were significantly higher in spring and winter compared to summer and autumn. Such disparities may be due to the massive use of heating devices in cold wintertime compared to the summertime in northern and central China (Liu et al., 2020). Additionally, the geographic and seasonal variations in $PM_{2.5}$ levels may be attributed to differences in $PM_{2.5}$ composition and energy structures. For instance, a study investigating $PM_{2.5}$ in a Chinese megacity from 2006 to 2014 found that higher proportions of Al, Si, Ca, and Fe were present in the summer, while concentrations of OC, NO_3^-, and SO_4^{2-} were elevated in the winter. Cement and crustal dust contributed more to $PM_{2.5}$ in the summer, whereas coal combustion, nitrate, and secondary organic compounds were more prominent in the winter. Vehicular and secondary sources were also significant contributors to $PM_{2.5}$ (Tian et al., 2016). Similarly, a study conducted at various sites in Taiwan reported that concentrations of Fe, Zn, V, Cu, and Mn—metals associated with industrial activities—were higher at the industrial site (Kaohsiung), while Ba, Cr, Ni, Mo, and Co—metals linked to traffic emissions—were more abundant at the urban site (Taipei). The rural site (Hualian) exhibited good air quality, with low levels of both $PM_{2.5}$ and metals. Across all sites, most metal concentrations were higher during the cold season, except at the rural location. Notably, ambient concentrations of Mn, Cr, and Pb at all sites posed a greater health risk (Hsu et al., 2021). The diverse chemical composition of $PM_{2.5}$ across regions and seasons highlights the complexity of air pollution and its health risks. Future research should prioritize long-term, high-resolution monitoring of $PM_{2.5}$ to clarify source contributions and transformations. Evaluating targeted emission reduction strategies and conducting comprehensive health risk assessments by considering both $PM_{2.5}$ concentrations and toxic components will be vital for effective public health policy and protection of vulnerable groups.

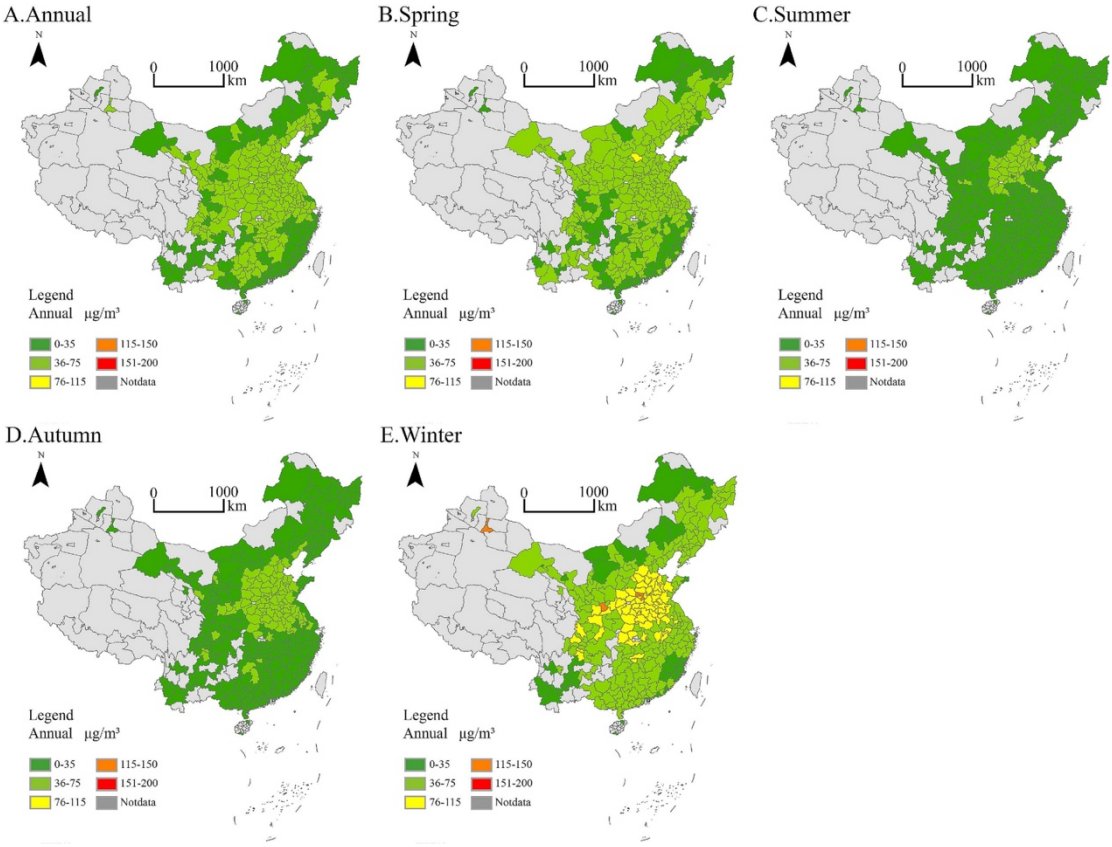

Figure 2-4. Spatial distribution of $PM_{2.5}$ concentrations by season. The $PM_{2.5}$ concentration data are from January to December 2018 for 284 cities in China (Liu et al., 2025).

2.2.3 $PM_{2.5}$-induced toxicity is shaped by its toxic components

A large number of epidemiological studies have confirmed the toxic effects of $PM_{2.5}$ on human health, including cardiovascular diseases (Liu et al., 2021), respiratory disease and lung cancer mortality (Pun et al., 2017), diabetes (Lao et al., 2019), ischemic stroke (Tian et al., 2017), dementia and Parkinson's diseases (Chen et al., 2017). However, although epidemiological studies reveal statistical links between exposure and health outcomes, they do not provide definitive evidence of causation. To better understand the toxicity of $PM_{2.5}$, it is crucial to identify the specific constituents contributing to its harmful effects. However, not all constituents in $PM_{2.5}$ contribute to the toxicity of mixture $PM_{2.5}$. The varying levels of organic substances (*e.g.*, PAHs) and transition metals (such as aluminum, iron, manganese, lead, and zinc) present in

the $PM_{2.5}$ samples may contribute to the observed toxicity, which appears to depend on both exposure duration and concentration, and is mediated by inflammatory mechanisms (Billet et al., 2007). Within the respiratory system, the bronchial epithelial layer serves to maintain pulmonary stability and functions as a physical barrier. Nevertheless, during this protective process, the release of cytokines and exposure to external factors can trigger both immediate and long-term reactions. Human bronchial epithelial cells are crucial in these responses, as their biological activities under stress are of significant importance (Jia et al., 2017). Toxicological studies further demonstrated that $PM_{2.5}$-induced toxicity depends on chemical composition (Perrone et al., 2010). For example, a study conducted on Singapore $PM_{2.5}$ found that PAHs and transition metals decreased the cell viability and increase the cell death (Pavagadhi et al., 2013). Another study also observed that cytotoxic effects were likely linked to the oxidative potential of metals and PAHs adsorbed onto the particles (Gualtieri et al., 2009). A recent *in vitro* study conducted in 10 Chinese megacities observed a strong positive correlation between heavy metals abundance and ROS production while a moderate correlation was noted between PAHs abundance and ROS levels (Sun et al., 2021). Similarly, another *in vitro* study revealed that $PM_{2.5}$-induced cytotoxicity and pulmonary toxicity were associated with particulate PAHs and heavy metals (Zhou et al., 2022). Moreover, a study conducted in 10 large Chinese cities noticed a significant correlation between endotoxins in $PM_{2.5}$ and inflammatory cytokines (interleukin (IL)-6 and IL-8) (Ma et al., 2019). Collectively, these findings highlight that the toxicity of $PM_{2.5}$ is strongly influenced by its chemical profile, which in turn varies with geographic location, pollution sources, climatic conditions, and land-use types.

In conclusion, extensive research has demonstrated that $PM_{2.5}$ poses significant health risks, with its toxicity largely influenced by its composition and source-specific characteristics. While epidemiological and toxicological studies have provided valuable insights into the associations between $PM_{2.5}$ exposure and various adverse health outcomes, there remains a need for further investigation to clarify the underlying molecular mechanisms, particularly the roles of specific chemical constituents such as

PAHs and transition metals. Future research should aim to disentangle the contributions of individual $PM_{2.5}$ components, explore the cellular pathways involved in oxidative stress and inflammation, and examine the effects of $PM_{2.5}$ from diverse sources and environments. Advancing our understanding in these areas will be crucial for developing targeted public health interventions and informing regulatory policies to reduce exposure and protect human health.

2.3 Biological composition of $PM_{2.5}$

In addition to the well-known chemical composition in $PM_{2.5}$, biological components are abundant and linked to a wide range of adverse health effects (Douwes et al., 2003). Bioaerosols (fur fibers, dandruff, skin fragments, plant fragments, pollen, spores, bacteria, algae, fungi, viruses, and proteins) comprise up to 25% of atmospheric aerosols and are responsible for various diseases and allergies (Jaenicke, 2005). The combination of chemical and biological constituents in PM could enhance allergic and asthmatic responses (Boreson et al., 2004). However, dose-response relationships for these airborne biological components have not been established (Degobbi et al., 2011; Samake et al., 2017) and information on their threshold values is limited.

2.3.1 Microorganisms in airborne particles

Extensive research has established that bioaerosols, comprising bacteria, fungi, and other microorganisms suspended in the atmosphere, play a crucial role in influencing atmospheric processes, including air quality, meteorological events, and the global climate system (Fuzzi et al., 2015; Kulmala et al., 2011; O′ Sullivan et al., 2015; Pöhlker et al., 2012; Steiner et al., 2015). A growing body of research highlights their critical roles in atmospheric processes. For example, bioaerosols contribute to the formation of cloud condensation and ice nuclei, thereby affecting weather patterns and climate. Additionally, atmospheric microorganisms can alter the photochemical and chemical properties of aerosols by metabolizing OC compounds and reducing radical concentrations (Husárová et al., 2011; Vaïtilingom et al., 2010; Vaïtilingom et al.,

2013). Beyond their environmental significance, bioaerosols have profound implications for public health and ecological systems. Pathogenic microorganisms in the air are associated with adverse health outcomes, including infectious diseases, allergic reactions, and respiratory as well as cardiovascular disorders (Douwes et al., 2003; Fung and Hughson, 2003; Jahne et al., 2015). After excluding bioaerosol components with size larger than 2.5 μm, prokaryotic microorganisms remain, with bacteria being the dominant group (Cao et al., 2014; Lim and Kim, 2024). The health risks posed by bioaerosols are particularly pronounced when they are associated with fine PM ($PM_{2.5}$). Due to their small size, $PM_{2.5}$ particles can penetrate deeply into the respiratory tract, reaching the tracheobronchial and alveolar regions, and thus present greater health hazards compared to larger particles, which are more likely to deposit in the upper airways (Brook et al., 2004; Kawanaka et al., 2009). Given these concerns, recent scientific inquiry and public discourse have increasingly focused on the health risks associated with fine aerosol particles, particularly $PM_{2.5}$. Bacteria and fungi, as the most abundant and widespread bioaerosols, are ubiquitous in the atmosphere. Numerous studies have sought to quantify airborne bacterial and fungal populations—especially those that are culturable—and to examine their relationships with air pollution levels and environmental factors (Dong et al., 2016; Fang et al., 2005; Gao et al., 2015; Haas et al., 2013). However, understanding only the concentration of these microorganisms is insufficient. Insights into their community composition and toxic potency and contributions are essential for assessing the health impacts of air pollution.

Furthermore, there remains a significant gap in knowledge regarding the long-term temporal dynamics of airborne bacteria in $PM_{2.5}$, particularly in different regions. Long-term, systematic sampling is essential for capturing the full range of variability in microbial populations and environmental conditions, which is critical for evaluating the roles of airborne microorganisms in air pollution (Zhen et al., 2017).

In summary, while considerable progress has been made in characterizing the abundance and diversity of airborne microorganisms—particularly in relation to $PM_{2.5}$—there is a pressing need for extended, longitudinal studies to better understand the temporal and spatial patterns of bioaerosol communities and their implications for air quality and public health.

2.3.2 Spatial and temporal variations of airborne microorganisms

The distribution and dynamics of bioaerosols are shaped by a complex interaction of factors, including emission sources, land-use characteristics, environmental variables, and meteorological conditions (Bowers et al., 2011; Brodie et al., 2007). Among these, fluctuations in air pollution levels have been identified as significant drivers influencing both the abundance and community composition of airborne microorganisms (Cao et al., 2014; Gao et al., 2015). Recent investigations that have simultaneously monitored airborne particles and microbial populations have revealed pronounced seasonal changes in bacterial assemblages. These shifts are often linked to local factors such as vehicular emissions, marine and terrestrial sources, and episodic events like Saharan dust intrusions, all of which can alter both the chemical and biological makeup of the atmosphere (Federici et al., 2018; Innocente et al., 2017; Romano et al., 2020). Several studies have further demonstrated that meteorological parameters, particularly temperature and relative humidity, exert a strong influence on the structure of airborne microbial communities (Bertolini et al., 2013; Fierer et al., 2008; Maron et al., 2006). Given the close association between bacteria and PM, it is reasonable that the chemical composition of PM also influences microbial community structure. This hypothesis is supported by research indicating that certain chemical constituents of PM can affect microbial abundance (Smith et al., 2012; Vaïtilingom et al., 2012). For instance, a comprehensive analysis of the chemical composition of total suspended particulates collected during a Saharan dust event in Spain, along with characterization of the associated microbial communities, revealed the complexity of these interactions

(Sanchez de la Campa et al., 2013) . However, the direct link between PM chemistry and microbial community structure remained unclear.

Spatial heterogeneity in airborne microbial communities has been reported at broad geographic scales. For example, the microbial composition of outdoor dust varies markedly across different regions of the United States (Barberán et al., 2015). Distinct bacterial communities have been identified in agricultural, suburban, and forested environments (Bowers et al., 2011), and specific microbial taxa have been shown to differ between urban centers (Gandolfi et al., 2015). Similarly, research in Munich revealed that bacterial diversity was lower in urban areas compared to rural areas (Després et al., 2007). These studies conducted in various regions highlight the influence of local environmental conditions. In China, studies have documented the taxonomic composition of airborne microorganisms under varying pollution scenarios. During severe smog events in Beijing, $PM_{2.5}$ samples were found to consist predominantly of bacteria (86.1%), with smaller proportions of other biological components such as eukaryotes, archaea, and viruses. Similar trends were observed in PM_{10} samples, though with slight variations in the relative abundances (Cao et al., 2014). In Hangzhou, the dominant bacterial phyla included *Proteobacteria*, *Cyanobacteria*, *Actinobacteria*, *Firmicutes*, and *Bacteroidetes* (Liu et al., 2018a). The local environment, particularly in rapidly urbanizing regions in China, plays a pivotal role in shaping airborne microbial communities. Urban areas typically experience elevated levels of air pollutants—including $PM_{2.5}$, PM_{10}, NO_2, SO_2, and CO—relative to rural settings (Chai et al., 2014; She et al., 2017). Consistent with this, numerous studies have established positive correlations between the concentrations of both particulate and gaseous pollutants and the abundance of airborne microorganisms (Dong et al., 2016; Gou et al., 2016; Waters et al., 2016), suggesting that air pollution not only affects microbial community structure but may also enhance the survival or emission of certain microorganisms.

In summary, the spatial and temporal distribution of airborne microorganisms is influenced by a combination of factors such as air pollution, meteorology, geography, and anthropogenic emissions. Current evidence, mostly correlative, highlights the need for more mechanistic studies to illustrate how specific PM chemical components directly affect the microbial community.

2.3.3 Endotoxins: a widely present but often overlooked component

As one of the important airborne biological components, endotoxins are a type of pyrogen produced by Gram-negative bacteria. Endotoxins are the most abundant antigen on the cell surface of most Gram-negative bacteria, contributing up to 80% of the outer membrane of *E. coli* and *Salmonella* (Avila-Calderón et al., 2021). Examples of Gram-negative bacteria that produce endotoxins include *E. coli*, *Salmonella*, *Shigella*, *Pseudomonas*, *Klebsiella*, and *Francisella tularensis* (Farhana and Khan, 2023). A single bacterial cell contains approximately 10–40 fg of lipopolysaccharide (LPS), and ambient concentrations of 10^6–10^8 CFU (colony-forming unit) m^{-3} of Gram-negative bacteria can produce 0.01–1.0 μg of airborne endotoxins (Duquenne et al., 2013). Endotoxins are prevalent in the atmosphere while usually neglected because of their low concentration. They are found across a wide range of particle sizes. For example, a study on PM ranging from 10 nm to 18 μm collected from Zürich, Switzerland and Beijing, China found that endotoxins existed across a wide PM size range, from 0.01μm to 13 μm and 30.2–52.1% of the total endotoxin contents were found in PM_1. Elevated airborne endotoxins levels have been reported in various occupational settings, including wastewater treatment plant (4–887 EU m^{-3}), flower houses (0.84–1097 EU m^{-3}), tomato greenhouses (5.4–4002 EU m^{-3}), as well as animal husbandry (9.2 – 370000 EU m^{-3}) (Basinas et al., 2013; Gioffrè et al., 2012; Thilsing et al., 2015; Visser et al., 2006). A study conducted in a school campus in Beijing detected a range of 37.9–97.6 EU m^{-3} airborne endotoxins in measured environments, with a total average of 72 EU m^{-3} (Liu et al., 2018b).

Structurally, endotoxins are predominantly composed of an oligosaccharide core, lipid A, and outer membrane components (Figure **2-5**). They are heat-resistant, chemically stable and difficult to remove or inactivate (Ruiz et al., 2009), which contributes to their environmental persistence and health relevance.

Exposure to low concentrations of airborne endotoxins has been systematically linked to adverse respiratory outcomes (Farokhi et al., 2018). Health effects include causing oxidative stress, damaging airway mucosa, impairing mucociliary clearance, enhancing the effects of inhaled allergens, and inducing airway sensitization and asthma (Gasana et al., 2012; Guarnieri and Balmes, 2014). Evidence indicates that simultaneous contact with both traffic-related PM and endotoxins may exacerbate persistent respiratory conditions in children up to three years old (Ryan et al., 2009). Increased frequency and severity of asthma have been observed in pediatric populations when endotoxin concentrations reach 0.05 EU m^{-3} (Rabinovitch et al., 2005). Within residential environments, respiratory effects associated with endotoxins exposure appear to be influenced by the presence of nitrogen dioxide indoors, whereas PM does not show a similar association (Matsui et al., 2013). The toxicity of endotoxins is primarily mediated by the production of ROS, apoptosis, inflammatory damage, and DNA damage (Yan et al., 2023), which are major mechanisms of endotoxin-induced toxicity. Despite these well-documented mechanisms, the quantitative contribution of endotoxins to $PM_{2.5}$ mixture toxicity remains unaddressed, particularly in comparison with other more abundant components in $PM_{2.5}$, like metals and PAHs. Addressing this knowledge gap is critical as it would provide valuable insights into the significance of the toxicity from biological components in $PM_{2.5}$.

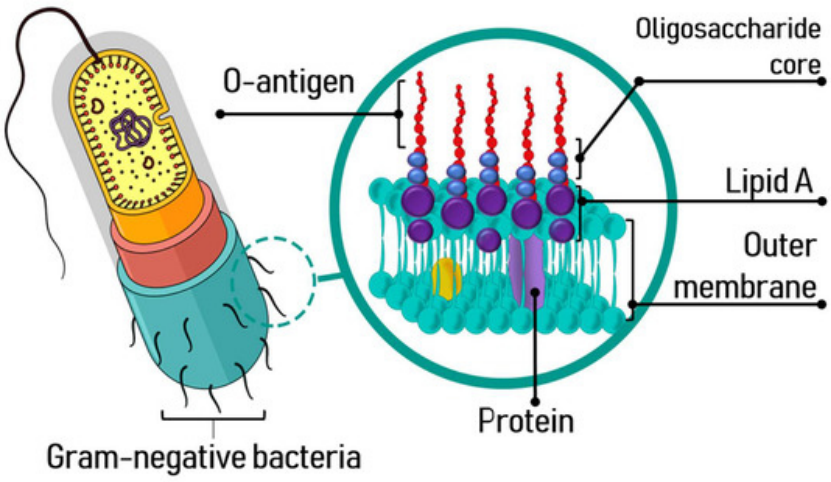

Figure 2-5. The structure of endotoxins (Marcano et al., 2021).

2.4 Component-resolved and source-resolved toxic contributions of $PM_{2.5}$

2.4.1 *In vitro* cell culture systems

Compared to *in vivo* models, *in vitro* approaches offer notable benefits such as reduced costs, greater time efficiency, and simplified experimental procedures. These systems provide enhanced opportunities to investigate complex cellular and subcellular processes, intercellular interactions, and underlying molecular pathways. As a result, recent years have seen a growing effort toward minimizing the use of animal testing by developing physiologically relevant models of the respiratory mucosa (Lee et al., 2009; Thai et al., 2005). The majority of *in vitro* investigations aimed at evaluating lung cytotoxicity have utilized either established lung cell lines or primary pulmonary cells maintained in submerged culture systems (Akhtar et al., 2014). In these models, test toxins such as PM, nanoparticles, or gases are introduced directly into the culture medium. While *in vitro* models cannot fully replicate human toxicological responses, they serve as a practical alternative for evaluating the impacts of $PM_{2.5}$ mixture and its constituents. A cellular-level investigation would generate foundational data that can guide more comprehensive toxicological assessments across experimental models and epidemiological studies.

2.4.2 Oxidative stress

Intracellular oxidative stress was selected as the endpoint for the toxicity analysis due to its well-documented role as a central molecular mechanism mediating $PM_{2.5}$-induced cellular damage (Al Housseiny et al., 2020; Gangwar et al., 2020). Exposure to $PM_{2.5}$ can impair antioxidant defense and decrease the antioxidant capacity in cells, resulting in the overproduction of intracellular ROS (Bai et al., 2018; Peng et al., 2021). This overproduction disrupts redox homeostasis, leading to oxidative damage to lipids, proteins, and DNA—a hallmark of cellular dysfunction and apoptosis (Juan et al., 2021). As evidenced by clinical correlations, oxidative stress mechanisms mediate $PM_{2.5}$-associated inflammatory responses and chronic diseases, which makes it both a sensitive biomarker of acute cellular stress (Abbas et al., 2019; Bo et al., 2016) and a predictive indicator of chronic disease risk (Hou et al., 2024; Liu et al., 2022; Traina et al., 2022).

Numerous investigations have demonstrated that inhalation of $PM_{2.5}$ can induce oxidative stress and cellular damage in both human and animal models (Dergham et al., 2012; Gualtieri et al., 2012; Kouassi et al., 2010; Longhin et al., 2013; Reche et al., 2012). Several factors contribute to this process. Firstly, $PM_{2.5}$, particularly particles originating from combustion, contains environmentally persistent free radicals (Gehling and Dellinger, 2013; Gehling et al., 2014). Secondly, a variety of organic compounds present on the surface of $PM_{2.5}$ can undergo metabolic activation, forming reactive electrophilic metabolites that elevate intracellular ROS levels (Gualtieri et al., 2012; Kouassi et al., 2010; Longhin et al., 2013; Torres-Ramos et al., 2011). Thirdly, transition metals such as iron, copper, vanadium, and manganese, which are often found in $PM_{2.5}$, may catalyze ROS generation through Fenton-type reactions or by interfering with enzyme activities (Huang et al., 2014a; Maciejczyk et al., 2010; Torres-Ramos et al., 2011). Additionally, $PM_{2.5}$ can activate inflammatory cells, which subsequently produce both ROS and reactive nitrogen species, further contributing to oxidative stress (Kannan et al., 2007). In addition to promoting oxidative stress, $PM_{2.5}$ exposure can compromise the antioxidant defense systems of affected cells. The transcription factor Nrf2 (nuclear factor erythroid-2-related factor 2) plays a pivotal role in cellular

protection against oxidative insults. ROS generated by $PM_{2.5}$ may act as signaling molecules, prompting the nuclear translocation of Nrf2 and altering the expression of genes encoding antioxidant enzymes (Deng et al., 2013). Evidence indicates that $PM_{2.5}$ exposure can modulate the levels and activities of key antioxidant enzymes, often resulting in their reduced activity (Davel et al., 2012; Kouassi et al., 2010; Wang et al., 2015). The ROS generated as a result of $PM_{2.5}$ exposure can interact with essential biomolecules—such as membrane lipids, proteins, and DNA—leading to structural and functional impairments and ultimately increasing cellular and tissue injury.

2.4.3 Mixture-toxicity modeling of $PM_{2.5}$

As previously indicated, the toxicity of $PM_{2.5}$ is not determined by total concentration alone, but also depends on its components, geographic characteristics, and other factors. For example, it has been demonstrated that, when compared at the same mass concentration, $PM_{2.5}$ collected from Beijing displayed higher toxicity than that from Guangzhou, and metals and PAHs accounted for 38% of $PM_{2.5}$-induced ROS in Beijing and 24% in Guangzhou (Jin et al., 2019). However, the remaining 60% of toxicity contributor is still unclear. One of this study's aims is to identify the contributors of the remaining 60% of toxicity.

To assess the contributions of individual components to $PM_{2.5}$-induced toxicity, the effect potency of each component should be quantified. Relative effect potencies can be determined directly using *in vitro* bioassays. Bioanalytical equivalent concentrations (BEQs) are subsequently calculated either by combining these potencies with measured chemical concentrations (BEQchem) or by utilizing the bioassay data itself (BEQbio) (Villeneuve et al., 2000). BEQs serve as a valuable means of connecting results, as they quantify the biological effect of an unknown sample in terms of the response produced by a specific reference compound. While the BEQ approach is most commonly employed for substances that exert their effects through receptor-mediated pathways, it can also be applied to nonspecific or reactive toxicological mechanisms (Escher et al., 2008).

2.4.4 Source apportionment of $PM_{2.5}$ toxicity

$PM_{2.5}$ from different regions with different climate features, pollution sources, and land-use types presents different component profiles, which result in different toxicity it induced. For instance, downtown $PM_{2.5}$ road dust induced much higher intracellular ROS levels than that from non-downtown areas, and northern cities exhibit a significantly higher ROS-inducing capacity than southern cities (Sun et al., 2021). Additionally, $PM_{2.5}$ from northern cities induced higher pro-inflammatory responses compared to those from southern cities (Ma et al., 2019). Moreover, $PM_{2.5}$ from the highway site induced higher cytotoxicity, oxidative stress and inflammatory response than the samples from the industry site and the toxicity of $PM_{2.5}$ samples in the winter was higher than that in the autumn (Zhou et al., 2022).

Previous studies have concluded major sources of $PM_{2.5}$ pollution. For example, industrial emissions, combustion, traffic emissions, secondary aerosol, dust, sea salt and so on (Xie et al., 2020). A possible reason for $PM_{2.5}$'s toxicity differences between seasons and regions may be the extensive use of residential heating in wintertime, which leads to a higher contribution from the burning of coal (Zhang and Cao, 2015). Previous studies have tracked possible sources that contribute qualitatively to $PM_{2.5}$ toxicity, and found that the $PM_{2.5}$ from vehicle emissions, coal combustion, and biomass burning have significant correlations with health risks such as oxidative potential and inflammatory responses (Li et al., 2022; Xu et al., 2020). Some studies have quantified the chronic health-risk oriented source apportionment (Xie et al., 2020; Yan et al., 2022). However, sources of *in vitro*, cell-based toxicity are yet to be investigated.

The *in vitro* cellular assays of this study can incorporate complex biological interactions, providing a more comprehensive understanding of the oxidative potential of $PM_{2.5}$ components and the toxicity source, which is essential for implementing effective pollution control measures.

2.5 Summary and outlook

Current research has established that $PM_{2.5}$ is a complex pollutant with diverse chemical and biological components, originating from both natural and anthropogenic sources. Its composition and concentration vary significantly by region and season. Epidemiological and toxicological studies have linked $PM_{2.5}$ exposure to a range of adverse health outcomes, including respiratory, cardiovascular, and neurological diseases. The toxicity of $PM_{2.5}$ is largely determined by specific components, such as metals, endotoxins and PAHs, which can induce oxidative stress, inflammation, and other cellular damage.

There are several gaps remaining for further investigation. First, the precise contributions of individual $PM_{2.5}$ components to overall $PM_{2.5}$ toxicity are not fully understood, particularly for biological components like endotoxins relative to chemical components. Second, the toxic sources to $PM_{2.5}$-induced toxicity require further research. Third, long-term, high-resolution monitoring of both chemical and biological $PM_{2.5}$ components is lacking, limiting studies in assessing temporal and spatial trends and their health implications. Addressing these gaps is essential for developing targeted interventions, informing regulatory policies, and reducing the health burden associated with $PM_{2.5}$ exposure.

While several studies have indicated that the health risk associated with $PM_{2.5}$ varies depending on its toxic composition from different pollution sources, few studies have focused on estimating $PM_{2.5}$ site-specific toxicity and the contribution of individual components. A previous study (Jin et al., 2019) analyzed the contribution of metals and PAHs to the intracellular ROS generation of $PM_{2.5}$ from Beijing and Guangzhou in 2013. However, there were still more than 60% of the total ROS induction effects unexplained back then. This study hypothesizes that endotoxins may be one of the other components responsible for the toxic effects. While the role of endotoxins in $PM_{2.5}$-induced oxidative stress and inflammation has been established in previous studies,

more research is needed to quantify its contribution to the $PM_{2.5}$ mixture toxicity, especially when compared with chemical components in $PM_{2.5}$, such as metals.

China, as one of the most rapidly developing countries in the world, is facing a significant issue of haze pollution, which has become a national public health and social problem over the past few decades. To investigate the challenges of quantifying toxic contributions of biological constituents and resolving source-specific toxicity profiles, we conducted an integrative study across six distinct land-use sites in two megacities in China: Nanjing and Guangzhou including its surrounding areas (referred to as Guangzhou in this study). Focusing on three key components in $PM_{2.5}$ (trace metals, endotoxins, and PAHs), an *in vitro* experiment was conducted on BEAS-2B cells to measure the production of intracellular ROS as the endpoint. The BEQ approach and the concentration addition (CA) concept were employed to calculate component-specific contributions to the overall toxicity of the $PM_{2.5}$ mixture. The PMF 5.0 model from the United States Environmental Protection Agency (USEPA) was used to identify the emission sources of $PM_{2.5}$. By integrating PMF models with *in vitro* experimental data, contributions of sources to $PM_{2.5}$ toxicity were quantified. This study challenges the traditional mass-based assessment of $PM_{2.5}$ toxicity and, for the first time, quantitatively reveals the significant contribution of biological components–endotoxins to the mixed toxicity of $PM_{2.5}$. It provides critical scientific evidence for establishing component-specific and source-specific air quality standards, and for implementing mitigation measures that take emission sources into account.

Chapter 3 Methodology

This chapter outlines the overall description of the sampling locations, explains the sampling methodology, and presents comprehensive details regarding the chemical and biological analyses, as well as the *in vitro* assays conducted in this study.

3.1 Description of sampling sites and the sampling strategy

To study $PM_{2.5}$ and its composition and toxicity in different regions, the $PM_{2.5}$ samples were collected in Nanjing in eastern China and Guangzhou in southern China from June 2019 to May 2020. These two cities are well-suited for health risk analysis due to their large populations and diverse land-use types (Appendix 1). In addition, they differ by approximately 30 degrees in latitude (Figure **3-1**), resulting in distinct climates. Nanjing experiences four distinct seasons, while Guangzhou remains generally warm throughout the year. These climatic differences may influence the profiles of biological components present in the air. A total of six sampling sites, each characterized by distinct land-use patterns, were chosen across the two cities (Figure **3-1**). In Nanjing, Xuanwu (XW) represents the urban environment, Pukou (PK) represents a suburban-industrial area, and Lishui (LS) represents a rural site. In Guangzhou, Tianhe (TH) represents the urban environment, Heshan (HS) represents a semirural-industrial site, and Conghua (CH) represents a suburban area. Further details of the sampling sites and samples can be found in Appendix 1. The $PM_{2.5}$ samples were typically collected once per week using a $PM_{2.5}$-PUF-1000 multifunctional high-volume air sampler (Guangzhou Mingye Environmental Technology Co., Ltd, China) with quartz filter membranes for 24 h for each sample. A $PM_{2.5}$ size-selective impactor was installed at the sampler inlet to remove particles larger than 2.5 μm in aerodynamic diameter, ensuring the collection of only $PM_{2.5}$ on the quartz filters. The sampling rate was 999 L min^{-1}. Tissue quartz filters of 8×10 inches (PALL, USA) were pre-baked at 500 °C for 5 h to remove organics and pyrogens, and weighed before and after sampling with a sensitivity of ± 0.0001 g. The filters were placed in a desiccator at 25 °C and a relative

humidity of 40–50% for 24 h before being weighed. Field blank filters were collected by placing filters in the sampler without operating the pump to evaluate potential contamination during handling and transport, for quality assurance and quality control (QA/QC) purposes. Information about the $PM_{2.5}$ samples extracted for cell toxicity analysis is shown in Appendix 1.

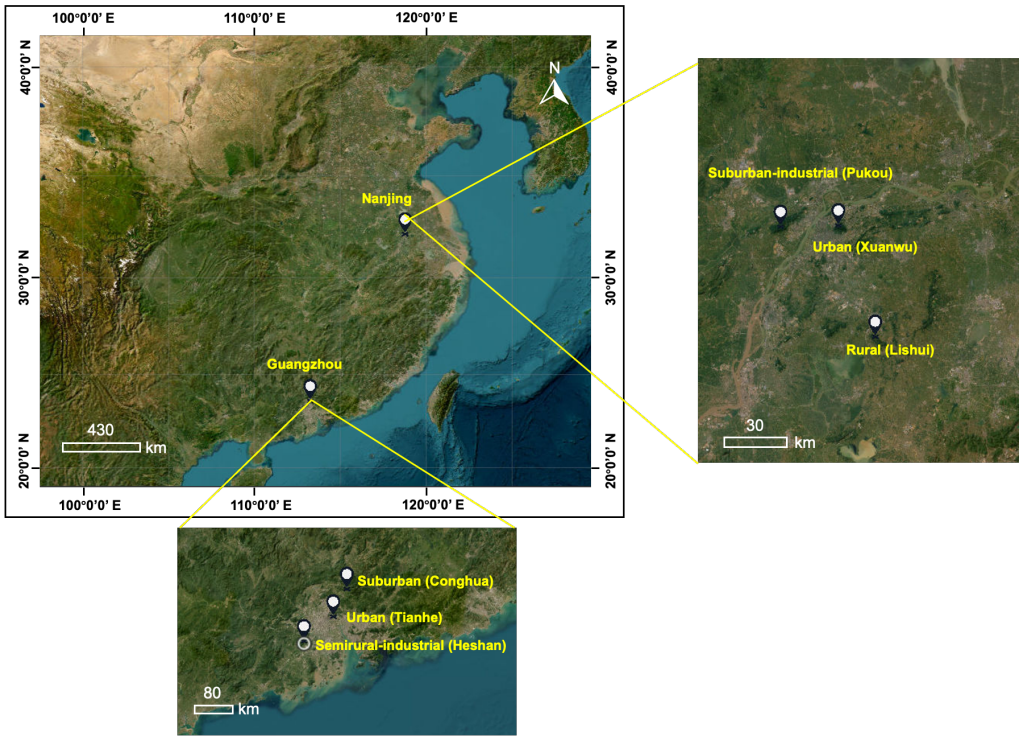

Figure 3-1. Map of the sampling sites (created using ArcGIS® Online)

3.2 Chemical analysis of $PM_{2.5}$

This section outlines the laboratory procedures used to analyze the fundamental chemical components of $PM_{2.5}$, including trace metals, WSI, OC, EC and PAHs. It also describes the risk assessment models applied.

3.2.1 Trace metals

The glass test tubes used for trace metal extraction were soaked in 10% regular HNO_3 overnight and rinsed thoroughly with Milli-Q water the following day. They were then soaked in 10% high-purity HNO_3 overnight. After removal from the high-purity HNO_3, they were rinsed with Milli-Q water and placed in a laboratory oven to dry.

For each $PM_{2.5}$ filter membrane, a section equivalent in size to 1/16 of an A4 sheet was cut and placed into a test tube. Plastic scissors and tweezers were used for this process. Three blank tubes, three blank filter tubes, and three tubes containing the standard reference material (NIST 1648a) were included and evenly distributed among the test tubes for QA/QC. After cutting each sample, 8 mL of 70% high-purity HNO_3 and 2 mL of 60% high-purity $HClO_4$ were added to the test tubes using auto-pipettes.

The tubes were vortexed and placed in a heating block, with the heating program set as follows: ramp to 50 °C for 30 minutes, ramp to 75 °C for 30 minutes, ramp to 100 °C for 120 minutes, ramp to 125 °C for 180 minutes, ramp to 150 °C for 180 minutes, and finally ramp to 190 °C until dry. When the temperature reaches 190 °C, the tubes were checked every 30 minutes. They were removed from the heating block once the residual samples were completely dry.

After the test tubes had cooled, 12 mL of 5% HNO_3 (prepared by diluting 70% high-purity HNO_3 to 5%) was added to each tube using a dispenser. The test tubes were

vortexed, returned to the heating block, and heated at 70 °C for 60 minutes. They were then removed, vortexed again, and allowed to cool.

The solution and remaining filter in each test tube were filtered through 0.45 μm filter membranes and poured into 10 mL plastic tubes. The solution was stored at 4 °C prior to analysis. Trace metals in each solution were analyzed using an inductively coupled plasma optical emission spectrometer (ICP-OES). For quality control, recovery tests were conducted at high and medium levels (with the medium level being half of the high level) for each metal. The recovery rates did not show significant differences during the analysis. Recovery rates of most metals in the reference materials ranged from 73.5% to 119%. Exceptions were Al and Cr, whose recoveries were low because the digestion procedure did not fully dissolve them, indicating a limitation of the method employed (Table **3-1**). Comparisons of analyzed metals in $PM_{2.5}$ samples and field blank filters are shown in Table **3-2**.

Table 3-1. Recovery of analyzed trace metals.

Component	Al	As	Cd	Co	Cr	Cu	Fe	Mn	Ni	Pb	V	Zn
Mean%	56.2	119	96.1	102	32.2	93.2	93.1	73.5	89.2	95.2	86.2	96.5
SD%	3.76	6.37	3.99	6.55	9.45	3.53	3.27	6.62	4.79	3.08	4.69	5.99

Table 3-2. Comparisons of analyzed metals in $PM_{2.5}$ samples and field blank filters.

Component	$PM_{2.5}$ sample (ng m^{-3})	Blank filter (ng m^{-3})	Blank filter/ $PM_{2.5}$ sample
Al	573±505	1.11±0.867	0.194%
As	5.20±3.22	0.171±0.282	3.27%
Cd	0.860±0.495	0.0404±0.0312	4.65%
Co	1.14±2.16	0.0717±0.0628	6.14%

Cr	3.84±2.90	0.235±0.283	6.25%
Cu	41.2±44.6	0.512±0.631	1.24%
Fe	529±298	2.73±1.65	0.516%
Mn	21.7±11.5	0.262±0.0668	1.20%
Ni	4.96±2.96	0.177±0.131	3.63%
Pb	25.6±20.8	0.310±0.390	1.21%
V	2.29±1.27	0.164±0.243	6.99%
Zn	105±63.8	0.892±0.853	0.850%

3.2.2 WSI

Each $PM_{2.5}$ filter membrane (with a size equivalent to 1/32 of an A4 sheet) was cut and put into a 50 mL plastic tube. Then, 15 mL of Milli-Q water was added to each tube. The tubes containing the samples were sonicated in ice water for 20 minutes. After sonication, the solution was filtered through a 0.45 μm filter membrane into a new 50 mL plastic tube. The $PM_{2.5}$ filters were left in the original tubes. 15 mL of Milli-Q water was added again, followed by sonication and a second filtration. The filtrate from the second filtration was combined with the solution obtained from the first filtration. The combined solution was stored in a laboratory refrigerator at 4 °C prior to analysis. Anions (Cl^-, SO_4^{2-}, NO_3^-) and cations (Na^+, K^+, NH_4^+, Ca^{2+}, Mg^{2+}), were measured separately using ion chromatography (IC).

3.2.3 OC/EC

A 0.526 cm² section of each $PM_{2.5}$ sample was cut using the customized cutter and placed into a carbon analyzer. After processing each sample, the cutter and tweezers were cleaned with Milli-Q water. Concentrations of OC and EC were analyzed using a thermal optical carbon analyzer (Model 2001, Desert Research Institute) and calculated based on the results of the thermal optical reflectance (TOR) protocol.

3.2.4 PAHs

Two to three 1 cm² sections of each $PM_{2.5}$ filter were cut using a customized cutter. Then, 5 μL of internal standard was introduced into every sample. PAHs (phenanthrene (Phe), anthracene (Ant), fluoranthene (FLA), pyrene (Pyr), benz[a]anthracene (BaA), chrysene (Chr), benzo[b]fluoranthene (BbF), benzo[k]fluoranthene (BkF), Benzo[a]pyrene (BaP), indeno[1,2,3-cd]pyrene (IcdP), benzo[g,h,i]perylene (BghiP), dibenz[a,h]anthracene (DahA)) were analyzed using an in-injection port thermal desorption, in which small strips of $PM_{2.5}$ filter were packed into a injector liner and analyzed by a gas chromatography-mass spectrometry (GC-MS) (Agilent 7890A) following a previous protocol (Ho and Yu, 2004). The physical properties, calibration slopes, intercepts and coefficients of determination for the PAH standards are shown in Table 3-3. And the GC-MS total ion chromatogram (TIC) of a $PM_{2.5}$ sample (CH-12, as an example) and a blank filter sample is shown in Figure **3-2**.

Table 3-3. Physical properties, calibration slopes, intercepts and coefficients of determination for the PAH standards.

PAH	Molecular weight (g mol^{-1})	Boiling point (°C)	Slope	Intercept	R^2
Phe	178	340	0.0377	-0.0522	0.992
Ant	178	340	0.118	0.00170	0.997
Fla	202	375	0.0915	-0.0772	0.992
Pyr	202	404	0.0883	-0.0623	0.996
BaA	228	438	0.105	-0.1166	0.992
Chr	228	448	0.0978	-0.0208	0.992
BbF	252	357	0.0647	-0.144	0.997
BkF	252	480	0.1591	-0.0533	0.997
BaP	252	495	0.068	-0.0185	0.971
IcdP	276	536	0.118	-0.149	0.991

BghiP	276	500	0.0879	-0.0847	0.996
DahA	278	524	0.0815	-0.123	0.997

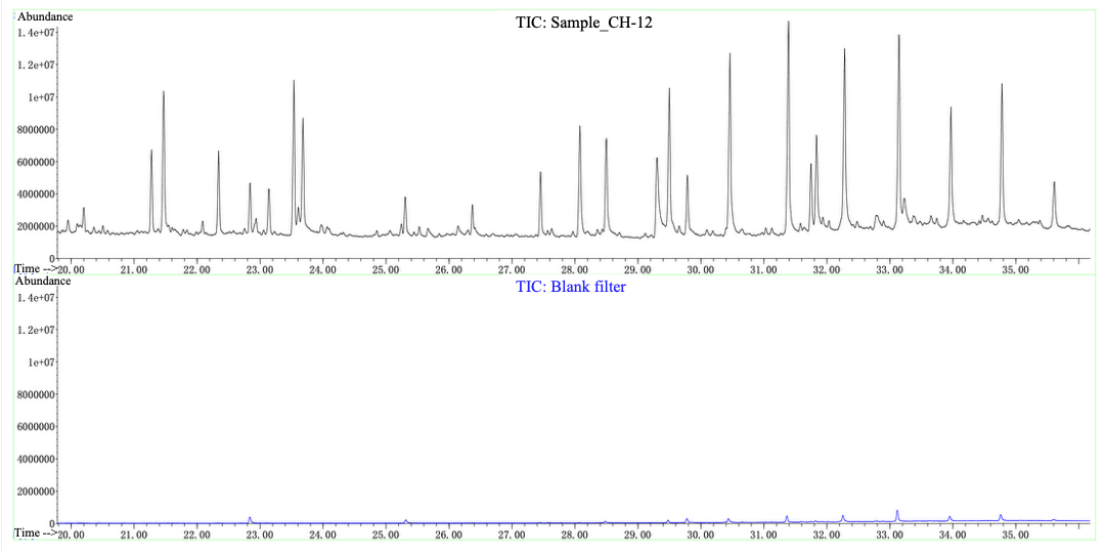

Figure 3-2. GC-MS total ion chromatogram (TIC) of a $PM_{2.5}$ sample (CH-12, as an example) and a blank filter sample.

3.3 Health risk assessment posed by chemical components

The evaluation of long-term inhalation health hazards posed by trace metals in $PM_{2.5}$ across the six sampling sites was conducted according to USEPA protocols, utilizing measured metal concentrations.

First, the exposure levels (μg m^{-3}) were adjusted using Equation 3-1. *CR* and *NCR*, represented by Hazard Quotients (*HQ*), were then determined through Equations 3-2 and 3-3, respectively (USEPA, 2009).

$$EC = (BC \times ET \times EF \times ED)/AT$$

Equation 3-1

The term *EC* (μg m^{-3}) refers to the concentration of exposure, and *BC* (μg m^{-3}) denotes the yearly mean concentration of the metal. Additionally, *ET*, *EF*, and *ED* stand for exposure time (hours per day), exposure frequency (days per year), and exposure duration (years), respectively. The averaging time (*AT*) represents the total lifetime

hours when assessing *CR*. For *HQ* calculations, *AT* is defined solely as the cumulative hours over the exposure period.

$$CR = IUR \times EC$$

Equation 3-2

$$HQ = EC/(RfC_i \times 1000\ \mu g/mg)$$

Equation 3-3

IUR denotes the Inhalation Unit Risk (per μg m^{-3}), and RfC_i represents the inhalation reference concentration (mg m^{-3}). Additional parameter values are provided in Table **3-4**. For As, the concentrations applied in risk assessments were modified using speciation information described in the previous study (Xie et al., 2020).

In summary, an adjusted approach for assessing As risk, which incorporates its speciation profile, was utilized for *CR* (Equation 3-4) and *NCR* (Equation 3-5).

$$CR_{cur} = \frac{CR_{ori}}{R_{ori,As(V)} * TR_{As(V)/As(III)} + R_{ori,As(III)}} \times (R_{cur,As(V)} * TR_{As(V)/As(III)} + R_{cur,As(III)})$$

Equation 3-4

$$HQ_{cur} = \frac{HQ_{ori}}{R_{ori,As(V)} * TR_{As(V)/As(III)} + R_{ori,As(III)}} \times (R_{cur,As(V)} * TR_{As(V)/As(III)} + R_{cur,As(III)})$$

Equation 3-5

CR_{cur} and CR_{ori} denote the adjusted and original CRs, respectively. R_{cur} indicates the fractions of As(V) or As(III) relative to total As in this study, whereas R_{ori} reflects the corresponding proportions cited in USEPA studies. The toxicity ratio of As(V) to As(III), $TR_{As(V)/As(III)}$, was set to 0.1. For the CR calculation, $R_{ori,As(V)}$ and $R_{ori,As(III)}$ were assigned values of 5/6 and 1/6, respectively. In NCR assessments, $R_{ori,As(V)} = R_{ori,As(III)} =$ 1/2.

Table 3-4. Parameters used in the calculation of CR and hazard quotients in this study.

Parameters	**adult**	**Metal**	**IUR [a] ($\mu g\ m^{-3})^{-1}$**	**RfC_i[a] ($mg\ m^{-3}$)**
ED (years)	20	V	--	1.00E-04
ET (hours day^{-1})	8	Mn	--	5.00E-05
EF (days $year^{-1}$)	350	Co	9.00E-03	6.00E-06
AT-non-carcinogens (h)	175200 (20 years)	Ni	2.60E-04[b]	9.00E-05
		As	4.30E-03	1.50E-05
AT-carcinogens (h)	613200 (70 years)	Cd	1.80E-03[c]	1.00E-05
		Pb	1.20E-05[d]	5.00E-04[e]
		Cr (VI)	8.40E-02	1.00E-04
		Fe	--	5.00E+00[e,f]
		Cu	--	1.00E+00[e]
		Zn	--	5.00E-01[e]

[a] IUR and RfC_i obtained from the USEPA(USEPA, 2018)

[b] for Ni soluble salts

[c] for Cd (Diet/Water)

[d] for Pb phosphate/acetate/subacetate

[e] benchmark value obtained from other standards (Oosthuizen et al., 2015)

[f] for Fe oxide (dust)

For estimating the excessive cancer risk (ECR) of PAHs, a point-estimate method developed by the Office of Environmental Health Hazard Assessment (OEHHA) of the California Environmental Protection Agency (CalEPA) (Collins et al., 1998) was employed. The concentration of each PAH was converted to its BaP equivalent (BaPeq) by multiplying by its relative potency factor (RPF). The overall inhalation cancer risk for the PAH mixture was calculated by multiplying the sum of the individual BaPeq

concentrations by the unit risk (UR) associated with BaP exposure. The equations for these calculations are provided in Equations 3-6 and 3-7.

$$Cancer\ Risk = \sum_{i=1}^{n} (C_{PAH_i} \times RPF_i) \times UR_{BAP}$$

Equation 3-6

$$Excess\ Cancer\ Risk = \sum_{i=1}^{n} (C_{PAH_i} \times RPF_i) \times UR_{BAP}$$

Equation 3-7

In this context, C_{PAHi} refers to the concentration of a specific PAH within $PM_{2.5}$ particles, RPF_i denotes the relative potency factor for each PAH,, and UR_{BaP} represents the inhalation unit risk associated with exposure to BaP. This risk is defined as the theoretical maximum probability of developing cancer from lifelong exposure to BaP at a concentration of one microgram per cubic meter of air over 70 years. The WHO has estimated UR_{BaP} at 8.7×10^{-5} per ng m^{-3}, based on a study involving coke-oven workers in Pennsylvania. The assessment of inhalation cancer risk included seventeen carcinogenic PAHs, among them twelve priority pollutants such as Ant, BaA, BbF, BghiP, BkF, Chr, DahA, FLA, IcdP, Phe, Pyr, and BaP and two MW 302 PAHs, dibenzo[a,e]pyrene (DBaeP) and dibenzo[a,l]pyrene (DBalP). The RPF were derived from tumor bioassay data provided by the USEPA's Integrated Risk Information System Program (USEPA, 2010). Although the USEPA reviewed RPF values for additional MW 302 PAH isomers, these were not adopted due to insufficient data. Table **3-5** details the individual PAHs and their corresponding RPF values.

Table 3-5. RPF of PAH for cancer risk assessment.

PAH	RPF
Phenanthrene	0
Anthracene	0
Fluoranthene	0.08
Pyrene	0

Benz[a]anthracene	0.2
Chrysene	0.1
Benzo[b]fluoranthene	0.1
Benzo[k]fluoranthene	0.1
Benzo[a]pyrene	1
Dibenz[ah]anthracene	10
Indeno[1,2,3-cd]pyrene	0.07
Benzo[ghi]perylene	0.009
Dibenzo[a,l]pyrene	30
Dibenzo[a,e]pyrene	0.4

3.4 Characterization of biological components

This section outlines the approach for biological characterization in this study, including assessment of endotoxins levels, preparation protocols for $PM_{2.5}$ samples, measurement of bacterial concentrations, and examination of microbial community through 16S rDNA sequence analysis.

3.4.1 Endotoxin analysis

The work surface was disinfected with 70% ethanol before the experiment. Two pieces of 0.526 cm^2 $PM_{2.5}$ filter samples were cut with pre-disinfected plastic scissors, then transferred using plastic tweezers into a pyrogen-free tube. 1 mL of pyrogen-free water was added to the tube, which was then vortexed for 30 minutes and sonicated for 30 minutes at room temperature, followed by centrifugation at 1000g for 15 minutes as described in Allen et al. (2011). The supernatant was used for endotoxins quantification using the LAL assay with the Pierce™ Chromogenic Endotoxin Quant Kit (Thermo Scientific), following the manufacturer's instructions. Blank filters and reference filters containing the endotoxin standard (0.5 EU mL^{-1}) were analyzed with the samples as ongoing analytical quality control throughout the entire process. Endotoxin

concentrations were measured using a microplate reader (SpectraMax iD3). For quality control, an endotoxin standard derived from *E. coli* strain O111: B4 (Thermo Scientific) was used as the standard reference material and the recovery rate of endotoxins was 96.8% ± 4.83%. The comparison of endotoxins in $PM_{2.5}$ samples and field blank filters is shown in Table **3-6**.

Table 3-6. Comparisons of endotoxins in $PM_{2.5}$ samples and field blank filters.

Component	$PM_{2.5}$ sample (ng m^{-3})	Blank filter (ng m^{-3})	Blank filter/ $PM_{2.5}$ sample
Endotoxins	0.00612±0.00584	0.000483±0.000402	7.89%

3.4.2 Pretreatment of $PM_{2.5}$ samples before DNA extraction

For $PM_{2.5}$ samples collected from June 2019 to May 2020 in six sites in Nanjing and Guangzhou, 1/32 of each selected filter sample (mostly four samples per month) was cut out. These four cut samples from the same month were combined as one sample (equivalent to 1/8 of the original filter) for DNA extraction. A blank filter underwent the same treatment procedure as the samples. The pretreatment of $PM_{2.5}$ samples was conducted based on the established protocol (Jiang et al., 2015) with minor adjustments implemented to suit the specific requirements of this study. In brief, following division of the filter into 1/32 equal segments, each section was sonicated in sterile 1× phosphate-buffered saline (PBS) within an ultrasonic bath cooled by ice water. This method did not result in notable DNA degradation as described in a previous study (He et al., 2021). The extracts were subsequently passed through a 0.2-μm polyether sulfone (PES) membrane disc filter (47 mm, PALL) to collect sufficient biological material for subsequent analyses, though this approach limited the temporal resolution to monthly averages. Prior to DNA extraction, all samples were stored at −80 °C. Throughout the procedure, all instruments, materials, and devices were thoroughly sterilized.

3.4.3 DNA extraction

Genomic DNA was isolated from the samples utilizing the FastDNA SPIN Kit for Soil (MP Biomedicals, USA), following the protocol provided by the manufacturer, with the exception of a modified purification step. For $PM_{2.5}$ samples, Agencourt AMPure XP beads (Beckman Coulter, USA) were employed during purification, as described in previous studies (Cao et al., 2014; Jiang et al., 2015). The 0.2 μm round membrane filters of $PM_{2.5}$ were initially cut into smaller fragments. As outlined in Section 3.4.2, a total of 59 monthly $PM_{2.5}$ DNA samples were collected from six monitoring locations in Nanjing (XW, PK, LS) and Guangzhou (TH, HS, CH), along with one field blank, and prepared for subsequent analyses. All extracted DNA samples were stored at -80 °C prior to further examination.

3.4.4 Real-Time qPCR (quantitative polymerase chain reaction) quantification of target genes

The 16S rRNA gene was utilized as a marker to estimate the overall bacterial abundance. Quantification was performed using a StepOnePlus Real-Time qPCR System (Applied Biosystems), employing the following primers: forward, 5'-TCCTACGGGAGGCAGCAGT-3', and reverse, 5'-GGACTACCAGGGTATCTAATCCTGTT-3' (Nadkarni et al., 2002). Absolute quantification of 16S rRNA gene copies was achieved by generating a standard curve with seven serial 10-fold dilutions, including a blank standard. Each sample, standard, and blank was measured three times, and the amplification efficiency varied from 90% to 110%. Melt curve analysis was employed to verify the specificity of the PCR products. Each 20 μL qPCR reaction mixture contained 10 μL of Power SYBR™ Green PCR Master Mix (Life Technologies, CA, USA), 1 μL of extracted DNA, 0.5 μL of each primer (100 nM), and RNase-free water to reach the final 20 μL volume. The amplification protocol consisted of an initial step at 95°C for 10 minutes to activate the enzyme, followed by 40 cycles of denaturation at 95°C for 10 seconds and hybridization

and elongation at 60°C for 1 min. The resulting amplicons were approximately 400–500 base pairs (bp) in length.

3.4.5 16S rRNA gene amplicon sequencing

Amplification of the V3–V4 region within the 16S rRNA gene was performed using 30 ng of high-quality DNA as template, together with 16S rRNA fusion primers for PCR. Following amplification, PCR products were purified utilizing Agencourt AMPure XP beads, resuspended in Elution Buffer, and subsequently indexed to complete the library preparation process. The resulting libraries were assessed for fragment size and concentration using an Agilent 2100 Bioanalyzer. Libraries meeting quality criteria were then sequenced on the DNB platform, with sequencing parameters adjusted according to the insert length. Figure **3-3** shows the experiment workflow.

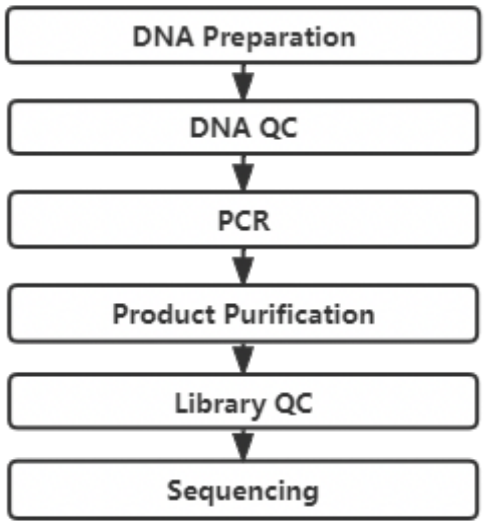

Figure 3-3. The experiment workflow of 16S rRNA gene amplicon sequencing

3.4.6 Bioinformatic analysis

Initial sequencing data underwent quality control to generate high-confidence clean reads. Overlapping clean reads were subsequently merged into tags, which were then grouped into operational taxonomic units (OTUs). Representative sequences from each OTU were taxonomically classified using the Ribosomal Database Project (RDP)

database. Downstream analyses—including assessments of alpha and beta diversity, identification of differentially abundant taxa, network construction, and predictive modeling—were conducted utilizing the OTU abundance table in conjunction with taxonomic annotation results. Figure **3-4** shows the bioinformatics analysis workflow.

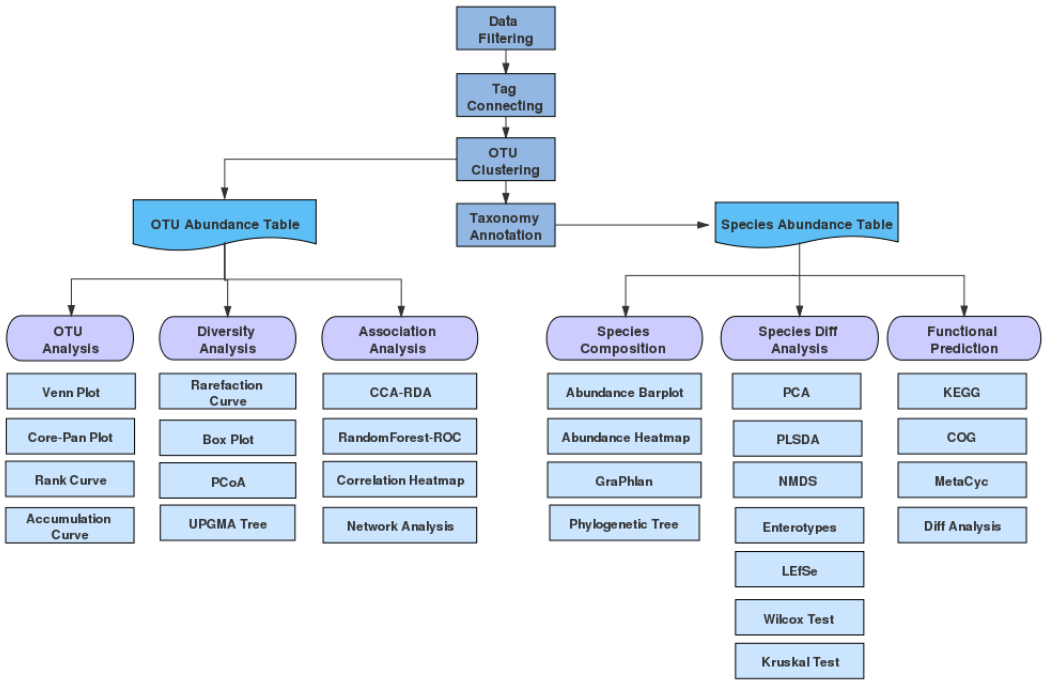

Figure 3-4. Bioinformatics analysis workflow.

Alpha diversity, which assesses the variety of species within an individual sample, was quantified in this study using the Shannon index, implemented via the cluster and clusterSim packages in R (v3.4.1). The Shannon index provides an estimate of community diversity by accounting for both the number of species present (richness) and their relative abundances (evenness). When species richness is held constant, higher evenness corresponds to increased diversity.

For taxonomic profiling, representative sequences from each OTU were classified using the Bayesian algorithm of the RDP classifier, enabling detailed characterization of microbial community composition. Following taxonomic annotation, species abundances were determined at seven hierarchical levels—phylum, class, order, family,

genus, and species—using the 'gplots' package in R (v3.1.1), with complete linkage clustering and Euclidean distance metrics applied.

Principal Coordinates Analysis (PCoA) was employed to investigate and visualize patterns of similarity or difference among samples. This technique begins with a matrix of pairwise similarities or dissimilarities and projects each sample into a reduced-dimensional space. The most informative axes are selected by ranking and extracting the leading eigenvalues from the distance matrix. For beta diversity analysis, QIIME (v1.80) was utilized, applying an iterative approach in which 75% of the sequence count from the sample with the lowest read number was randomly subsampled 100 times, considering both unweighted and weighted species abundances. The resulting data were visualized using PCoA plots. A Venn diagram was used to display the number of common and unique OTUs between Nanjing and Guangzhou samples (Software: Venn Diagram package in R (v3.1.1)). Linear discriminant analysis (LDA), a widely used supervised dimensionality reduction method in machine learning, was applied to maximize the separation between predefined groups based on their features. This approach leverages group labels to enhance the reliability of the results. The linear discriminant analysis effect size (LEfSe) tool (https://huttenhower.sph.harvard.edu/galaxy/) was used to perform LDA in this context.

Species accumulation curves are used to show the increase of species detected with the addition of each sample. It is an effective tool to understand the composition of the community and predict the richness of species, which is widely used for the estimation of the sufficiency of the sampling quantity and species richness in the survey of the biodiversity and community. In this study, A total of over 4000 species was recorded after 59 sampling units (Figure **3-5**). The accumulation curve approached an asymptote after these 59 samples, indicating that most species present were likely detected.

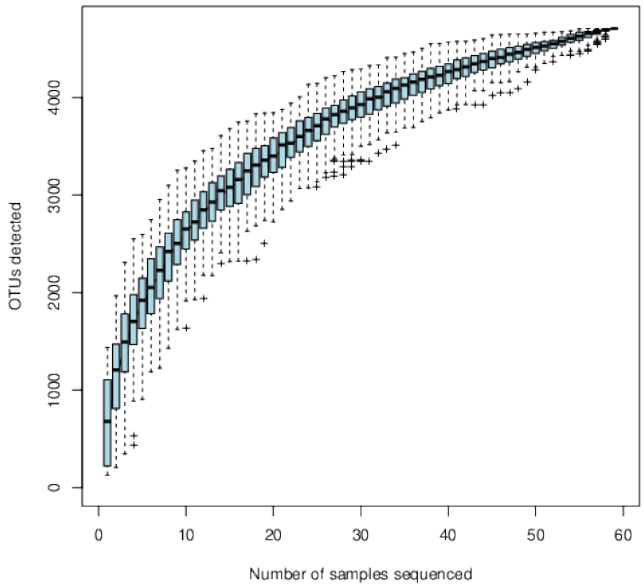

Figure 3-5. Species accumulation analysis.

3.5 $PM_{2.5}$ cell toxicity analysis

This section describes the procedure of preparation of PM extracts for cell exposure, *in vitro* cell experiments, mixture-toxicity modeling and related data analysis.

3.5.1 Preparation of PM extracts for cell exposure

Each $PM_{2.5}$ sample was extracted using MilliQ water (pyrogen-free) and methanol (100%) following previously established protocols (Jin et al., 2019). Each quartz filter (of a size equivalent to one-sixteenth of the sampling quartz filter) was extracted in 7.5 mL of Milli-Q water by 30 mins of sonication and extracted again in 7.5 mL of methanol by 30 mins of sonication in pre-weighed, sterile centrifuge tubes. The $PM_{2.5}$ extracts that were extracted using Milli-Q water were stored at –80 °C overnight and lyophilized. The $PM_{2.5}$ extracts that were extracted using methanol were evaporated under nitrogen gas until dry. Both centrifuge tubes were reweighed to quantify the amount of $PM_{2.5}$ removed from the quartz filter. The combined $PM_{2.5}$ extracts were resuspended in the cell culture medium at 1000 mg L^{-1} for cellular assays. The rest were stored at –20 °C for further analysis.

3.5.2 Cell culture and bioassays

BEAS-2B cells were purchased from American Type Culture Collection (ATCC). They were cultured in Dulbecco's Modified Eagle's Medium (DMEM) supplemented with 10% heat-inactivated fetal bovine serum and 1% penicillin-streptomycin antibiotics under conditions of 37 °C and 5% CO_2 in a humidified incubator. An MTS assay (Abcam) was used to measure the viability of the cells. The production of intracellular ROS was assessed using the DCFH-DA (2,7-dichlorofluorescein diacetate) assay (Abcam).

Cells were inoculated in black 96-well plates at a density of 1.5×10^5 cells mL^{-1} and incubated for 24 h to achieve confluence. Once the medium was discarded, cells were rinsed twice with PBS and then treated with 100 μL of serially diluted $PM_{2.5}$ samples, test substances, or field blanks in fresh medium. The exposure concentration of $PM_{2.5}$ samples ranged from 0 to 500 mg L^{-1}. Tert-butyl hydroperoxide (TBHP), known as an intracellular ROS inducer, served as a reference chemical in each plate. After exposure for 24 h, the medium was discarded and a total of 100 μL of 1× buffer containing 20 μM DCFH-DA was added to the cells. After 45 mins of incubation at 37 °C, the fluorescence intensity was assessed at 0 h and 2 h by a microplate reader (excitation: 485 nm, emission: 535 nm). The ROS induction ratio (*IR*) was expressed as the optical density (*OD*) of samples relative to that of controls at 2 h using Equation 3-8. We employed linear concentration-effect curves as described (Escher et al., 2018), featuring an intercept of 1 and a calculated slope (Equation 3-9) to determine the effect concentration at an ROS induction ratio of 1.5 ($EC_{IR1.5}$, Equation 3-10).

$$IR = \frac{OD_{sample,2h}}{OD_{control,2h}}$$

Equation 3-8

$$IR = 1 + slope \times concentration$$

Equation 3-9

$$EC_{IR1.5} = \frac{0.5}{slope}$$

Equation 3-10

During the extraction procedure, there were quartz fiber debris extracted along with $PM_{2.5}$ particles. To quantify this, we performed "procedure blank" tests by extracting blank quartz fiber filters using the same protocol as for $PM_{2.5}$-loaded samples. Based on six replicates, it was found that the amount of extracted quartz fiber debris accounted for 16.2 ± 3.03% of the total mass in the $PM_{2.5}$ extracts. To check if the quartz fiber debris affects the toxicity induced by $PM_{2.5}$ itself, the biological responses induced by blank filter extracts were measured. As shown in the Figure **3-6**, blank filter extracts did not induce significant ROS production ($p > 0.05$) or affect cell viability ($p > 0.05$) at concentrations up to 500 mg L^{-1}, which matches the maximum concentration used in the cell experiments.

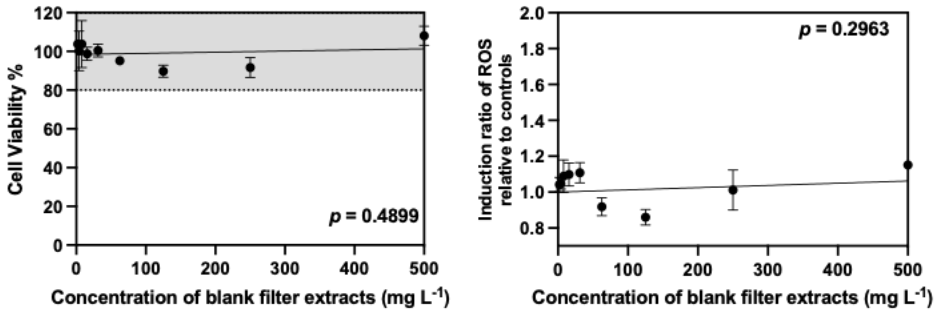

Figure 3-6. Concentration-effect curves of cytotoxicity and oxidative stress induced by field blank filters. $p > 0.05$ means no significant toxicity.

3.5.3 Estimation of realistic daily exposure concentration for adults of each component

Minute ventilation (*MV*), including breath in and breath out, in humans ranges between 6.02 and 7.5 L min^{-1} (Arms and Travis, 1988). Here we employ 7.5 L min^{-1} for calculation. It is assumed that the volume of air breathed in equals that breathed out, and that all inhaled particles deposit on lungs without loss. The total volume of

epithelial lining fluid (V_{ELF}) in the lungs is in the range of 10–40 mL. Based on this, a mean value of 25 mL (CV = 20%) was used (Gaohua et al., 2015). The realistic daily exposure concentration (C_{RDE}) for adults of each component is calculated by Equation 3-11, where C_i is the mass concentration of individual component.

$$C_{RDE} = C_i \times \frac{\frac{MV}{2} \times 60\ min \times 24\ h}{V_{ELF}}$$

Equation 3-11

3.5.4 Mixture-toxicity modeling

To quantify the contribution of identified components to $PM_{2.5}$-induced toxicity, intracellular ROS was employed as an exemplary endpoint. The mixture-toxicity modeling was conducted according to methods that have been validated (Jin et al., 2019). Based on BEAS-2B cell assays, the following effect concentrations were obtained: for each tested component ($EC_{IR1.5,\ i}$), for the reference compound TBHP ($EC_{IR1.5,\ TBHP}$), for defined mixtures of selected components ($EC_{IR1.5,\ mix}$), and for $PM_{2.5}$ extract samples ($EC_{IR1.5,\ PM2.5}$). The ROS-inducing ability of individual active components, expressed as relative effect potency (REP_i), was calculated through normalization to the reference chemical TBHP (Equation 3-12).

$$REP_i = \frac{EC_{IR1.5,TBHP}}{EC_{IR1.5,i}}$$

Equation 3-12

$PM_{2.5}$ extracts comprise an unidentified mixture of components at unknown concentrations. BEQ offers a quantitative approach for assessing the combined effects of $PM_{2.5}$ components ($BEQ_{bio,\ PM2.5}$). $BEQ_{bio,\ PM2.5}$ refers to the concentration of TBHP that produces the equivalent effect (the 1.5-fold induction of ROS) as that caused by the $PM_{2.5}$ extract (Equation 3-13).

$$BEQ_{bio,PM_{2.5}} = \frac{EC_{IR1.5,TBHP}}{EC_{IR1.5,PM_{2.5}}}$$

Equation 3-13

Determination the BEQ_{comp} for each identified component or their mixtures was based on Equation 3-14, where C_i is the mass concentration of a certain component per unit mass of $PM_{2.5}$. This enables the calculation of the proportional contribution of identified components in the samples to the overall $PM_{2.5}$ toxicity (i.e., *percent contribution of components*), using Equation 3-15.

$$BEQ_{comp} = \sum_{i=1}^{n} (C_i REP_i)$$

Equation 3-14

$$percent\ contribution\ of\ components = \frac{BEQ_{comp}}{BEQ_{bio,PM_{2.5}}} \times 100\%$$

Equation 3-15

The CA model has been extensively applied to estimate the combined effects of organic compounds on general endpoints, including baseline toxicity and responses related to oxidative stress, both of which are influenced by various underlying mechanisms (Escher et al., 2013; Tang et al., 2013). Confirmation is still needed regarding the joint effects of metals, endotoxins, and PAHs on intracellular ROS induction. In this research, the CA model was employed to test the hypothesis that the aggregate impact of individual components on ROS production closely reflects the overall effect observed when these substances are combined. This approach enabled us to quantitatively determine the contribution of each identified component. The CA model was utilized to estimate the effect concentrations ($EC_{IR1.5,CA}$) for ROS induction, based on representative mixtures of metals, endotoxins, and PAHs. These mixtures reflected the average mass percentage (p_i) of each component found in samples from each site.

$EC_{IR1.5,CA}$ is calculated with Equation 3-16, which translates the mass proportion in the mixture into its toxic contribution (Backhaus and Faust, 2012).

$$EC_{IR1.5,CA} = \frac{1}{\sum_{i=1}^{n} \frac{p_i}{EC_{IR1.5,i}}}$$

Equation 3-16

The index of prediction quality (IPQ) was applied to evaluate how much the predicted mixture effects differed from the experimentally observed outcomes (Altenburger et al., 1996). An *IPQ* value of zero means complete concordance between the model's predictions and the experimental results. When the *IPQ* is positive, the $EC_{IR1.5}$ estimated by the CA model ($EC_{IR1.5,CA}$) exceeds the experimentally determined $EC_{IR1.5}$ ($EC_{IR1.5,exp}$); conversely, a negative *IPQ* reflects a lower CA-predicted $EC_{IR1.5}$ compared to the experimental value, as described in Equations 3-17 and 3-18.

$$\text{If } EC_{IR1.5,CA} > EC_{IR1.5,exp}, \text{ then } IPQ = \frac{EC_{IR1.5,CA}}{EC_{IR1.5,exp}} - 1$$

Equation 3-17

$$\text{If } EC_{IR1.5,CA} < EC_{IR1.5,exp}, \text{ then } IPQ = 1 - \frac{EC_{IR1.5,exp}}{EC_{IR1.5,CA}}$$

Equation 3-18

If the IPQ is between –1 and +1, it indicates a strong agreement between the experimental results and the model prediction, which suggests that the combined effects of metals, endotoxins, and PAHs align well with the prediction of the CA model.

The total concentrations of metals, endotoxins, and PAHs in each $PM_{2.5}$ sample, as shown in Appendix 1, were determined using acid digestion, pyrogenic water extraction, and thermal desorption (TD), respectively. These concentrations did not fully align with those in $PM_{2.5}$ extracts (obtained using Milli-Q water and methanol) when exposed to cells. Therefore, the concentrations of components in half of the $PM_{2.5}$ extract samples were analyzed again for correction purposes. For metals, dried particles extracted with MilliQ water and methanol were soaked in acid, digested using a heating block, and analyzed by ICP-OES, as described in Section 3.2.1. For endotoxins, dried particles

extracted with MilliQ water and methanol were dissolved in pyrogen-free water and analyzed according to the protocol outlined in Section 3.4.1. For PAHs, particles extracted in methanol were centrifuged, and the supernatant was concentrated under nitrogen gas and adjusted to 1 mL with methanol. The solution was then filtered through a 0.22 μm membrane filter prior to analysis by GC-MS. The correction ratio represents the ratio of the concentration of an individual component in $PM_{2.5}$ extracts to its total concentration as described in Appendix 1. Prior to calculating the fractional contribution of metals, endotoxins, and PAHs to $PM_{2.5}$-induced intracellular ROS generation, the concentration of each component was adjusted by multiplying the correction ratio.

3.5.5 Error propagation

To estimate the standard errors of the parameter "percent contribution of components", an uncertainty analysis was conducted by propagating the errors of all variables involved in the calculation. Error propagation was applied to the $EC_{IR1.5}$ for each component and sample tested, REP for each active component (REP_i), BEQ of identified components (*BEQcomp*), and $PM_{2.5}$ extracts ($BEQ_{bio,PM2.5}$), as well as their percentage contributions, using the following equations. The standard errors for the slopes of the concentration-effect curves from the BEAS-2B intracellular ROS assay were used in the regression analysis to calculate the propagated errors for these parameters.

For experimentally determined $EC_{IR1.5}$ for $PM_{2.5}$ samples, individual component, and mixtures of metals, endotoxins and PAHs,

$$\sigma EC_{IR1.5} = \frac{0.5}{slope^2} \cdot \sigma slope$$

Equation 3-19

For CA predicted $EC_{IR1.5}$ for mixtures of metals, endotoxins and PAHs,

$$\sigma EC_{IR1.5,CA} = \sqrt{\sum_{i=1}^{n} \left(\frac{p_i}{EC_{IR1.5,i}} \cdot \sigma EC_{IR1.5,i} \right)^2}$$

Equation 3-20

$$\sigma REP_i = \frac{1}{slope_{TBHP}} \sqrt{\sigma slope^2 + \left(\frac{slope_i}{slope_{TBHP}} \cdot \sigma slope_{TBHP} \right)^2}$$

Equation 3-21

$$\sigma BEQ_{bio,PM2.5} = \frac{1}{slope_{TBHP}} \sqrt{\sigma slope_{PM2.5}{}^2 + \left(\frac{slope_{PM2.5}}{slope_{TBHP}} \cdot \sigma slope_{TBHP} \right)^2}$$

Equation 3-22

$$\sigma BEQ_{comp} = \sqrt{\sum \left(\frac{C_i}{slope_{TBHP}} \sqrt{\sigma slope_i{}^2 + \left(\frac{slope_i}{slope_{TBHP}} \cdot \sigma slope_{TBHP} \right)^2} \right)^2}$$

Equation 3-23

$$\sigma\%\ contribution =$$

$$\frac{1}{BEQ_{bio,PM2.5}} \sqrt{\sum \frac{\left(\frac{C_i}{slope_{TBHP}} \sqrt{\sigma slope_i{}^2 + (REP_i \cdot \sigma slope_{TBHP})^2} \right)^2 + }{\left(\frac{BEQ_{comp}}{slope_{PM2.5}} \sqrt{\sigma slope_{PM2.5}{}^2 + \left(BEQ_{bio,PM2.5} \cdot \sigma slope_{TBHP} \right)^2} \right)^2}}$$

Equation 3-24

3.6 Source apportionment

The EF of trace metals in $PM_{2.5}$ were calculated using Fe as the reference element, following the method used in previous studies (Acciai et al., 2017; Nirmalkar et al.,

2023; Xie et al., 2020; Yadav et al., 2022), with their values compared to the geochemical background values of metals (baseline) in soils in Guangzhou and Jiangmen (Survey, 2010) and in Nanjing (Liao et al., 2011). The *EF* was calculated using Equation 3-25.

$$EF = \frac{(\frac{C_i}{C_n})_{sample}}{(\frac{C_i}{C_n})_{baseline}}$$

Equation 3-25

Where C_i (ng m^{-3}) means the concentration of element i, and C_n (μg g^{-1}) means the concentration of reference element. The geochemical background values of each metal are listed in Table **3-7**.

Table 3-7. The geochemical background values of metals (μg g^{-1})

	As	Cd	Co	Cr	Cu	Fe	Mn	Ni	Pb	V	Zn
Nanjing	9.7	0.15	15.2	80.6	30.4	35500	579	35.8	29.4	91	72.2
Guangzhou	10.2	0.044	6.3	39	10.4	31500	235	12.3	41	74	275
Jiangmen	8.9	0.045	3.9	48	12.7	31500	162	11.4	38	79	260

The identified PAHs were divided into three groups based on their ring number (Chen et al., 2019a). PAHs with 2–3 rings are assumed as low-molecular-weight (LMW) PAHs, those with 4 rings are moderate-molecular-weight (MMW) PAHs, and those with 5–6 rings are high-molecular-weight (HMW) PAHs. To identify the potential origins of PAHs, diagnostic ratios such as FLA/(FLA + Pyr), BaA/(BaA + Chr), ANT/(ANT + Phe), IcdP/(IcdP + BghiP), and BaP/(BaP + BeP) were computed.

The PMF model from USEPA (PMF 5.0) was applied to investigate the sources of $PM_{2.5}$ in the six sampling sites. A data set of over 100 samples for PMF modeling is generally accepted (Norris, 2014), thus, the compositional data from three sites in Nanjing and three sites in Guangzhou were combined respectively for a PMF analysis

on the assumption that sites in the same city were under the influence of similar source profiles (Liao et al., 2021). This is a reasonable assumption considering that the direct distances among the three sites in Nanjing and Guangzhou were less than 65 km and 85 km, respectively. Previous PMF studies have also combined datasets collected at multiple sites for a more robust analysis, based on the assumption that the profiles of the same source type remain consistent at all sites (Mooibroek et al., 2011; Xie et al., 2012). Concentrations and uncertainties of $PM_{2.5}$ and its major components, including trace metals, WSI, OC/EC, and endotoxins, were input to run the model. To evaluate the uncertainty associated with the modeling outcomes, a bootstrap procedure was performed 100 times following the base run. The resulting error estimates were then utilized to determine the 95% confidence interval (CI). Based on the results of PMF source apportionment and the effect of individual $PM_{2.5}$-bound major toxic components on ROS generation, the contribution (percent contribution of sources) of each source to $PM_{2.5}$-induced intracellular ROS was calculated using Equations 3-26, 3-27 and 3-28.

$$BEQ_{i,l} = REP_i \times C_{i,l}$$

Equation 3-26

$$BEQ_{s,l} = \sum_i (BEQ_{i,l} \times RC_{i,s,l})$$

Equation 3-27

$$percent\ contribution\ of\ sources = \frac{BEQ_{s,l}}{\sum_s BEQ_{s,l}}$$

Equation 3-28

Where *s* represents emission sources and *l* represents sampling locations. $BEQ_{i,l}$ is the equivalent concentration of TBHP that causes the same effect toxicity as a certain component in a certain location. $C_{i,l}$ is the mass concentration of a certain component per unit mass of $PM_{2.5}$ in a targeted location. $BEQ_{s,l}$ is the equivalent concentration of TBHP that causes the same toxicity from a certain source in a certain location. $RC_{i,s,l}$ is the relative contribution of a certain source to an individual component in a targeted

location, and *percent contribution of sources* refers to the percent contribution of each source to $PM_{2.5}$-induced toxicity.

3.7 Data analysis

The data were analyzed using GraphPad Prism 9, Excel and Origin. Non-parametric Mann-Whitney tests and the non-parametric Kruskal-Wallis one-way analysis of variance (ANOVA) were employed to compare differences among the sampling groups in data distribution (*$p < 0.05$, **$p < 0.01$, ***$p < 0.001$, ****$p < 0.001$).

Chapter 4 Chemical Characterization and Health Risk Assessment of $PM_{2.5}$ in Nanjing and Guangzhou

This chapter presents a comprehensive chemical characterization and health risk assessment of $PM_{2.5}$ across all sampling sites with varying land-use types in Nanjing and Guangzhou from 2019 to 2020, alongside long-term trends from 2013 to 2020. Chemical analysis revealed regional differences in $PM_{2.5}$ composition and identified trace metals (notably Cr, As, and Mn) and PAHs (especially DahA and BaP) as major health risk contributors. Long-term trends showed significant reductions in $PM_{2.5}$ levels and associated risks, reflecting effective air quality policies. Persistent and site-specific risks highlight the need for ongoing, targeted pollution control strategies focusing on specific harmful components.

4.1 Inter-city and intra-city comparisons of $PM_{2.5}$ concentration and chemical composition profiles

In general, people live in both Nanjing and Guangzhou were exposed to polluted air during almost the entire evaluated year (June 2019 to May 2020) with excessive $PM_{2.5}$ concentrations that were above the WHO guideline value (25 μg m^{-3} for 24 h in average, applicable during 2006–2021) (Figure **4-1**). Most of the highly polluted days in both cities fell in autumn and winter, which may result from the increasing use of heaters in cold weather. According to government documents, coal combustion is the primary source of electricity in Nanjing (Nanjing Municipal Bureau of Statistics, 2020), while both coal and oil combustion are the main sources in Guangzhou (Guangzhou Statistics Bureau, 2023). The use of heaters can increase electricity consumption, leading to greater coal and oil combustion and, consequently, the release of aerosol particles. In addition, the extensive use of residential heating during winter in northern China leads to increased coal burning and $PM_{2.5}$ release (Huang et al., 2014b; Zhang and Cao, 2015), which could affect southern regions through atmospheric transport (Ping et al., 2023). There was a decrease in $PM_{2.5}$ concentration from 2019–2020 winter to 2020 spring in

the urban (XW) site ($p < 0.01$) and the suburban-industrial PK site ($p < 0.05$) in Nanjing. There is a possibility that the decrease was related to the Shut Down Policy in February due to COVID-19. There were no significant seasonal changes at the three sites in Guangzhou. $PM_{2.5}$ concentration seemed to share similar patterns of fluctuation in the same city. The annual average at all six sites was above the WHO guideline (2016–2021) value for $PM_{2.5}$ concentration (25 μg m^{-3} for 24 h in average) based on short-time monitoring, but below the Grade II value (75 μg m^{-3} for 24 h in average) of the Chinese National Ambient Air Quality Standard (NAAQS) (Figure **4-2**). In Nanjing, the urban (XW) (75.5 μg m^{-3}) and suburban-industrial (PK) (72.0 μg m^{-3}) sites presented significantly higher pollution than the rural (LS) (49.0 μg m^{-3}) site, which may be the result of stronger anthropogenic activity in these two sites than the rural site, while the three studied sites in Guangzhou had similar concentration. When focusing on industrial sites, $PM_{2.5}$ concentration in Nanjing was 52.1% higher than that in Guangzhou ($p < 0.05$), suggesting regional differences of air pollution under similar land-use types. This difference can be attributed to the distinct industrial structure of the two cities: the industrial site in Guangzhou consists of light industries such as electroplate factories and hardware and battery manufacturers (Xie et al., 2020), while in Nanjing, heavy industries like steel plants dominate (Jiangsu News Network, 2022), which are extremely energy-intensive and major emitters of primary $PM_{2.5}$.

Figure **4-3**A shows analyzed chemical profiles of $PM_{2.5}$ from the six sampling sites. In Nanjing, WSI were major components in the three sampling sites, with organic matter and EC being the second and third contributors. In Guangzhou, organic matter and EC were the top two contributors while WSI became the third. In Nanjing, the fraction of WSI associated with secondary aerosols (such as SO_4^{2-}, $NH4^{+}$, and NO_3^{-}) among the total identified constituents was higher, while the share of carbonaceous substances (OC and EC), likely originating from combustion processes, was lower in comparison to Guangzhou. Such regional differentiation had been observed in the same sampling

sites three years ago, with decrease in the $PM_{2.5}$ and components concentrations but the components profiles (details are shown in Section 4.3). Figure **4-3**B shows the seasonal variations of $PM_{2.5}$ composition in the six sampling sites. In general, the seasonal composition patterns were consistent within cities. The total concentrations of analyzed components were higher in autumn and winter compared to in spring and summer in all sites except the CH site, which has higher concentrations in summer and autumn. In addition to the identified components, a fraction of $PM_{2.5}$ mass remained unidentified. This unidentified fraction, which may include unmeasured organic compounds or other trace constituents, varied both spatially and seasonally. Generally, the proportion of unidentified $PM_{2.5}$ was higher in summer, possibly due to increased formation of secondary organic aerosols or the presence of volatile compounds that were not fully captured by current analytical methods. Spatially, sites with higher contributions from combustion sources, such as those in Guangzhou, tended to have a lower unidentified fraction, likely because a greater proportion of the $PM_{2.5}$ mass could be attributed to measured carbonaceous components. Conversely, sites dominated by secondary aerosols, such as those in Nanjing, exhibited a higher unidentified fraction. In addition, the conversion factor 1.8 for transferring OC to OM is an average and may not be accurate for all locations or sources, as the composition of organic matter can vary. Some studies use factors ranging from 1.4 to 1.7 depending on the aerosol source and chemical environment (Russell, 2003), which could explain why the total concentrations of analyzed components exceeded the measured $PM_{2.5}$ mass at the CH site during summer. These findings highlight the complexity of $PM_{2.5}$ composition and the need for further research to better characterize the unidentified portion, which may have important implications for health risk assessments and source apportionment.

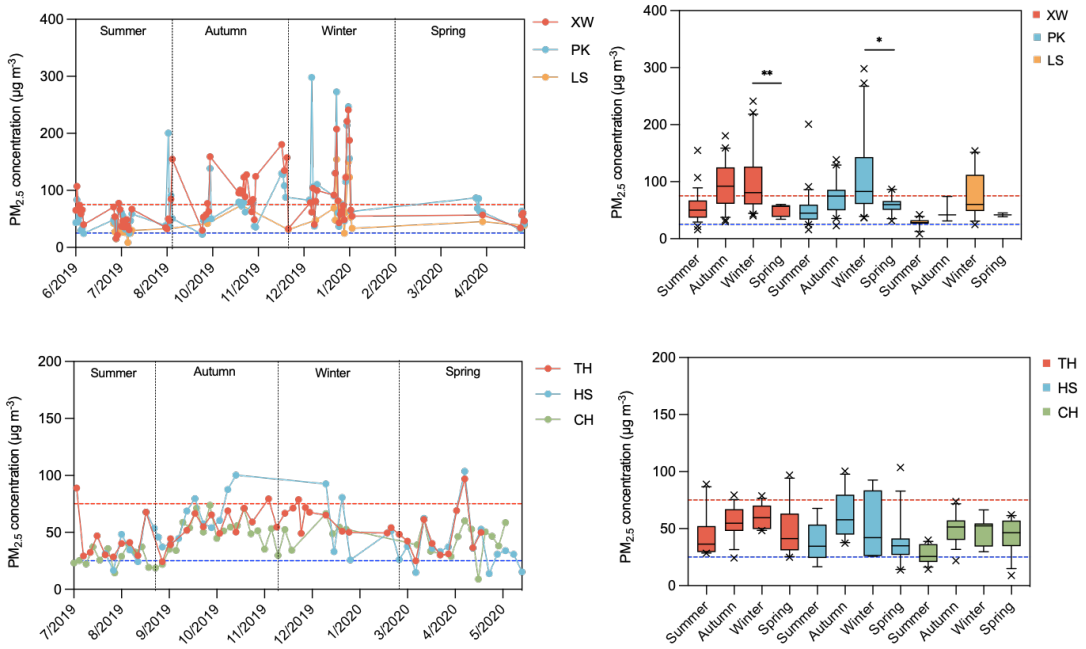

Figure 4-1. Changes in $PM_{2.5}$ concentration levels over time and across locations at selected sites in Nanjing (XW, PK, LS) and Guangzhou (TH, HS, CH). The blue dashed line indicates the WHO recommended limit for $PM_{2.5}$ concentration (25 μg m^{-3} for a 24 h period) as set between 2016 and 2021. The red dashed line represents the Grade II threshold (75 μg m^{-3} averaged over 24 h) specified by the NAAQS.

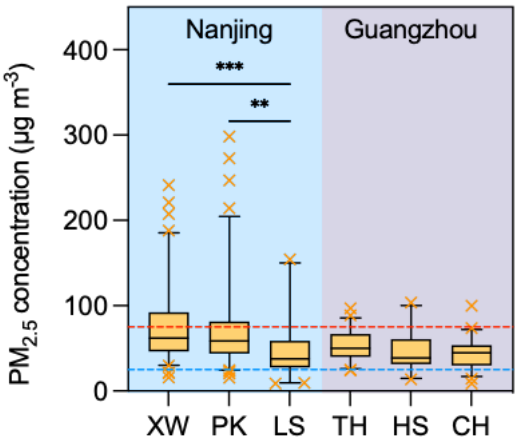

Figure 4-2. Annual average $PM_{2.5}$ concentration at the sampling sites in Nanjing (XW, PK and LS) and Guangzhou (TH, HS and CH). Line and error bars display the average values with the 95% CI. The blue dashed line indicates the WHO recommended limit for $PM_{2.5}$ concentration (25 μg m^{-3} for a 24 h period) as set between 2016 and 2021.

The red dashed line represents the Grade II threshold (75 μg m^{-3} averaged over 24 h) specified by the NAAQS.

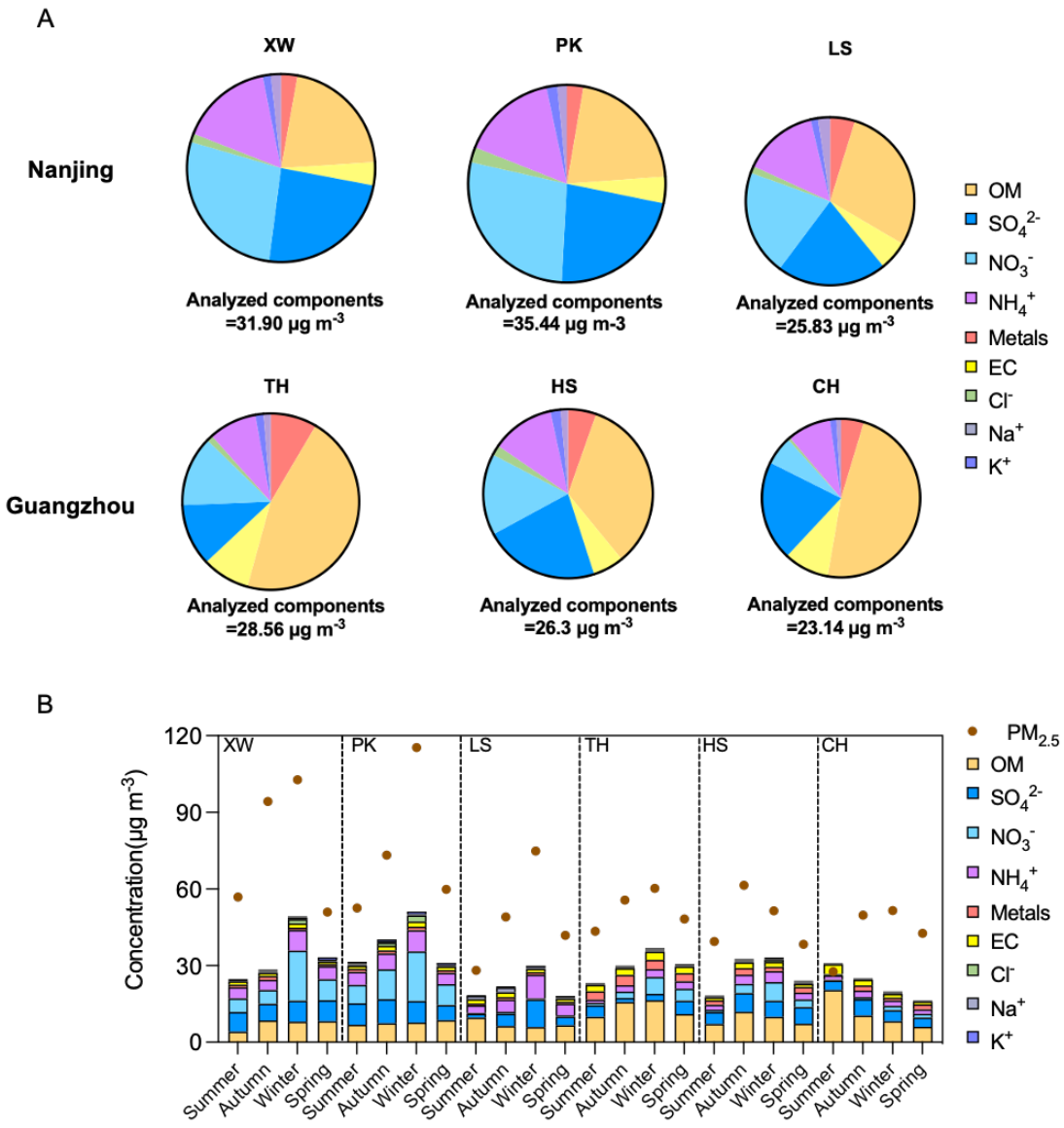

Figure 4-3. Component profiles of $PM_{2.5}$ in six sites in Nanjing (XW, PK and LS) and Guangzhou (TH, HS and CH). (A) Annual average major chemical components analyzed in $PM_{2.5}$. The pie charts illustrate the relative abundance of each analyzed component, expressed as a proportion of the total measured components based on their concentrations in $PM_{2.5}$ samples. Organic matter (OM) is calculated as the OC concentration multiplied by 1.8 (Malm et al., 2017). (B) Seasonal variations of major chemical components and $PM_{2.5}$ concentrations.

4.2 Characteristics of analyzed $PM_{2.5}$-bound trace metals and PAHs

4.2.1 Concentrations of $PM_{2.5}$-bound metals

Trace metals constituted only a small proportion of the analyzed chemicals in both cities. However, despite their low abundance, metals may have a significant impact on health. To further investigate the health effects of these metals, EFs, CR and NCR of analyzed metals were calculated for the analyzed metals.

Figure **4-4** shows the concentrations $PM_{2.5}$-bound trace metals in Nanjing and Guangzhou based on annual averages. In Nanjing, the annual average concentrations of elements with EF ranging between 1 and 10 like Co, Cr and V had the highest concentrations in the semirural-industrial (PK) site ($p < 0.05$), and the rural (LS) site had the lowest concentrations of Mn and V ($p < 0.05$). Among moderately enriched elements ($10 < EF < 100$), As, Ni and Pb had the highest concentrations in the semirual-industrial (PK) site ($p < 0.05$), meanwhile, the rural (LS) site had the lowest concentration of Zn ($p < 0.05$). The elevated concentrations of As, Ni, and Pb at the semi-rural industrial site could reflect substantial contributions from coal combustion, metal processing, and other industrial activities (Siudek, 2020; Wang et al., 2017). As to highly enriched elements ($EF > 100$), Cu and Cd had the highest concentrations in the semirual-industrial (PK) site while Cu has the lowest concentration in the rural (LS) site. This may be because Cu and Cd are mostly associated with metal manufacturing and wear abrasion from transport activities (Ekman Nilsson et al., 2017; Li et al., 2020; Sandoval and Silva, 2023). In Guangzhou, the annual average concentrations of elements with EF ranging between 1 and 10 like Mn, Co, V had the highest concentrations in the (TH) urban site ($p < 0.05$) and the lowest concentrations in the semirural-industrial (HS) site ($p < 0.05$), these traffic-related elements suggesting that vehicle emissions are dominant contributors to $PM_{2.5}$ in the urban site compared to the semirural-industrial site (Xia and Gao, 2011). As for moderately enriched elements (10

< EF < 100) like Ni, Pb and Zn, the suburban (CH) site had the lowest annual average concentrations ($p < 0.05$). In highly enriched elements (EF > 100), Cu had the highest concentration in the (TH) urban site and the lowest concentration in the suburban (CH) site, and Cd had the lowest concentration in the suburban (CH) site, which can be explained by the fact that brake wear from vehicles is an important source of atmospheric particulate copper concentrations (Van der Gon et al., 2007). In summary, these differences between sites may result from varying degrees of industrialization and urbanization and different emission source profiles. Details of EF are shown in Figure **4-5**.

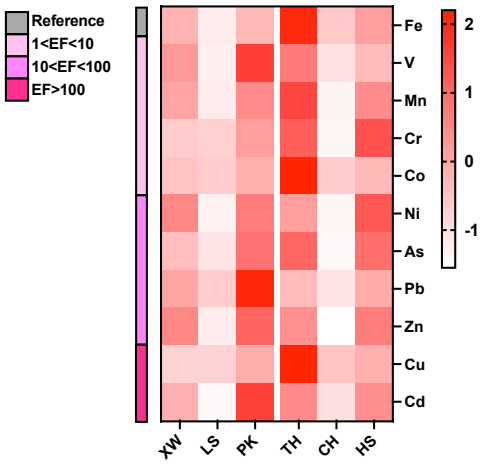

Figure 4-4. Trace metal concentrations in $PM_{2.5}$ in Nanjing (XW, PK, and LS) and Guangzhou (TH, HS and CH) based on annual average. Prior to plotting, each metal's concentration value underwent an independent normalization procedure. Metals were categorized according to the average EF calculated across all sampling sites.

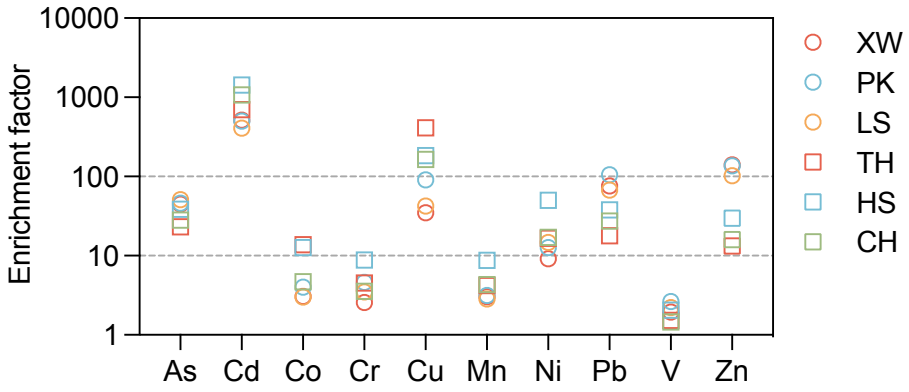

Figure 4-5. Average EFs for the analyzed trace elements in each site, using Fe concentration as the reference.

4.2.2 Health risk assessment of CR and NCR posed by metals

The CR and NCR (represented by HQ) induced by trace metals at six sites in Nanjing and Guangzhou are shown in Figures **4-6**A and **4-6**B. At all six sites, the CR values exceeded the acceptable risk level for carcinogens (10^{-6}), while the HQ values remained below the reference threshold of 1.0. In Nanjing, the three sampling sites did not exhibit significant differences in CR. In Guangzhou, however, the CR at the suburban (CH) site was significantly lower than at both the urban (TH) site ($p < 0.0001$) and the semirural-industrial (HS) site ($p < 0.0001$). Regarding NCR, both the urban (XW) and suburban-industrial (PK) sites in Nanjing had higher NCRs than the rural (LS) site ($p < 0.05$). Additionally, the suburban-industrial (PK) site showed a significantly higher NCR than the urban (XW) site. In Guangzhou, both the urban (TH) and semirural-industrial (HS) sites exhibited higher NCRs compared to the suburban (CH) site ($p < 0.001$). These results suggest spatial variations in health risks associated with trace metal exposure, emphasizing the need for targeted pollution control strategies in different urban, industrial and suburban environments.

To assess the contribution of each metal element to health risks, Figures **4-6**C and **4-6**D were plotted. Among the six sampling sites, Cr contributed the most to the total CR, accounting for over 90% in Nanjing and over 86% in Guangzhou. As was the second

largest contributor, responsible for more than 4% and 3% of the total CR in Nanjing and Guangzhou, respectively. These results are generally consistent with previous studies (Xie et al., 2020). In terms of NCR, Mn emerged as the predominant contributor, with risk contributions exceeding 43% in Nanjing and 38% in Guangzhou, followed by As, which contributed over 13% and 10%, respectively. Notably, although Fe, Zn, and Cu exhibited higher mass contributions than other elements (as shown in Figure **4-7**), they contributed least to health risks. These findings highlight the importance of focusing on the specific chemical components of $PM_{2.5}$, rather than solely on its mass concentration, for effective and accurate pollution control.

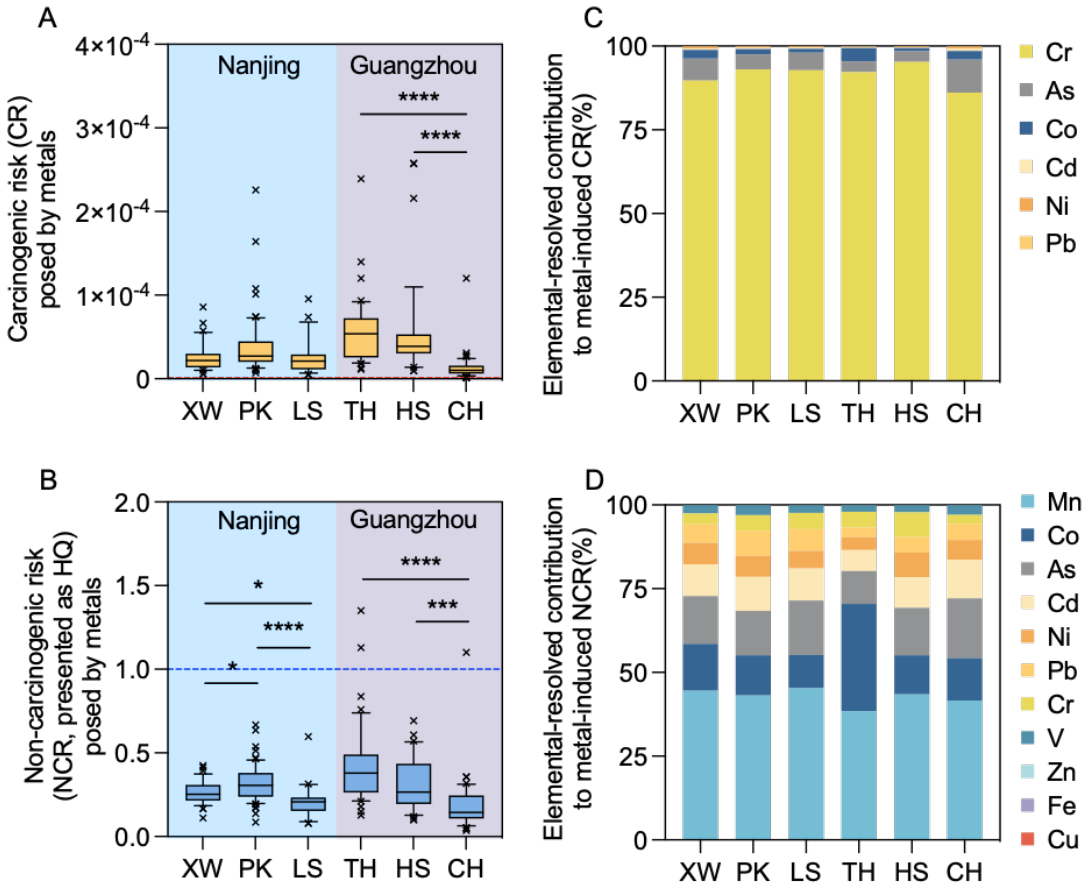

Figure 4-6. Health risk assessment of $PM_{2.5}$-bound metals in six sites in Nanjing (XW, PK, and LS) and Guangzhou (TH, HS and CH). (A) & (B) Metals-posed CR and NCR in six sampling sites based on average metal concentrations, incorporating adjustment on arsenic speciation. The box plots with whiskers present the mean with a 90% CI.

The red dashed line represents the threshold for acceptable CR (10^{-6}), while the blue dashed line indicates the reference value for hazard quotients (1.0) related to non-carcinogenic effects, as recommended by the USEPA. (C)&(D) Relative contributions of individual metals to the CR and NCR.

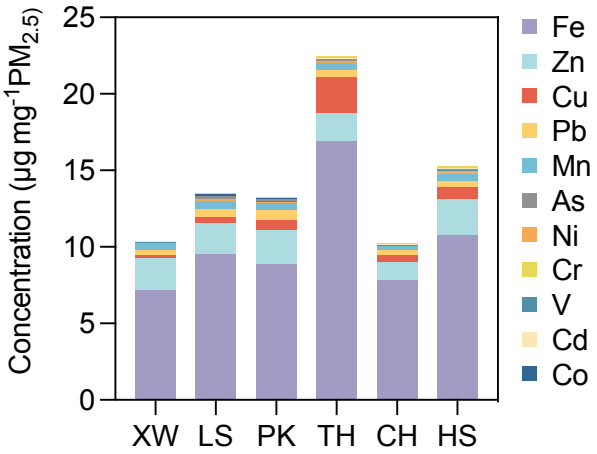

Figure 4-7. Concentrations of analyzed trace metals per unit mass of $PM_{2.5}$ in six sites in Nanjing and Guangzhou.

4.2.3 Concentrations of $PM_{2.5}$-bound PAHs

Overall, 12 kinds of PAHs were identified in $PM_{2.5}$ samples from six sites in Nanjing and Guangzhou, including Phe, Ant, FLA, Pyr, BaA, Chr, BbF, BaP, IcdP, BghiP, and DahA (Figure **4-8**). Nanjing showed significantly elevated levels of PAHs ($p < 0.0001$) compared to Guangzhou, with extraordinarily higher levels of PAHs in the suburban-industrial site (PK). The suburban-industrial (PK) site of Nanjing had higher levels of most PAHs compared to the rural (LS) site in Nanjing and all three sites in Guangzhou ($p < 0.05$). This may be due to soot and coke oven emissions from heavy industries in the industrial areas of Nanjing (Chen et al., 2019b). In contrast, the semirural-industrial (HS) site in Guangzhou does not emit much PAHs, possibly because it primarily consists of light industries such as electroplate factories and hardware and battery manufacturers (Xie et al., 2020).

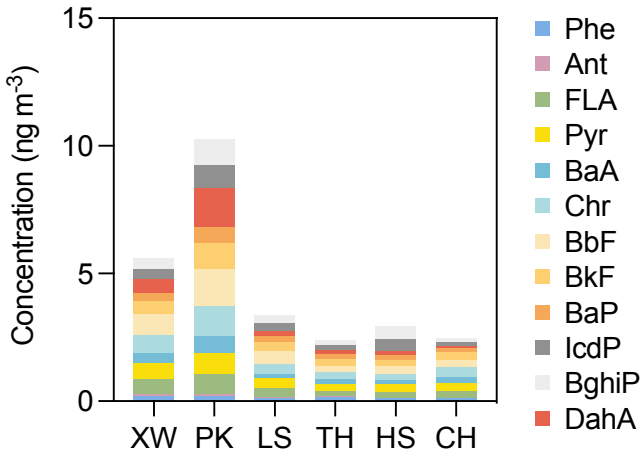

Figure 4-8. Concentrations of analyzed PAHs in six sites in Nanjing and Guangzhou.

4.2.4 Assessment of ECR posed by $PM_{2.5}$-bound PAHs

The ECR posed by DahA, BaP, Chr, BaA, BbF, BkF, FLA, IcdP and BghiP are plotted in Figure **4-9**A. All ECRs in six sites were over the guideline for ECR (10^{-6}) recommended by the USEPA. The intra-city ECR posed by these PAHs did not show significant differences. Contributions of each PAH to the ECR were also calculated and shown in Figure **4-9**B. Among the 9 PAHs, DahA was the dominant health risk contributor, accounting for over 75%, followed by BaP (>4%).

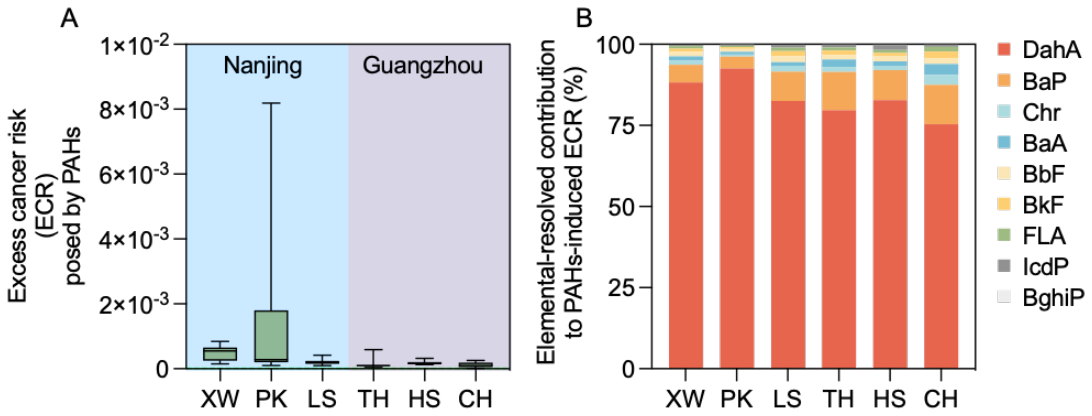

Figure 4-9. Health risk assessment of $PM_{2.5}$-bound PAHs in six sites in Nanjing (XW, PK, and LS) and Guangzhou (TH, HS and CH). (A) ECR posed by $PM_{2.5}$-bound PAHs. The box plots with whiskers present the mean with a 90% CI, and the green dashed line stands for the guideline for ECR (10^{-6}) recommended by the USEPA. (B) Relative contributions of various PAHs to the ECR.

4.2.5 Sources of $PM_{2.5}$-bound PAHs

PAHs with different ring numbers have distinct properties (Cao et al., 2019). The 16 PAHs are generally divided into three groups based on their ring number (Chen et al., 2019a). Figure **4-10** shows the composition characteristics of PAHs in $PM_{2.5}$ from six sampling sites in Nanjing and Guangzhou. These sites did not show significant differences in ring distributions. The proportions of LMW PAHs, MMW PAHs and HMW PAHs were 1.4%–19%, 12%–60% and 33%–86%, respectively, which indicated that $PM_{2.5}$-bound PAHs in both cities were dominated by HMW PAHs. As reported by previous studies (Bouloubassi et al., 2012; Yunker et al., 2002), LMW PAHs are majorly from petrogenic source, while HMW PAHs play a dominant role in PAH composition from pyrogenic source. Thus, $PM_{2.5}$-bound PAHs of these sampling sites were from the pyrogenic source rather than the petrogenic source. This conclusion is also verified by PAHs diagnostic ratios (Figure **4-11**), confirming that PAHs were mainly from non-petrogenic sources, including fossil fuel combustion, grass, wood, coal combustion, vehicle emission, and petroleum combustion. LMW PAHs exhibit comparatively weak hydrophobicity, whereas HMW PAHs, which are more

hydrophobic, tend to associate more readily with solid materials and are commonly found in atmospheric PM, soils, and sediments (Andersson et al., 2014; Liu et al., 2019). Their persistence in the environment increases the likelihood of human exposure and poses potential health risks.

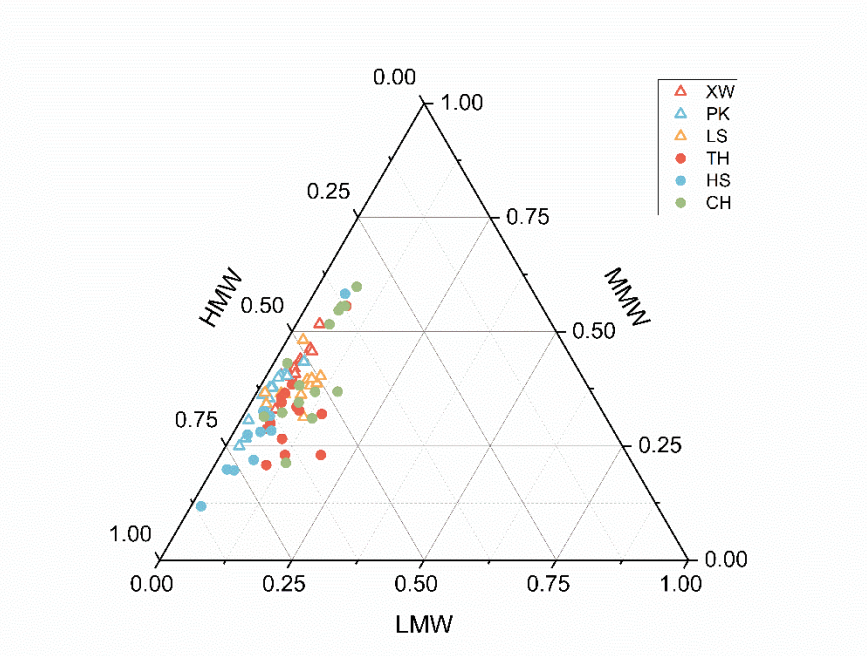

Figure 4-10. Ternary plots of $PM_{2.5}$-bound PAHs distribution in Nanjing (XW, PK and LS) and Guangzhou (TH, HS and CH). LMW: PAHs with 2-3 rings. MMW: PAHs with 4 rings. HMW: PAHs with 5 or more rings.

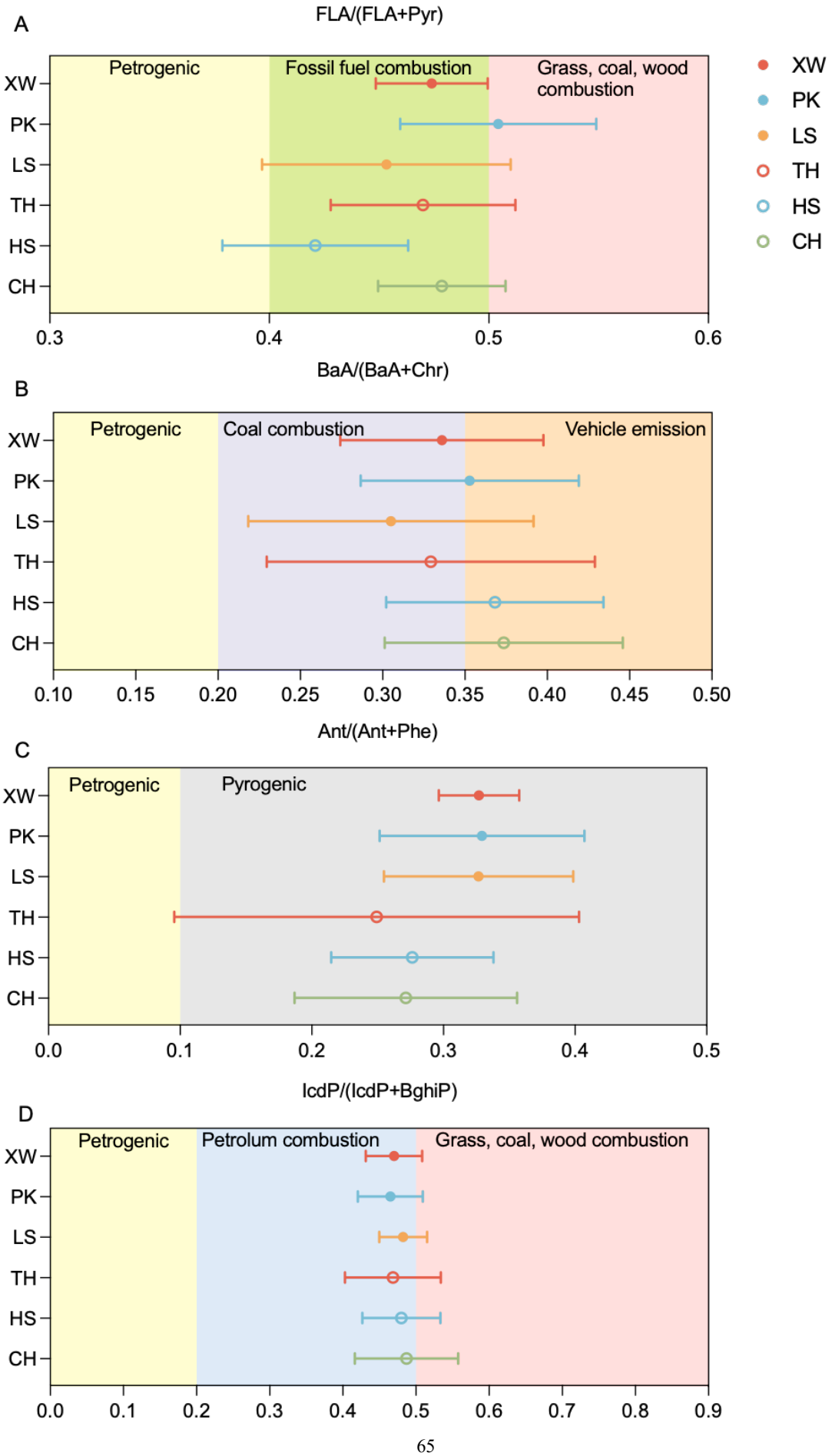
A
FLA/(FLA+Pyr)
Petrogenic
Fossil fuel combustion
Grass, coal, wood combustion
XW
PK
LS
TH
HS
CH
0.3
0.4
0.5
0.6
B
BaA/(BaA+Chr)
Petrogenic
Coal combustion
Vehicle emission
0.10
0.15
0.20
0.25
0.30
0.35
0.40
0.45
0.50
C
Ant/(Ant+Phe)
Petrogenic
Pyrogenic
0.0
0.1
0.2
0.3
0.4
0.5
D
IcdP/(IcdP+BghiP)
Petrogenic
Petrolum combustion
Grass, coal, wood combustion
0.6
0.7
0.8
0.9

Figure 4-11. The mean values and standard deviations (SD) of PAH diagnostic ratios of six sites in Nanjing (XW, PK, and LS) and Guangzhou (TH, HS and CH). (A) FLA/(FLA + Pyr), (B) BaA/(BaA + Chr), (C) Ant/(Ant + Phe), and (D) IcdP/(IcdP + BghiP) determined for $PM_{2.5}$ samples collected from six sites in Nanjing and Guangzhou. The characteristic diagnostic ratios differentiating various sources are from references (Katsoyiannis et al., 2011; Ravindra et al., 2008).

4.3 $PM_{2.5}$ and its chemical composition trends from 2013 to 2020 in urban Nanjing and urban Guangzhou

Few studies have investigated the long-term trends of $PM_{2.5}$ and its chemical composition, particularly regarding health risk assessments based on extended monitoring periods. In this section, we analyzed a long-term dataset of $PM_{2.5}$ collected during three periods: 2013–2014, 2016–2017, and 2019–2020. For each period, samples were obtained from three sites in Nanjing—XW (urban), PK (suburban-industrial), and LS (rural)—and three sites in Guangzhou—TH (urban), HS (semirural-industrial), and CH (suburban). To examine long-term trends in $PM_{2.5}$-related health risks and to identify key chemical components driving these changes, we focused on the CR and NCR associated with $PM_{2.5}$-bound metals at the urban sites: XW in Nanjing (referred to as "urban Nanjing" in Section 4.3) and TH in Guangzhou (referred to as "urban Guangzhou" in Section 4.3). Additionally, we analyzed the element-specific contributions to metal-induced health risks.

As shown in Figure **4-12**, during the 2013–2014 sampling period, many days recorded $PM_{2.5}$ concentrations exceeding the Grade II value (75 μg m^{-3}, 24-hour average) of the Chinese NAAQS. In contrast, during 2016–2017 and 2019–2020, only the most heavily polluted days surpassed this threshold. Throughout all three sampling periods (August 2013 to August 2014, March 2016 to February 2017, and June 2019 to May 2020), residents at the sampling sites in both Nanjing and Guangzhou were almost

continuously exposed to $PM_{2.5}$ concentrations above the WHO guideline of 25 μg m^{-3}. Most of the highly polluted days occurred in autumn and winter, highlighting the pronounced seasonal characteristics of PM pollution over the long term. Generally, $PM_{2.5}$ concentrations exhibited similar fluctuation patterns within each city, except for occasional site-specific pollution episodes. For example, the semi-rural (HS) industrial site in Guangzhou experienced relatively high $PM_{2.5}$ concentrations during the winter of 2016.

Regarding annual $PM_{2.5}$ concentration trends from 2013 to 2020, Figure **4-13** shows a significant decline in urban sites of both cities. In Nanjing, the annual $PM_{2.5}$ concentration dropped by 35%, from 97.8 μg m^{-3} in 2013 to 63.9 μg m^{-3} in 2020 ($p < 0.0001$). Similarly, Guangzhou saw a 36% reduction, from 81.5 μg m^{-3} to 52.6 μg m^{-3} over the same period ($p < 0.0001$). This marked improvement in air quality can be largely attributed to the implementation of China's "Action Plan for Air Pollution Prevention and Control" in September 2013. Further analysis of major toxic components—specifically metals—in $PM_{2.5}$ samples from Nanjing and Guangzhou during the sampling periods is presented in Figure **4-14**. Na, Ca, K, and Fe were the four most abundant metals, collectively accounting for over 75% of the total analyzed metals. Among the trace metals with significant health risks, Fe and Zn were the most prevalent, with Cu becoming more prominent in the 2019–2020 period. In Nanjing, the total concentration of analyzed metals in $PM_{2.5}$ decreased by 57%, from 4.5 μg m^{-3} in 2013–2014 to 2.0 μg m^{-3} in 2019–2020. In Guangzhou, metal concentrations declined from 3.9 μg m^{-3} in 2013–2014 to 2.2 μg m^{-3} in 2016–2017, but then increased to 3.2 μg m^{-3} in 2019–2020. This latter increase was primarily driven by a rise in Cu concentrations.

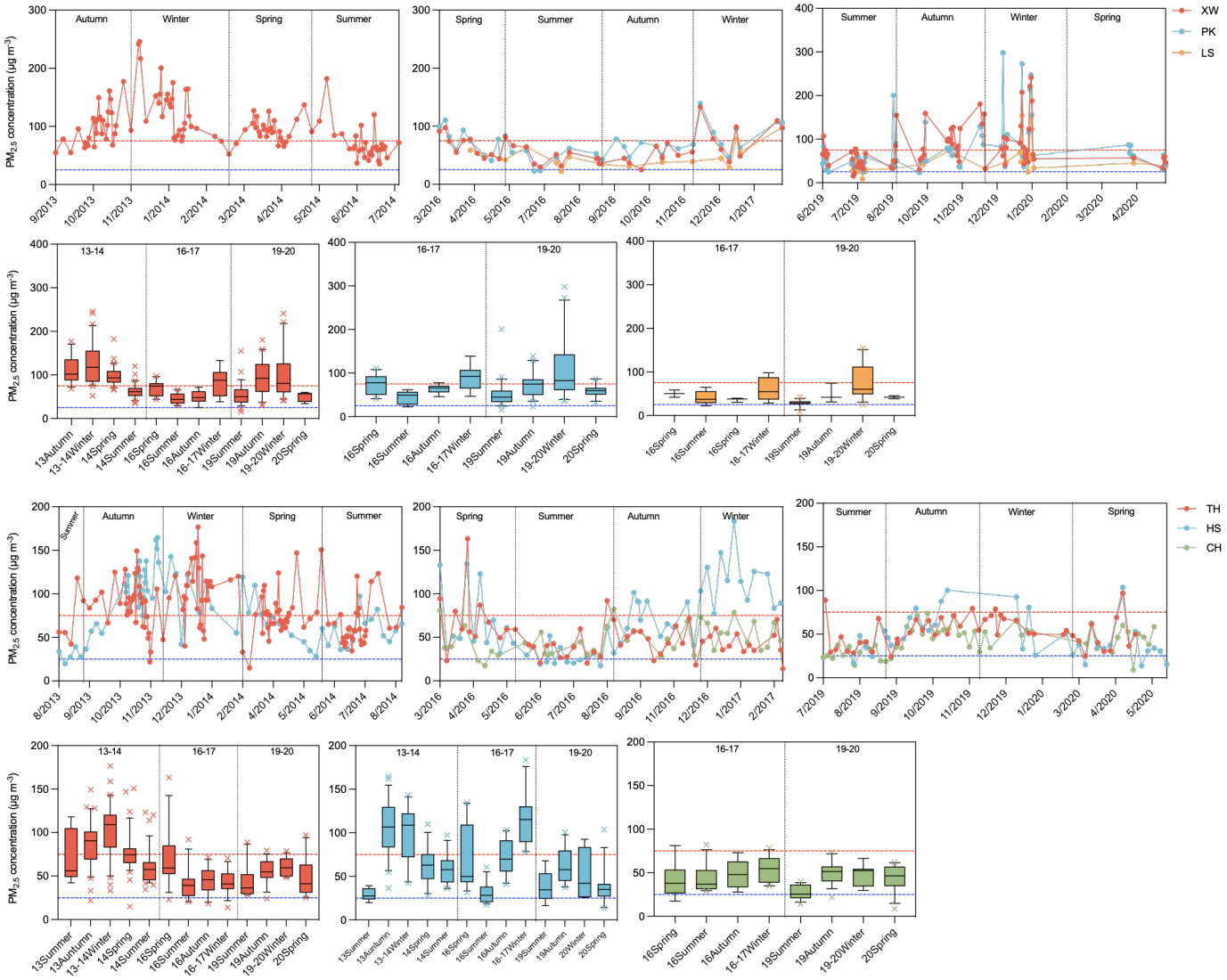
PM2.5 concentration (μg m-3)
Autumn
Winter
Spring
Summer
XW
PK
LS
13-14
16-17
19-20
TH
HS
CH

Figure 4-12. Spatiotemporal variations in $PM_{2.5}$ concentrations during three sampling periods at the studied sites in Nanjing (XW, PK and LS) and Guangzhou (TH, HS and CH). The blue dashed line indicates the WHO recommended limit for $PM_{2.5}$ concentration (25 μg m^{-3} for a 24 h period) as set between 2016 and 2021. The red dashed line represents the Grade II threshold (75 μg m^{-3} averaged over 24 h) specified by the NAAQS.

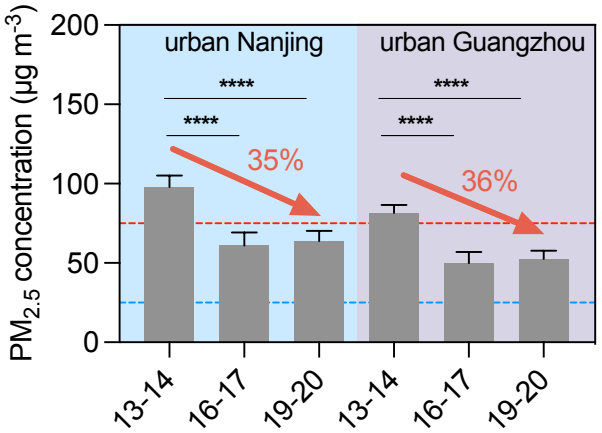

Figure 4-13. The trends of $PM_{2.5}$ concentration in urban sites of Nanjing and Guangzhou during the three sampling periods (August 2013 to August 2014, March 2016 to February 2017, and June 2019 to May 2020). The blue dashed line indicates the WHO recommended limit for $PM_{2.5}$ concentration (25 μg m^{-3} for a 24 h period) as set between 2016 and 2021. The red dashed line represents the Grade II threshold (75 μg m^{-3} averaged over 24 h) specified by the NAAQS.

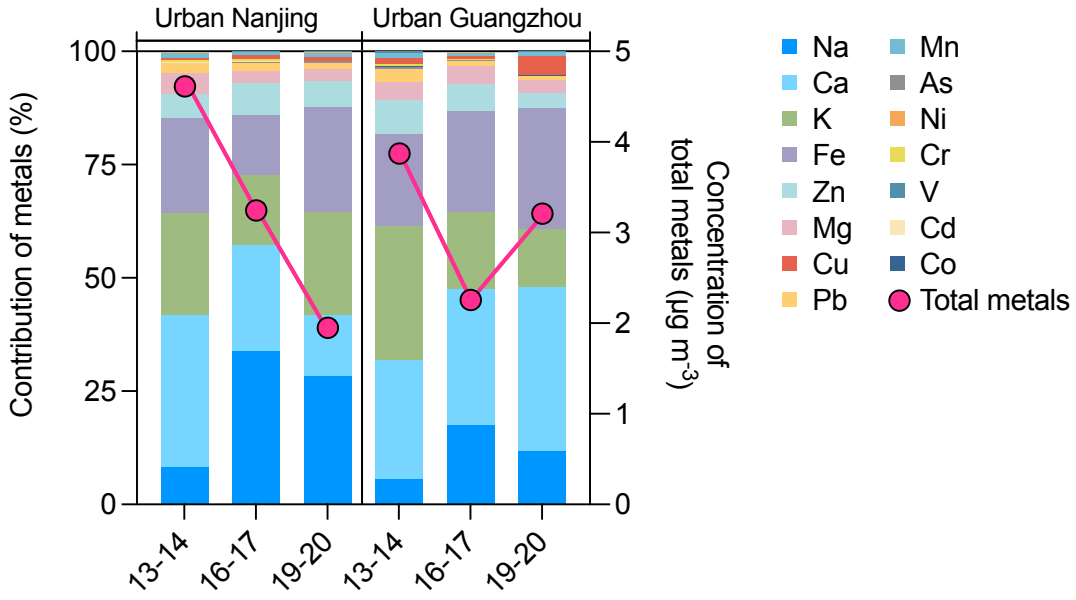

Figure 4-14. Contributions of analyzed metals in $PM_{2.5}$ in urban sites of Nanjing and Guangzhou during the three sampling periods (August 2013 to August 2014, March 2016 to February 2017, and June 2019 to May 2020). The contributions of metals were plotted on the left Y axis and the concentrations of total metals were plotted on the right Y axis.

The CR and NCR posed by metals in $PM_{2.5}$ at the urban sites were calculated for each sampling period (Figure **4-15**). The CR values associated with $PM_{2.5}$-bound metals in both urban Nanjing and urban Guangzhou exceeded the reference threshold across all three sampling periods, while the NCR values generally remained below the reference level. In Nanjing, both CR and NCR attributable to $PM_{2.5}$-bound metals declined significantly from 2013 to 2020, by 55% and 61% respectively. In Guangzhou, both CR and NCR showed a downward trend from 2013–2014 to 2016–2017, but rebounded after 2019. Overall, from 2013 to 2020, CR and NCR in Guangzhou decreased by 64% and 52%, respectively. The slight increase observed after 2017 was primarily due to elevated concentrations of Cr and Mn (Figure **4-16**A). Cr and As were the main contributors to CR (Figure **4-16**A), while Mn, As, and Co were the primary contributors to NCR (Figure **4-16**B). The observed reduction in health risks associated with $PM_{2.5}$-

bound metals highlights the effectiveness of air pollution control measures and their positive impact on public health. These findings identify Cr, As, Mn, and Co as major contributors to health risks, indicating that future mitigation efforts and health risk assessments should prioritize these specific metals. Moreover, understanding which metals drive health risk and monitoring changes in their concentrations over time will enable better prediction and prevention of adverse health outcomes in urban populations. However, the persistent exceedance of cancer risk thresholds and the rebound in risk after 2017 highlight the need for continuous monitoring and adaptive management strategies to ensure sustained improvements in air quality and public health.

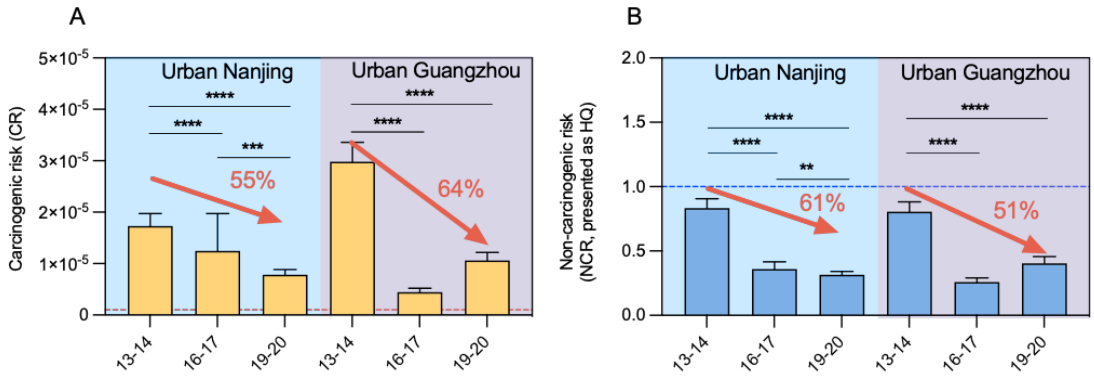

Figure 4-15. Assessment of (A) CR and (B) NCR induced by analyzed trace metals in $PM_{2.5}$ in urban sites in Nanjing and Guangzhou during the three sampling periods (August 2013 to August 2014, March 2016 to February 2017, and June 2019 to May 2020). The red dashed line represents the threshold for acceptable CR (10^{-6}), while the blue dashed line indicates the reference value for hazard quotients (1.0) related to non-carcinogenic effects, as recommended by the USEPA.

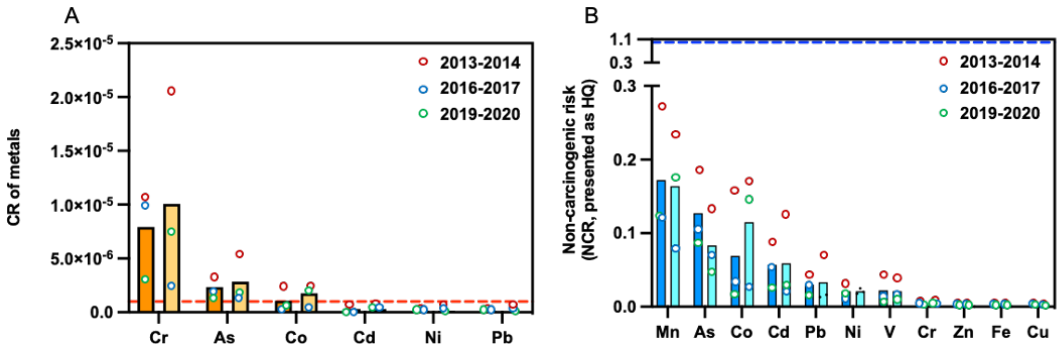

Figure 4-16. Average (A) CR and (B) NCR (presented as HQ) values of different metals in $PM_{2.5}$ samples collected during the three sampling periods (August 2013 to August 2014, March 2016 to February 2017, and June 2019 to May 2020). The red dashed line represents the threshold for acceptable CR (10^{-6}), while the blue dashed line indicates the reference value for hazard quotients (1.0) related to non-carcinogenic effects, as recommended by the USEPA. Circles of different colors represent the CR or NCR for different periods, as shown in the figure.

4.4 Summary

This chapter presents a comprehensive analysis of $PM_{2.5}$ pollution in six sites across Nanjing and Guangzhou, representing different land-use types (urban, suburban-industrial, semirural-industrial, suburban and rural). The study covers the period from June 2019 to May 2020, with additional long-term trend analysis from 2013 to 2020. The chapter examines spatial and temporal variations in $PM_{2.5}$ concentration, chemical composition (including WSI, OC/EC, trace metals, and PAHs), and assesses the associated health risks posed by $PM_{2.5}$-bound metals and PAHs. The sources of PAHs are also investigated. Finally, the chapter evaluates the effectiveness of air pollution control policies by analyzing trends in $PM_{2.5}$ and its toxic components over seven years. The major findings of chapter 4 are listed below:

1. Residents in both Nanjing and Guangzhou were exposed to $PM_{2.5}$ concentrations exceeding the WHO guideline (25 μg m^{-3}, 24 h average) for almost the entire year studied. Most highly polluted days occurred in autumn and winter, likely influenced by human activities and meteorological conditions.

2. In Nanjing, urban and suburban-industrial sites had significantly higher $PM_{2.5}$ concentrations than the rural site, reflecting more frequent anthropogenic activity. In Guangzhou, $PM_{2.5}$ concentrations were similar across urban, suburban, and semi-rural industrial sites. A significant decrease in $PM_{2.5}$ was observed in Nanjing during the COVID-19 shutdown, but not in Guangzhou. In Nanjing, WSI were the major $PM_{2.5}$ components, followed by OM and EC. While in Guangzhou, OM and EC dominated, with WSI as the third largest contributors. Nanjing had a higher proportion of secondary aerosols, while Guangzhou had more carbonaceous material, indicating regional differences in sources and atmospheric processes.

3. Trace metals, though a small fraction of $PM_{2.5}$ mass, posed significant health risks. CR from metals exceeded the acceptable threshold at all sites, while NCR remained below the reference level. Cr was the dominant contributor to CR (> 90%), while Mn

was the main contributor to NCR. Urban and industrial sites generally had higher health risks than rural and suburban sites.

4. Nanjing had significantly higher $PM_{2.5}$-bound PAHs than Guangzhou, especially at the suburban-industrial site, likely due to heavy industry emissions. All sites exceeded the USEPA guideline for ECR from PAHs. DahA was the largest contributor to PAH-induced ECR (> 75%). PAHs were majorly from pyrogenic sources (combustion of fossil fuels, biomass, and vehicles) rather than petrogenic sources.

5. Both cities had significant reductions in $PM_{2.5}$ concentrations (Nanjing: 35%, Guangzhou: 36%) and metal concentrations (Nanjing: 57%, Guangzhou: 18%) over the study period (2013–2020), reflecting the effectiveness of air pollution control policies. Health risks from $PM_{2.5}$-bound metals (CR and NCR) declined significantly in both cities. The main contributors to health risks remained consistent over time (Cr and As for CR; Mn, As, and Co for NCR).

6. The findings highlight the need for targeted pollution control strategies, focusing not only on reducing $PM_{2.5}$ mass but also on specific toxic components. Continued monitoring and source-specific interventions are essential for further improving air quality and reducing health risks.

While Chapter 4 provided a comprehensive assessment of the chemical characteristics, sources, and health risks associated with $PM_{2.5}$ and its components in Nanjing and Guangzhou, it is increasingly recognized that the biological components of $PM_{2.5}$ also play a critical role in determining its overall impact on air quality and public health. In particular, bioaerosols such as bacteria and endotoxins can contribute to the toxicity induced by $PM_{2.5}$, but these components are often overlooked in conventional air pollution studies. Based on the results from the chemical analysis and health risk assessment in Chapter 4, Chapter 5 shifts the focus to the biological components of $PM_{2.5}$. Chapter 5 explores the abundance, diversity, and community structure of

airborne bacteria, as well as the distribution of endotoxins in $PM_{2.5}$ across different land-use types in both cities. By integrating biological and chemical perspectives, the following chapter aims to provide a more comprehensive understanding of $PM_{2.5}$ composition and its potential health implications, thereby offering new insights for air quality management and risk assessment.

Chapter 5 Biological Components of $PM_{2.5}$–Endotoxins and Bacteria Profiles in Nanjing and Guangzhou

This chapter investigates the biological components of $PM_{2.5}$, focusing on endotoxins and bacterial profiles in Nanjing and Guangzhou. Distinct bacterial community structures exist between cities, shaped by local environment and land use. Gram-negative bacteria predominated and were strongly correlated with endotoxin concentrations. This chapter also highlights the association between the chemical components of $PM_{2.5}$ and biological factors.

5.1 Inter-city and intra-city comparisons of the concentrations of endotoxins

The composition analysis revealed distinct inter-city profiles of $PM_{2.5}$ (Figure **5-1**). The concentration of endotoxins per unit mass of $PM_{2.5}$ in Guangzhou (0.179 ± 0.138 ng mg^{-1}) was significantly higher than that in Nanjing (0.0862 ± 0.0600 ng mg^{-1}) ($p < 0.0001$). This difference may be attributed to Guangzhou's southern subtropical monsoon climate, which results in a warmer annual mean temperature (23.1 °C) compared to Nanjing (17.1 °C) (Guangzhou Meteorological Observatory, 2020; Nanjing Municipal Bureau Statistics, 2019). This warm environment could create favorable conditions for the proliferation of Gram-negative bacteria in the atmosphere, accelerating the release of endotoxins into bioaerosols (Carty et al., 2003; Park et al., 2013). The intra-city variation in concentrations in Guangzhou was more distinct than in Nanjing, reflecting the impacts of land use. In Guangzhou, the urban (TH) site exhibited nearly double the level of endotoxins of the suburban (CH) site ($p < 0.05$), which may have resulted from more frequent human activities such as the discharge of domestic waste and domestic sewage (Rasuli et al., 2022), wastewater treatment (Madsen et al., 2023), food processing activities (Fayyaz et al., 2022) and household dust (Zhao et al., 2024). Endotoxins can become airborne through the disturbance and aerosolization of materials contaminated with Gram-negative bacteria. In urban areas, frequent human activities may facilitate the release of endotoxin-containing particles into the atmosphere. The annual average endotoxin concentrations at the sampling sites are of similar magnitude to those measured ten years ago (Table **5-1**).

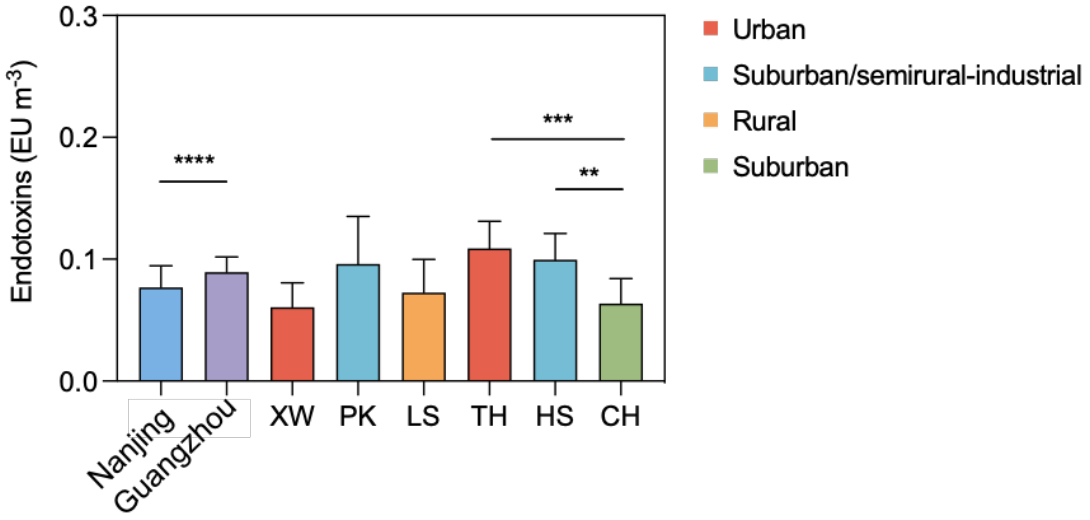

Figure 5-1. Annual average $PM_{2.5}$-bound endotoxins levels in Nanjing (XW, PK and LS) and Guangzhou (TH, HS and CH).

Table 5-1. Summary of endotoxins concentration measured in different studies.

Location	Size fraction	Endotoxin level (EU m^{-3})	Sampling time	Reference
Guangzhou, China	$PM_{2.5}$	0.148	2008-2009	(Cheng et al., 2012)
	PM_{10}	0.386	2008-2009	
Hong Kong, China	$PM_{2.5}$	0.099	2008-2009	
	PM_{10}	0.350	2008-2009	
XW, Nanjing, China	$PM_{2.5}$	0.061	2019-2020	This study
LS, Nanjing, China	$PM_{2.5}$	0.073	2019-2020	
PK, Nanjing, China	$PM_{2.5}$	0.096	2019-2020	
TH, Guangzhou, China	$PM_{2.5}$	0.109	2019-2020	
CH, Guangzhou, China	$PM_{2.5}$	0.064	2019-2020	
HS, Jiangmen, China	$PM_{2.5}$	0.010	2019-2020	

As shown in Figure **5-2**, in Nanjing, higher levels of endotoxins usually fell in July, October, November and December. In the HS site of Guangzhou, there was a peak of endotoxins levels in July, and in the TH site of Guangzhou, peaks existed in July, September, October, November, December and March. In general, $PM_{2.5}$-bound endotoxins were abundant in autumn and winter together with July. A previous study conducted on PM_{10} collected in 2008-2009 shared similar results with slight difference as this study (Figure **5-3**). In the previous study, peaks of PM_{10}-bound endotoxins levels in Guangzhou appear in July, August, November, December and January while in Hong Kong, the concentration start to increase in summer and remained high in winter. The seasonal pattern in this study is more similar to Hong Kong PM_{10}-related endotoxins in 2008-2009.

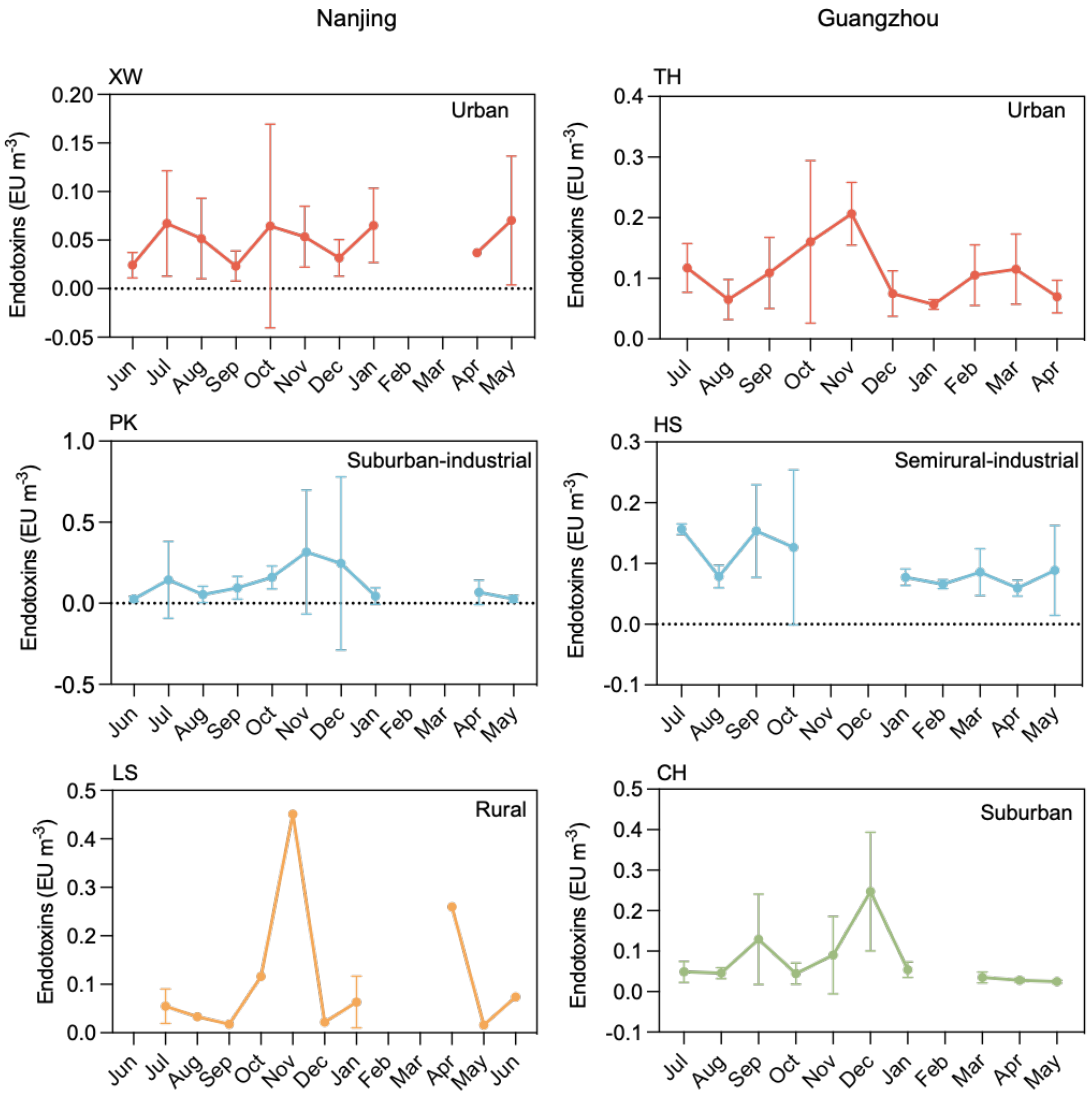

Figure 5-2. Monthly variations of $PM_{2.5}$-bound endotoxins levels in three sites in Nanjing (XW, LS, and PK) and Guangzhou (TH, CH, and HS), respectively.

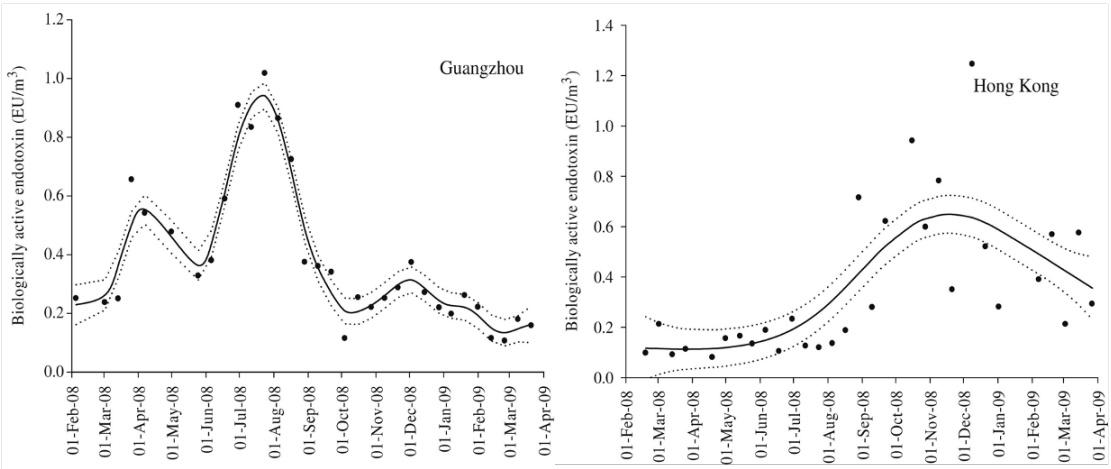

Figure 5-3. Smoothed plots of the atmospheric bioactive endotoxin in PM_{10} at Guangzhou and Hong Kong over the sampling period. Dotted lines represent the 95% CI of the smoothing spline (Cheng et al., 2012).

To further investigate how meteorological parameters influence the concentrations of $PM_{2.5}$-bound endotoxins, the trends in airborne endotoxin levels associated with temperature and humidity were plotted using nonparametric LOESS smoothing (Figure **5-4**). It can be estimated that 21 °C was a critical threshold in both Nanjing and Guangzhou – below it, the correlation was positive, while above it, the correlation was negative. The general trend was consistent with the trend achieved by a previous study in Beijing, although the threshold in Beijing was 4 °C (Figure **5-5**) (Guan et al., 2014). For relative humidity, between 30% and 100%, endotoxin concentration decreased as humidity increased in both cities. Between 80% and 100%, the decrease was slower in Guangzhou. This pattern is similar to that observed in Beijing, where endotoxin concentrations also decreased as relative humidity increased from 40% to 80% (Figure 5-5) (Guan et al., 2014). Therefore, weather differences may partly explain the differences in endotoxin concentrations.

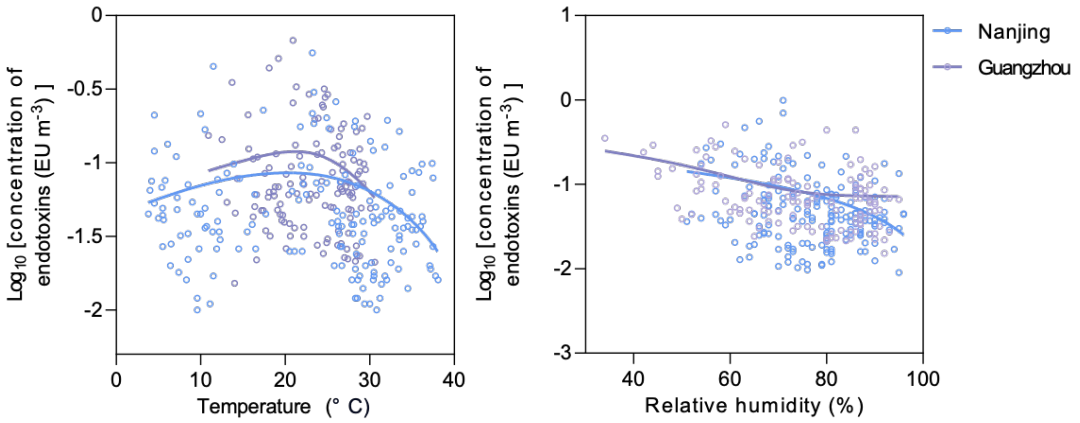

Figure 5-4. Changes in endotoxins concentration with the increase in temperature and relative humidity.

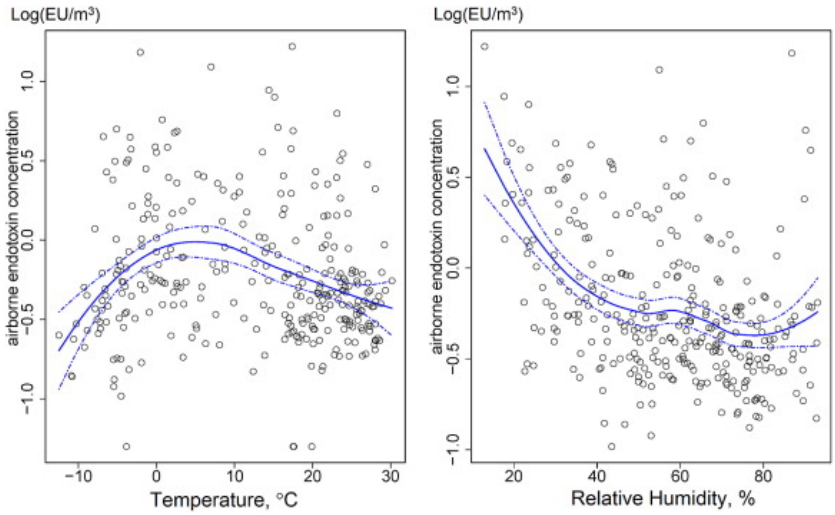

Figure 5-5. Changes in $PM_{2.5}$-bound endotoxins concentration with the increase in temperature and relative humidity (1 March 2012 to 27 February 2013 in Beijing) (Guan et al., 2014).

5.2 Relationships between $PM_{2.5}$-bound endotoxins and $PM_{2.5}$

To further investigate the associations of the $PM_{2.5}$-bound endotoxins with $PM_{2.5}$, the Pearson correlation was conducted between endotoxin mass per 10μg of $PM_{2.5}$ and the ambient $PM_{2.5}$ mass concentrations. As shown in Figure **5-6**, endotoxin levels per unit mass of $PM_{2.5}$ on relatively clean days were higher than on polluted days. It indicates that when assessing the potential toxicity posed by $PM_{2.5}$, mass concentration is not the only parameter that needs consideration since $PM_{2.5}$ is a mixture of various components.

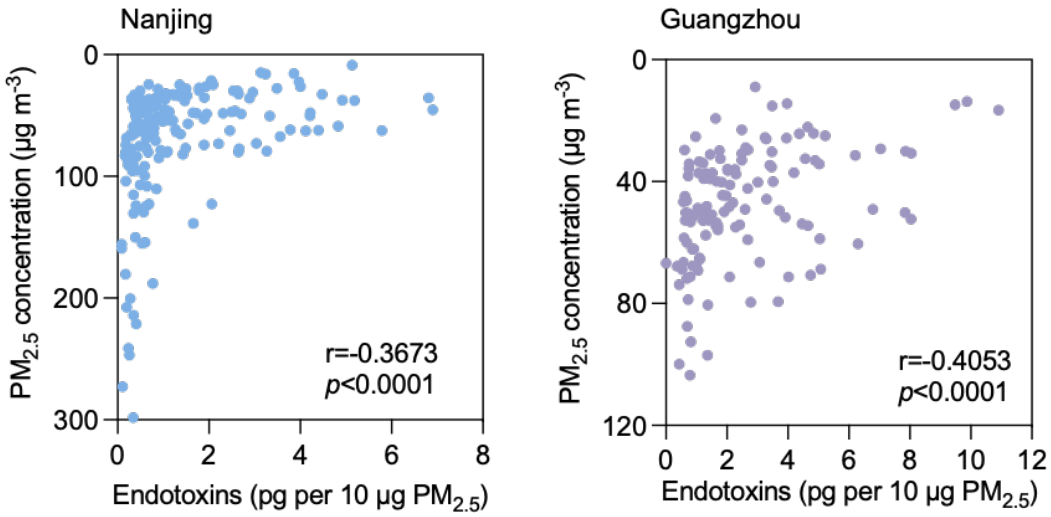

Figure 5-6. Relationship between endotoxin mass per 10 μg of $PM_{2.5}$ and ambient $PM_{2.5}$ mass concentrations. Correlation was conducted by the Pearson correlation in GraphPad Prism 9.

5.3 Inter-city and intra-city comparisons of $PM_{2.5}$-bound bacteria profiles

The annual absolute abundance of 16S rRNA genes of Nanjing and Guangzhou did not show significant difference (Figure **5-7**A) and remained relatively stable during the sampling period, with limited variations constrained to one order of magnitude (10^3-10^4 copy m^{-3}) (Figure **5-7**B). However, the total bacteria load was more distinct among the three sites in Nanjing, with the rural (LS) site exhibiting the highest load compared to both the urban (XW) ($p < 0.001$) and suburban-industrial (PK) sites ($p < 0.01$) (Figure **5-7**C). In contrast, the total bacterial load remained consistent across the three sites in Guangzhou (Figure **5-7**D). The observed stability in the annual absolute abundance of 16S rRNA genes in both Nanjing and Guangzhou, as well as the limited variation in total bacterial load, are generally consistent with a previous study conducted in the same cities (Xie et al., 2018). The higher bacterial load observed at the rural site in Nanjing compared to urban and suburban-industrial sites aligns with findings from other studies, which have revealed that rural or less urbanized areas often exhibit greater airborne bacterial abundance, likely due to increased vegetation, soil exposure, and reduced anthropogenic disturbance (Bowers et al., 2013; Bowers et al., 2011; Lymperopoulou et al., 2016). These results suggest that local land use and environmental factors play a critical role in shaping the spatial distribution of airborne bacterial communities. Similarly, Guangzhou had significantly higher bacterial diversity compared to Nanjing ($p < 0.05$) (Figure **5-8**A). The rural (LS) site had significantly higher Shannon diversity than the urban (XW) site in Nanjing ($p < 0.01$) (Figure **5-8**B), while the three sampling sites in Guangzhou had consistent bacterial diversity (Figure **5-8**C).

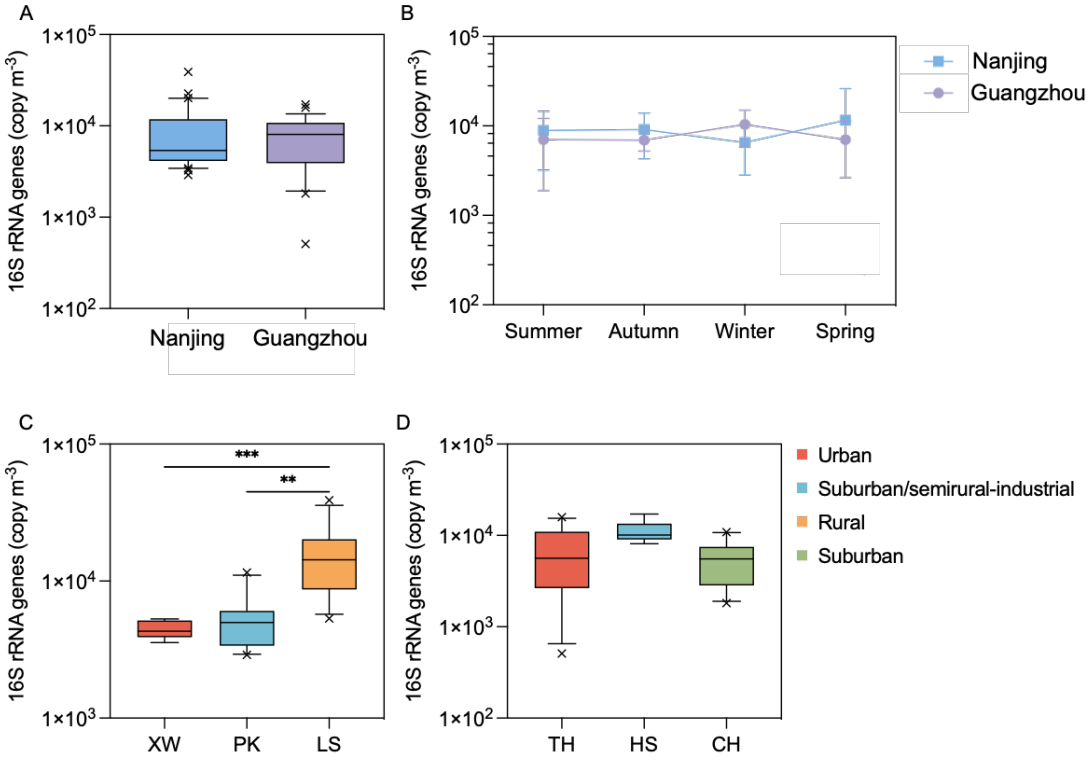

Figure 5-7. (A) Annual $PM_{2.5}$-bound 16S rRNA genes of $PM_{2.5}$ samples in Nanjing and Guangzhou. (B) Seasonal $PM_{2.5}$-bound 16S rRNA genes in Nanjing and Guangzhou. Annual $PM_{2.5}$-bound 16S rRNA genes in (C) three sites in Nanjing (XW, PK, and LS) and (D) three sites in Guangzhou (TH, HS, and CH).

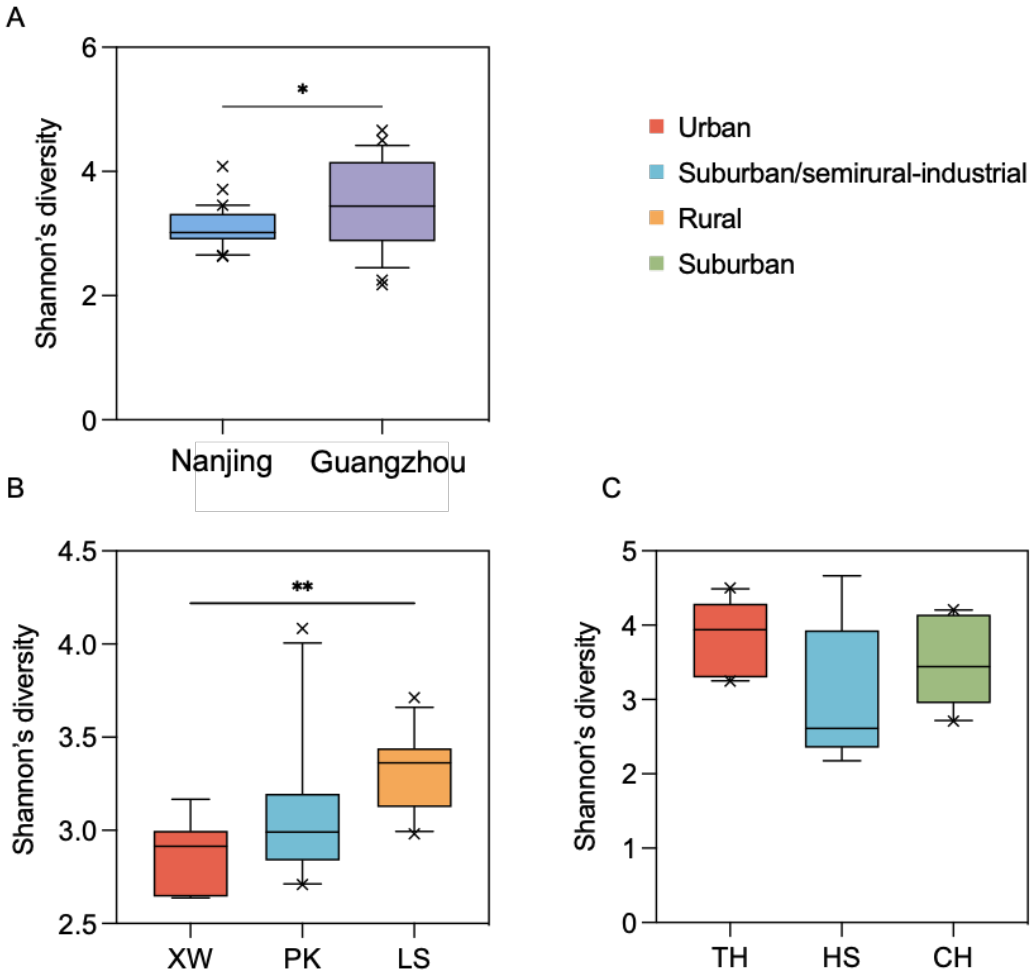

Figure 5-8. Annual Shannon diversity indices of $PM_{2.5}$ samples in (A) Nanjing and Guangzhou, (B) three sites in Nanjing (XW, PK, and LS) and (C) three sites in Guangzhou (TH, HS, and CH).

A total of 28 bacterial phyla were identified in $PM_{2.5}$ samples from Nanjing and Guangzhou (Figure **5-9**A). The top nine phyla were plotted in the figure, and the remaining phyla with unidentified phyla were grouped as "other" (< 5%). The dominant phyla differed between the two cities. In Nanjing, the dominant phylum was *Pseudomonadota*, alone accounting for over 78% of the total, followed by *Bacillota*, *Bacteroidota*, *Cyanobacteriota* and *Actinomycetota*, which together accounted for 18% of the total phyla. In Guangzhou, the dominant phylum was *Cyanobacteriota*, with a relative abundance of over 41%, followed by *Pseudomonadota* (30%) and *Bacillota*

(17%). The three sites in Nanjing shared similar bacteria profile (Figure **5-9**B), with the rural (LS) site having slightly lower *Pseudomonadota* and higher *Cyanobacteriota* abundance compared to the urban (XW) and suburban-industrial (PK) sites. Likewise, the three sites in Guangzhou also shared similar bacteria profile (Figure **5-9**C), with the semirural-industrial (HS) site having slightly lower *Pseudomonadota* and higher *Cyanobacteriota* abundance compared to other two sites. These results are consistent with previous studies that have identified *Proteobacteria*, *Firmicutes*, *Actinobacteria*, *Bacteroidetes*, and *Cyanobacteria* as the dominant phyla in airborne $PM_{2.5}$ in Chinese cities (Gao et al., 2017; Pan et al., 2019; Wang et al., 2021a). The higher abundance of *Cyanobacteriota* in Guangzhou may be related to the warmer and more humid climate, which favors the growth and aerosolization of cyanobacteria (Luo et al., 2014; Yao et al., 2020).

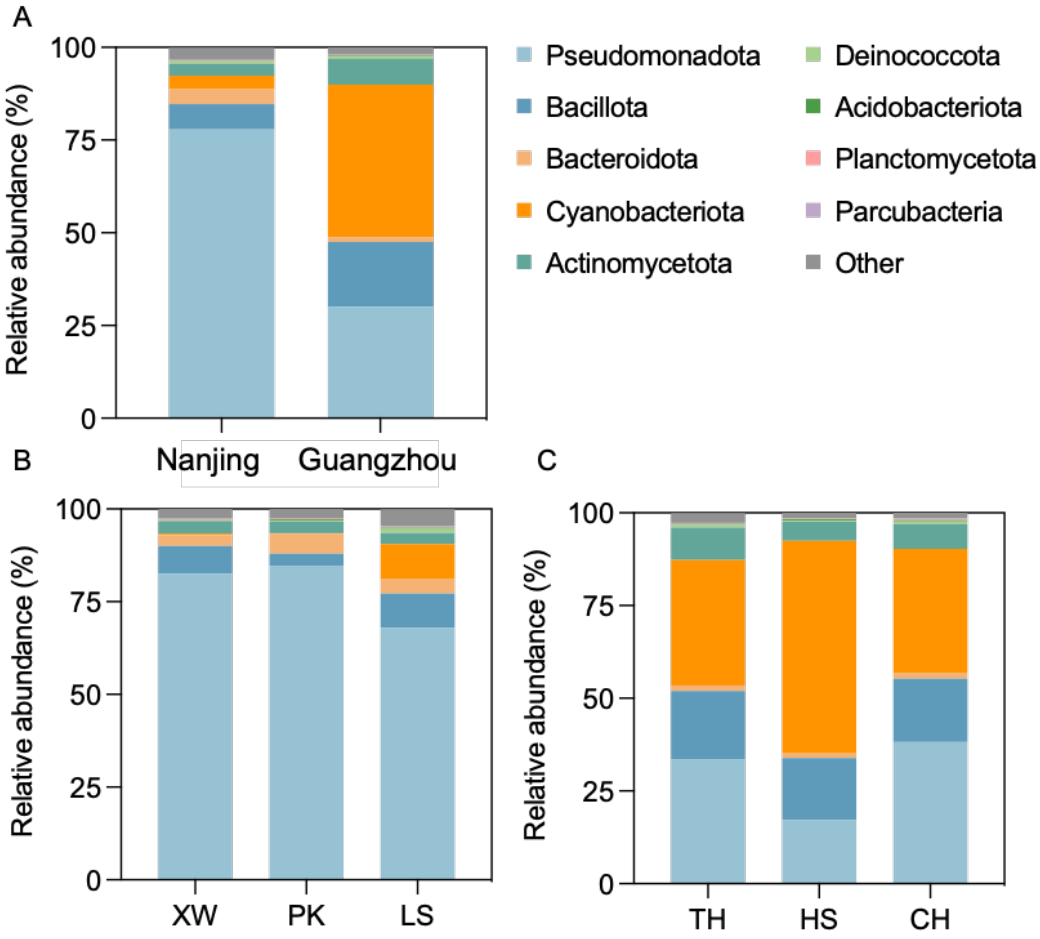

Figure 5-9. Phylum-level bacteria community structures of $PM_{2.5}$ samples in (A) Nanjing and Guangzhou, (B) three sites in Nanjing (XW, PK, and LS) and (C) three sites in Guangzhou (TH, HS, and CH).

To visualize differences in bacterial community composition among samples, the PCoA analysis based on Bray-Curtis dissimilarities calculated from OTU-level abundance data were conducted. Between Nanjing and Guangzhou (Figure **5-10**A), the first principal coordinate (PCo1) accounted for 49.1% of the total variation, while the second principal coordinate (PCo2) explained 16.5%. The resulting PCoA plot showed that $PM_{2.5}$ bacterial community of Nanjing clustered separately from those of Guangzhou, suggesting distinct community structures between these two cities. Statistical analysis using Permutational multivariate analysis of variance (PERMANOVA) indicated that these differences were significant (p = 0.001). The bacterial community structures among the three sites in Nanjing exhibit distinct differences, with the PCo1 accounting for 57.0% of the total variation and the PCo2 explaining 10.5% (Figure **5-10**B). The $PM_{2.5}$-bound bacterial community in the semirural-industrial (HS) site in Guangzhou clustered separately from those in the urban (TH) site and the suburban (CH) site, with the PCo1 accounting for 30.5% of the total variation and the PCo2 explaining 17.4% (Figure **5-10**C). Statistical analysis using PERMANOVA confirmed that these differences were significant ($p < 0.05$).

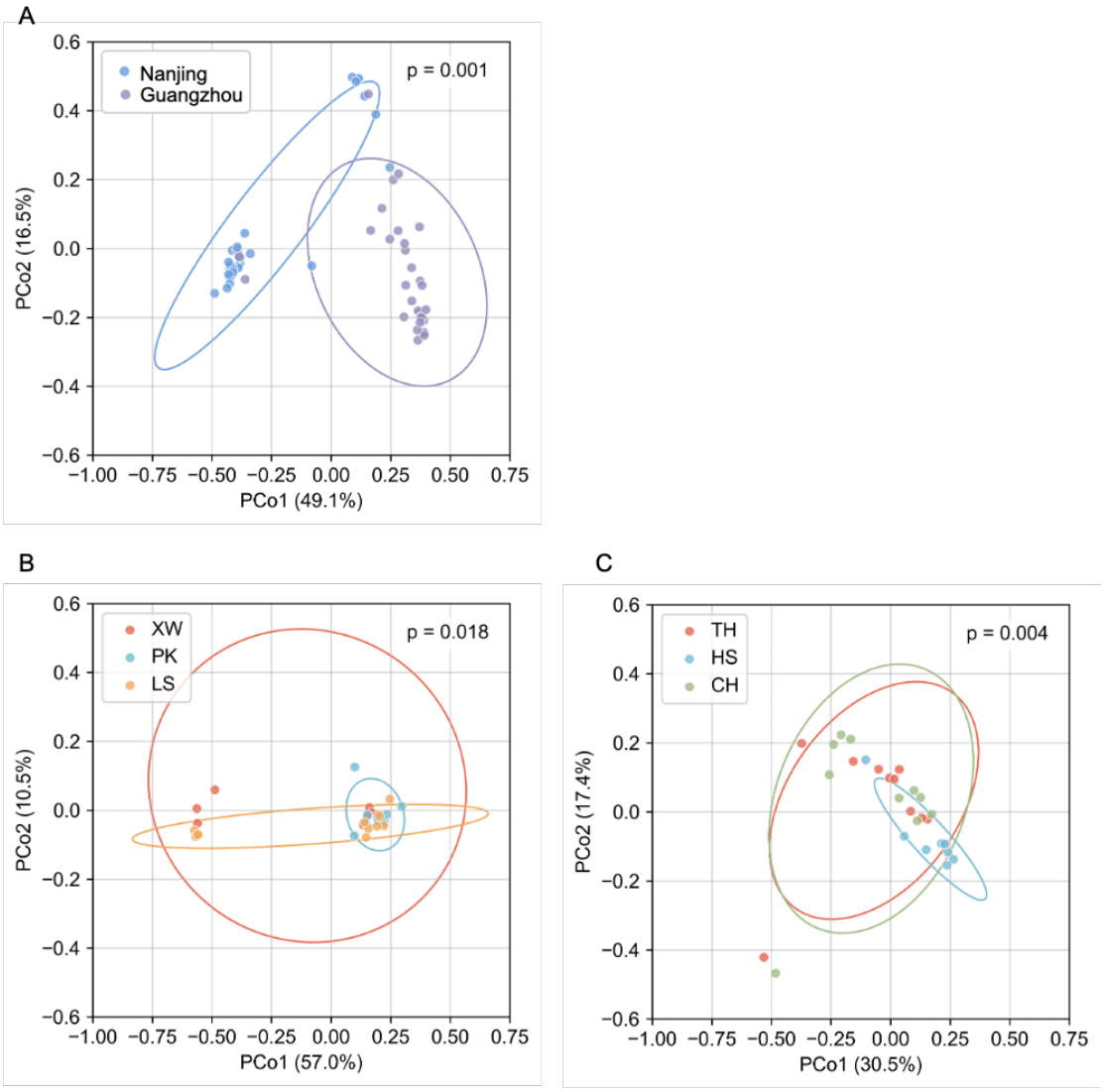

Figure 5-10. PCoA on Bray-Curtis dissimilarities of bacterial communities on the OTU level from (A) Nanjing and Guangzhou, (B) three sites in Nanjing (XW, PK, and LS) and (C) three sites in Guangzhou (TH, HS, and CH).

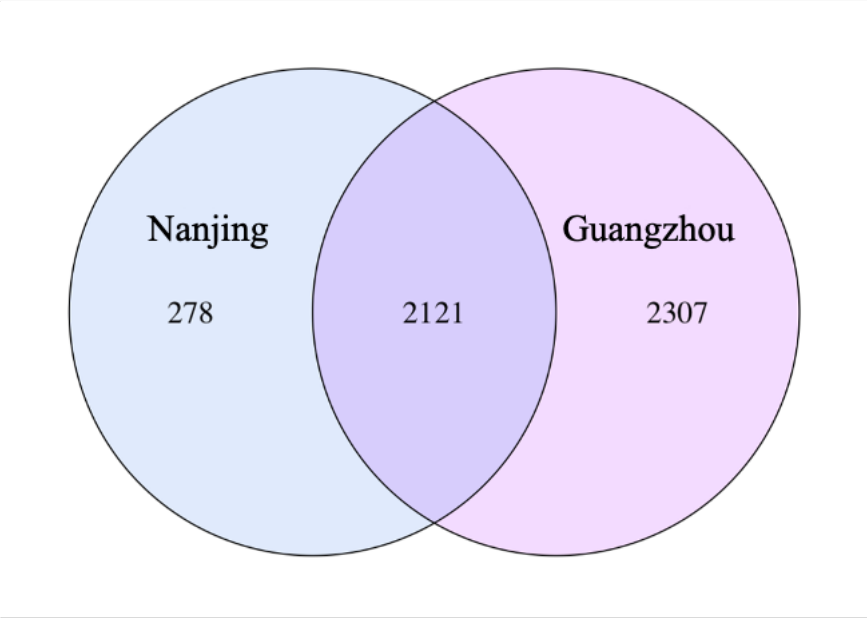

Figure 5-11. Venn diagram of unique and shared bacterial OTUs in $PM_{2.5}$ collected from Nanjing and Guangzhou.

The Venn diagram is shown in Figure **5-11** to compare the bacterial OTUs present in $PM_{2.5}$ samples from Nanjing and Guangzhou. The analysis revealed that 278 OTUs were unique to Nanjing, and 2307 OTUs were unique to Guangzhou. Importantly, 2121 OTUs were shared between the two cities, representing a considerable proportion of the total OTUs detected. This substantial overlap suggests that, despite geographical and environmental differences, there is a core set of bacterial taxa commonly present in $PM_{2.5}$ across both environments. The higher number of unique OTUs in Guangzhou compared to Nanjing could be attributed to several factors, including differences in climate, local sources of $PM_{2.5}$, population density, and industrial activities. Guangzhou's warmer and more humid climate may support a greater diversity of airborne bacteria, as has been suggested in previous studies (Carty et al., 2003; Park et al., 2013). Additionally, local land use and emission sources can introduce unique bacterial taxa into the atmosphere, contributing to the observed differences.

LDA was conducted to identify OTUs that significantly distinguished the bacterial communities between Nanjing and Guangzhou. Using an LDA score threshold of 4.0, a total of 17 OTUs were found to be significantly enriched in at least one site ($p < 0.05$).

The most discriminative OTUs, as indicated by their high LDA scores, are shown in Figure **5-12**.

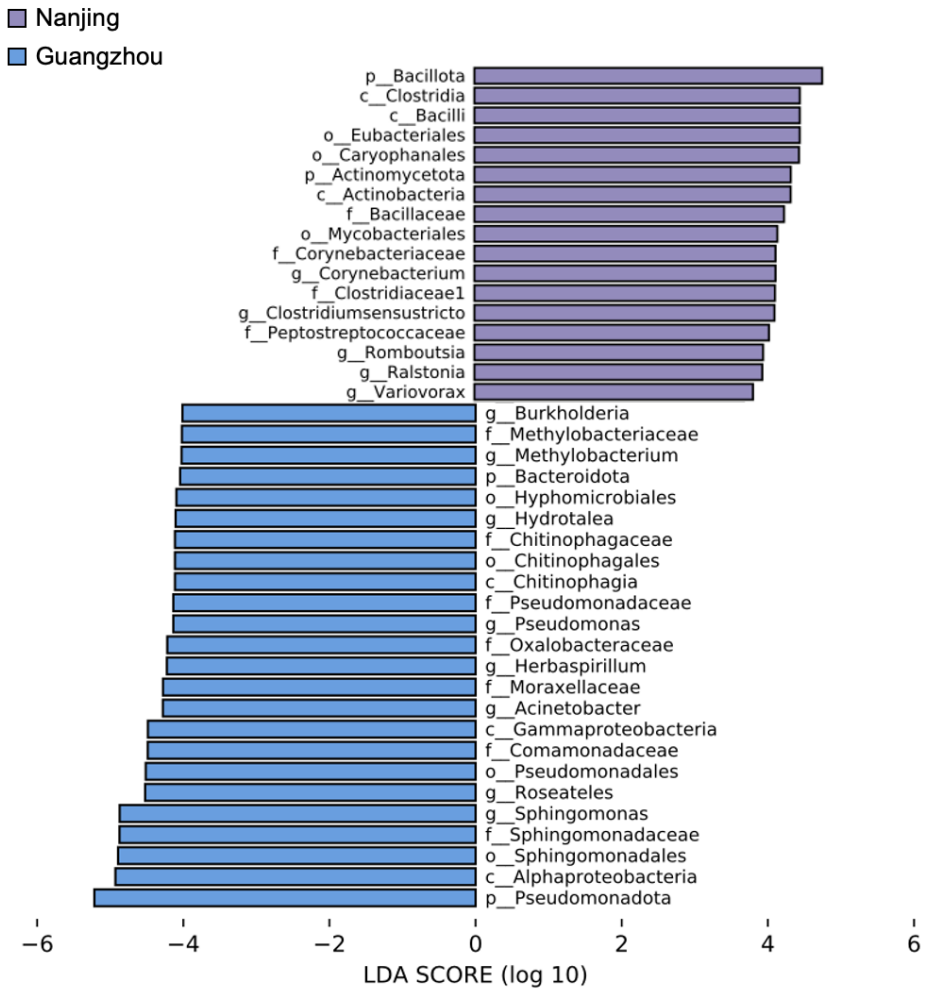

Figure 5-12. LDA scores (log 10) computed for OTUs differentially abundant between Nanjing and Guangzhou.

5.4 Gram-positive and gram-negative bacteria, and their correlations with endotoxins

Gram-negative bacteria predominated over Gram-positive bacteria in Nanjing and Guangzhou (Figure **5-13**A) and across all six sampling sites (Figure **5-13**B and C), accounting for over 80% and 68% of bacterial profiles in Nanjing and Guangzhou, respectively. Concentration of endotoxins is significantly positively correlated with the relative abundance of most Gram-negative bacteria ($p < 0.01$), including *Hydrotalea* (*r*

= 0.95), *Roseateles* (r = 0.89), *Herbaspirillum* (r = 0.87), *Burkholderia* (r = 0.84), *Sphingomonas* (r = 0.81), *Methylobacterium* (r = 0.75), *Aquabacterium* (r = 0.67), *Acinetobacter* (r = 0.65), *Pseudomonas* (r =0.64), and *Novosphingobium* (r = 0.53). In contrast, endotoxin concentration was significantly negatively correlated with most Gram-positive bacteria (p < 0.05), including *Clostridiumsensustricto* (r = –0.59), *Priestia* (r = –0.41), *Bacillus* (r = –0.39), *Romboutsia* (r = –0.39), *Corynebacterium* (r = –0.33) (Figure **5-14**). A prior study similarly identified significant correlations between endotoxin levels and the relative abundance of the three Gram-negative phyla: *Proteobacteria* (r = 0.32), *Bacteroidota* (r = 0.17), and *Myxococcota* (r = 0.071) (Amin et al., 2023). The results demonstrate a significant positive correlation between endotoxin concentrations and the relative abundance of most Gram-negative bacteria, highlighting the importance of monitoring Gram-negative bacterial populations in $PM_{2.5}$, as well as their associated endotoxins, due to their potential impact on air quality and public health.

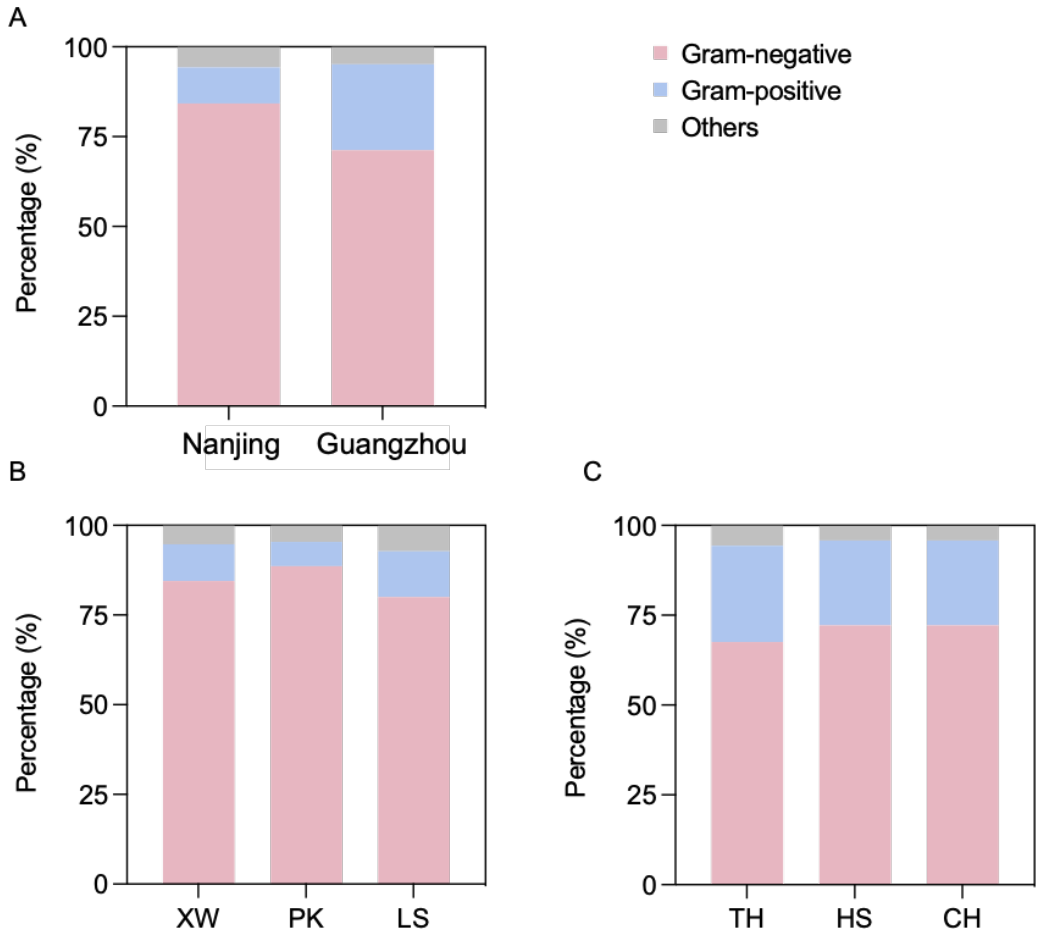

Figure 5-13. Relative abundance of Gram-negative and Gram-positive bacteria of (A) Nanjing and Guangzhou, (B) three sites in Nanjing (XW, PK, and LS) and (C) three sites in Guangzhou (TH, HS, and CH).

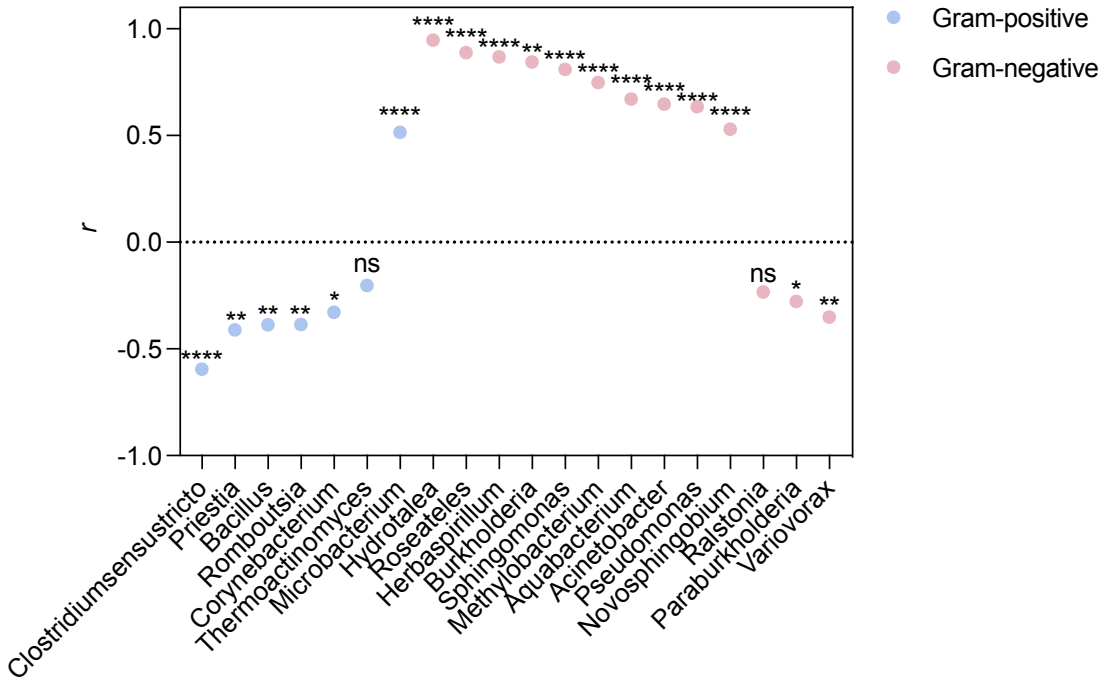

Figure 5-14. Spearman correlation coefficients for the concentration of endotoxins against the relative abundance of bacteria at the genus level (*$p < 0.05$, **$p < 0.01$, ****$p < 0.0001$).

5.5 Associations between $PM_{2.5}$-bound chemical components and biological components

To investigate the relationship between chemical components of $PM_{2.5}$ and biological components, the Pearson correlation was conducted (Figure **5-15**). The concentrations of endotoxins were positively correlated with those of Al, Mg^{2+}, and Ca^{2+}, likely because they share similar sources such as dust. Most Gram-negative bacteria showed positive correlations with WSI, which may be attributed to shared sources such as sea spray, dust, and secondary aerosol resuspension. In addition, WSI may provide essential nutrients that support bacterial survival. The presence of WSI may enhance

the attachment and persistence of Gram-negative bacteria, whose outer membranes can interact with ionic environments (Gottenbos et al., 2001; Sheng et al., 2008).

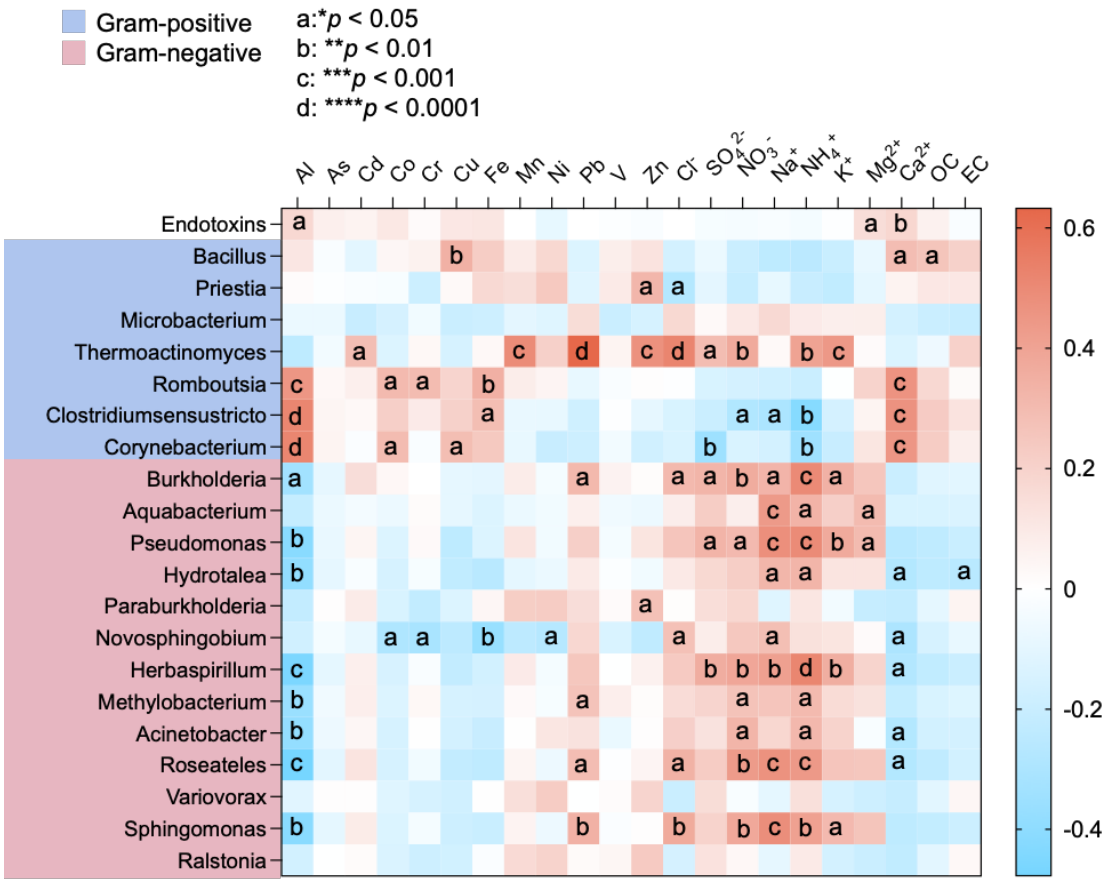

Figure 5-15. Pearson correlation coefficients between the mass concentrations of endotoxins and the relative abundance of bacteria at the genus level versus chemical components.

5.6 Summary

Chapter 5 investigates the biological components of $PM_{2.5}$, focusing on endotoxins and bacterial community profiles in Nanjing and Guangzhou. This chapter compares inter-city and intra-city variations in endotoxins concentrations, explores the relationships between endotoxins and $PM_{2.5}$ chemical components, characterizes bacterial abundance and diversity, and examines the correlations between bacterial taxa and chemical constituents, including endotoxins. The major findings of chapter 5 are listed below:

1. $PM_{2.5}$ samples from Guangzhou exhibited nearly double the endotoxin load per unit mass of $PM_{2.5}$ compared to Nanjing. The intra-city variation was more pronounced in Guangzhou, with urban sites showing higher endotoxins levels than suburban sites, likely due to increased human activities. Seasonal peaks in endotoxins concentrations were observed in autumn, winter, and July, with patterns similar to previous studies in Guangzhou and Hong Kong.

2. Endotoxin levels per unit mass of $PM_{2.5}$ were higher on relatively clean days than on polluted days, indicating that $PM_{2.5}$ mass alone does not fully reflect toxicity.

3. The annual absolute abundance of 16S rRNA genes (bacterial load) was similar between Nanjing and Guangzhou, but the rural site in Nanjing had significantly higher bacterial load than urban and suburban-industrial sites. Bacterial diversity (Shannon index) was significantly higher in Guangzhou than in Nanjing. Within Nanjing, the rural site had higher diversity than the urban site. Diversity was consistent across sites in Guangzhou.

4. A total of 28 bacterial phyla were identified. In Nanjing, *Pseudomonadota* dominated, while in Guangzhou, *Cyanobacteriota* was most abundant. Both cities shared a core set of bacterial OTUs (2121 OTUs), but Guangzhou had a higher number of unique OTUs, likely due to its warmer, more humid climate and diverse emission sources.

5. PCoA and PERMANOVA analyses showed distinct bacterial community structures between Nanjing and Guangzhou. Within Guangzhou, the semirural-industrial site had a distinct community compared to urban and suburban sites. No significant differences were observed among Nanjing sites.

6. Gram-negative bacteria predominated in both cities. Endotoxin concentrations were significantly positively correlated with the abundance of most Gram-negative

bacteria, and negatively correlated with most Gram-positive bacteria.

7. There are associations between chemical and biological components in $PM_{2.5}$. The concentrations of endotoxins were positively correlated with Al, Mg^{2+}, and Ca^{2+}, likely due to shared sources such as dust. Most Gram-negative bacteria also showed positive correlations with WSI, which may provide nutrients for bacteria and enhance their attachment.

Chapter 5 expands the perspective to include biological components such as bacteria and endotoxins in $PM_{2.5}$, highlighting their potential health implications. Based on Chapter 4 and chapter 5, Chapter 6 integrates both chemical and biological analyses to assess the toxicological impacts of $PM_{2.5}$ using *in vitro* cellular assays. By linking specific $PM_{2.5}$ components and emission sources to measured intracellular oxidative stress, Chapter 6 advances the understanding of how the complex mixture of $PM_{2.5}$ induce toxicity, providing an integrated view of $PM_{2.5}$ toxicity and directing more targeted air quality management strategies.

Chapter 6 The Critical Role of Chemical and Biological Composition and Sources in $PM_{2.5}$ Toxicity in Nanjing and Guangzhou

This chapter demonstrates that the toxicity of $PM_{2.5}$ in Nanjing and Guangzhou is determined more by its chemical and biological composition than by its mass concentration. Source apportionment indicated that the main contributors to $PM_{2.5}$ mass were not always the main sources of toxicity. Biological emissions played a significant role in inducing oxidative stress. Overall, the findings highlight the need for targeted pollution control strategies that focus on the most toxic $PM_{2.5}$ components and sources, rather than solely on reducing $PM_{2.5}$ mass, to better protect public health.

6.1 Spatially heterogeneous composition of $PM_{2.5}$

The CR and the NCR induced by metals, and the ECR posed by PAHs in the six sampling sites were calculated following USEPA methods in Chapter 4. It was observed that elements with relatively higher concentrations did not necessarily contribute the most to the risks. This observation supports the previously mentioned hypothesis that equal mass concentrations of $PM_{2.5}$ or its constituents do not result in equivalent toxicity. Such estimations are based on long-term low-dose exposure scenarios (such as lifetime exposure) (USEPA, 2018). However, the risk associated with short-term, high-concentration exposure in real-world environments—such as industrial accidents or extreme pollution events, which can have immediate and severe health impacts—may have been underestimated. Thus, the *in vitro* experiments in this study offer advantages by providing insights into the immediate effects of real environmental exposure, delivering a detailed mechanistic understanding of cellular responses to toxicants, and allowing for controlled experimentation to assess specific pathways or cellular responses. Thus, to further validate this hypothesis, 76 samples were selected from six sampling sites (11–14 samples in each site) for an *in vitro* study (Appendix 1). Cell viability and oxidative stress were measured as biotoxicity endpoints. Contribution of $PM_{2.5}$-bound metals, endotoxins and PAHs to the mixture toxicity were calculated to find out the toxic key components.

The composition analysis revealed distinct inter-city profiles of $PM_{2.5}$ (Figure **6-1**). The concentration of endotoxins per unit mass of $PM_{2.5}$ in Guangzhou (0.179 ± 0.138 ng mg^{-1}) was significantly higher than that in Nanjing (0.0862 ± 0.0600 ng mg^{-1}) ($p < 0.0001$). This difference may be attributed to Guangzhou's southern subtropical monsoon climate, which results in a warmer annual mean temperature (23.1 °C) compared to Nanjing (17.1 °C) (Guangzhou Meteorological Observatory, 2020; Nanjing Municipal Bureau Statistics, 2019). The association between airborne endotoxin levels and temperature and humidity is discussed in Section 5.1. The total concentration of trace metals in Guangzhou (15.6 ± 4.64 μg mg^{-1}) was 35.7% higher than that of Nanjing (11.5 ± 6.58 μg mg^{-1}) ($p < 0.01$), whereas Nanjing showed significantly elevated levels of PAHs (79.6 ± 92.9 μg mg^{-1}) than Guangzhou (32.6 ± 26.2 μg mg^{-1}) ($p < 0.0001$), with extraordinarily higher levels of PAHs in the suburban-industrial (PK) site. The intra-city variation in component concentrations in Guangzhou was more distinct than in Nanjing, reflecting the impacts of land use (Figure **6-2**A). In Guangzhou, the urban (TH) site exhibited nearly double the level of endotoxins of the suburban (CH) site ($p < 0.05$), which may have resulted from more frequent human activities, which is discussed in Section 5.1. The urban (TH) site and the suburban-industrial (HS) site exhibited higher levels of total trace metals per unit mass of $PM_{2.5}$ than the suburban (CH) site ($p < 0.05$). As shown in Figure **6-2**B, the $PM_{2.5}$ mass-normalized concentration of highly enriched element Cd (EF > 100) was significantly higher in the semirural-industrial (HS) site than in the suburban (CH) site ($p < 0.05$), and the concentration of Cu (EF > 100) was significantly higher in the urban (TH) site than in the semirural-industrial (HS) site and the suburban (CH) site ($p < 0.01$). The $PM_{2.5}$ mass normalized concentrations of moderate (10 < EF < 100) and slightly (1 < EF < 10) enriched elements were significantly higher in the urban (TH) site or the semirural-industrial (HS) site than in the suburban (CH) site ($p < 0.05$). This is likely attributed to higher anthropogenic emissions in urban and industrial areas, such as those from industries and traffic emissions, which produce abundant metals compared to suburban areas (Hsu et al., 2021; Hueglin et al., 2005). Such trends are consistent with

those noted in previous studies (Xie et al., 2020). The suburban-industrial (PK) site of Nanjing had the highest levels of BbF, BkF, Chr, and BaA compared to the rural (LS) site in Nanjing and all three sites in Guangzhou. This may be due to soot and coke oven emissions from heavy industries in the industrial areas of Nanjing (Chen et al., 2019b). In contrast, the semirural-industrial (HS) site in Guangzhou does not emit much PAHs, possibly because it primarily consists of light industries such as electroplate factories and hardware and battery manufacturers (Xie et al., 2020).

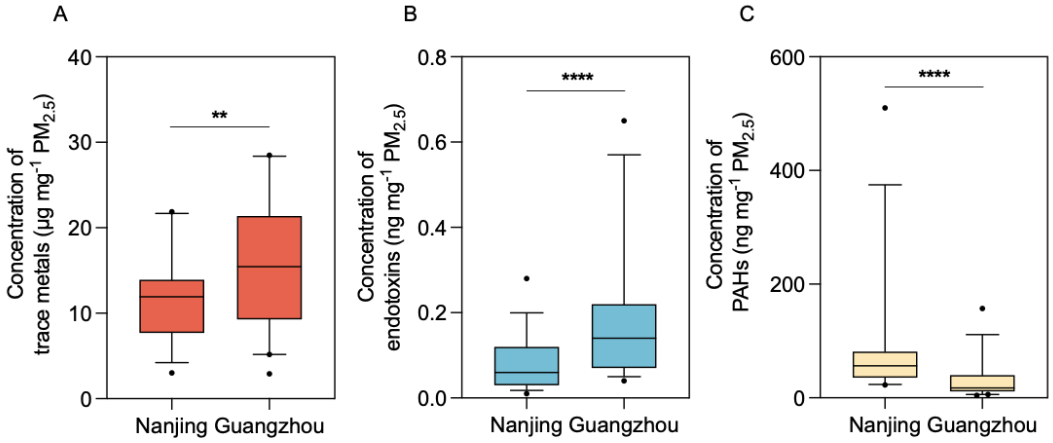

Figure 6-1. Concentrations of (A) total trace metals, (B) endotoxins and (C) PAHs per unit mass of $PM_{2.5}$ in Nanjing and Guangzhou. The box plots with whiskers present the mean with a 95% CI. The dots show individual data points that are considered outliers, lying outside the 5th to 95th percentile range.

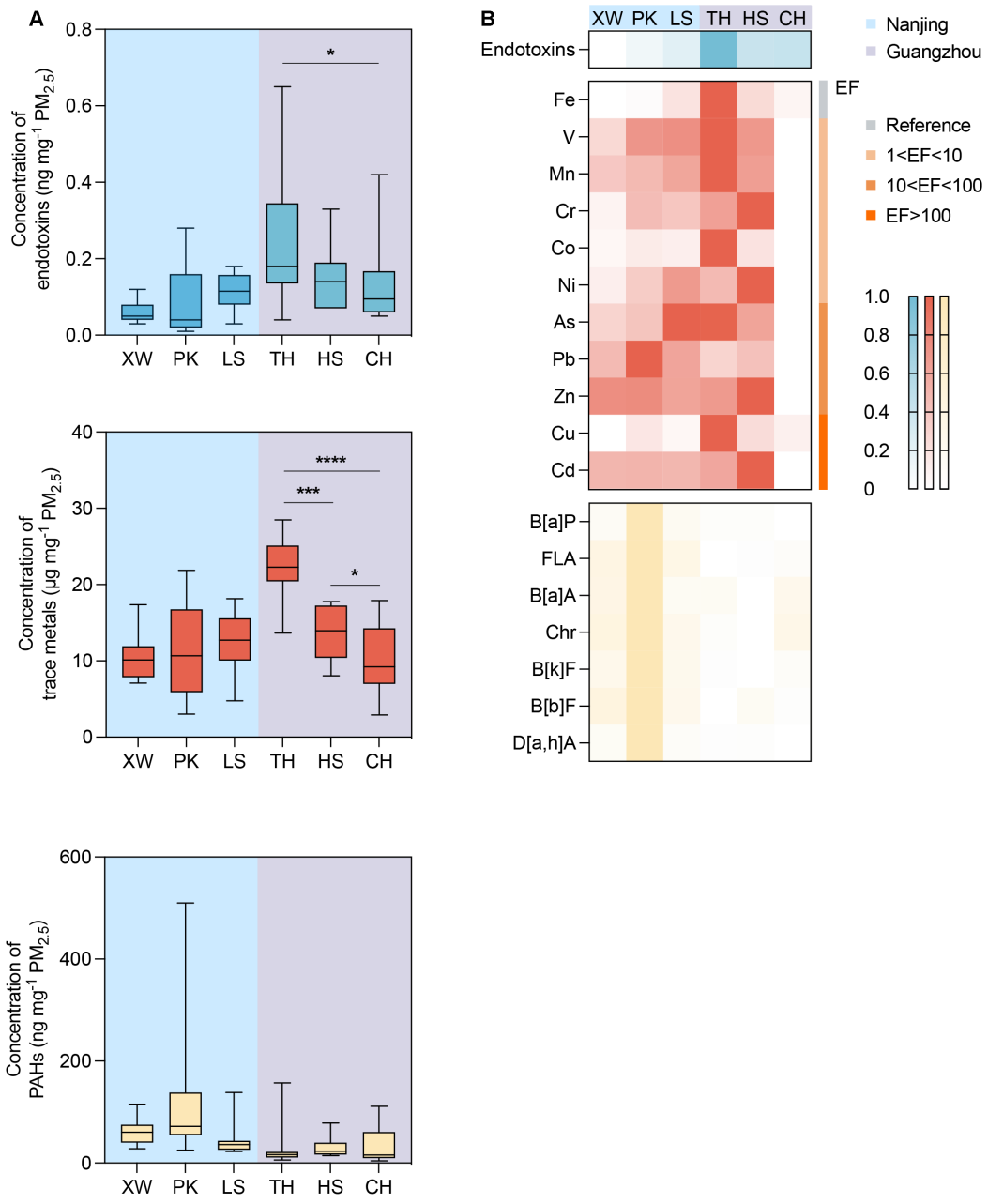

Figure 6-2. Analyzed chemical and biological component profiles in six sites in Nanjing (XW, PK, and LS) and Guangzhou (TH, HS and CH). (A) Mass concentrations of endotoxins, trace metals, and PAHs per unit mass of $PM_{2.5}$ from six sites in Nanjing and Guangzhou. The box plots with whiskers present the mean with a 95% CI. (B) Heatmaps of mass concentrations of the analyzed components per unit mass of $PM_{2.5}$. Prior to plotting the figures, the concentration of each individual component was separately normalized. The metals analyzed here were categorized according to the average EFs of all sampling sites. The original data are provided in Appendix 1.

6.2 Spatial diversity in $PM_{2.5}$-induced intracellular oxidative stress potency

To compare the toxicity induced by $PM_{2.5}$ from sites with different land-use types and to investigate the effects of anthropogenic activities on the toxicity of $PM_{2.5}$, we examined $PM_{2.5}$-induced intracellular oxidative stress. When the exposure concentration of $PM_{2.5}$ was under 500 mg L^{-1}, the average cell viability of six sampling sites was all over 50%, mostly 80% (Figure **6-3**), which means exposure to $PM_{2.5}$ samples from six sites did not induce significant cytotoxicity when the exposure concentration was under 500 mg L^{-1}. When the exposure concentration reaches 1000 mg L^{-1}, the $PM_{2.5}$ extracts became cloudy, which affected the absorbance of wavelength when measured by the microplate reader. Thus, the highest exposure concentration of $PM_{2.5}$ extracts to cells was selected as 500 mg L^{-1} in the intracellular ROS generation analysis. $PM_{2.5}$-induced intracellular oxidative stress potency exhibited pronounced spatial diversity across land-use types in Nanjing and Guangzhou, as quantified by concentration-effect curve slopes (Figure **6-4**A). The Nanjing suburban-industrial (PK) $PM_{2.5}$ (0.00398 ± 0.00125) demonstrated double the toxicity of rural (LS) samples (0.00212 ± 0.00206) ($p < 0.05$), while the urban (XW) site did not show significantly higher toxicity, despite higher $PM_{2.5}$ mass concentrations at both the suburban-industrial (PK) and urban (XW) sites compared to the rural (LS) site ($p < 0.01$). Similarly, in Guangzhou, urban (TH) (0.00543 ± 0.00201) and semirural-industrial (HS) (0.00514 ± 0.00172) $PM_{2.5}$ induced double the oxidative stress potency of suburban (CH) samples (0.00238 ± 0.00200) ($p < 0.01$), even with statistically indistinguishable $PM_{2.5}$ mass concentrations across sites (TH: 53.1 ± 11.6 μg m^{-3}; HS: 51.8 ± 22.1 μg m^{-3}; CH: 46.5 ± 12.3 μg m^{-3}; $p>0.05$). Figure **6-4**B shows that there is no significant linear relationship between $PM_{2.5}$ mass concentration and its toxicity (represented as slopes of $PM_{2.5}$ concentration-effect curves) in both Nanjing ($p > 0.05$) and Guangzhou ($p > 0.05$), indicating that $PM_{2.5}$ mass alone poorly predicts oxidative stress potential. Such poor linear relationships were also found in recent studies with 385 $PM_{2.5}$ samples

collected from 14 different sites across four continents and using five different oxidative potential (and cytotoxicity) endpoints (Salana et al., 2024). Integrating our findings with existing evidence, we propose that spatial variations in $PM_{2.5}$-induced intracellular oxidative stress predominantly result from disparities in composition rather than from $PM_{2.5}$ mass concentration gradients. This highlights the critical need to characterize the toxic contributions of individual components and identify key toxic components in order to make accurate evaluations of the toxicity induced by $PM_{2.5}$.

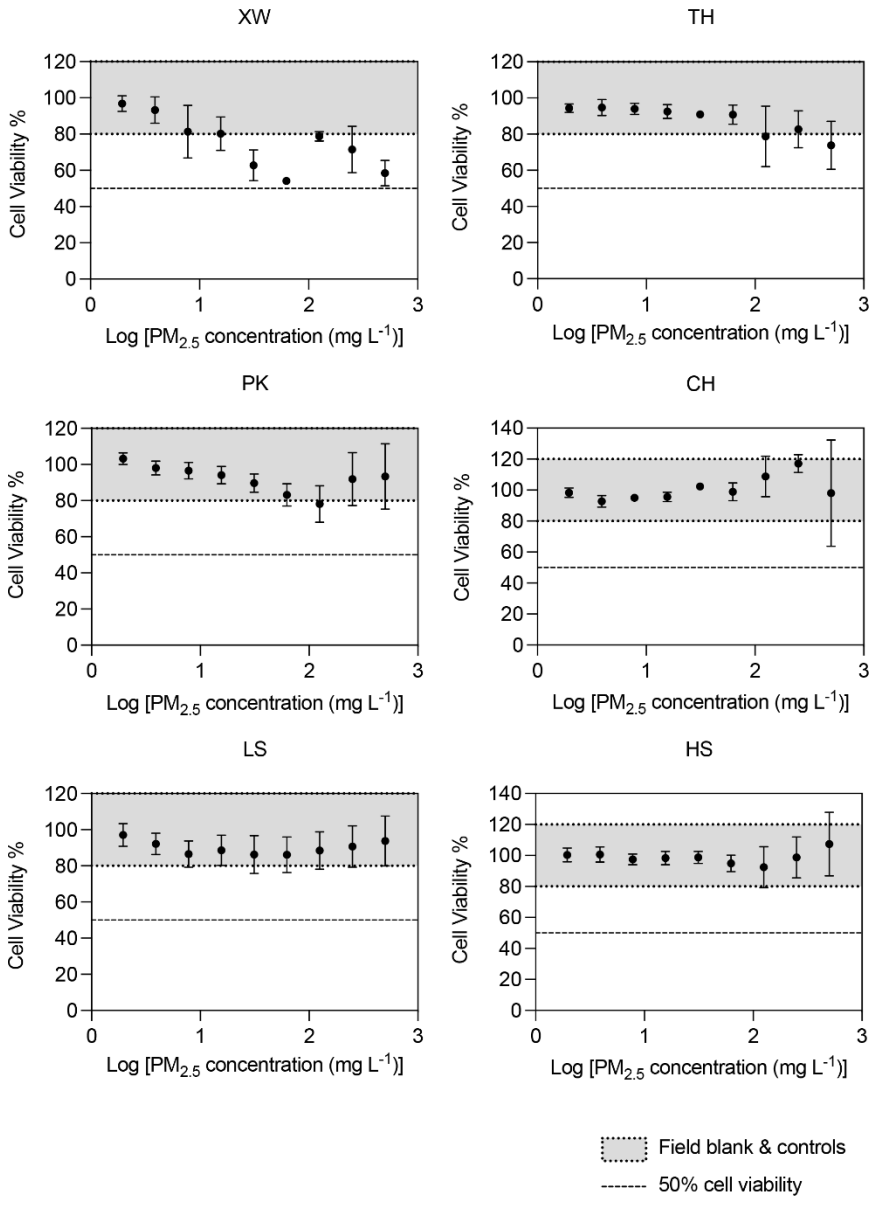

Figure 6-3. Dose-response relationships for mean cytotoxic effects induced by $PM_{2.5}$ extracts collected from six sites in Nanjing and Guangzhou.

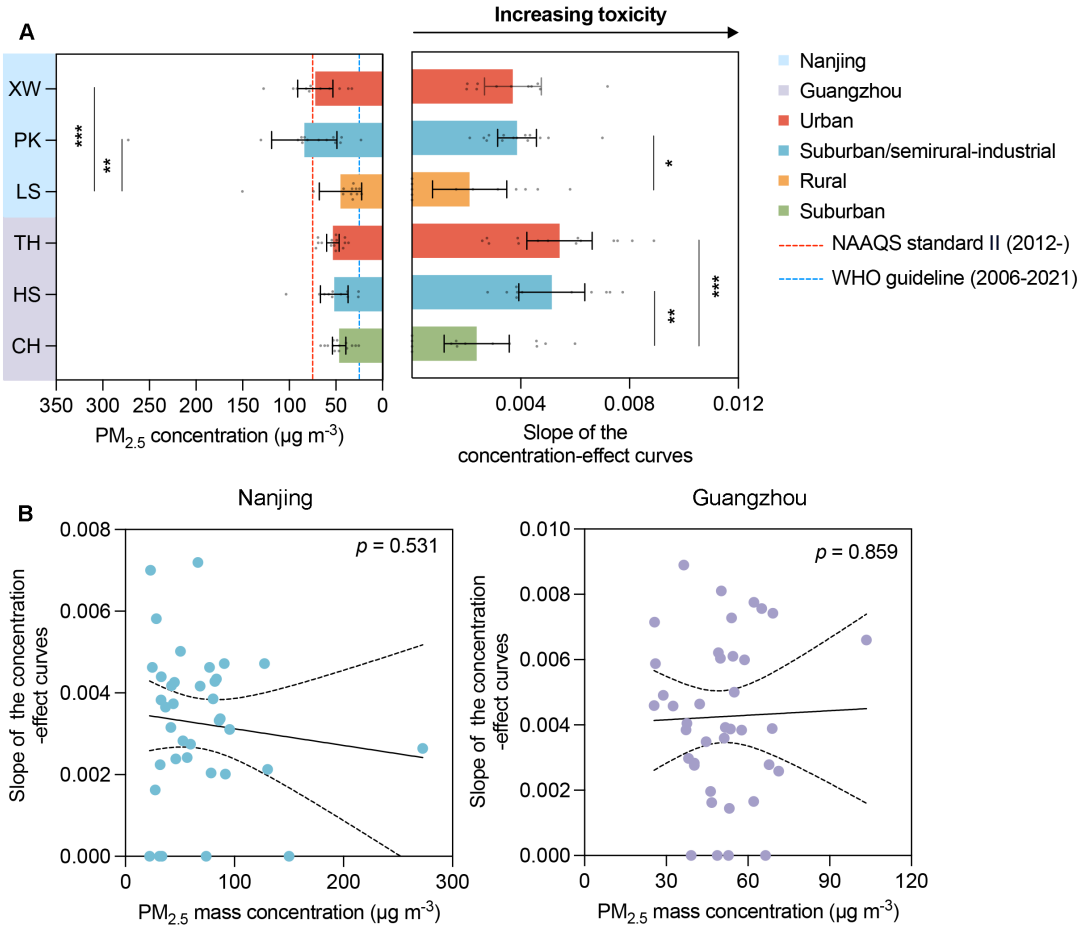

Figure 6-4. (A) $PM_{2.5}$ mass concentration (left panel) and slopes of $PM_{2.5}$ concentration-effect curves (right panel) of samples from six sites in Nanjing and Guangzhou. Note that the higher the slope of a sample, the greater its effect potency. The bar with whiskers presents the mean with a 95% CI. The blue dashed line indicates the WHO recommended limit for $PM_{2.5}$ concentration (25 μg m^{-3} for a 24 h period) as set between 2016 and 2021. The red dashed line represents the Grade II threshold (75 μg m^{-3} averaged over 24 h) specified by the NAAQS. The concentration-effect curve of each sample is provided in Appendix 2. (B) Linear regression analysis of the $PM_{2.5}$ mass concentration against its toxicity (represented by slopes of $PM_{2.5}$ concentration-effect curves) in Nanjing and Guangzhou ($p > 0.05$ means no significant linear relationships).

6.3 Contributions of metals, endotoxins, and PAHs to $PM_{2.5}$-induced intracellular oxidative stress

The intracellular oxidative stress potency of individual $PM_{2.5}$ components is shown in Figure **6-5**A. $EC_{IR1.5}$ values spanned five orders of magnitude across components, with endotoxins exhibiting the highest toxicity ($EC_{IR1.5}$ = $(18.7\pm2.02)\times10^{-5}$ mg L^{-1}), followed by metals and PAHs in general. Element-specific variations were observed among metals: Cd demonstrated the highest toxic effect ($EC_{IR1.5}$ = 0.0460 ± 0.00316 mg L^{-1}), while As showed no detectable ROS induction in this study. Among PAHs, DahA ($EC_{IR1.5}$ = 4.651 ± 0.327 mg L^{-1}) was the most toxic compound, and BaP ($EC_{IR1.5}$ = 46.1 ± 6.58 mg L^{-1}) was the least. Detailed concentration-effect profiles and associated derivations for each individual component are presented in Appendix 2. Most acute toxicity studies typically employ concentrations much higher than those found in the environment or encountered by organisms under real-world conditions (Wolf and Segner, 2023). According to the USEPA, the acceptable margin of exposure (a ratio of the toxicity effect level to the estimated exposure dose) for *in vivo* assessment is 100, which means that if the ratio is lower than 100, there may be a potential health risk (USEPA, 2012). Figure **6-5**B presents the ratio of $EC_{IR1.5}$ to the estimated realistic daily exposure concentration for adults of each component in Nanjing and Guangzhou. The ratios of endotoxins in Guangzhou (81 ± 48), Fe in Nanjing (43 ± 23) and Guangzhou (42 ± 32), and Mn in Nanjing (33 ± 18) and Guangzhou (41 ± 24) were lower than 100, suggesting that the realistic daily exposure to these components may pose a potential toxicity to humans. For endotoxins, Cd, Ni, Pb and Zn in Nanjing samples, and Cd, Ni, Pb and Zn in Guangzhou samples, the ratios were higher than 100 but lower than 1000, indicating that the potential daily toxicity was relatively low but cannot be completely ruled out. Cumulative exposure over time may be required for these components to induce oxidative stress and adversely affect human health. The ratios for PAHs exceeded 10,000 in Nanjing and 100,000 in Guangzhou, indicating that there is little concern that the realistic exposure concentration will reach levels where

toxicity is possible on a daily basis. However, potential long-term health impacts, including CR, should be considered (USEPA, 2012). Although the default ratios of 100 and 1000 are primarily established for *in vivo* studies, these thresholds were adopted here as a conservative reference in the absence of specific guidance for *in vitro* data. It should be noted that additional uncertainty may exist due to the lack of *in vivo* metabolic processes in *in vitro* systems.

Comparisons between $EC_{IR1.5}$ achieved by this study and established health risk parameters by the USEPA are shown in Figure **6-6**. The results showed that the ranking of metals based on $EC_{IR1.5}$ was generally consistent with the RfC rankings, with the exception of Co, V, As and Cu. However, when compared to the IUR^{-1} ranking, differences were observed. We also compared the effect potency of PAHs observed in our *in vitro* study with the relative potency factor (RPF) by the USEPA. The results also showed that the ranking of PAHs based on $EC_{IR1.5}$ was generally consistent with the RPF^{-1} rankings, with the exception of BaP and BaA.

We then mixed the identified metals, endotoxins, and PAHs together at the average mass concentration measured in the field samples of each site for a screening of their combined effects. Since the IPQ values for mixtures containing average concentrations of metals, endotoxins, and PAHs from all six sites were between -1 and +1, the ROS induction predicted by the CA model for these mixtures of active components closely matched the ROS effects observed in experimental measurements (Figure **6-7**). Therefore, the CA model supported the hypothesis that the aggregate impact of individual components on ROS production is comparable to the overall effect observed when these substances are present together in a mixture. Details are given in Appendix 2.

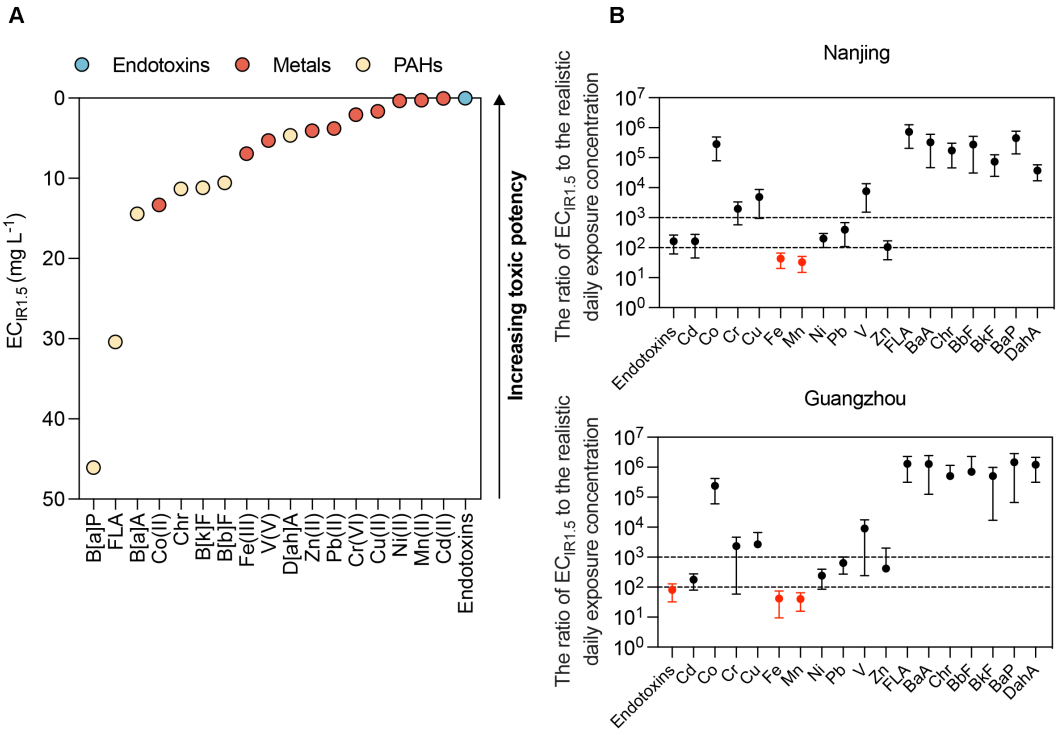

Figure 6-5. (A) $EC_{IR1.5}$ of each component identified in the $PM_{2.5}$ samples in inducing intracellular oxidative stress potency. Note that the lower the $EC_{IR1.5}$ value of a component, the greater its effect potency. Detailed concentration-effect profiles and associated derivations for each individual component are presented in Appendix 2. (B) The ratio of $EC_{IR1.5}$ to the estimated realistic daily exposure concentration for adults of each component in Nanjing and Guangzhou. Realistic daily exposure concentration: the concentration inhaled by a healthy adult and deposited in the epithelial lining fluid of the lungs daily. The dashed lines mean the ratio = 100 and 1000, respectively.

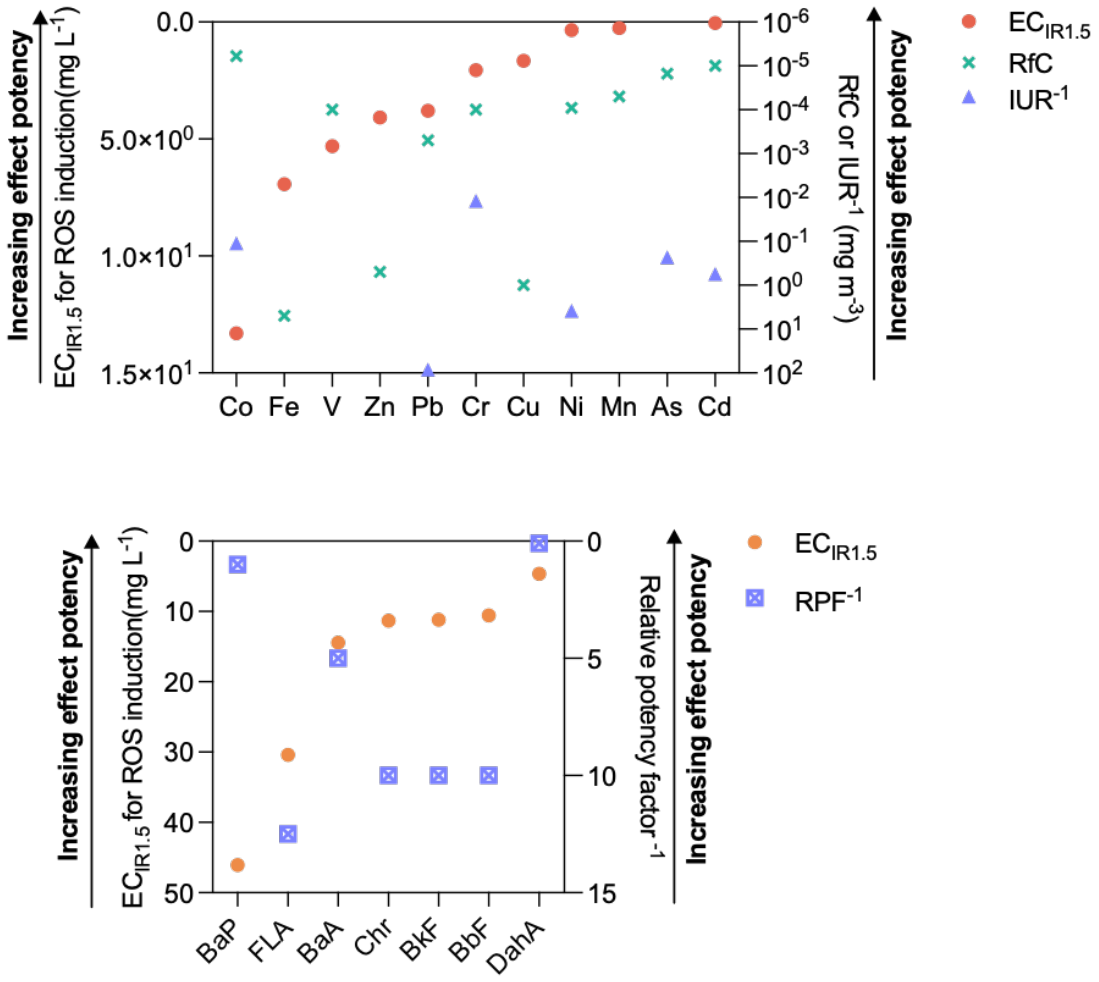

Figure 6-6. Comparisons between $EC_{IR1.5}$ achieved by this study and established health risk parameters (RfC for metal-induced CR, IUR^{-1} for metal-induced NCR and RPF^{-1} for PAH-induced ECR) by the USEPA (USEPA, 2018).

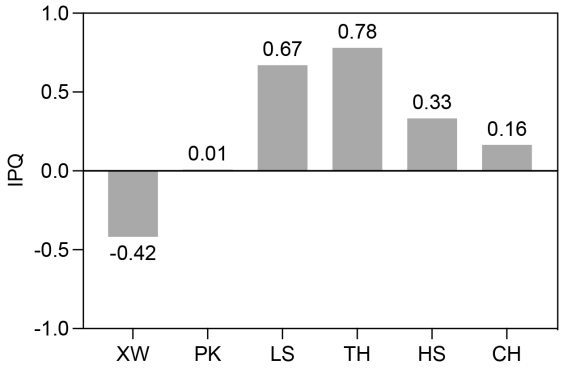

Figure 6-7. IPQs for the mixtures of average metals, endotoxins, and PAHs of all six sites (a detailed derivation is given in Appendix 2) in Nanjing (XW, PK and LS) and Guangzhou (TH, HS and CH).

The BEQ concept was adopted to quantify the contribution of individual components to the overall $PM_{2.5}$ toxicity. Samples induced no significant oxidative stress potency (slope = 0) were excluded from this quantification of contributions. The mass concentrations of analyzed components used in the toxic calculation were corrected by multiplying the correction ratio (Table **6-1**). The contribution to $PM_{2.5}$-induced ROS generation of each identified component is shown in Figure **6-8**A, and detailed deviation is shown in Appendix 2. Despite constituting only 1.01–2.23% of the total $PM_{2.5}$ mass, trace metals, endotoxins, and PAHs together explained 35.9–56.9% of intracellular oxidative stress induced by $PM_{2.5}$ in six sampling sites, with metals as the dominant contributors (31.6–46.7%), followed by endotoxins (4.24–12.2%) and PAHs (0.0218–0.135%). The toxic contribution of endotoxins in Guangzhou (10.1% ± 5.63%) was significantly higher than in Nanjing (5.39% ± 4.84%) (p = 0.0001), which is consistent with the elevated concentration of endotoxins in Guangzhou, further confirming that the local conditions in Guangzhou favor the toxic contribution of endotoxins. The toxic contribution of PAHs in the suburban-industrial (PK) site in Nanjing was significantly higher than that in the Nanjing rural (LS) site and all three sites in Guangzhou ($p < 0.05$), which is also consistent with the higher concentrations of PAHs observed in the PK site compared to other sites. Fe and Mn were the primary metal contributors (> 50.0% combined), and DahA, BbF, BkF, and Chr accounted for 75.6% of PAH-associated effects (Figure **6-8**B). These findings quantify for the first time the crucial contribution of endotoxins to the $PM_{2.5}$ mixture toxicity and, at the same time, echo previous opinions that metals dominate the oxidative potential induced by typical ambient $PM_{2.5}$ samples (Charrier and Anastasio, 2012; Lyu et al., 2018). Different from previous studies, PAHs did not serve as a major toxic contributor in this

study. One reason may be the significant decrease in their mass concentrations following the implementation of the Air Pollution Prevention and Control Action Plan since 2013. There are notable similarities in the dominant contributors identified by this *in vitro* assay and those determined by the existing USEPA health risk assessment protocol (Figure **6-9**). Mn was the primary contributor to intracellular oxidative stress, followed by Fe. Similarly, Mn was also the dominant contributor to NCR. While as to CR, Cr was the dominant contributor. For PAHs, DahA was the dominant contributor to both intracellular oxidative stress and ECR. The alignment between *in vitro* assay results and established health risk assessment protocols supports the relevance of these findings to human health, emphasizing the importance of specific $PM_{2.5}$ components such as Fe, Mn, Cr and DahA in driving biological toxicity and associated health outcomes. Comparison of toxicity contributions and mass contributions to $PM_{2.5}$ of each component are shown in Figure **6-10**. The toxicity contribution of endotoxins was 100,000 times greater than their contribution to the $PM_{2.5}$ mass. The toxicity contribution of trace metals was approximately 10 –1,000 times their mass contribution, and for PAHs, it was approximately 10 times. The disparity between mass contribution and toxicity contribution of a component has also been observed in previous studies. For example, the toxicity contribution of PAHs ranged from 58 to 592 times their mass contribution (Chen et al., 2024), and was about 421 times in another study (Jin et al., 2019). As for trace metals, the factor was approximately 5 times (Jin et al., 2019). The contribution of an individual component to the overall $PM_{2.5}$-induced ROS depends on both the mass concentration of the component and its REP. For example, as the most abundant component among analyzed toxic composition, the mass concentration of Fe was approximately 6.54×10^4 times that of endotoxins, which is comparable to the findings of previous studies (Moretti et al., 2019; Shen et al., 2024). However, the REP of endotoxins was around 3.70×10^4 times that of Fe, which resulted in comparable toxic contributions of Fe (6.86–13.8%) and endotoxins (4.24–12.2%) to the overall ROS generation. These results indicate that mass contribution does not equate to the

toxicity contribution of $PM_{2.5}$. Even though components like endotoxins are a small fraction in $PM_{2.5}$ compared to elements like Fe and Zn, they still stimulate ROS generation on a large scale. This finding reveals the importance of endotoxins in inducing $PM_{2.5}$ ROS generation and quantifies the contribution of endotoxins to the $PM_{2.5}$-induced ROS for the first time. Thus, in future, much more attention should be paid to biological components when evaluating $PM_{2.5}$-induced toxicity and control policies.

Table 6-1. Correction Ratio of analyzed components extracted by MilliQ water and methanol for cell exposure.

Component	Correction Ratio %	SD%	Component	Correction Ratio %	SD%
As	57.5	14.7	**FLA**	58.3	6.61
Cd	70.0	11.1	**BaA**	83.3	6.94
Co	80.7	18.3	**Chr**	65.4	10.2
Cr	15.1	8.46	**BbF**	57.2	5.34
Cu	71.1	14.1	**BkF**	46.5	4.13
Fe	51.0	12.5	**BaP**	68.1	3.90
Mn	47.8	14.1	**DahA**	93.3	6.47
Ni	83.0	20.1			
Pb	56.9	12.5			
V	57.3	15.3			
Zn	79.6	10.5			
Endotoxins	91.6	6.68			

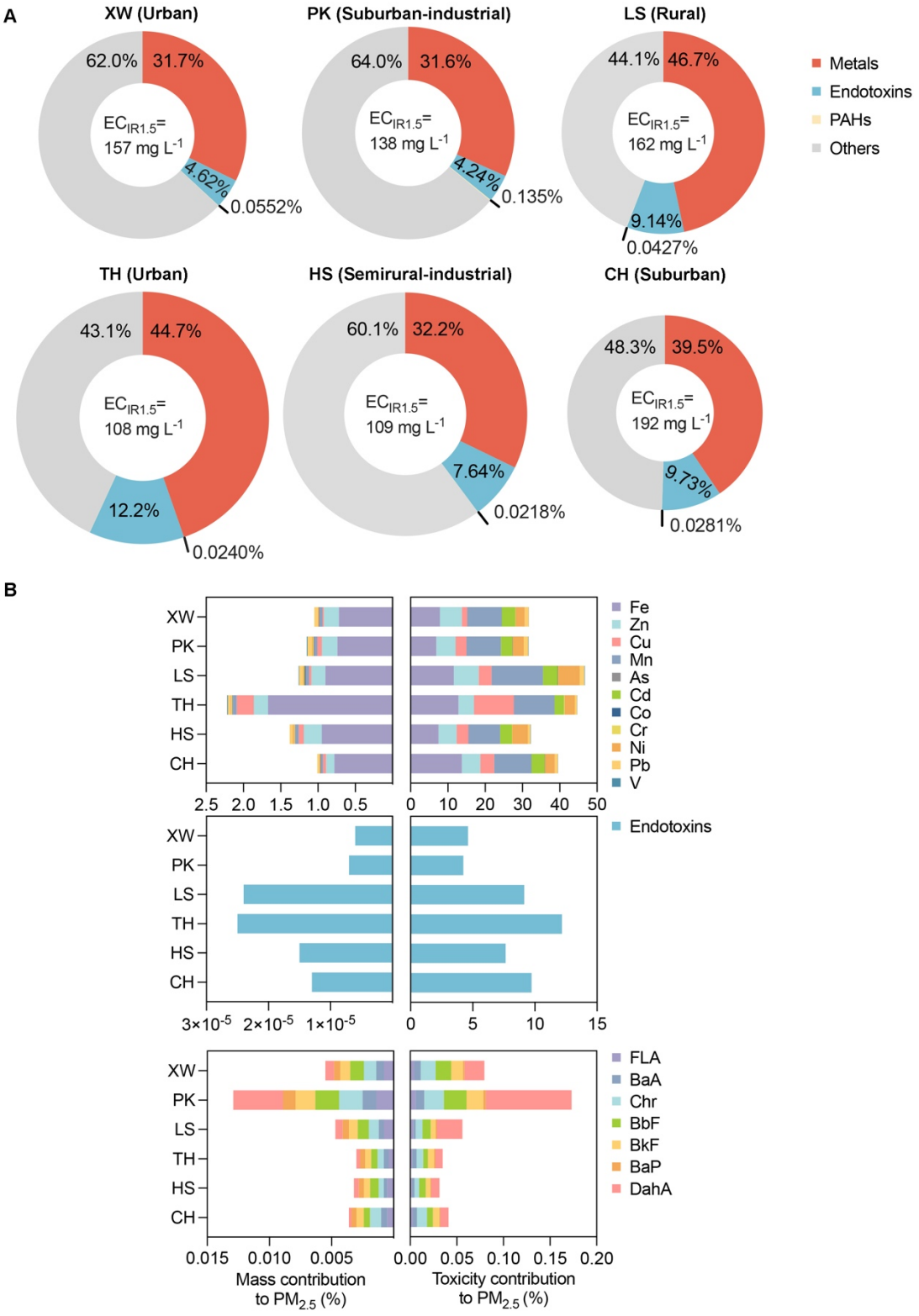

Figure 6-8. (A) Relative contributions from trace metals, endotoxins, and PAHs to intracellular oxidative stress induced by $PM_{2.5}$ in six sites in Nanjing (XW, PK and LS) and Guangzhou (TH, HS and CH). The size of the pie chart represents the toxic potency of the $PM_{2.5}$ at each site. The larger the pie chart, the more toxic the $PM_{2.5}$ from the

sampling site. The detailed derivation can be found in Appendix 2. (B) Mass contributions (left panel) and toxic contributions (right panel) of individual trace metals, endotoxins, and individual PAHs at the six sampling sites in Nanjing and Guangzhou.

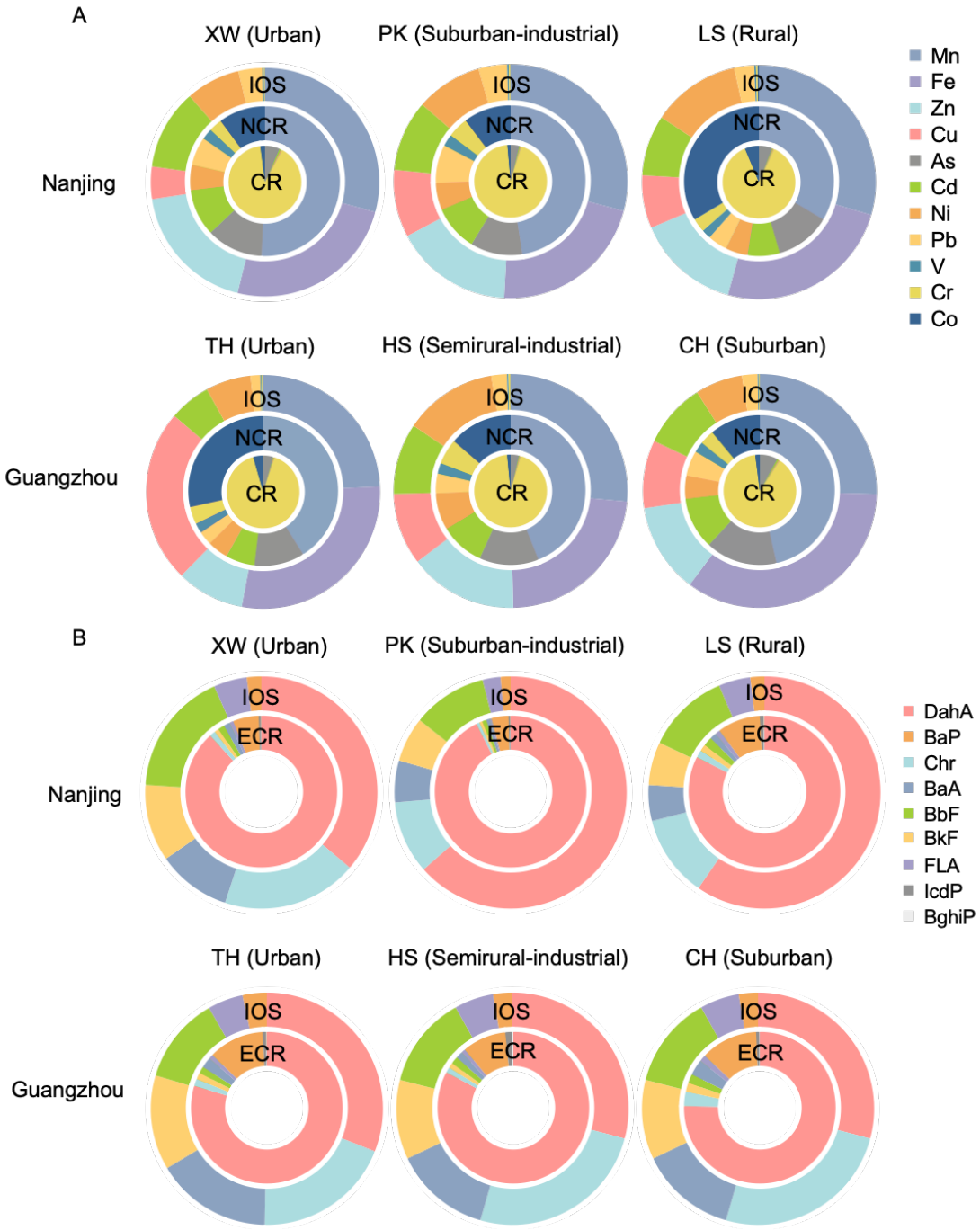

Figure 6-9. Comparisons between contributions of individual components to intracellular oxidative stress (IOS) and (A) CR and NCR, and (B) ECR.

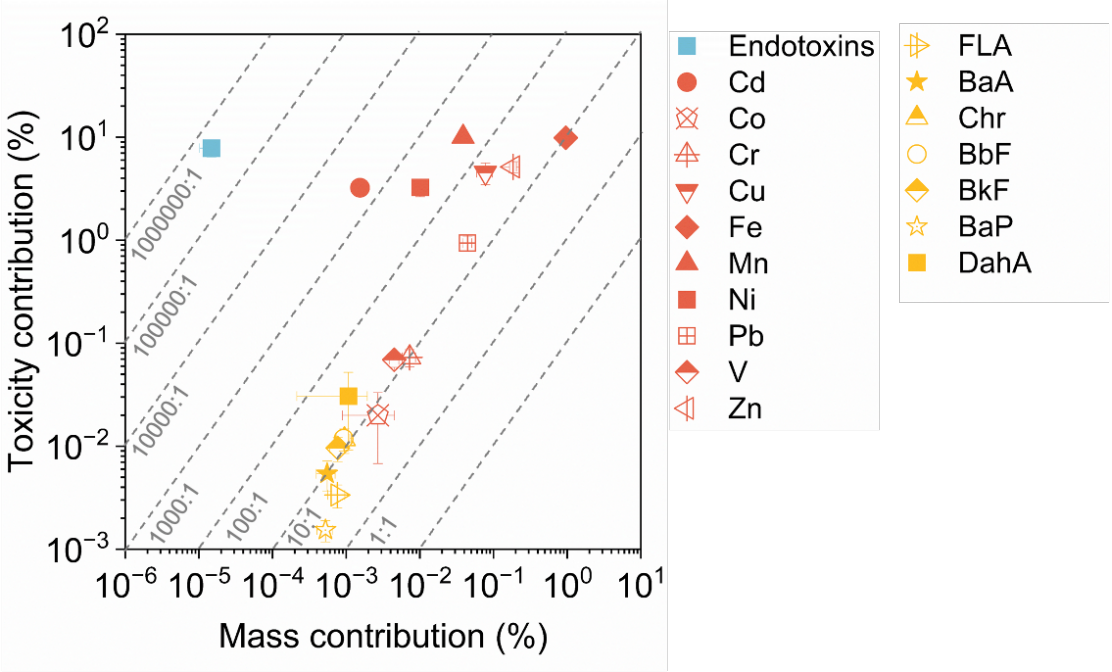

Figure 6-10. Comparisons of toxicity contributions and mass contributions to $PM_{2.5}$ of trace metals, endotoxins, and PAHs.

6.4 Contributions of emission sources to $PM_{2.5}$ mass and intracellular oxidative stress

To further investigate the emission sources of $PM_{2.5}$ and their contributions to $PM_{2.5}$-induced intracellular oxidative stress at each sampling site, the PMF model was applied based on major $PM_{2.5}$ components, including trace metals, WSI, OC/EC, and endotoxins. The combined composition input data of three sites in Nanjing and three sites in Guangzhou are shown in Figures **4-3** and **6-11**. The resolved source profiles are presented in Figure **6-12**. After excluding data that resulted in out-of-range dots, the scaled residuals varied between -3 and +3 (the percentage of used data was over 90%). The ratio of Q (robust) to Q (true) was close to 1 (smaller than 1.5). For the majority of species, the slopes comparing predicted values to input data fell between 0.58 and 1.02, while the corresponding correlation coefficients (R^2) ranged from 0.51 to 0.98. These results indicate that the model demonstrated satisfactory performance. Notable exceptions included Al, Co, Cr, Cu, Ni, and V in the Nanjing dataset, which exhibited lower slopes (ranging from 0.02 to 0.33) and reduced R^2 values (between 0.03 and 0.29). Similarly, in the Guangzhou samples, V, Na^+, Cl, OC, EC, and Co displayed lower slopes (0.10 to 0.56) and correlation coefficients (0.12 to 0.50). These outcomes may be attributed to the relatively small sample sizes and the complex mixture of sources contributing to these elements (Zeng et al., 2019). The subsequent analysis using the F-peak model produced a G-space plot with poor factor correlations, reflecting little presence of rotational ambiguity. Summary of error estimation results, and bootstrap (BS) mapping of Nanjing and Guangzhou samples are shown in Appendix 2. In general, the BS runs were performed 100 times. Most bootstrapped factors explicitly mapped to factors resolved in the base solution. No error was found in the DISP assessment. The drop in Q value was less than 1%.

Eight source factors were identified for Nanjing and Guangzhou respectively. Factors 1 of $PM_{2.5}$ in both Nanjing and Guangzhou were identified as combustion (coal, biomass and waste), dominated by trace metals like As, Cd and Pb, OC/EC, and some other trace metals, representing coal combustion and waste incineration. K^+ was the marker of biomass burning. Factor 2 of Nanjing $PM_{2.5}$ had high a abundance of SO_4^{2-} and NH_4^+, which could be markers of secondary sulfate formation. Factor 2 of Guangzhou $PM_{2.5}$ was ship emissions mixed with secondary sulfate characterized by abundant Ni and V, OC/EC, and high loadings of SO_4^{2-}. Factors 3 of Nanjing and Guangzhou, with high abundance of NO_3^- and the presence of NH_4^+ and other ions were characterized as secondary nitrate. Factors 4 of $PM_{2.5}$ in both Nanjing and Guangzhou represented fugitive dust, considering their rich abundance of Al, Fe, Mn, Mg^{2+}, Ca^{2+}, and the presence of other trace metals. Factors 5 of $PM_{2.5}$ in both Nanjing and Guangzhou were characterized as biological emissions, considering the extremely high abundance of endotoxins. Factor 6 of Nanjing was traffic emissions, including vehicle emissions and ship emissions, considering high loadings of Cu and other trace metals, and OC/EC, which are usually markers of vehicle emission. V, Ni and OC/EC are markers of ship emissions which majorly consume heavy oil. Factor 6 of Guangzhou was vehicle emissions, which was identified by the high loadings of Cu and OC/EC. Concentrations of hopanes and steranes were not measured in this study. Including these and other organic components would make the identification of traffic emissions more accurate. Factors 7 of both Nanjing and Guangzhou were sea salts, with high abundance of Na^+, Mg^{2+}, Ca^{2+}, and the presence of Cl^-. Factors 8 in both cities were industrial emissions, characterized by high loadings of trace metals like Cd, Co, Cr, Cu, Pb, V and Zn, and low abundance of OC/EC.

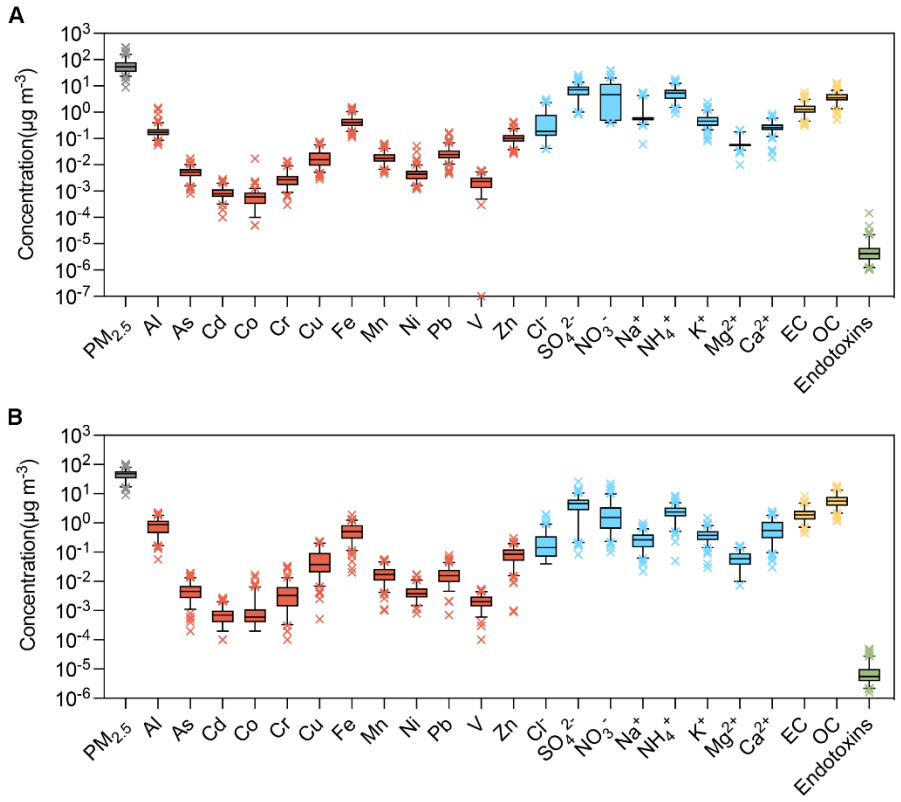

Figure 6-11. Concentration distributions of $PM_{2.5}$ and individual components in $PM_{2.5}$ from (A) Nanjing and (B) Guangzhou. The box plots with whiskers present the mean with a 95% CI.

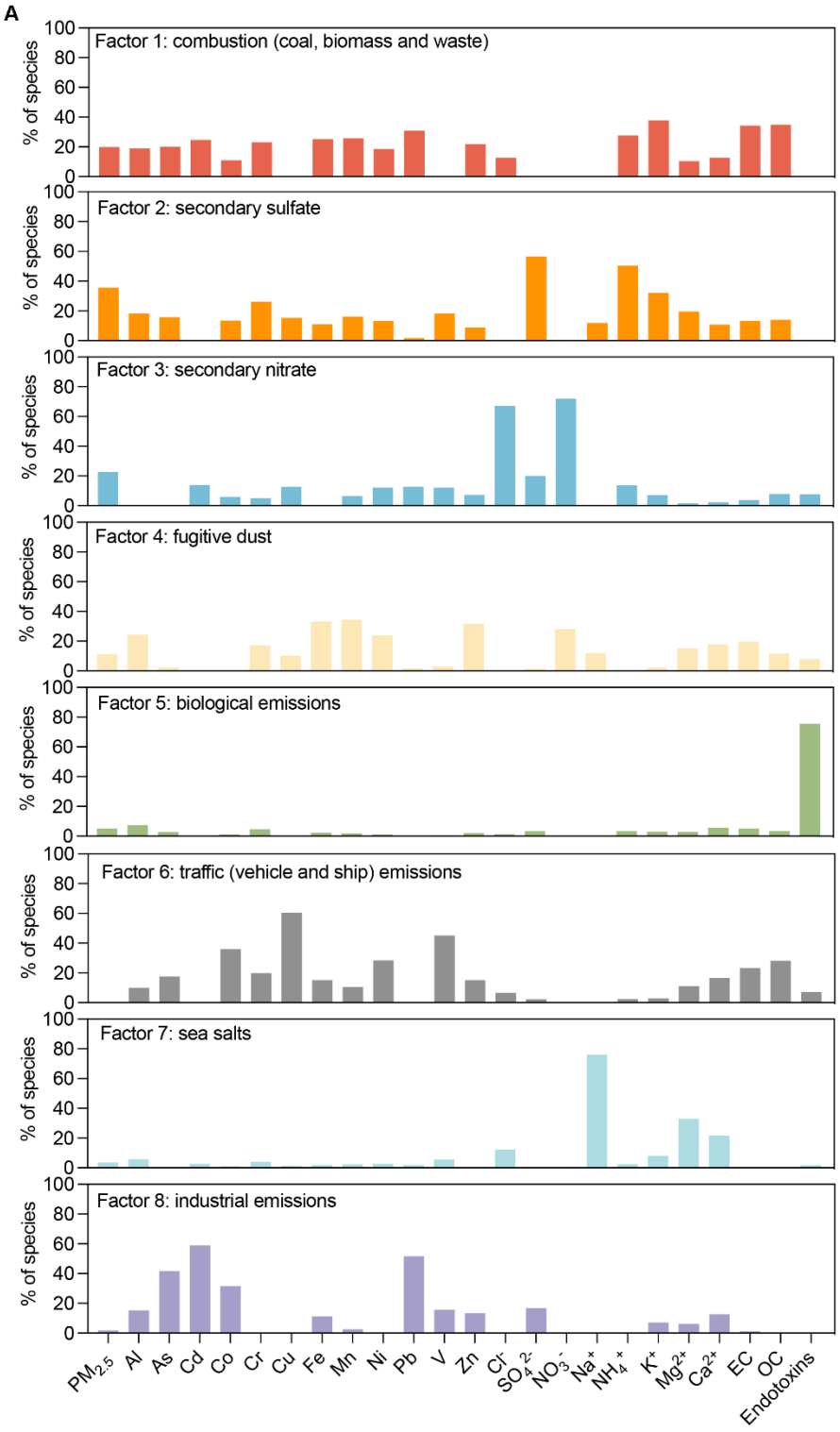
A
Factor 1: combustion (coal, biomass and waste)
Factor 2: secondary sulfate
Factor 3: secondary nitrate
Factor 4: fugitive dust
Factor 5: biological emissions
Factor 6: traffic (vehicle and ship) emissions
Factor 7: sea salts
Factor 8: industrial emissions
% of species
0
20
40
60
80
100
PM2.5
Al
As
Cd
Co
Cr
Cu
Fe
Mn
Ni
Pb
V
Zn
Cl-
SO4 2-
NO3-
Na+
NH4+
K+
Mg2+
Ca2+
EC
OC
Endotoxins

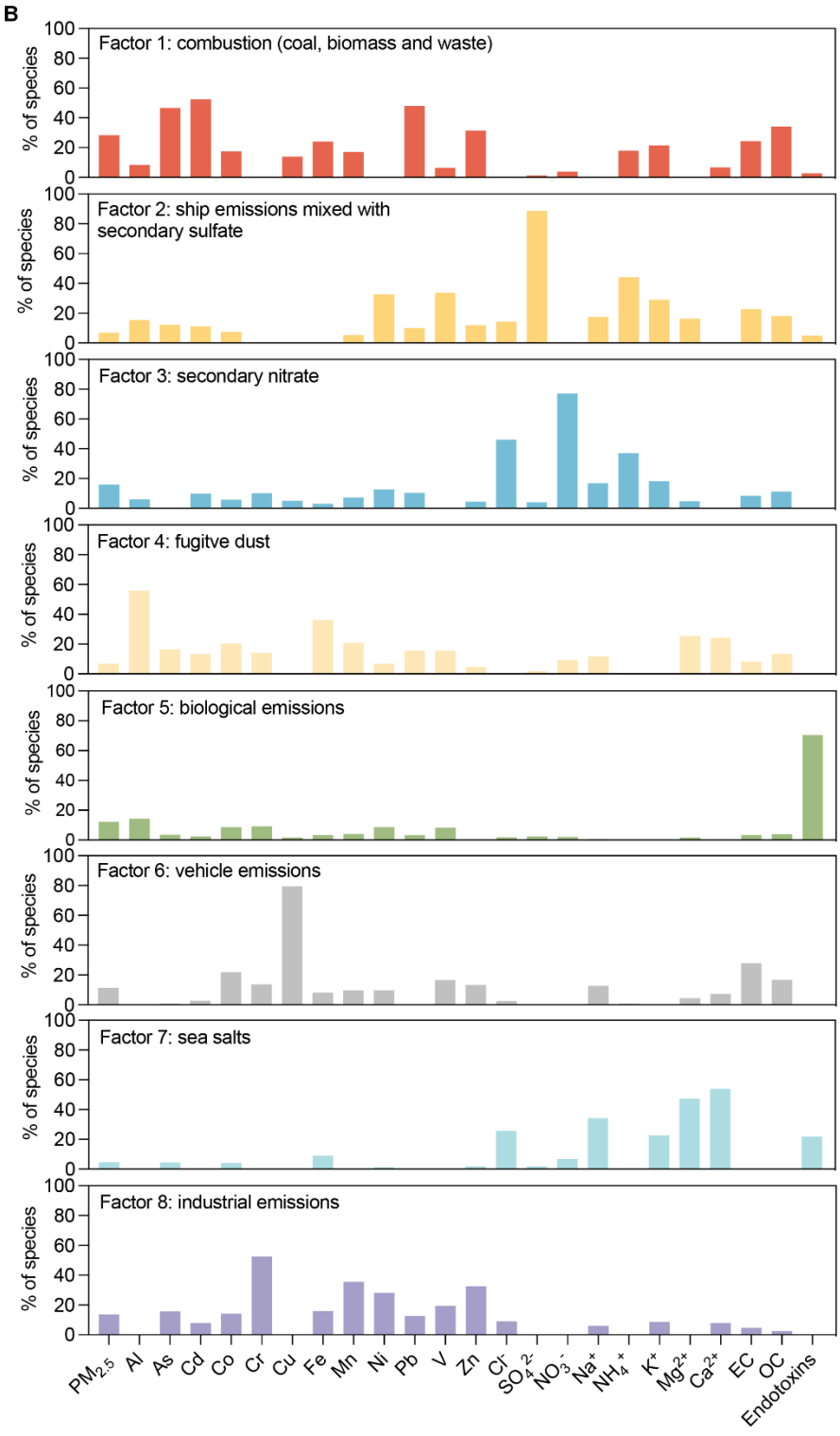

Figure 6-12. Resolved source profiles of major components in $PM_{2.5}$ from (A) Nanjing and (B) Guangzhou. The colored bars represent the percentage of certain species contributed by certain sources.

Overall, ten sources contributed to $PM_{2.5}$ mass in these two cities: secondary nitrate, secondary sulfate, fugitive dust, combustion (coal, biomass, and waste), traffic (vehicle and ship) emissions, vehicle emissions, ship emissions mixed with secondary sulfate, industrial emissions, sea salts, and biological emissions (Figure **6-13**). Notably, the dominant mass contributors differed significantly from the key toxicity drivers, with distinct spatial patterns observed between cities. In Nanjing, secondary aerosol (secondary nitrate and sulfate) and combustion were dominant sources of $PM_{2.5}$ mass, contributing 47.3–62.3% and 10.6–33.8%, respectively. Similar results were also reported in previous studies (Li et al., 2016; Xie et al., 2020; Zheng et al., 2019). However, toxicity apportionment identified fugitive dust (23.2–24.6%) and combustion (19.0–20.5%) as the primary contributors to $PM_{2.5}$-induced intracellular oxidative stress. Biological emissions also contributed significant proportions to the $PM_{2.5}$-induced toxicity across three sites in Nanjing, ranging from 10.3% to 12.7%. In contrast, Guangzhou exhibited different patterns: in the urban (TH) site, vehicle emissions (21.1%) were the dominant source of $PM_{2.5}$ mass, while combustion dominated in the semirural-industrial (HS) (29.0%) and suburban (CH) (19.9%) sites, aligning with the findings of previous studies (Guangzhou Municipal Ecological Environment Bureau, 2019; Xie et al., 2020; Zhou et al., 2018). The spatial distribution of toxic sources in Guangzhou exhibited stronger land-use differentiation compared to Nanjing, revealing distinct source-specific patterns across anthropogenic gradients. Vehicle emissions (19.8%) were the dominant toxic source in the urban (TH) site, followed by biological emissions (18.4%) and combustion (17.0%). Comparable proportions from industrial emissions (18.4%) and combustion (18.5%) were the primary toxic contributors to the semirural-industrial (HS) site, slightly exceeding biological emissions (16.6%). Biological emissions (20.0%) were the largest toxic contributor in the suburban (CH) site, followed by combustion (18.4%) and industrial emissions (16.1%). This study highlights the significant role of biological emissions in contributing to $PM_{2.5}$ mass and

toxicity, accounting for 2.71–17.4% and 10.3–20.0%, respectively. This is the first quantitative evidence linking bioaerosols (via endotoxin markers) to $PM_{2.5}$-induced intracellular oxidative stress, extending current understanding by establishing biological components as persistent contributors to toxicity. Although previous studies demonstrated that $PM_{2.5}$ components from traffic emissions promoted *in vitro* cellular response to oxidative stress in Beijing (Xu et al., 2020), and proved that industry and soil sources were strongly correlated with ROS activity in Seoul (Park et al., 2018), these findings uniquely link $PM_{2.5}$-induced intracellular oxidative stress with $PM_{2.5}$ mass sources. This allows for a quantitative assessment of the toxicity-related sources of $PM_{2.5}$ in different regions of China, revealing that $PM_{2.5}$ mass sources do not equate to toxicity sources. Such disparities in mass sources and toxicity sources of $PM_{2.5}$ were also observed in previous studies that assessed the health risks of $PM_{2.5}$-related metals (Yan et al., 2022). It is evident that the key toxic components in $PM_{2.5}$ that induce *in vitro* toxicity can originate from specific dominant sources, providing valuable guidance for developing strategies to effectively control $PM_{2.5}$ emissions in accordance with local conditions.

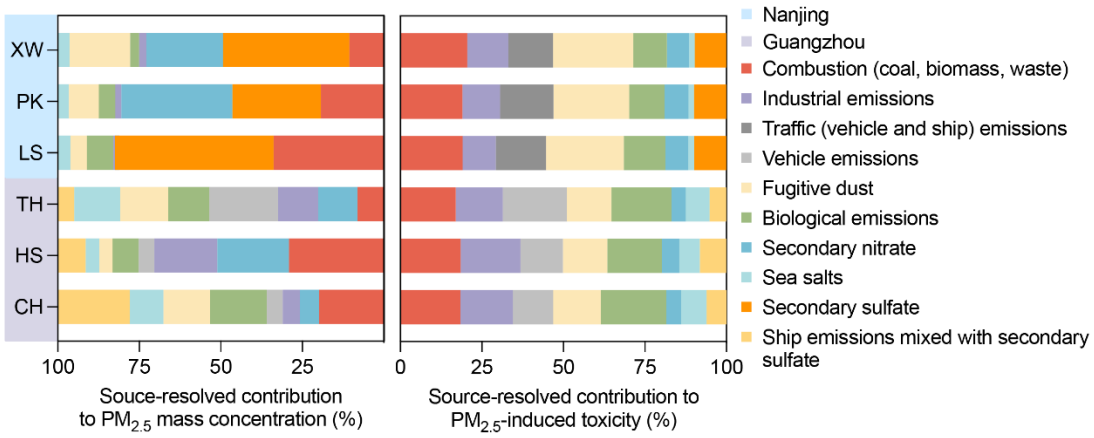

Figure 6-13. Source-resolved contributions to $PM_{2.5}$ mass (left panel) and $PM_{2.5}$-induced intracellular oxidative stress (right panel).

In recent years, evidence has accumulated suggesting that reducing mass concentrations of PM may not lower oxidative potential, and if oxidative potential is linked to major health impacts, targeting specific sources could be more effective than reducing overall particulate mass (Daellenbach et al., 2020). In this section, endotoxins, a significant biological component of $PM_{2.5}$, were found to play a crucial role in inducing intracellular oxidative stress, even though they constitute only a small fraction compared to $PM_{2.5}$-related trace metals. Aside from the quantified contribution of endotoxins to the $PM_{2.5}$ mixture toxicity, this chapter also identified and quantified biological emissions as a possible $PM_{2.5}$ toxic source for the first time, together with other well-known sources (*e.g.*, vehicle emissions, industrial emissions, combustion), highlighting the importance of $PM_{2.5}$-related biological emissions. This section calls for a broader perspective on air quality regulations that include biological and chemical components and suggests that regulatory frameworks should incorporate component-specific and source-specific toxicity assessments. This could lead to more effective pollution mitigation strategies that better protect public health by targeting the most harmful components and sources of $PM_{2.5}$.

Previous studies often assessed the chemical oxidative potential of airborne endotoxins using acellular assays, such as the dithiothreitol (DTT) assay (Yue et al., 2018). These chemical-based, cell-free methods only measure the redox activity of substances in a simplified environment without accounting for real biological processes. Some PM components (*e.g.*, transition metals, organic compounds) may react strongly with DTT (Guo et al., 2020; Lin and Yu, 2019) but are less affected in biological systems due to the existence of antioxidants (Bates et al., 2019). In contrast, the *in vitro* cellular assays of this section can incorporate complex biological interactions, providing a more comprehensive understanding of the oxidative potential of endotoxins and other $PM_{2.5}$ components. The BEAS-2B human bronchial epithelial cell model closely resembles bronchial mucosa in terms of transcript profiling, making it one of the most relevant *in*

vitro models for studying the metabolism and bioactivation of toxicants and drugs in the bronchial epithelium (Courcot et al., 2012). Although such *in vitro* methods cannot fully predict the toxicity of $PM_{2.5}$ and its composition, they complement previous cell-free analyses and help provide a simple yet comprehensive understanding of $PM_{2.5}$ mixture toxicity and the role that endotoxins play in it. The realistic daily exposure to endotoxins in Guangzhou $PM_{2.5}$ may pose a potential toxicity to humans, implying that the airborne endotoxins levels were sufficient to cause health impacts even with daily exposure, highlighting the urgent need to establish a threshold for airborne endotoxins exposure.

Numerous studies have examined $PM_{2.5}$ emission sources in China (Xu et al., 2019; Zhang et al., 2013; Zhang et al., 2024b), and some studies have linked the oxidative potential of $PM_{2.5}$ to quantified emission sources using model-based estimations (Grange et al., 2022; Zhang et al., 2024a), but the causality of the identified sources (and PM constituents) in driving oxidative potential could be questioned because the underlying biological mechanisms were not included. In this section, we identified the toxic potency of each determined component and verified how their mixtures perform in the CA model before quantifying their toxic contributions and source contributions to toxicity, to ensure the full consideration of the unique toxic potencies of different components and their interactions in mixtures.

Current air quality management strategies often focus on reducing $PM_{2.5}$ mass and neglect the specific toxicities of its components and toxic sources, which can lead to a cost-benefit imbalance in pollution mitigation efforts. These findings, supported by recent studies, suggest that both key toxic components, such as metals and endotoxins, and key toxic emission sources, including bioaerosols, should be prioritized in regulations.

6.5 Summary

Chapter 6 investigates how the chemical and biological composition and sources of $PM_{2.5}$ influence its toxicity in Nanjing and Guangzhou. The chapter combines *in vitro* cellular assays and source apportionment to evaluate the contributions of specific $PM_{2.5}$ components and sources to intracellular oxidative stress. The study highlights spatial heterogeneity in $PM_{2.5}$ composition and toxicity across different land-use types and cities, quantifies the toxic contributions of individual components, and uses source apportionment modeling to link emission sources to both $PM_{2.5}$ mass and toxicity. The major findings of chapter 6 are listed below:

1. Spatial heterogeneity in $PM_{2.5}$ composition was observed, with Guangzhou exhibiting significantly higher concentrations (normalized to $PM_{2.5}$ mass) of endotoxins and trace metals, while Nanjing had higher levels of PAHs, particularly in the suburban-industrial site. Within each city, urban and industrial areas generally showed higher concentrations of analyzed components compared to suburban or rural sites.

2. The toxicity associated with $PM_{2.5}$ is not directly proportional to its mass concentration. Components present in higher concentrations do not necessarily contribute most to toxicity. Instead, specific chemical and biological composition of $PM_{2.5}$ plays a critical role in determining its toxic potency. The research demonstrated that endotoxins, trace metals, and PAHs together accounted for 35.9–56.9% of the $PM_{2.5}$-induced intracellular oxidative stress, despite representing only a small fraction of the total $PM_{2.5}$ mass. Among these, metals were the dominant contributors to oxidative stress, followed by endotoxins, and then PAHs. Notably, endotoxins had a disproportionately high contribution to toxicity relative to their mass. Specific metals such as Fe and Mn, as well as PAHs like DahA, BbF, BkF, and Chr, were identified as key toxic drivers. The findings also revealed that the toxicity contribution of these

components was greater than their mass contribution, emphasizing that health risk assessments and control strategies should focus on specific toxic components rather than on total $PM_{2.5}$ mass.

3. Source apportionment analysis revealed that the sources contributing most to $PM_{2.5}$ mass were not always the same as those driving toxicity. In Nanjing, secondary aerosols and combustion were the main contributors to $PM_{2.5}$ mass, but fugitive dust and combustion were the primary sources of toxicity. In Guangzhou, vehicle emissions were the main source of $PM_{2.5}$ mass in the urban area, while combustion dominated in the semirural-industrial and suburban sites. The sources of $PM_{2.5}$ toxicity showed even greater land-use differences in Guangzhou: with vehicle emissions as the leading toxic source in the urban site, industrial emissions and combustion as the most important in the semirural-industrial site, and biological emissions as the largest contributor to toxicity in the suburban site. Biological emissions, as indicated by the endotoxin marker, were found to be significant contributors to both $PM_{2.5}$ mass and toxicity, providing the first quantitative evidence of their role in $PM_{2.5}$-induced oxidative stress.

In conclusion, Chapter 6 follows the chemical characterization (Chapter 4) and biological profiling (Chapter 5) of $PM_{2.5}$ to provide an integrated assessment of its toxicological impacts. By demonstrating that oxidative stress associated with adverse health effects is driven more by specific toxic components (*e.g.*, trace metals, endotoxins, and PAHs) than by total $PM_{2.5}$ mass, this chapter emphasizes the importance of component-specific evaluation for effective air quality management. Moreover, Chapter 6 provides the first quantitative evidence of the disproportionate toxic contributions from biological emissions, particularly endotoxins, thereby stressing the need to include biological factors in future $PM_{2.5}$ health risk assessments. The source apportionment analysis further highlights that emission sources responsible for $PM_{2.5}$ mass are not always consistent with those driving toxicity, highlighting the

necessity of adjusting control strategies to targeted key toxic sources, including combustion, vehicular emissions, and biological emissions.

Chapter 7 Conclusions and Recommendations

7.1 Overall summary and major conclusions

The overall aim of this study is to comprehensively characterize the chemical and biological composition of $PM_{2.5}$ in Nanjing and Guangzhou (two megacities in China), assess its spatial and temporal variations, identify its sources, evaluate the associated health risks and toxicity, and inform targeted air pollution control strategies for public health protection. Chapter 4 aims to analyze the spatial and temporal variations in $PM_{2.5}$ concentrations and chemical composition across six sites representing different land-use types in both cities, and to assess the health risks associated with $PM_{2.5}$-bound toxic components. This chapter presents detailed comparisons of $PM_{2.5}$ concentrations and chemical profiles, evaluates CR, NCR and ECR posed by metals and PAHs, and examines long-term trends of $PM_{2.5}$ to assess the effectiveness of air pollution control policies. Chapter 5 focuses on the biological components of $PM_{2.5}$, specifically endotoxins and bacterial community profiles, aiming to compare their concentrations and diversity between and within cities, explore their relationships with chemical constituents, and analyze the correlations between bacterial taxa and endotoxins. Chapter 6 investigates how the chemical and biological composition and sources of $PM_{2.5}$ influence its toxicity in Nanjing and Guangzhou, combining *in vitro* cellular assays and source apportionment modeling to quantify the contributions of specific $PM_{2.5}$ components and emission sources to intracellular oxidative stress. Each chapter thus addresses a key aspect, namely chemical composition and health risk characterization, biological profiling, and toxicity/source analysis, contributing to a comprehensive understanding of $PM_{2.5}$ pollution and its implications for air quality management and public health. The major findings and conclusions of this thesis are listed below.

1. Residents in both Nanjing and Guangzhou were exposed to $PM_{2.5}$ concentrations exceeding WHO guidelines for most of the year, with urban and industrial areas

generally experiencing higher pollution and health risks than rural or suburban sites. Seasonal peaks in pollution were observed in autumn and winter, reflecting the influence of human activities and meteorological conditions.

2. The chemical composition of $PM_{2.5}$ showed clear regional and land-use differences: Nanjing was characterized by higher proportions of secondary aerosols and PAHs (especially in industrial areas), while Guangzhou had higher levels of carbonaceous material, trace metals, and endotoxins, particularly in urban sites. These differences were linked to local emission sources and climatic conditions.

3. Trace metals and PAHs, although minor in mass, posed significant health risks, with Cr and Mn being the main contributors to CR and NCR, respectively, and DahA dominating PAH-related ECR. All sites exceeded health risk thresholds for metal-induced CR and PAH-induced ECR, highlighting the importance of component control in air pollution regulation.

4. Abundance of biological components in $PM_{2.5}$, especially endotoxins and Gram-negative bacteria, was closely associated with certain chemical components (*e.g.*, trace metals, WSI).

5. The toxicity of $PM_{2.5}$, as measured by *in vitro* oxidative stress assays, was not directly proportional to $PM_{2.5}$ mass concentration. Instead, specific components, trace metals and endotoxins, were identified as the key drivers of toxicity, with their toxic contributions far exceeding their mass fractions. This finding highlights the inadequacy of using $PM_{2.5}$ mass alone as a standard for toxicity analysis.

6. Source apportionment revealed that the sources contributing most to $PM_{2.5}$ mass (*e.g.*, secondary aerosols, combustion, vehicle emissions) were not always the same as those

driving toxicity. Biological emissions, fugitive dust, and industrial or traffic sources played an important role in oxidative stress induction, indicating that targeted source control is essential for effective health risk reduction.

7.2 Limitations and future outlook

This study offers a comprehensive assessment of $PM_{2.5}$ pollution in the Chinese megacities of Nanjing and Guangzhou by integrating both chemical and biological analyses and evaluating component- and source-specific contributions to toxicity. This approach extends beyond the scope of many previous studies, which have largely focused on the toxicity induced by $PM_{2.5}$-bound chemical constituents alone. However, the current study has several limitations, including insufficient components analysis, choice of toxic endpoints and source tracker models, experimental techniques applied, and so on. These limitations, along with corresponding recommendations for future research, are briefly discussed below.

First, our extraction method introduces some quartz fiber debris (16.2 ± 3.03%), does not remove insoluble particles, and may miss certain hydrophobic compounds, which could potentially affect the accuracy of toxicity analysis. Advanced approaches like cyclonic separation (Honda et al., 2021), which collect $PM_{2.5}$ in powder form for cell exposure, should be considered in future research.

Second, a single correction ratio value was applied to each metal across all samples in this study, due to sample limitations. It is acknowledged that metal solubility in $PM_{2.5}$ can vary depending on aerosol pH, anion concentrations (*e.g.*, nitrate and sulfate), and chelating agent concentrations (*e.g.*, oxalate) (Song et al., 2003; Taira et al., 2020). Therefore, using a uniform correction ratio for all samples may not fully account for sample-specific variations in metal solubility. However, the observed variation in correction ratios among the analyzed extracts was relatively low and is unlikely to

significantly affect the conclusion that metals are the dominant contributors to $PM_{2.5}$-induced oxidative stress in this study. Future work should aim to analyze correction ratios for individual samples to improve accuracy and better account for chemical variability.

Third, this study did not account for oxidative stress induced by insoluble components like EC (Zou et al., 2016), biological components such as proteins and β-glucans (Li et al., 2023; Li et al., 2022), or specific PAH derivatives (oxygenated, nitrated, and alkylated PAHs) (Wang et al., 2022; Zhang et al., 2024c) due to limited time and resources. These unmeasured components may also be important toxic contributors to the unexplained fraction of $PM_{2.5}$-induced toxicity.

Fourth, although BEAS-2B cells are a widely used epithelial cell line relevant to respiratory exposure to $PM_{2.5}$, they do not respond like A549, Calu-3, and other pulmonary cell lines, resulting in limitations in the toxic reaction (Salana et al., 2024). Additionally, PAHs are known to cause genotoxicity, DNA damage, inflammatory responses (Bekki et al., 2016; Santibáñez-Andrade et al., 2023; Wierzbicka et al., 2022) and endotoxins are recognized for their role in activating inflammatory responses (Yoda et al., 2019). By focusing only on oxidative stress, this study may have underestimated the toxicity induced by PAHs and endotoxins associated with these pathways. A broader range of biological endpoints, such as apoptosis, genotoxicity and inflammatory response, are needed in future studies for a more comprehensive understanding of $PM_{2.5}$-induced toxicity.

In addition, biological sources in this study were identified solely by endotoxins, which do not capture the full spectrum of bioaerosol constituents, such as Gram-positive bacteria, fungi, spores, and pollen. Compared to the chemical fraction of $PM_{2.5}$, the biological components remain significantly underexplored. Biological sources of $PM_{2.5}$

can be further traced to plants, soil, farms, livestock, hospitals, wastewater treatment facilities, and other related environments (Basinas et al., 2015; Liu et al., 2018b; Schaeffer et al., 2017; Wang et al., 2018; Zhang et al., 2019). This represents an important perspective for future studies. Although the study characterized bacterial community profiles and endotoxins in both cities, endotoxins alone cannot fully explain the toxicity of Gram-negative bacteria. Moreover, the health effects of specific bacterial taxa remain unclear. While Gram-negative bacteria are considered to induce stronger health effects in some studies (Jalava et al., 2015), Gram-positive bacteria remain important as possible pathogens, particularly in immune compromised individuals (Karimi et al., 2020). A more comprehensive analysis of $PM_{2.5}$-bound biological components is needed to improve health risk assessments.

Finally, the study employed the CA model to evaluate the combined toxicity of $PM_{2.5}$ mixtures. Although widely used, the CA model assumes that all components share a common mode of action and exhibit linear dose-response relationships. It cannot account for synergistic, antagonistic, or independent effects, nor for nonlinear interactions and metabolic transformations (Cedergreen et al., 2008; Kim et al., 2022). These limitations can lead to inaccurate toxicity predictions, especially in complex mixtures with numerous components and varying exposure conditions. To enhance the reliability of mixture toxicity evaluations, alternative models like the independent action (IA) model, mechanism-based models, and systems toxicology approaches, along with probabilistic assessments such as Monte Carlo simulations, can be adopted in future studies. Further research should, therefore, explore a broader range of toxicological endpoints and component profiles, including bacterial taxa associated with endotoxins, while employing more advanced and mechanistically relevant toxicity models. These efforts will contribute to a more comprehensive understanding of $PM_{2.5}$ toxicity and help identify its most harmful constituents and emission sources, supporting evidence-based air quality regulation and public health protection.

Although limitations were identified in component analysis, experimental techniques, toxicity endpoints, and modeling approaches, these highlight clear opportunities for future research. Enhancing exposure models, expanding the range of toxicological endpoints, and improving mixture toxicity assessment methods will be critical for advancing health risk evaluation and supporting more effective air quality management strategies.

Appendix 1

1.1 Description of the sampling sites.

City	District	Land-use type	Sampling site	Description
Nanjing (Eastern China)	Pukou	Suburban-industrial	Nanjing University of Information Science and Technology	Sampling site at the rooftop of a twelve-floor building; surrounded by petrochemical plants, steel plants and highways; mixed industrial-residential areas
	Xuanwu	Urban	Institution of Soil Science, Chinese Academy of Sciences	Sampling site at the rooftop of a five-floor building; downtown area surrounded by school, residential, and commercial buildings, with complex traffic networks
	Lishui	Rural	Lishui Fujiabian Agricultural Science and Technology Park	Sampling site on the ground; distant from main roads, with massive vegetation cover
Guangzhou and its surrounding areas (Southern China)	Tianhe	Urban	Guangzhou Institution of Geochemistry, Chinese Academy of Sciences	Sampling site at the rooftop of a five-floor building, adjacent to two expressways with heavy traffic, and surrounded by dwellings and schools
	Conghua	Suburban	Tianhu Park	Sampling site on the ground upon a hill; located in a recreation area around 60 km northeast from Guangzhou downtown areas
	Heshan	Semirural-industrial	Guangdong Atmospheric Monitoring Supersite of China	Sampling site at the rooftop of a four-floor building; located on a hill surrounded by vegetation, farmlands and country roads in the vicinity, as well as some industrial activities and highways in the outer space

1.2. Demographic and economic information of the sampling districts.

City	Land-use type	District	Area (km^2)	Residential Population (1000 capita)	Population Density (capita km^{-2})	Urbanization ratio (population) (%)	GDP (billion RMB)	Percentage of GDP (%)			GDP Density (million RMB km^{-2})		
								Primary Industry	Secondary Industry	Tertiary Industry	Primary Industry	Secondary Industry	Tertiary Industry
Nanjing (Eastern China)	Urban	Xuanwu	75	634	8646	100	79.6	0	4.48	95.52	0.00	47.55	1013.79
	Suburban-industrial	Pukou	910	769	823	69.87	88.5	4.68	47.96	47.37	4.55	46.64	46.07
	Rural	Lishui	1063	432	399	25.69	64.2	6.23	51.15	42.62	3.76	30.89	25.74
Guangzhou and its surrounding areas (Southern China)	Urban	Tianhe	96	1631	16931	100	380	0.02	9.96	90.03	0.79	394.25	3563.69
	Suburban	Conghua	1974	635	322	44.81	37.5	6.75	43.83	49.43	1.28	8.33	9.39
	Semirural-industrial	Heshan	1082	505	344	61.01	28.7	8.05	52.12	39.83	2.14	13.82	10.56

The statistical data was sought from (Guangdong Statistics Bureau, 2017; Jiangmen Statistics Bureau, 2017; Nanjing Municipal Statistics Bureau, 2017)

1.3. Sampling period, frequency and sample size.

Region	District	Sampling period	Sampling frequency	Sampling size
Nanjing (Eastern China)	Pukou	June 2019 – May 2020	4 – 5 samples per month	52
	Xuanwu	June 2019 – May 2020	4 – 5 samples per month	52
	Lishui	July 2019 – May 2020	1 sample per month in June, August, September, October, November and December 2019, and April and May 2020. 4 – 5 samples in July 2019 and January 2020.	18
Guangzhou and its surrounding areas (Southern China)	Tianhe	July 2019 – April 2020	3 – 5 samples per month	46
	Conghua	July 2019 – May 2020	2 – 7 samples per month	51
	Heshan	July 2019 – May 2020	2 – 6 samples per week (except November and December 2019)	38

1.4. Information about the $PM_{2.5}$ samples extracted for cell toxicity analysis.

Sampling site	Sample ID	Sampling date	$PM_{2.5}$ ($\mu g\ m^{-3}$)
Xuanwu (XW), Nanjing	XW-1	22 July 2019	66.6
	XW-2	23 July 2019	36.8
	XW-3	24 July 2019	46.1
	XW-4	27 Sep 2019	77.2
	XW-5	21 Oct 2019	95.7
	XW-6	27 Oct 2019	128
	XW-7	28 Nov 2019	32.9
	XW-8	15 Dec 2019	78.5
	XW-9	2 Jan 2020	91.8
	XW-10	5 Jan 2020	81.9
	XW-11	25 Apr 2020	56.7
Pukou (PK), Nanjing	PK-1	19 Jun 2019	115
	PK-2	20 Jun 2019	117
	PK-3	18 Jul 2019	134
	PK-4	30 Aug 2019	106
	PK-5	31 Aug 2019	99.6
	PK-6	23 Sep 2019	71.4
	PK-7	25 Sep 2019	177
	PK-8	15 Dec 2019	130
	PK-9	3 Jan 2020	235
	PK-10	4 Jan 2020	189
	PK-11	20 Apr 2020	148
	PK-12	21 Apr 2020	120
	PK-13	22 Apr 2020	150

	PK-14	26 May 2020	182
Lishui (LS), Nanjing	LS-1	17 Jul 2019	42.3
	LS-2	18 Jul 2019	27.3
	LS-3	20 Jul 2019	28.3
	LS-4	22 Jul 2019	31.9
	LS-5	30 Jul 2019	24.8
	LS-6	27 Aug 2019	32.6
	LS-7	27 Sep 2019	41.8
	LS-8	23 Oct 2019	74.1
	LS-9	28 Nov 2019	31.3
	LS-10	13 Jan 2020	150
	LS-11	16 Jan 2020	33.5
	LS-12	20 Jun 2020	22.3
Tianhe (TH), Guangzhou	TH-1	6 Aug 2019	176
	TH-2	23 Sep 2019	51.7
	TH-3	5 Oct 2019	55.0
	TH-4	17 Oct 2019	49.2
	TH-5	23 Oct 2019	68.9
	TH-6	29 Oct 2019	50.2
	TH-7	28 Nov 2019	54.5
	TH-8	10 Dec 2019	71.3
	TH-9	3 Jan 2020	65.1
	TH-10	3 Mar 2020	42.3
	TH-11	21 Mar 2020	40.3
	TH-12	8 Apr 2020	69.1
	TH-13	20 Apr 2020	36.4

	TH-14	26 Apr 2020	49.8
Conghua (CH), Guangzhou	CH-1	21 Jul 2019	25.5
	CH-2	6 Aug 2019	28.9
	CH-3	16 Aug 2019	32.5
	CH-4	20 Sep 2019	58.7
	CH-5	20 Oct 2019	51.3
	CH-6	24 Nov 2019	53.2
	CH-7	3 Jan 2020	66.5
	CH-8	8 Jan 2020	48.7
	CH-9	18 Jan 2020	52.8
	CH-10	10 Mar 2020	39.1
	CH-11	15 Mar 2020	62.1
	CH-12	9 Apr 2020	46.3
	CH-13	4 May 2020	46.6
	CH-14	9 May 2020	38.2
Heshan (HS), Guangzhou	HS-1	24 Aug 2019	67.7
	HS-2	30 Aug 2019	53.5
	HS-3	17 Sep 2019	44.6
	HS-4	5 Oct 2019	57.6
	HS-5	11 Oct 2019	54.0
	HS-6	21 Jan 2020	25.7
	HS-7	26 Feb 2020	26.0
	HS-8	3 Mar 2020	37.6
	HS-9	15 Mar 2020	62.2
	HS-10	2 Apr 2020	37.3
	HS-11	14 Apr 2020	104

1.5. Concentrations of analyzed metals per unit mass of $PM_{2.5}$ (μg mg-1)

	Al	As	Cd	Co	Cr	Cu	Fe	Mn	Ni	Pb	V	Zn
Xuanwu, Nanjing												
XW-1	2.33	0.122	0.0270	0.0120	0.0631	0.239	7.97	0.457	0.0811	0.592	0.0601	2.31
XW-2	3.43	0.212	0.0299	0.0190	0.0897	0.201	7.81	0.253	0.0625	0.612	0.0517	1.41
XW-3	3.57	0.189	0.0260	0.0130	0.0390	0.174	6.68	0.223	0.0455	0.980	0.0434	1.69
XW-4	4.10	0.0143	0.0143	0	0.0337	0.152	8.21	0.511	0.0907	0.298	0.0389	3.48
XW-5	2.85	0.0199	0.00836	0.00314	0.0136	0.106	5.49	0.328	0.0429	0.261	0.0272	2.18
XW-6	2.05	0.036	0.00705	0.00235	0.0360	0.157	5.02	0.284	0.0376	0.354	0.00392	1.40
XW-7	4.05	0.0669	0.00912	0.00608	0.0213	0.259	12.9	0.663	0.0639	0.350	0.0335	3.00
XW-8	2.28	0.0369	0.00891	0.00382	0.0140	0.208	5.59	0.188	0.0688	0.292	0.0471	1.41
XW-9	1.56	0.0338	0.00763	0.0109	0.0218	0.279	4.45	0.226	0.0828	0.277	0.0262	1.69
XW-10	1.95	0.0830	0.00976	0.0134	0.0390	0.270	6.81	0.382	0.0866	0.359	0.0293	1.41
XW-11	11.0	0.150	0.0229	0.0194	0.0881	0.303	7.79	0.382	0.0670	0.582	0.0300	2.46
Average	3.56	0.0875	0.0155	0.00938	0.0418	0.213	7.16	0.354	0.0663	0.451	0.0356	2.03

Pukou, Nanjing												
PK-1	3.18	0.0838	0.0156	0.0120	0.0455	0.853	8.33	0.373	0.0790	0.627	0.0419	2.91
PK-2	2.37	0.122	0.0289	0.0200	0.0711	1.28	10.9	0.520	0.149	1.01	0.0933	2.44
PK-3	2.78	0.109	0.0114	0.0205	0.148	0.689	4.11	0.262	0.123	0.322	0.0844	1.54
PK-4	2.32	0.0728	0.0143	0.0110	0.0276	0.475	4.50	0.212	0.0629	0.759	0.0408	1.46
PK-5	3.51	0.145	0.0258	0.0218	0.0575	0.888	10.5	0.456	0.161	1.32	0.0932	3.45
PK-6	6.92	0.283	0.0261	0.0435	0.161	1.45	15.7	0.714	0.183	0.731	0.122	2.45
PK-7	2.65	0.154	0.0227	0.0208	0.112	0.800	8.32	0.390	0.171	0.654	0.0967	1.86
PK-8	2.37	0.0734	0.0274	0.00871	0.0585	0.811	13.3	0.654	0.0858	1.87	0.0597	4.67
PK-9	1.67	0.0399	0.00997	0.00460	0.0422	0.123	3.59	0.284	0.0560	0.394	0.0199	1.13
PK-10	0.821	0.0194	0.00880	0.00183	0.0264	0.0451	1.99	0.159	0.0260	0.240	0.00770	0.513
PK-11	1.13	0.0414	0.00575	0.00230	0.0138	0.145	3.99	0.202	0.0402	0.184	0.00805	1.33
PK-12	1.38	0.0481	0.00729	0.00437	0.203	0.143	9.36	0.548	0.0904	0.329	0.0146	2.47
PK-13	0.844	0.0465	0.00698	0.00233	0.0895	0.0791	2.72	0.230	0.0372	0.209	0.00814	0.991
PK-14	1.97	0.0602	0.00837	0.00335	0.0218	0.241	6.13	0.328	0.0586	0.397	0.0100	1.49

Average	2.42	0.0927	0.0157	0.0127	0.0770	0.573	7.39	0.381	0.0944	0.646	0.0500	2.05
Lishui, Nanjing												
LS-1	5.27	0.100	0.0160	0.00705	0.0604	0.438	8.89	0.420	0.111	0.387	0.0598	2.23
LS-2	4.40	0.125	0.00897	0.0107	0.103	0.677	8.31	0.415	0.0924	0.349	0.0565	1.86
LS-3	7.46	0.105	0.0102	0.0127	0.0906	0.206	11.0	0.347	0.0673	0.896	0.0415	1.35
LS-4	6.22	0.215	0.0202	0.0138	0.111	0.478	8.28	0.375	0.0840	0.498	0.0634	2.45
LS-5	9.28	0.269	0.0304	0.693	0.103	0.464	11.9	0.671	0.643	0.633	0.0668	2.34
LS-6	5.15	0.118	0.0183	0.0143	0.0516	0.230	9.41	0.514	0.0962	0.476	0.0445	1.74
LS-7	6.42	0.118	0.0145	0.0157	0.078	0.580	13.0	0.587	0.129	0.811	0.112	2.68
LS-8	3.50	0.0602	0.0181	0.00829	0.0416	0.111	5.43	0.273	0.0639	0.415	0.0376	1.39
LS-9	6.06	0.106	0.0145	0.0155	0.0492	0.182	11.2	0.521	0.0968	0.566	0.0462	2.84
LS-10	5.62	0.111	0.0140	0.0134	0.0618	0.132	8.17	0.264	0.0220	0.352	0.0195	0.868
LS-11	1.68	0.0513	0.00533	0.00402	0.0298	0.0829	3.38	0.179	0.0604	0.158	0.0148	0.797
LS-12	3.23	0.191	0.0211	0.0227	0.0615	0.271	6.57	0.364	0.110	0.562	0.0545	1.89
Average	5.36	0.131	0.0160	0.0693	0.0701	0.321	8.79	0.411	0.131	0.509	0.0514	1.87

Tianhe, Guangzhou												
TH-1	22.4	0.0947	0.0108	0.0311	0.169	3.36	16.5	0.889	0.114	0.361	0.071	2.89
TH-2	30.6	0.139	0.0159	0.0350	0.170	3.76	21.3	0.292	0.142	0.426	0.048	2.00
TH-3	21.6	0.0696	0.0148	0.0208	0.0374	2.37	16.9	0.431	0.0749	0.306	0.064	1.98
TH-4	19.6	0.182	0.0246	0.0786	0.0993	1.87	15.0	0.368	0.109	0.643	0.0232	2.03
TH-5	16.8	0.0987	0.0131	0.0230	0.129	2.03	14.9	0.555	0.0801	0.347	0.0528	2.13
TH-6	22.9	0.0894	0.0135	0.114	0.0599	1.95	17.5	0.345	0.0596	0.410	0.0267	1.19
TH-7	31.7	0.110	0.0126	0.110	0.0514	1.72	22.7	0.396	0.0731	0.312	0.0361	1.56
TH-8	17.3	0.0811	0.0165	0.0260	0.120	1.68	17.2	0.606	0.084	0.369	0.0450	2.09
TH-9	12.6	0.0538	0.0139	0.0152	0.121	3.19	14.5	0.632	0.136	0.389	0.0328	2.31
TH-10	22.7	0.111	0.0122	0.0627	0.0540	2.42	10.8	0.390	0.157	0.200	0.0548	1.19
TH-11	16.2	0.108	0.0122	0.0186	0.0288	1.79	9.12	0.583	0.144	0.229	0.118	1.49
TH-12	21.5	0.113	0.0126	0.0171	0.139	2.10	18.0	0.830	0.0911	0.315	0.0538	2.12
TH-13	35.3	0.130	0.0135	0.0318	0.0724	1.87	23.2	0.638	0.193	0.310	0.148	1.82
TH-14	28.2	0.369	0.0418	0.0583	0.054	1.68	16.3	0.398	0.0575	0.819	0.0650	2.44

Average	22.8	0.125	0.0163	0.0459	0.0933	2.27	16.7	0.525	0.108	0.388	0.0599	1.95
Heshan, Guangzhou												
HS-1	17.2	0.216	0.0256	0.0269	0.0505	0.471	11.5	0.385	0.0863	0.598	0.0431	2.17
HS-2	5.33	0.115	0.00882	0.0117	0.120	0.692	5.88	0.450	0.0741	0.160	0.0365	1.40
HS-3	8.37	0.163	0.0195	0.0156	0.0787	0.593	10.1	0.381	0.211	0.396	0.0373	1.98
HS-4	12.5	0.132	0.0179	0.0114	0.101	0.894	10.8	0.581	0.199	0.540	0.0640	3.42
HS-5	10.1	0.124	0.0254	0.0136	0.196	0.915	6.92	0.384	0.168	0.630	0.0755	4.24
HS-6	25.9	0.136	0.0342	0.0187	0.144	1.03	12.3	0.484	0.193	0.773	0.0937	2.09
HS-7	13.9	0.0671	0.0215	0.0164	0.477	0.933	10.9	0.543	0.660	0.482	0.0496	3.33
HS-8	8.47	0.0165	0.0121	0.00757	0.0324	0.712	5.33	0.184	0.0893	0.243	0.0361	1.38
HS-9	18.5	0.0681	0.0143	0.0119	0.0762	0.309	14.6	0.443	0.0897	0.354	0.0466	1.81
HS-10	4.46	0.0389	0.0184	0.00772	0.0717	0.503	6.63	0.473	0.0698	0.358	0.0418	2.17
HS-11	17.6	0.0741	0.0161	0.0225	0.0574	0.751	10.1	0.415	0.0563	0.255	0.0183	1.91
Average	12.9	0.105	0.0194	0.0149	0.128	0.710	9.54	0.429	0.172	0.435	0.0493	2.35

Conghua, Guangzhou												
CH-1	6.49	0.0819	0.0106	0.0110	0.0455	0.924	5.73	0.288	0.115	0.180	0.0474	1.84
CH-2	6.01	0.0858	0.0104	0.00934	0.0529	0.637	4.06	0.273	0.0837	0.228	0.0602	1.79
CH-3	8.60	0.0953	0.0200	0.00922	0.0184	0.628	5.78	0.284	0.0550	0.282	0.0237	1.97
CH-4	16.0	0.159	0.0232	0.00970	0.00698	0.663	14.36	0.355	0.0483	0.630	0.0322	1.62
CH-5	16.0	0.104	0.0177	0.00877	0.0388	0.777	10.66	0.363	0.0565	0.494	0.0329	1.84
CH-6	14.7	0.108	0.0186	0.00865	0.0137	0.519	11.92	0.303	0.0466	0.447	0.0318	2.15
CH-7	7.27	0.0486	0.00903	0.00301	0.0414	0.225	3.87	0.142	0.0257	0.175	0.0120	0.633
CH-8	13.3	0.0369	0.00821	0.00493	0.0271	0.204	6.83	0.152	0.0242	0.177	0.0127	0.195
CH-9	5.40	0.0203	0.00757	0.00360	0.0291	0.143	2.16	0.0939	0.0218	0.166	0.00492	0.248
CH-10	29.1	0.0703	0.00945	0.00537	0.0215	0.0639	5.32	0.199	0.0376	0.293	0.00894	0.0238
CH-11	26.1	0.0620	0.00967	0.00660	0.0301	0.274	10.7	0.252	0.0362	0.276	0.0219	0.431
CH-12	21.8	0.0527	0.00778	0.00605	0.0650	0.160	5.85	0.272	0.0510	0.206	0.0125	0.747
CH-13	38.9	0.0440	0.00707	0.00836	0.0414	0.270	12.3	0.250	0.0602	0.183	0.0347	1.07
CH-14	32.7	0.0317	0.00550	0.00812	0.0500	0.468	10.1	0.285	0.0684	0.180	0.0367	0.800

Average	17.3	0.0715	0.0118	0.00734	0.0344	0.425	7.83	0.251	0.0522	0.280	0.0266	1.10

1.6. Concentrations of analyzed endotoxins and PAHs per unit mass of $PM_{2.5}$ (ng mg^{-1})

	Endotoxins	Phe	Ant	Fla	Pyr	BaA	Chr	BbF	BkF	BaP	IcdP	BghiP	DahA
Xuanwu, Nanjing													
XW-1	0.0261	2.81	1.18	9.96	12.4	5.22	10.2	11.4	5.23	4.83	6.88	6.19	13.6
XW-2	0.0434	3.34	1.22	9.39	9.31	15.3	19.4	9.20	15.2	7.05	5.24	5.52	3.13
XW-3	0.0416	2.67	1.49	7.09	6.17	6.56	16.5	7.73	13.1	5.57	3.04	4.35	4.06
XW-4	0.0581	1.86	1.01	6.26	7.73	2.47	7.46	7.93	3.56	3.91	3.50	4.99	8.93
XW-5	0.0264	1.68	0.973	5.60	6.82	2.76	5.02	3.13	2.63	2.63	3.26	3.51	6.22
XW-6	0.0350	1.75	0.876	6.99	7.93	3.65	6.26	9.19	3.76	3.08	3.67	3.85	5.47
XW-7	0.0960	5.91	3.10	20.3	23.4	9.71	17.2	30.2	12.0	9.03	12.0	13.5	16.8
XW-8	0.0783							Lack data					
XW-9	0.0489	1.93	0.942	7.73	8.42	9.82	16.9	13.7	18.5	5.34	10.1	10.5	1.96
XW-10	0.119	2.69	1.15	6.86	7.32	2.20	7.15	13.6	5.00	3.51	6.46	8.09	7.32
XW-11	0.0660	3.34	1.53	12.4	13.9	5.17	9.11	15.4	6.15	5.19	5.94	6.15	9.37
Average	0.0581	2.80	1.35	9.26	10.3	6.29	11.5	12.2	8.52	5.01	6.01	6.66	7.69

Pukou, Nanjing													
PK-1	0.0351	1.29	0.734	5.68	5.48	5.07	13.3	11.2	15.2	5.08	5.01	7.69	2.49
PK-2	0.0857	2.82	1.26	9.63	8.31	12.8	19.1	25.9	17.7	5.27	8.09	8.43	3.26
PK-3	0.0283	8.40	5.82	34.9	53.9	14.8	33.6	14.9	19.3	23.2	58.3	72.3	211
PK-4	0.0188	1.51	0.721	7.14	6.68	6.55	13.5	13.3	13.6	5.49	6.35	7.04	2.02
PK-5	0.278	2.75	1.29	13.9	13.1	12.7	25.9	26.8	26.5	10.7	12.9	14.1	3.62
PK-6	0.172	13.4	9.26	55.7	64.8	34.9	52.7	26.2	32.5	38.4	104	85.4	263
PK-7	0.158	4.29	3.72	21.9	27.5	12.0	19.8	14.3	13.2	11.6	18.0	18.4	36.7
PK-8	0.0894	2.09	1.35	14.4	13.5	17.3	24.0	53.0	17.5	15.8	21.0	22.3	23.6
PK-9	0.0291	1.75	0.354	8.22	6.63	10.1	15.8	23.9	15.5	6.37	7.80	9.62	2.13
PK-10	0.00911	0.816	0.280	4.38	3.72	1.75	3.11	8.21	2.74	2.02	3.33	3.13	3.12
PK-11	0.0179	0.788	0.342	4.68	4.54	8.82	11.2	12.3	15.7	6.23	5.79	7.90	2.72
PK-12	0.0157	1.42	0.875	5.31	5.16	3.39	11.3	16.9	11.5	4.74	4.89	6.65	1.69
PK-13	0.0225	1.24	0.416	5.40	5.11	7.06	9.65	15.3	9.90	5.30	5.38	5.66	1.59
PK-14	0.0293	1.91	0.712	4.90	4.10	2.89	8.55	5.83	7.93	3.02	2.43	3.43	1.38

Average	0.0706	3.17	1.94	14.0	15.9	10.7	18.7	19.2	15.6	10.2	18.8	19.4	39.9
Lishui, Nanjing													
LS-1	0.0750	3.16	1.60	5.72	10.1	1.79	5.54	6.65	3.31	3.46	4.45	4.22	8.55
LS-2	0.156	4.41	2.02	7.27	10.9	1.99	6.13	8.03	4.06	3.31	5.49	5.70	9.38
LS-3	0.0768	3.74	2.67	7.55	7.52	3.58	6.48	4.47	3.97	3.92	4.95	5.19	8.31
LS-4	0.119	3.69	1.97	5.03	8.31	3.18	4.60	3.39	3.57	3.64	4.55	4.70	7.94
LS-5	0.182	2.63	0.715	7.23	7.03	1.91	5.82	4.69	4.71	3.51	5.56	7.14	9.63
LS-6	0.106	3.65	3.23	4.94	6.46	2.63	4.58	6.16	4.00	3.74	5.45	7.84	6.75
LS-7	0.0458	2.31	1.43	4.73	6.32	1.18	3.47	4.26	3.25	3.30	4.38	5.13	3.60
LS-8	0.164	0.929	0.385	4.96	6.00	0.963	2.69	5.52	3.67	2.90	6.43	6.21	2.09
LS-9	1.51	3.84	1.81	19.7	18.3	22.1	29.9	19.8	28.5	14.6	11.8	12.9	3.54
LS-10	0.0342	1.10	0.417	8.82	7.83	4.45	14.2	19.4	14.3	7.47	8.26	8.27	1.77
LS-11	0.132	2.86	1.24	11.0	11.6	1.75	7.30	11.2	6.83	2.61	13.8	12.3	4.18
LS-12	0.0811	2.96	1.01	5.35	6.70	2.50	3.18	3.87	3.15	1.91	4.70	5.06	4.23
Average	0.109	2.94	1.54	7.69	8.91	4.00	7.83	8.12	6.94	4.53	6.65	7.05	5.83

Tianhe, Guangzhou													
TH-1	0.251	8.84	7.22	24.9	26.1	34.1	33.7	9.49	26.1	15.4	7.48	6.79	13.6
TH-2	0.326	2.52	0.108	1.78	1.93	0.449	1.58	2.61	0.847	2.13	1.28	2.17	0.524
TH-3	0.190	2.39	0.0977	0.909	1.04	0.269	0.801	1.84	0.368	1.14	1.41	2.09	0.775
TH-4	0.566	1.4	0.427	3.58	4.47	0.704	2.15	3.41	2.32	2.84	4.28	3.72	2.25
TH-5	0.0440	0.78	0.477	1.10	1.31	0.765	0.965	1.12	0.900	0.881	1.69	1.48	1.15
TH-6	0.653	1.24	0.615	3.11	3.35	0.695	2.19	3.41	1.44	2.47	5.41	4.94	2.28
TH-7	0.388	1.18	0.566	3.95	3.66	1.68	2.51	3.56	2.32	2.11	4.35	4.20	2.19
TH-8	0.175	3.75	3.12	8.78	8.93	12.2	15.5	10.3	22.2	12.2	6.93	7.38	6.82
TH-9	0.0916	3.2	0.168	1.74	2.21	1.22	3.90	7.09	2.30	4.40	2.74	4.35	0.840
TH-10	0.223	1.19	0.499	2.49	2.40	1.51	1.88	3.39	1.56	2.27	5.01	4.23	2.36
TH-11	0.153	1.94	0.500	1.46	2.65	1.63	3.23	3.33	1.70	2.43	2.45	3.52	1.91
TH-12	0.0878	2.76	0.0996	1.34	1.69	0.511	1.87	4.95	0.866	2.44	2.32	3.99	0.673
TH-13	0.170	2.02	1.17	2.06	2.32	0.666	1.75	6.01	1.95	2.58	4.61	4.76	2.75
TH-14	0.160	1.51	0.641	5.34	5.03	1.60	2.89	5.70	2.77	2.90	5.44	5.72	2.16

Average	0.248	2.48	1.12	4.47	4.80	4.14	5.35	4.73	4.84	4.01	3.96	4.24	2.88
Heshan, Guangzhou													
HS-1	0.0725	4.27	2.03	11.2	14.5	15.1	21.5	7.45	12.4	6.92	3.70	3.86	3.95
HS-2	0.138	1.58	0.686	1.99	2.97	0.957	1.47	5.86	2.02	1.87	5.89	5.83	2.49
HS-3	0.164	1.67	0.317	2.52	3.20	1.01	1.37	2.57	1.66	2.33	4.67	4.32	2.99
HS-4	0.108	1.12	0.320	2.56	3.53	1.04	1.86	5.84	3.90	4.04	16.0	32.2	3.55
HS-5	0.138	1.39	0.601	2.45	3.46	0.970	2.34	8.18	2.84	3.73	8.33	9.85	2.77
HS-6	0.329	2.91	1.93	7.06	11.0	3.72	5.31	16.9	6.19	5.77	15.0	14.0	6.67
HS-7	0.274	2.25	0.788	7.83	14.9	2.67	3.31	7.25	6.21	6.47	15.4	14.6	6.10
HS-8	0.190	1.82	0.791	4.19	6.96	2.22	3.04	5.56	3.94	3.45	8.16	8.12	3.70
HS-9	0.0718	0.833	0.267	3.36	3.96	1.25	2.14	3.47	2.45	2.08	5.36	5.69	2.05
HS-10	0.109	1.68	0.560	5.05	5.72	1.42	3.83	9.99	6.30	5.36	16.6	18.7	5.45
HS-11	0.0662	0.640	0.266	3.02	3.24	0.631	1.81	3.62	2.45	2.22	6.02	5.97	1.78
Average	0.151	1.83	0.778	4.66	6.67	2.81	4.37	6.97	4.58	4.02	9.57	11.2	3.77

Conghua, Guangzhou													
CH-1	0.270	2.99	0.84	2.74	2.78	1.64	1.78	2.33	1.48	1.92	3.8	3.66	2.82
CH-2	0.217	1.79	1.01	2.15	2.45	1.06	1.15	1.14	1.01	1.25	2.02	1.64	1.77
CH-3	0.149	8.29	2.89	17.0	22.8	17.7	33.1	10.4	16.8	9.45	3.34	2.80	6.96
CH-4	0.421	3.67	1.80	9.07	9.92	9.32	17.7	9.09	8.86	5.94	2.22	3.03	3.50
CH-5	0.0710	1.30	0.634	2.30	2.19	0.774	1.24	1.76	1.26	0.941	2.17	1.79	1.29
CH-6	0.0678	3.47	1.80	7.40	9.46	7.97	15.7	4.08	9.97	5.38	2.01	2.54	3.07
CH-7	0.0478	2.51	0.885	5.99	6.45	5.59	9.77	6.43	6.60	3.27	1.80	2.45	2.14
CH-8	0.107	3.78	1.62	8.14	8.14	8.15	20.7	4.88	9.92	5.20	3.72	3.96	3.06
CH-9	0.139	2.72	0.635	10.7	12.2	14.1	19.2	21.2	17.8	10.5	9.68	9.47	2.12
CH-10	0.121	1.00	0.450	2.06	2.22	1.01	1.40	2.29	1.34	1.33	3.15	3.00	1.47
CH-11	0.0762	0.760	0.346	3.19	2.89	0.690	1.93	5.52	1.72	1.71	3.76	3.31	1.86
CH-12	0.0564	0.884	0.299	1.96	1.86	0.935	1.46	2.24	1.00	1.04	1.87	1.51	1.19
CH-13	0.0476	0.823	0.366	1.48	1.58	0.666	0.824	0.942	0.648	0.716	2.00	1.90	1.25
CH-14	0.0610	1.16	0.0395	0.497	0.672	0.202	0.559	1.33	0.210	1.26	0.857	1.98	0.300

Average	0.132	2.51	0.973	5.33	6.11	4.99	9.03	5.26	5.61	3.57	3.03	3.07	2.34

Appendix 2

2.1. Concentration-effect curve of ROS induction by $PM_{2.5}$ extracts and derivation of BEQ.

Sample ID	Concentration-effect curve	Slope	*p* value*	$EC_{IR1.5, PM2.5}$ (mg L^{-1})**	$BEQ_{bio, PM2.5}$ (μg mg^{-1})***
PK-1	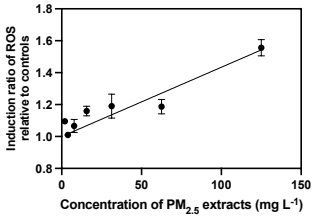	0.00434±0.000299	<0.0001	115±7.95	6.42±0.351
PK-2	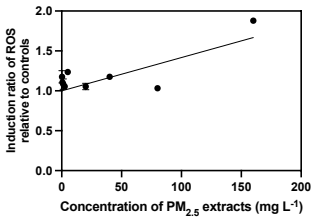	0.00426±0.000584	<0.0001	117±16.1	6.30±0.344
PK-3	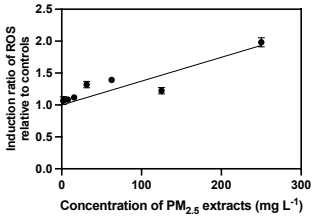	0.00373±0.000289	<0.0001	134±10.4	5.52±0.302

PK-4	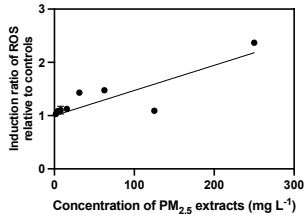	0.00472±0.000470	<0.0001	106±10.5	6.98±0.382
PK-5	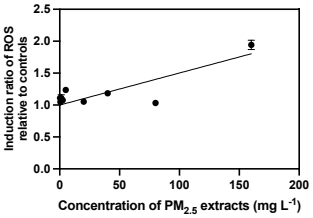	0.00502±0.000584	<0.0001	99.6±9.34	7.43±0.406
PK-6	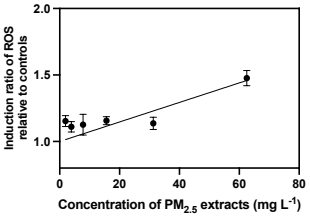	0.00734±0.000765	<0.0001	71.4±7.81	10.4±0.566
PK-7	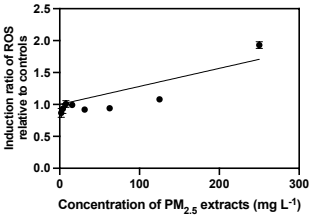	0.00283±0.000312	<0.0001	177±19.5	4.18±0.229

PK-8	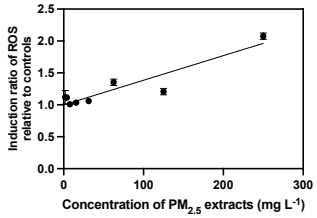	0.00385±0.000290	<0.0001	130±9.78	5.70±0.312
PK-9	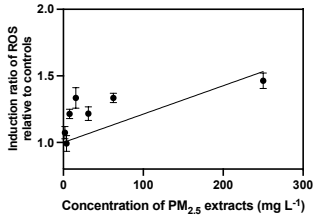	0.00213±0.000364	<0.0001	235±40.1	3.15±0.172
PK-10	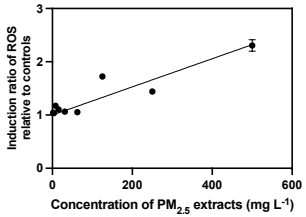	0.00264±0.000183	<0.0001	189±13.1	3.91±0.214
PK-11	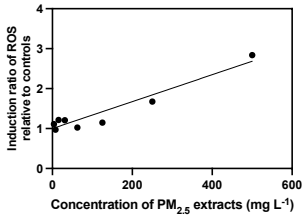	0.00337±0.000171	<0.0001	148±7.52	4.98±0.272

PK-12	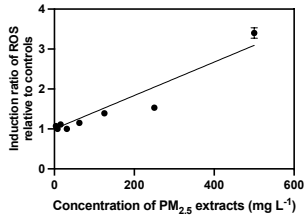	0.00417±0.000237	<0.0001	120±6.82	6.17±0.337
PK-13	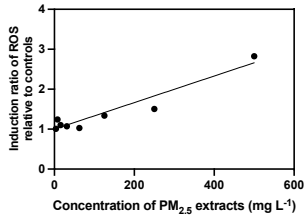	0.00332±0.000144	<0.0001	150±6.49	4.92±0.269
PK-14	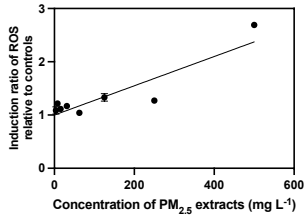	0.00275±0.000247	<0.0001	182±16.4	4.06±0.222
XW-1	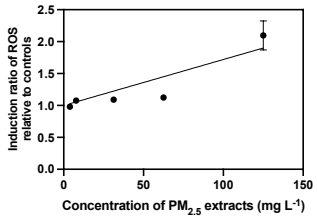	0.00720±0.000844	<0.0001	69.5±8.15	10.6±1.38

XW-2	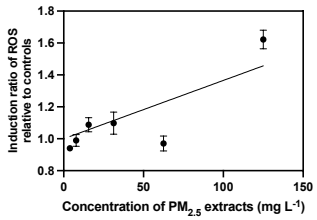	0.00366±0.000490	<0.0001	137±18.3	5.41±0.782
XW-3	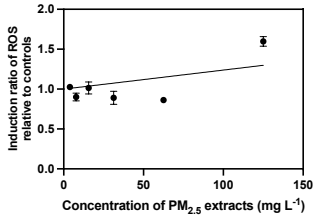	0.00238±0.000628	<0.0001	210±55.3	3.53±0.949
XW-4	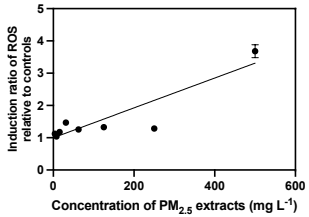	0.00462±0.000315	<0.0001	108±7.36	6.84±0.597
XW-5	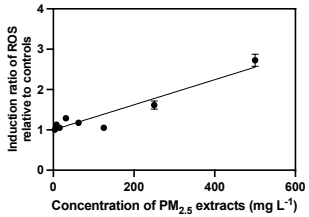	0.00311±0.000183	<0.0001	161±9.45	4.59±0.369

XW-6	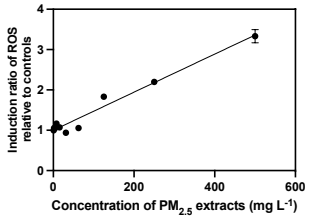	0.00472±0.000144	<0.0001	106±3.24	6.98±0.437
XW-7	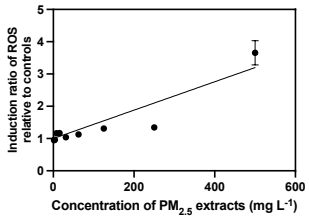	0.00440±0.000341	<0.0001	114±8.81	6.50±0.617
XW-8	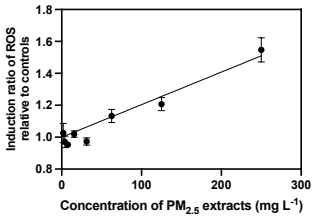	0.00204±0.000121	<0.0001	245±14.6	3.02±0.244
XW-9	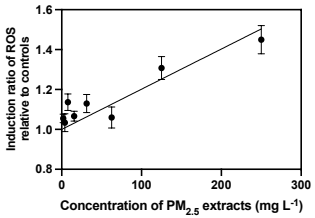	0.00201±0.000173	<0.0001	248±21.3	2.98±0.303

XW-10	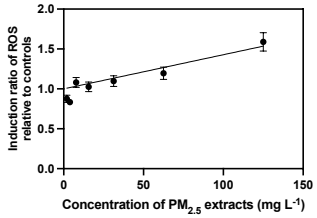	0.00428±0.000458	<0.0001	117±12.5	6.33±0.760
XW-11	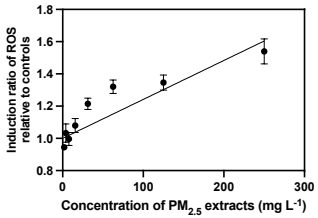	0.00242±0.000182	<0.0001	207±15.6	3.57±0.333
LS-1	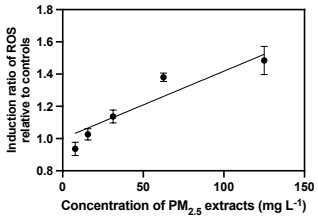	0.00418±0.000312	<0.0001	120±8.93	6.18±0.337
LS-2	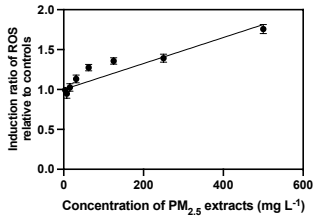	0.00163±0.000102	<0.0001	307±19.3	2.41±0.132

LS-3	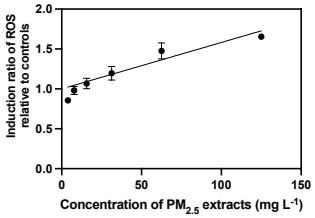	0.00582±0.000512	<0.0001	86.0±7.58	8.60±0.470
LS-4	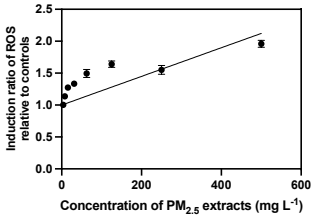	0.00224±0.000224	<0.0001	223±22.2	3.32±0.182
LS-5	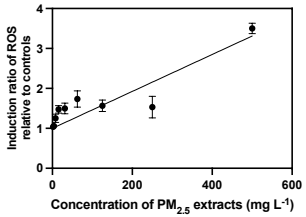	0.00462±0.000347	<0.0001	108±8.12	6.84±0.374
LS-6	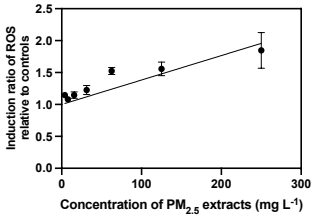	0.00383±0.000318	<0.0001	131±10.8	5.66±0.310

LS-7	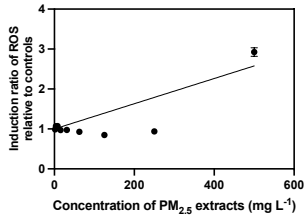	0.00316±0.000321	<0.0001	158±16.1	4.67±0.255
LS-8	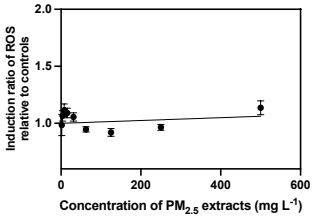	0	0.152		
LS-9	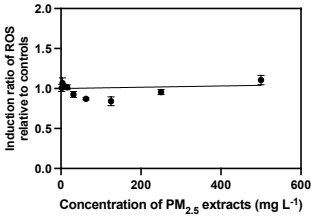	0	0.292		
LS-10	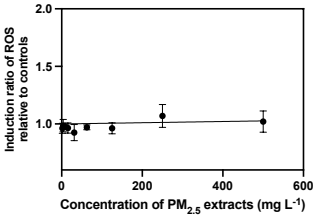	0	0.376		

LS-11	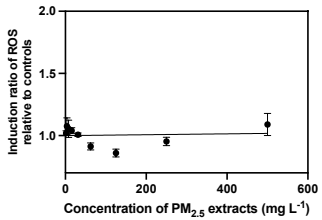	0	0.637		
LS-12	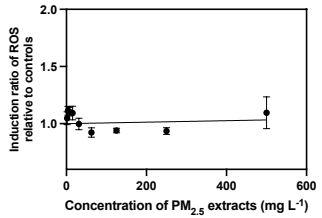	0	0.444		
TH-1	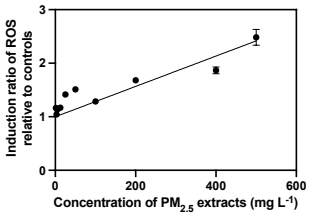	0.00283±0.000196	<0.0001	176±12.2	4.19±0.370
TH-2	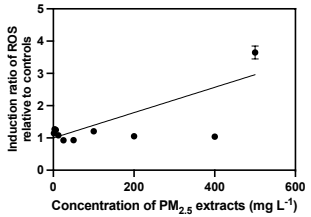	0.00392±0.000356	<0.0001	128±1.59	5.80±0.615

TH-3	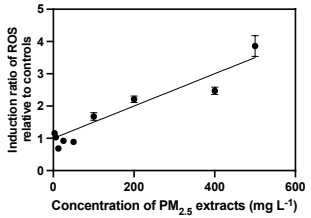	0.00500±0.000160	<0.0001	99.9±3.19	7.40±0.469
TH-4	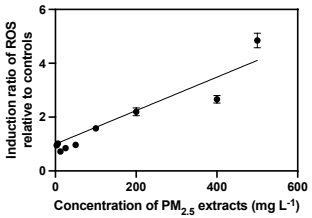	0.00621±0.000214	<0.0001	80.5±2.77	9.19±0.594
TH-5	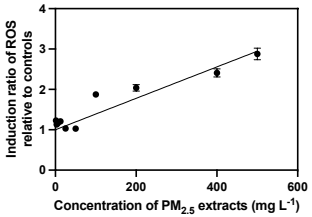	0.00389±0.000112	<0.0001	128±3.69	5.76±0.356
TH-6	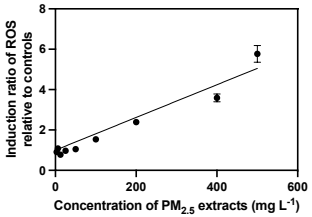	0.00810±0.000207	<0.0001	61.7±1.58	12.0±0.723

TH-7	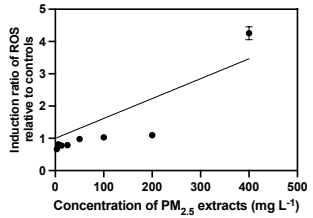	0.00610±0.000431	<0.0001	82.0±5.79	9.02±0.806
TH-8	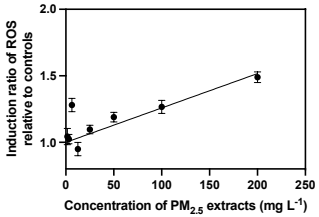	0.00258±0.000283	<0.0001	194±21.2	3.82±0.468
TH-9	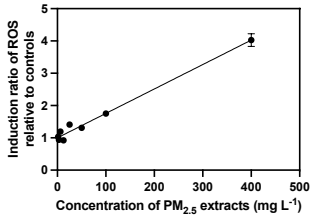	0.00756±0.000120	<0.0001	66.1±1.05	11.2±0.637
TH-10	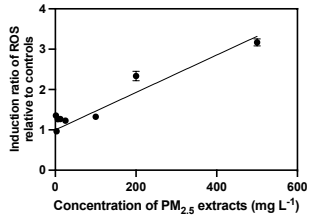	0.00464±0.000149	<0.0001	108±3.46	6.86±0.435

TH-11	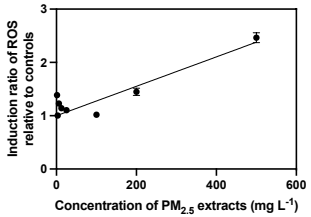	0.00276±0.000121	<0.0001	181±7.92	4.08±0.286
TH-12	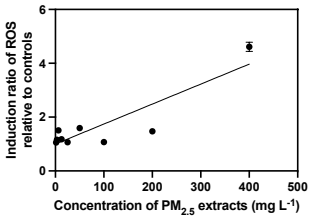	0.00742±0.000362	<0.0001	67.4±3.29	11.0±0.805
TH-13	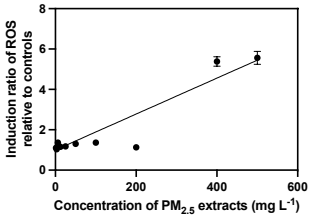	0.00890±0.000312	<0.0001	56.2±1.97	13.2±0.854
TH-14	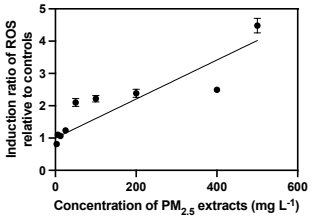	0.00604±0.000247	<0.0001	82.8±3.39	8.93±0.610

CH-1	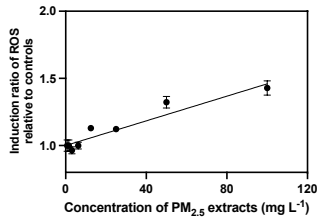	0.00459±0.000200	<0.0001	109±4.74	6.80±0.475
CH-2	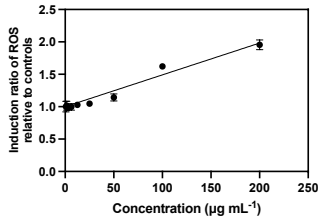	0.00491±0.000177	<0.0001	102±3.68	7.26±0.476
CH-3	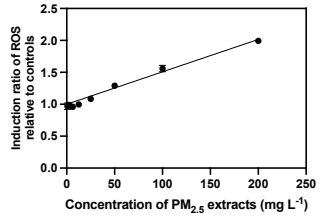	0.00458±0.000126	<0.0001	109±3.00	6.78±0.414
CH-4	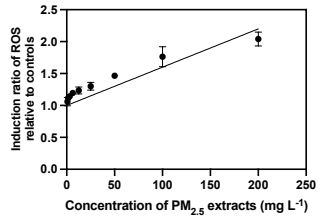	0.00600±0.000345	<0.0001	83.4±4.80	8.87±0.704

CH-5	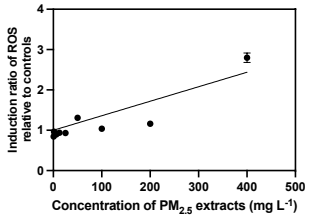	0.00360±0.000190	<0.0001	139±7.35	5.32±0.405
CH-6	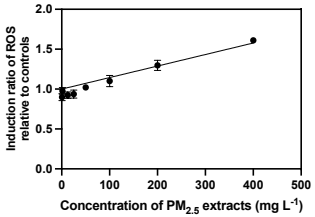	0.00144±0.0000829	<0.0001	347±19.9	2.13±0.169
CH-7	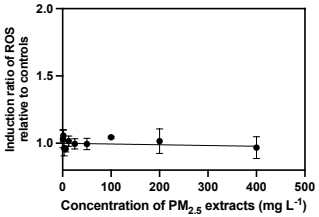	0	0.339		
CH-8	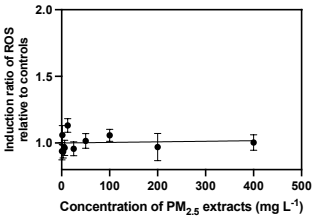	0	0.652		

CH-9	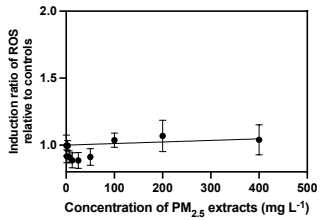	0	0.163		
CH-10	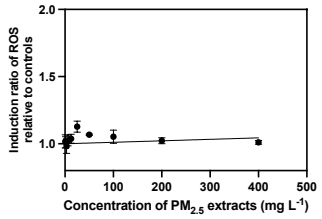	0	0.116		
CH-11	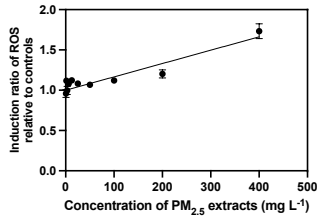	0.00166±0.0000920	<0.0001	302±16.8	2.45±0.191
CH-12	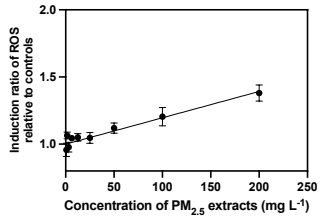	0.00196±0.000108	<0.0001	255±14.1	2.90±0.225

CH-13	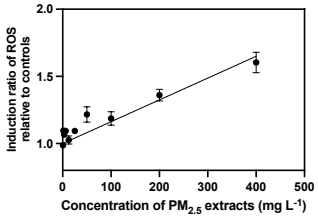	0.001620±0.0000946	<0.0001	308±17.9	2.40±0.192
CH-14	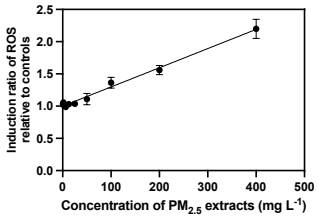	0.00298±0.0000566	<0.0001	168±3.19	4.40±0.255
HS-1	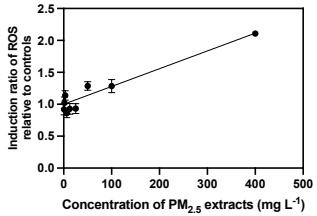	0.00278±0.000104	<0.0001	180±6.71	4.12±0.273
HS-2	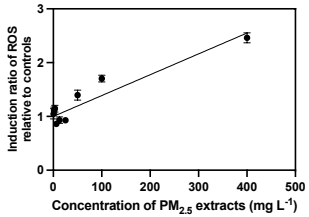	0.00388±0.000145	<0.0001	129±4.82	5.73±0.380

HS-3	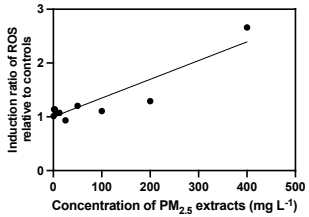	0.00349±0.000238	<0.0001	143±9.77	5.16±0.451
HS-4	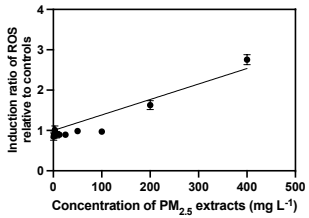	0.00384±0.000157	<0.0001	130±5.31	5.68±0.310
HS-5	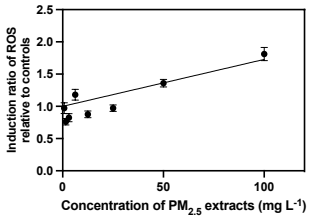	0.00728±0.000517	<0.0001	68.7±4.88	10.8±0.589
HS-6	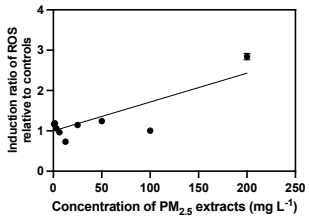	0.00715±0.000461	<0.0001	69.9±4.50	10.6±0.578

HS-7	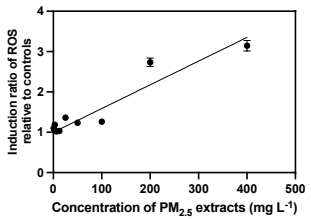	0.00588±0.000178	<0.0001	85.1±2.57	8.69±0.475
HS-8	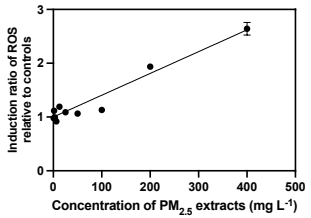	0.00405±0.0000975	<0.0001	123±2.97	5.99±0.327
HS-9	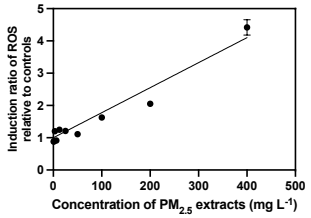	0.00775±0.000182	<0.0001	64.5±1.51	11.5±0.627
HS-10	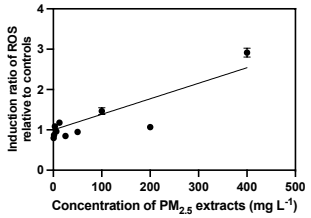	0.00385±0.000215	<0.0001	130±7.25	5.70±0.311

HS-11	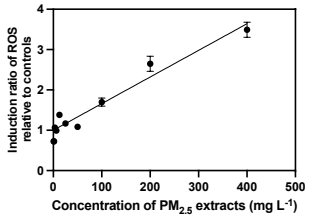	0.00660±0.000168	<0.0001	75.8±1.93	9.76±0.534

[*] p value < 0.05 means that the slope is significantly non-zero; otherwise, it is not.

[**]Calculated using Equation 3-10 with the slope provided in the regression analysis; standard errors calculated using Equation 3-19.

[***]Calculated using Equation 3-13; standard error calculated using Equation 3-22.

2.2. Profiling individual components for their potencies in inducing intracellular ROS.

Component	Concentration-effect curve*	$EC_{IR1.5}$ (μg mL^{-1}) **	REP_i ***
TBHP	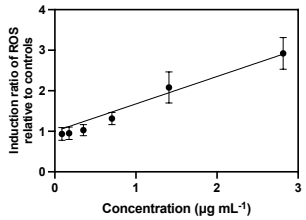	0.740±0.0404	1
Cd	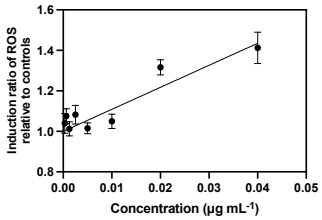	0.0460±0.00316	16.1±1.41
Co	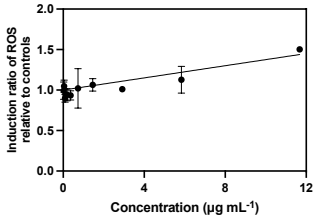	13.3±1.14	0.0556±0.00566

Cr	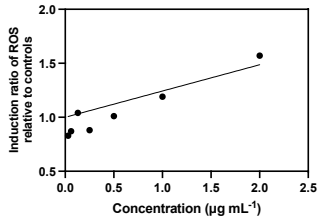	2.06±0.490	0.360±0.0879
Cu	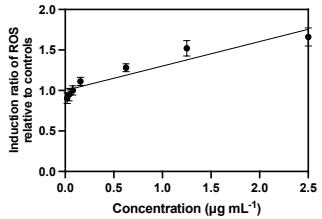	1.66±0.108	0.447±0.0381
Fe	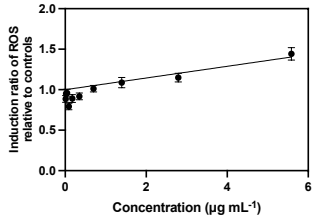	6.93±0.737	0.107±0.0128
Mn	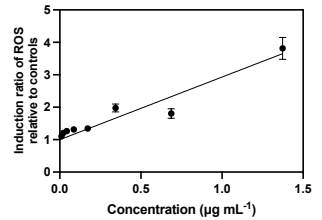	0.259±0.0119	2.86±0.204

Ni	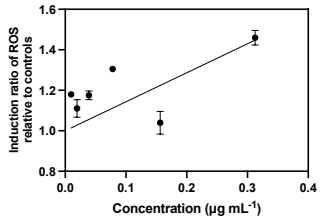	0.349±0.0562	2.12±0.360
Pb	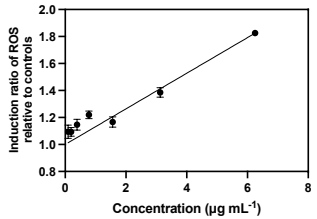	3.80±0.456	0.195±0.257
V	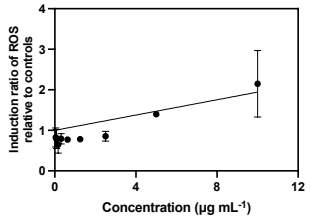	5.30±1.41	0.140±0.0378
Zn	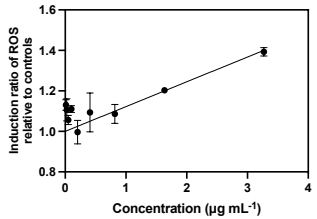	4.09±0.408	0.181±0.0206

Endotoxins	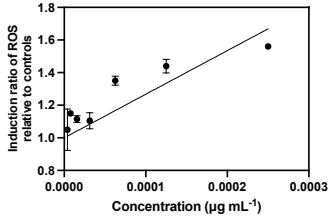	(18.7±2.02)×10^{-5}	3958±478
FLA	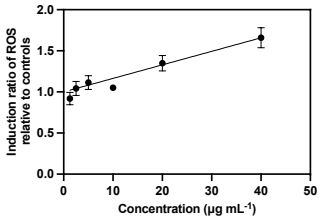	30.4±1.39	0.0243±0.00174
BaA	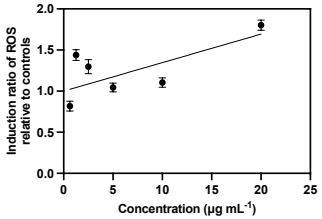	14.4±1.47	0.0513±0.00593
Chr	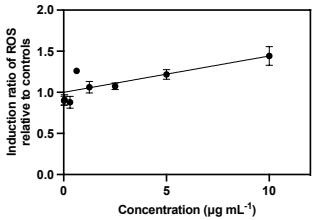	11.3±0.904	0.0654±0.00633

BbF	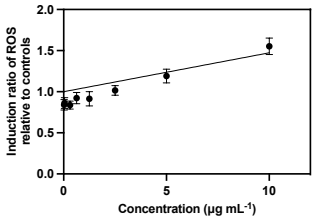	10.6±0.935	0.0700±0.00729
BkF	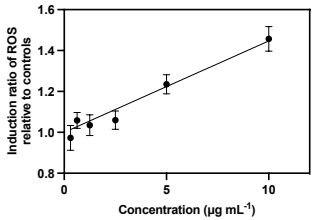	11.2±0.517	0.0661±0.00473
BaP	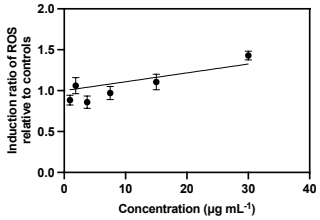	46.1±6.58	0.0161±0.00245
DahA	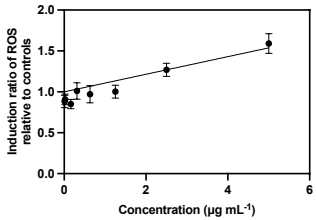	4.65±0.327	0.159±0.0142

* All concentration-effect curves have $p < 0.0001$.

** Calculated using Equation 3-10 with the slope provided in the regression analysis; standard errors calculated using Equation 3-19.

***Calculated using Equation 3-12 with the standard error calculated using Equation 3-21.

2.3. Experimental vs. modeled concentration-effect curves for mixtures of active metals, endotoxins and PAHs present at the measured mass composition in $PM_{2.5}$.

Mixture samples	Concentration-effect curve	$EC_{IR1.5,exp}$ (μg mL^{-1})*	$EC_{IR1.5,CA}$ (μg mL^{-1}) **	IPQ***
XW, Nanjing	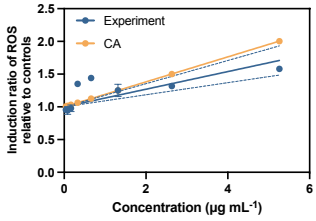	3.71±0.569	2.62±0.0751	-0.417
PK, Nanjing	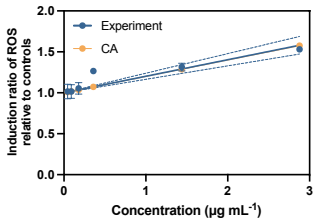	2.48±0.218	2.50±0.0710	0.0855
LS, Nanjing	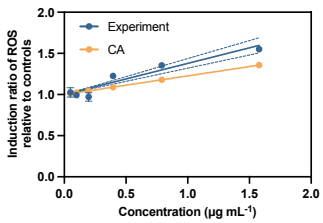	1.32±0.0958	2.21±0.0775	0.669
TH, Guangzhou	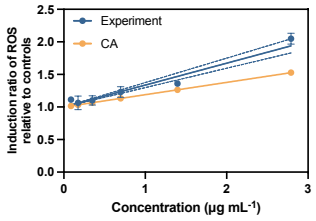	1.49±0.0821	2.64±0.0805	0.778
CH, Guangzhou	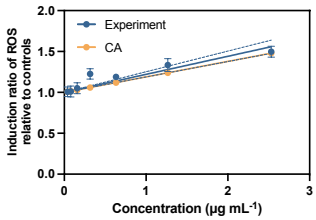	2.27±0.0.159	2.64±0.0831	0.164
HS, Guangzhou	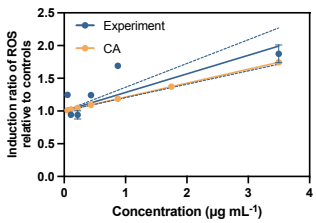	1.76±0.233	2.35±0.0747	0.333

*Calculated using Equation 3-10 with the slope provided in the regression analysis; standard error calculated using Equation 3-19.

**Predicted using Equation 3-16 with the standard error calculated using Equation 3-20.

***Calculated using Equations 3-17 or 3-18.

2.4. Derivation for fractional contribution (%) of metals, endotoxins and PAHs to $PM_{2.5}$-induced intracellular ROS generation.

Sample ID	$BEQ_{bio,\ PM2.5}$ ($\mu g\ mg^{-1}$) [a]	BEQ_{comp} of metals ($\mu g\ mg^{-1}$) [b]	BEQ_{comp} of endotoxins ($\mu g\ mg^{-1}$) [c]	BEQ_{comp} of PAHs ($ng\ mg^{-1}$) [d]	Effect explained by metals [e]	Effect explained by endotoxins [f]	Effect explained by PAHs [g]
XW, Nanjing							
XW-1	10.6±1.38	1.99±0.0868	0.0950±0.0114	3.48±0.193	18.7%±1.02%	0.889%±0.0486%	0.0327%±0.00179%
XW-2	5.41±0.782	1.56±0.0712	0.157±0.0190	3.00±0.129	28.9%±1.58%	2.91%±0.159%	0.0554%±0.00303%
XW-3	3.53±0.949	1.46±0.0649	0.151±0.0182	2.46±0.103	41.3%±2.26%	4.28%±0.234%	0.0698%±0.00382%
XW-4	6.84±0.597	2.05±0.979	0.211±0.0255	2.31±0.128	30.0%±1.64%	3.08%±0.168%	0.0337%±0.00184%
XW-5	4.59±0.369	1.30±0.0620	0.0955±0.0116	1.57±0.0874	28.2%±1.54%	2.08%±0.114%	0.0341%±0.00187%
XW-6	6.98±0.437	1.10±0.0508	0.127±0.0154	1.85±0.0886	15.8%±0.861%	1.82%±0.0994%	0.0265%±0.00145%
XW-7	6.50±0.617	2.37±0.119	0.348±0.0421	5.62±0.272	36.5%±2.00%	5.35%±0.292%	0.0864%±0.00472%
XW-8	3.02±0.244	1.09±0.0524	0.284±0.0341	Lack data	36.1%±1.97%	9.40%±0.514%	Lack data
XW-9	2.98±0.303	1.15±0.0532	0.177±0.0214	2.72±0.114	38.5%±2.10%	5.95%±0.325%	0.0913%±0.00499%
XW-10	6.33±0.760	1.49±0.0688	0.432±0.0523	2.32±0.117	23.5%±1.28%	6.83%±0.373%	0.0366%±0.002%
XW-11	3.57±0.333	1.85±0.0816	0.239±0.0289	3.04±0.148	51.6%±2.8%	6.69%±0.366%	0.085%±0.00465%

				Average	**31.7%**	**4.62%**	**0.0552%**
PK, Nanjing							
PK-1	6.42±0.351	2.04±0.0893	0.127±0.0154	3.63±0.160	31.8%±1.74%	1.98%±0.108%	0.0343%±0.00188%
PK-2	6.30±0.344	2.77±0.116	0.311±0.0375	35.2±2.79	44.0%±2.41%	4.93%±0.269%	0.0576%±0.00315%
PK-3	5.52±0.302	1.42±0.0623	0.102±0.0124	2.27±0.0949	25.7%±1.40%	1.85%±0.101%	0.638%±0.0349%
PK-4	6.98±0.382	1.26±0.0521	0.0681±0.00824	4.39±0.185	18.0%±0.984%	0.976%±0.0533%	0.0325%±0.00178%
PK-5	7.43±0.406	2.70±0.117	1.01±0.122	46.1±3.49	36.4%±1.99%	13.6%±0.741%	0.0591%±0.00323%
PK-6	10.4±0.566	3.36±0.149	0.624±0.0755	8.21±0.500	32.5%±1.77%	6.03%±0.33%	0.445%±0.0243%
PK-7	4.18±0.229	2.15±0.0949	0.572±0.0691	8.30±0.407	51.4%±2.81%	13.7%±0.747%	0.196%±0.0107%
PK-8	5.70±0.312	3.22±0.142	0.324±0.0392	3.04±0.137	56.6%±3.09%	5.69%±0.311%	0.146%±0.00796%
PK-9	3.15±0.172	1.04±0.0456	0.105±0.0128	1.17±0.0564	33.1%±1.81%	3.35%±0.183%	0.0965%±0.00527%
PK-10	3.91±0.214	0.586±0.0251	0.0330±0.00399	2.37±0.0965	15.0%±0.820%	0.844%±0.0461%	0.0299%±0.00163%
PK-11	4.98±0.272	0.889±0.0418	0.0650±0.00785	2.04±0.0930	17.8%±0.975%	1.30%±0.0713%	0.0476%±0.0026%
PK-12	6.17±0.337	1.95±0.951	0.0567±0.00686	2.00±0.0890	31.6%±1.73%	0.920%±0.0503%	0.033%±0.00181%
PK-13	4.92±0.269	0.803±0.0357	0.0815±0.00986	1.27±0.0523	16.3%±0.893%	1.66%±0.0906%	0.0407%±0.00223%
PK-14	4.06±0.222	1.32±0.0606	0.106±0.0128	3.63±0.160	32.4%±1.77%	2.61%±0.143%	0.0314%±0.00171%

				Average	**31.6%**	**4.24%**	**0.135%**
LS, Nanjing							
LS-1	6.18±0.337	1.94±0.0889	0.272±0.0329	2.07±0.120	31.5%±1.72%	4.40%±0.240%	0.0335%±0.00183%
LS-2	2.41±0.132	1.82±0.0820	0.563±0.0681	2.32±0.132	75.4%±4.21%	23.4%±1.28%	0.0966%±0.00528%
LS-3	8.60±0.470	1.67±0.0865	0.278±0.0336	2.12±0.117	19.5%±1.06%	3.23%±0.177%	0.0246%±0.00134%
LS-4	3.32±0.182	1.91±0.0844	0.430±0.0520	1.87±0.109	57.5%±3.14%	13.0%±0.708%	0.0562%±0.00307%
LS-5	6.84±0.374	3.63±0.223	0.661±0.0780	2.23±0.132	53.1%±2.90%	9.66%±0.528%	0.0326%±0.00178%
LS-6	5.66±0.310	1.97±0.0913	0.384±0.0465	1.79±0.0964	34.8%±1.90%	6.79%±0.371%	0.0316%±0.00173%
LS-7	4.67±0.255	2.57±0.120	0.166±0.0201	1.11±0.0541	55.2%±3.01%	3.56%±0.194%	0.0237%±0.0013%
				Average	**46.7%**	**9.14%**	**0.0427%**
TH, Guangzhou							
TH-1	4.19±0.370	3.97±0.176	0.908±0.110	6.62±0.294	94.8%±5.18%	21.7%±1.18%	0.158%±0.00863%
TH-2	5.80±0.615	3.54±0.184	1.18±0.143	0.344±0.0153	61.0%±3.33%	20.4%±1.11%	0.00593%±0.00032 4%
TH-3	7.40±0.469	2.89±0.141	0.688±0.0831	0.271±0.0135	39.0%±2.13%	9.29%±0.508%	0.00366%±0.0002%

TH-4	9.19±0.594	2.76±0.128	2.05±0.248	0.746±0.0353	30.0%±1.64%	22.3%±1.22%	0.00812%±0.000444%
TH-5	5.76±0.356	2.86±0.132	0.159±0.0193	0.342±0.017	49.7%±2.71%	2.77%±0.151%	0.00594%±0.000325%
TH-6	12.0±0.723	2.53±0.134	2.37±0.286	0.713±0.0352	21.1%±1.15%	19.8%±1.08%	0.00595%±0.000325%
TH-7	9.02±0.806	2.87±0.164	1.41±0.170	0.797±0.0359	31.8%±1.74%	15.6%±0.852%	0.00883%±0.000483%
TH-8	3.82±0.468	2.98±0.142	0.632±0.0764	3.55±0.143	78.1%±4.27%	16.5%±0.904%	0.0928%±0.00507%
TH-9	11.2±0.637	3.45±0.153	0.332±0.0401	0.771±0.0371	30.8%±1.68%	2.97%±0.162%	0.00689%±0.000377%
TH-10	6.86±0.435	2.51±0.116	0.809±0.0978	0.739±0.0363	36.5%±2.00%	11.8%±0.644%	0.0108%±0.000588%
TH-11	4.08±0.286	2.50±0.108	0.553±0.0668	0.34±0.016	61.4%±3.35%	13.5%±0.740%	0.00832%±0.000455%

TH-12	11.0±0.805	3.44±0.160	0.318±0.0385	0.472±0.0244	31.3%±1.71%	2.90%±0.158%	0.0043%±0.000235%
TH-13	13.2±0.854	3.54±0.184	0.614±0.0743	0.869±0.0453	26.9%±1.47%	4.67%±0.255%	0.0066%±0.000361%
TH-14	8.93±0.610	2.99±0.137	0.578±0.0699	0.934±0.041	33.5%±1.83%	6.47%±0.354%	0.0105%±0.000571%
				Average	**44.7%**	**12.2%**	**0.0240%**
HS, Guangzhou							
HS-1	4.12±0.273	2.13±0.0992	0.263±0.0318	3.07±0.135	51.6%±2.82%	6.38%±0.348%	0.0744%±0.00407%
HS-2	5.73±0.380	1.61±0.0696	0.501±0.0606	0.818±0.0421	28.1%±1.54%	8.74%±0.478%	0.0143%±0.00078%
HS-3	5.16±0.451	2.18±0.107	0.595±0.0720	0.761±0.0420	42.4%±2.31%	11.5%±0.631%	0.0147%±0.000806%
HS-4	5.68±0.310	2.78±0.126	0.392±0.0474	1.08±0.0548	49.0%±2.68%	6.91%±0.378%	0.0191%±0.00104%
HS-5	10.8±0.589	2.47±0.110	0.501±0.0606	1.04±0.0520	23.0%±1.25%	4.65%±0.254%	0.00969%±0.00053%

HS-6	10.6±0.578	2.79±0.123	1.19±0.144	2.41±0.118	26.3%±1.44%	11.3%±0.616%	0.0227%±0.00124%
HS-7	8.69±0.475	3.60±0.226	0.993±0.120	1.82±0.0903	41.4%±2.26%	11.4%±0.625%	0.021%±0.00115%
HS-8	5.99±0.327	1.29±0.0573	0.690±0.0834	1.22±0.0578	21.6%±1.18%	11.5%±0.629%	0.0203%±0.00111%
HS-9	11.5±0.627	2.12±0.113	0.260±0.0314	0.733±0.0333	18.5%±1.01%	2.27%±0.124%	0.00639%±0.00034 9%
HS-10	5.70±0.311	1.86±0.0790	0.394±0.0477	1.76±0.0867	32.6%±1.78%	6.92%±0.378%	0.0308%±0.00169%
HS-11	9.76±0.534	1.95±0.0892	0.240±0.0290	0.656±0.0300	20.0%±1.09%	2.46%±0.134%	0.00672%±0.00036 7%
				Average	**32.2%**	**7.64%**	**0.0218%**
CH, Guangzhou							
CH-1	6.80±0.475	1.61±0.0709	0.980±0.118	0.763±0.0404	23.7%±1.30%	14.4%±0.788%	0.0112%±0.000614 %
CH-2	7.26±0.476	1.35±0.0576	0.787±0.0952	0.477±0.0252	18.6%±1.02%	10.8%±0.593%	0.00657%±0.00035 9%
CH-3	6.78±0.414	1.54±0.0648	0.539±0.0651	4.48±0.197	22.8%±1.24%	8.00%±0.435%	0.0661%±0.00361%

CH-4	8.87±0.704	2.13±0.109	1.53±0.184	2.50±0.108	24.0%±1.31%	17.2%±0.940%	0.0282%±0.00154%
CH-5	5.32±0.405	1.95±0.0899	0.257±0.0311	0.43±0.0201	36.6%±2.00%	4.84%±0.264%	0.00808%±0.000442%
CH-6	2.13±0.169	1.88±0.0945	0.246±0.0297	2.10±0.0912	88.2%±4.82%	11.5%±0.629%	0.0984%±0.00538%
CH-11	2.45±0.191	1.28±0.0761	0.276±0.0334	0.726±0.0353	52.4%±2.86%	11.3%±0.616%	0.0296%±0.00162%
CH-12	2.90±0.225	1.05±0.0513	0.204±0.0247	0.439±0.0201	36.3%±1.99%	7.04%±0.385%	0.0151%±0.000827%
CH-13	2.40±0.192	1.46±0.0879	0.173±0.0209	0.335±0.0178	60.8%±3.32%	7.18%±0.393%	0.0139%±0.000762%
CH-14	4.40±0.255	1.41±0.0767	0.221±0.0267	0.157±0.00757	32.1%±1.75%	5.02%±0.275%	0.00357%±0.000195%
				Average	**39.5%**	**9.73%**	**0.0281%**

[a] Data from Appendix 2.1.

[b, c, d] Calculated using Equation 3-14 with mass concentrations in Appendix 1.5 and 1.6 and REP values from Appendix 2.2; standard errors calculated using Equation 3-23.

[e, f, g] Calculated using Equation 3-15; standard errors calculated using Equation 3-24.

2.5. Summary of error estimation results of PMF apportionment.

	Nanjing	Guangzhou
Robust model	Yes	Yes
Seed value	Random	Random
# of Base Model Runs	100	100
# of BS Runs	100	100
Mean R-value in BS	0.6	0.6
DISP error code	0	0
DISP %dQ	0.28	0.84
Qtrue/Qrobust	1.06	1.04

2.6. BS mapping of Nanjing samples of PMF apportionment.

		Factor 1	Factor 2	Factor 3	Factor 4	Factor 5	Factor 6	Factor 7	Factor 8	Unmapped	Mapping Frequency
Combustion (coal biomass and waste)	Boot Factor 1	73	2	6	4	0	0	0	15	0	73%
Secondary sulfate	Boot Factor 2	0	98	0	0	0	0	0	2	0	98%
Secondary nitrate	Boot Factor 3	0	0	99	0	0	0	0	1	0	99%
Fugitive dust	Boot Factor 4	1	1	8	74	0	1	0	15	0	74%
Biological emissions	Boot Factor 5	5	1	8	0	73	2	0	9	2	73%
Traffic (vehicle and ship) emissions	Boot Factor 6	4	4	7	1	0	79	0	4	1	79%

Sea salt	Boot Factor 7	1	0	1	0	0	0	96	2	0	96%
Industrial emissions	Boot Factor 8	1	0	0	0	0	0	0	99	0	99%

2.7. BS mapping of Guangzhou samples of PMF apportionment.

		Factor 1	Factor 2	Factor 3	Factor 4	Factor 5	Factor 6	Factor 7	Factor 8	Unmapped	Mapping Frequency
Combustion (coal biomass and waste)	Boot Factor 1	100	0	0	0	0	0	0	0	0	100%
Ship emissions mixed with secondary sulfate	Boot Factor 2	0	100	0	0	0	0	0	0	0	100%
Secondary nitrate	Boot Factor 3	0	0	100	0	0	0	0	0	0	100%
Fugitive dust	Boot Factor 4	0	0	0	100	0	0	0	0	0	100%
Biological emissions	Boot Factor 5	0	0	0	0	100	0	0	0	0	100%
Vehicle emissions	Boot Factor 6	0	0	0	0	0	100	0	0	0	100%

Sea salts	Boot Factor 7	5	10	0	5	0	5	70	5	5	70%
Industrial emissions	Boot Factor 8	0	5	0	0	0	0	0	95	0	95%

References

Abbas, I., Badran, G., Verdin, A., Ledoux, F., Roumie, M., Guidice, J.-M. L., Courcot, D., and Garçon, G. (2019). *In vitro* evaluation of organic extractable matter from ambient $PM_{2.5}$ using human bronchial epithelial BEAS-2B cells: Cytotoxicity, oxidative stress, pro-inflammatory response, genotoxicity, and cell cycle deregulation. *Environmental Research*, *171*, 510–522.

Acciai, C., Zhang, Z., Wang, F., Zhong, Z., and Lonati, G. (2017). Characteristics and source analysis of trace elements in $PM_{2.5}$ in the urban atmosphere of Wuhan in spring. *Aerosol and Air Quality Research*, *17*(9), 2224–2234.

Akhtar, M. J., Ahamed, M., Khan, M. M., Alrokayan, S. A., Ahmad, I., and Kumar, S. (2014). Cytotoxicity and apoptosis induction by nanoscale talc particles from two different geographical regions in human lung epithelial cells. *Environmental toxicology*, *29*(4), 394–406.

Al Housseiny, H., Singh, M., Emile, S., Nicoleau, M., Wal, R. L. V., and Silveyra, P. (2020). Identification of toxicity parameters associated with combustion produced soot surface chemistry and particle structure by *in vitro* assays. *Biomedicines*, *8*(9), 345.

Allen, J., Bartlett, K., Graham, M., and Jackson, P. (2011). Ambient concentrations of airborne endotoxin in two cities in the interior of British Columbia, Canada. *Journal of Environmental Monitoring*, *13*(3), 631–640.

Almeida, S. M., Manousakas, M., Diapouli, E., Kertesz, Z., Samek, L., Hristova, E., Šega, K., Alvarez, R. P., Belis, C. A., and Eleftheriadis, K. (2020). Ambient particulate matter source apportionment using receptor modelling in European and Central Asia urban areas. *Environmental Pollution*, *266*, 115199.

Altenburger, R., Boedeker, W., Faust, M., and Grimme, L. (1996). Regulations for combined effects of pollutants: Consequences from risk assessment in aquatic toxicology. *Food and Chemical Toxicology*, *34*(11-12), 1155–1157.

Amin, H., Šantl-Temkiv, T., Cramer, C., Finster, K., Real, F. G., Gislason, T., Holm, M., Janson, C., Jögi, N. O., and Jogi, R. (2023). Indoor airborne microbiome and endotoxin: meteorological events and occupant characteristics are important determinants. *Environmental Science & Technology*, *57*(32), 11750–11766.

Apte, J. S., Brauer, M., Cohen, A. J., Ezzati, M., and Pope III, C. A. (2018). Ambient PM2. 5 reduces global and regional life expectancy. *Environmental Science & Technology Letters*, *5*(9), 546–551.

Arms, A., and Travis, C. (1988). *Reference Physiological Parameters in Pharmacokinetic Modeling. Washington, DC: Office of Health and Environmental Assessment, Office of Research and Development*.

Avila-Calderón, E. D., Ruiz-Palma, M. d. S., Aguilera-Arreola, M. G., Velázquez-Guadarrama, N., Ruiz, E. A., Gomez-Lunar, Z., Witonsky, S., and Contreras-Rodríguez, A. (2021). Outer membrane vesicles of gram-negative bacteria: an outlook on biogenesis. *Frontiers in microbiology*, *12*, 557902.

Backhaus, T., and Faust, M. (2012). Predictive environmental risk assessment of chemical mixtures: a conceptual framework. *Environmental Science & Technology*, *46*(5), 2564–2573.

Bai, X., Liu, Y., Wang, S., Liu, C., Liu, F., Su, G., Peng, X., Yuan, C., Jiang, Y., and Yan, B. (2018). Ultrafine particle libraries for exploring mechanisms of $PM_{2.5}$-induced toxicity in human cells. *Ecotoxicology and Environmental Safety*, *157*, 380–387.

Basinas, I., Schlünssen, V., Takai, H., Heederik, D., Omland, Ø., Wouters, I. M., Sigsgaard, T., and Kromhout, H. (2013). Exposure to inhalable dust and endotoxin among Danish pig farmers affected by work tasks and stable characteristics. *Annals of Occupational Hygiene*, *57*(8), 1005–1019.

Basinas, I., Sigsgaard, T., Kromhout, H., Heederik, D., Wouters, I. M., and Schlünssen, V. (2015). A comprehensive review of levels and determinants of personal exposure to dust and endotoxin in livestock farming. *Journal of Exposure Science & Environmental Epidemiology*, *25*(2), 123–137.

Bates, J. T., Fang, T., Verma, V., Zeng, L., Weber, R. J., Tolbert, P. E., Abrams, J. Y., Sarnat, S. E., Klein, M., and Mulholland, J. A. (2019). Review of acellular assays of ambient particulate matter oxidative potential: methods and relationships with composition, sources, and health effects. *Environmental Science & Technology*, *53*(8), 4003–4019.

Bekki, K., Ito, T., Yoshida, Y., He, C., Arashidani, K., He, M., Sun, G., Zeng, Y., Sone, H., and Kunugita, N. (2016). $PM_{2.5}$ collected in China causes inflammatory and oxidative stress responses in macrophages through the multiple pathways. *Environmental Toxicology and Pharmacology*, *45*, 362–369.

Bertolini, V., Gandolfi, I., Ambrosini, R., Bestetti, G., Innocente, E., Rampazzo, G., and Franzetti, A. (2013). Temporal variability and effect of environmental variables on airborne bacterial communities in an urban area of Northern Italy. *Applied microbiology and biotechnology*, *97*, 6561–6570.

Billet, S., Garçon, G., Dagher, Z., Verdin, A., Ledoux, F., Cazier, F., Courcot, D., Aboukais, A., and Shirali, P. (2007). Ambient particulate matter ($PM_{2.5}$):

physicochemical characterization and metabolic activation of the organic fraction in human lung epithelial cells (A549). *Environmental Research*, *105*(2), 212–223.

Bo, L., Jiang, S., Xie, Y., Kan, H., Song, W., and Zhao, J. (2016). Effect of vitamin E and omega-3 fatty acids on protecting ambient $PM_{2.5}$-induced inflammatory response and oxidative stress in vascular endothelial cells. *PLoS One*, *11*(3), e0152216.

Boreson, J., Dillner, A. M., and Peccia, J. (2004). Correlating bioaerosol load with $PM_{2.5}$ and PM_{10cf} concentrations: a comparison between natural desert and urban-fringe aerosols. *Atmospheric Environment*, *38*(35), 6029–6041.

Bouloubassi, I., Roussiez, V., Azzoug, M., and Lorre, A. (2012). Sources, dispersal pathways and mass budget of sedimentary polycyclic aromatic hydrocarbons (PAH) in the NW Mediterranean margin, Gulf of Lions. *Marine Chemistry*, *142-144*, 18–28.

Bowers, R. M., Clements, N., Emerson, J. B., Wiedinmyer, C., Hannigan, M. P., and Fierer, N. (2013). Seasonal variability in bacterial and fungal diversity of the near-surface atmosphere. *Environmental Science & Technology*, *47*(21), 12097–12106.

Bowers, R. M., McLetchie, S., Knight, R., and Fierer, N. (2011). Spatial variability in airborne bacterial communities across land-use types and their relationship to the bacterial communities of potential source environments. *The ISME journal*, *5*(4), 601–612.

Brodie, E. L., DeSantis, T. Z., Parker, J. P. M., Zubietta, I. X., Piceno, Y. M., and Andersen, G. L. (2007). Urban aerosols harbor diverse and dynamic bacterial populations. *Proceedings of the National Academy of Sciences*, *104*(1), 299–304.

Brook, R. D., Franklin, B., Cascio, W., Hong, Y., Howard, G., Lipsett, M., Luepker, R., Mittleman, M., Samet, J., and Smith Jr, S. C. (2004). Air pollution and cardiovascular disease: a statement for healthcare professionals from the Expert Panel on Population and Prevention Science of the American Heart Association. *Circulation*, *109*(21), 2655–2671.

Cao, C., Jiang, W., Wang, B., Fang, J., Lang, J., Tian, G., Jiang, J., and Zhu, T. F. (2014). Inhalable microorganisms in Beijing's $PM_{2.5}$ and PM_{10} pollutants during a severe smog event. *Environmental Science & Technology*, *48*(3), 1499–1507.

Cao, W., Yin, L., Zhang, D., Wang, Y., Yuan, J., Zhu, Y., and Dou, J. (2019). Contamination, Sources, and Health Risks Associated with Soil PAHs in Rebuilt Land from a Coking Plant, Beijing, China. *International Journal of Environmental Research and Public Health*, *16*(4), 670.

Carty, C. L., Gehring, U., Cyrys, J., Bischof, W., and Heinrich, J. (2003). Seasonal variability of endotoxin in ambient fine particulate matter. *Journal of Environmental Monitoring*, *5*(6), 953–958.

Cedergreen, N., Christensen, A. M., Kamper, A., Kudsk, P., Mathiassen, S. K., Streibig, J. C., and Sørensen, H. (2008). A review of independent action compared to concentration addition as reference models for mixtures of compounds with different molecular target sites. *Environmental Toxicology and Chemistry*, *27*(7), 1621–1632.

Chai, F., Gao, J., Chen, Z., Wang, S., Zhang, Y., Zhang, J., Zhang, H., Yun, Y., and Ren, C. (2014). Spatial and temporal variation of particulate matter and gaseous pollutants in 26 cities in China. *Journal of Environmental Sciences*, *26*(1), 75–82.

Chang, L., Chong, W. T., Wang, X., Pei, F., Zhang, X., Wang, T., Wang, C., and Pan, S. (2021). Recent progress in research on $PM_{2.5}$ in subways. *Environmental Science: Processes & Impacts*, *23*(5), 642–663.

Charrier, J. G., and Anastasio, C. (2012). On dithiothreitol (DTT) as a measure of oxidative potential for ambient particles: evidence for the importance of soluble transition metals. *Atmospheric Chemistry and Physics (Print)*, *12*(5), 11317.

Chen, D., Feng, Q., Liang, H., Gao, B., and Alam, E. (2019a). Distribution characteristics and ecological risk assessment of polycyclic aromatic hydrocarbons (PAHs) in underground coal mining environment of Xuzhou. *Human and Ecological Risk Assessment: An International Journal*, *25*(6), 1564–1578.

Chen, H., Kwong, J. C., Copes, R., Tu, K., Villeneuve, P. J., Van Donkelaar, A., Hystad, P., Martin, R. V., Murray, B. J., and Jessiman, B. (2017). Living near major roads and the incidence of dementia, Parkinson's disease, and multiple sclerosis: a population-based cohort study. *The Lancet*, *389*(10070), 718–726.

Chen, J., Tan, M., Li, Y., Zheng, J., Zhang, Y., Shan, Z., Zhang, G., and Li, Y. (2008). Characteristics of trace elements and lead isotope ratios in PM2. 5 from four sites in Shanghai. *Journal of Hazardous Materials*, *156*(1-3), 36–43.

Chen, Q., Chen, Y., Luo, X.-S., Hong, Y., Hong, Z., Zhao, Z., and Chen, J. (2019b). Seasonal characteristics and health risks of $PM_{2.5}$-bound organic pollutants in industrial and urban areas of a China megacity. *Journal of Environmental Management*, *245*, 273–281.

Chen, X., Wu, D., Tan, Y., Song, X., Chen, J., and Li, Q. (2024). Absence of a causal link between elemental carbon exposure and short-term respiratory toxicity in human-derived organoids and cellular models. *Environmental Science & Technology*.

Chen, Y., Xie, S.-d., Luo, B., and Zhai, C. (2019c). Characteristics and sources of water-soluble ions in PM2. 5 in the Sichuan Basin, China. *Atmosphere*, *10*(2), 78.

Cheng, J. Y. W., Hui, E. L. C., and Lau, A. P. S. (2012). Bioactive and total endotoxins in atmospheric aerosols in the Pearl River Delta region, China. *Atmospheric Environment*, *47*, 3–11.

Churg, A., and Brauer, M. (1997). Human lung parenchyma retains PM2. 5. *American journal of respiratory and critical care medicine*, *155*(6), 2109–2111.

Collins, J. F., Brown, J. P., Alexeeff, G. V., and Salmon, A. G. (1998). Potency Equivalency Factors for Some Polycyclic Aromatic Hydrocarbons and Polycyclic Aromatic Hydrocarbon Derivatives. *Regulatory Toxicology and Pharmacology*, *28*(1), 45–54.

Courcot, E., Leclerc, J., Lafitte, J.-J., Mensier, E., Jaillard, S., Gosset, P., Shirali, P., Pottier, N., Broly, F., and Lo-Guidice, J.-M. (2012). Xenobiotic metabolism and disposition in human lung cell models: comparison with *in vivo* expression profiles. *Drug Metabolism and Disposition*, *40*(10), 1953–1965.

Currie, L. A. (2000). Evolution and Multidisciplinary Frontiers of 14C Aerosol Science1. *Radiocarbon*, *42*(1), 115–126.

Daellenbach, K. R., Uzu, G., Jiang, J., Cassagnes, L.-E., Leni, Z., Vlachou, A., Stefenelli, G., Canonaco, F., Weber, S., and Segers, A. (2020). Sources of particulate-matter air pollution and its oxidative potential in Europe. *Nature*, *587*(7834), 414–419.

Davel, A. P., Lemos, M., Pastro, L. M., Pedro, S. C., de André, P. A., Hebeda, C., Farsky, S. H., Saldiva, P. H., and Rossoni, L. V. (2012). Endothelial dysfunction in the pulmonary artery induced by concentrated fine particulate matter exposure is associated with local but not systemic inflammation. *Toxicology*, *295*(1-3), 39–46.

Degobbi, C., Lopes, F. D., Carvalho-Oliveira, R., Muñoz, J. E., and Saldiva, P. H. (2011). Correlation of fungi and endotoxin with $PM_{2.5}$ and meteorological parameters in atmosphere of Sao Paulo, Brazil. *Atmospheric Environment*, *45*(13), 2277–2283.

Deng, X., Rui, W., Zhang, F., and Ding, W. (2013). $PM_{2.5}$ induces Nrf2-mediated defense mechanisms against oxidative stress by activating PIK3/AKT signaling pathway in human lung alveolar epithelial A549 cells. *Cell biology and toxicology*, *29*, 143–157.

Dergham, M., Lepers, C., Verdin, A., Billet, S., Cazier, F., Courcot, D., Shirali, P., and Garçon, G. (2012). Prooxidant and proinflammatory potency of air pollution particulate matter ($PM_{2.5–0.3}$) produced in rural, urban, or industrial surroundings in human bronchial epithelial cells (BEAS-2B). *Chemical research in toxicology*, *25*(4), 904–919.

Dong, L., Qi, J., Shao, C., Zhong, X., Gao, D., Cao, W., Gao, J., Bai, R., Long, G., and Chu, C. (2016). Concentration and size distribution of total airborne microbes in hazy and foggy weather. *Science of the Total Environment*, *541*, 1011–1018.

Douwes, J., Thorne, P., Pearce, N., and Heederik, D. (2003). Bioaerosol health effects and exposure assessment: progress and prospects. *Annals of Occupational Hygiene*, *47*(3), 187–200.

Duquenne, P., Marchand, G., and Duchaine, C. (2013). Measurement of endotoxins in bioaerosols at workplace: a critical review of literature and a standardization issue. *Annals of Occupational Hygiene*, *57*(2), 137–172.

Ekman Nilsson, A., Macias Aragonés, M., Arroyo Torralvo, F., Dunon, V., Angel, H., Komnitsas, K., and Willquist, K. (2017). A review of the carbon footprint of Cu and Zn production from primary and secondary sources. *Minerals*, *7*(9), 168.

Escher, B. I., Bramaz, N., Mueller, J. F., Quayle, P., Rutishauser, S., and Vermeirssen, E. L. (2008). Toxic equivalent concentrations (TEQs) for baseline toxicity and specific modes of action as a tool to improve interpretation of ecotoxicity testing of environmental samples. *Journal of Environmental Monitoring*, *10*(5), 612–621.

Escher, B. I., Neale, P. A., and Villeneuve, D. L. (2018). The advantages of linear concentration–response curves for in vitro bioassays with environmental samples. *Environmental Toxicology and Chemistry*, *37*(9), 2273–2280.

Escher, B. I., van Daele, C., Dutt, M., Tang, J. Y., and Altenburger, R. (2013). Most oxidative stress response in water samples comes from unknown chemicals: the need for effect-based water quality trigger values. *Environmental Science & Technology*, *47*(13), 7002–7011.

Fang, Z., Ouyang, Z., Hu, L., Wang, X., Zheng, H., and Lin, X. (2005). Culturable airborne fungi in outdoor environments in Beijing, China. *Science of the Total Environment*, *350*(1-3), 47–58.

Fayyaz, K., Nawaz, A., Olaimat, A. N., Akram, K., Farooq, U., Fatima, M., Siddiqui, S. A., Rana, I. S., and Shahbaz, H. M. (2022). Microbial toxins in fermented foods: health implications and analytical techniques for detection. *Journal of food and drug analysis*, *30*(4), 523.

Federici, E., Petroselli, C., Montalbani, E., Casagrande, C., Ceci, E., Moroni, B., La Porta, G., Castellini, S., Selvaggi, R., and Sebastiani, B. (2018). Airborne bacteria and persistent organic pollutants associated with an intense Saharan dust event in the Central Mediterranean. *Science of the Total Environment*, *645*, 401–410.

Fierer, N., Liu, Z., Rodríguez-Hernández, M., Knight, R., Henn, M., and Hernandez, M. T. (2008). Short-term temporal variability in airborne bacterial and fungal populations. *Applied and environmental microbiology*, *74*(1), 200–207.

Fung, F., and Hughson, W. G. (2003). Health effects of indoor fungal bioaerosol exposure. *Applied occupational and environmental hygiene*, *18*(7), 535–544.

Fuzzi, S., Andreae, M. O., Huebert, B. J., Kulmala, M., Bond, T. C., Boy, M., Doherty, S. J., Guenther, A., Kanakidou, M., and Kawamura, K. (2006). Critical assessment of the current state of scientific knowledge, terminology, and research needs concerning the role of organic aerosols in the atmosphere, climate, and global change. *Atmospheric Chemistry and Physics*, *6*(7), 2017–2038.

Fuzzi, S., Baltensperger, U., Carslaw, K., Decesari, S., Denier van der Gon, H., Facchini, M. C., Fowler, D., Koren, I., Langford, B., and Lohmann, U. (2015). Particulate matter, air quality and climate: lessons learned and future needs. *Atmospheric Chemistry and Physics*, *15*(14), 8217–8299.

Gangwar, R. S., Bevan, G. H., Palanivel, R., Das, L., and Rajagopalan, S. (2020). Oxidative stress pathways of air pollution mediated toxicity: Recent insights. *Redox Biology*, *34*, 101545.

Gao, J. F., Fan, X. Y., Li, H. Y., and Pan, K. L. (2017). Airborne bacterial communities of $PM_{2.5}$ in Beijing-Tianjin-Hebei megalopolis, China as revealed by Illumina MiSeq sequencing: a case study. *Aerosol and Air Quality Research*, *17*(3), 788–798.

Gao, M., Jia, R., Qiu, T., Han, M., Song, Y., and Wang, X. (2015). Seasonal size distribution of airborne culturable bacteria and fungi and preliminary estimation of their deposition in human lungs during non-haze and haze days. *Atmospheric Environment*, *118*, 203–210.

Gaohua, L., Wedagedera, J., Small, B., Almond, L., Romero, K., Hermann, D., Hanna, D., Jamei, M., and Gardner, I. (2015). Development of a multicompartment permeability-limited lung PBPK model and its application in predicting pulmonary pharmacokinetics of antituberculosis drugs. *CPT: pharmacometrics & systems pharmacology*, *4*(10), 605–613.

Gasana, J., Dillikar, D., Mendy, A., Forno, E., and Vieira, E. R. (2012). Motor vehicle air pollution and asthma in children: a meta-analysis. *Environmental Research*, *117*, 36–45.

Gehling, W., and Dellinger, B. (2013). Environmentally persistent free radicals and their lifetimes in $PM_{2.5}$. *Environmental Science & Technology*, *47*(15), 8172–8178.

Gehling, W., Khachatryan, L., and Dellinger, B. (2014). Hydroxyl radical generation from environmentally persistent free radicals (EPFRs) in $PM_{2.5}$. *Environmental Science & Technology*, *48*(8), 4266–4272.

Gioffrè, A., Marramao, A., and IannÒ, A. (2012). Airborne microorganisms, endotoxin, and dust concentration in wood factories in Italy. *Annals of Occupational Hygiene*, *56*(2), 161–169.

Gottenbos, B., Grijpma, D. W., van der Mei, H. C., Feijen, J., and Busscher, H. J. (2001). Antimicrobial effects of positively charged surfaces on adhering Gram-positive and Gram-negative bacteria. *Journal of antimicrobial chemotherapy*, *48*(1), 7–13.

Gou, H., Lu, J., Li, S., Tong, Y., Xie, C., and Zheng, X. (2016). Assessment of microbial communities in PM_1 and PM_{10} of Urumqi during winter. *Environmental Pollution*, *214*, 202–210.

Grange, S. K., Uzu, G., Weber, S., Jaffrezo, J.-L., and Hueglin, C. (2022). Linking Switzerland's PM_{10} and $PM_{2.5}$ oxidative potential (OP) with emission sources. *Atmospheric Chemistry and Physics*, *22*(10), 7029–7050.

Gualtieri, M., Longhin, E., Mattioli, M., Mantecca, P., Tinaglia, V., Mangano, E., Proverbio, M. C., Bestetti, G., Camatini, M., and Battaglia, C. (2012). Gene expression profiling of A549 cells exposed to Milan $PM_{2.5}$. *Toxicology letters*, *209*(2), 136–145.

Gualtieri, M., Mantecca, P., Corvaja, V., Longhin, E., Perrone, M. G., Bolzacchini, E., and Camatini, M. (2009). Winter fine particulate matter from Milan induces morphological and functional alterations in human pulmonary epithelial cells (A549). *Toxicology letters*, *188*(1), 52–62.

Guan, T., Yao, M., Wang, J., Fang, Y., Hu, S., Wang, Y., Dutta, A., Yang, J., Wu, Y., and Hu, M. (2014). Airborne endotoxin in fine particulate matter in Beijing. *Atmospheric Environment*, *97*, 35–42.

Guangdong Statistics Bureau. (2017). Guangdong Statistical Yearbook 2017. In: China Statistics Press. Retrieved from http://stats.gd.gov.cn/gdtjnj/content/post_1424896.html.

Guangzhou Meteorological Observatory. (2020). 2020 Guangzhou Climate Bulletin, Guangzhou, China.

Guangzhou Municipal Ecological Environment Bureau. (2019). Guangzhou Releases 2019 $PM_{2.5}$ Source Analysis Results, Guangzhou, China.

Guangzhou Statistics Bureau. (2023). *Controlling total volume and reducing intensity: dual energy control yields fruitful results; peaking carbon emissions and achieving*

carbon neutrality: green and low-carbon initiatives embark on a new chapter — Guangzhou energy production and consumption report during the "13th Five-Year Plan" period.

Guarnieri, M., and Balmes, J. R. (2014). Outdoor air pollution and asthma. *The Lancet*, *383*(9928), 1581–1592.

Guo, H., Jin, L., and Huang, S. (2020). Effect of PM characterization on PM oxidative potential by acellular assays: a review. *Reviews on Environmental Health*, *35*(4), 461–470.

Haas, D., Galler, H., Luxner, J., Zarfel, G., Buzina, W., Friedl, H., Marth, E., Habib, J., and Reinthaler, F. F. (2013). The concentrations of culturable microorganisms in relation to particulate matter in urban air. *Atmospheric Environment*, *65*, 215–222.

Hao, Y., Luo, B., Simayi, M., Zhang, W., Jiang, Y., He, J., and Xie, S. (2020). Spatiotemporal patterns of $PM_{2.5}$ elemental composition over China and associated health risks. *Environmental Pollution*, *265*, 114910.

He, T., Jin, L., Xie, J., Yue, S., Fu, P., and Li, X. (2021). Intracellular and extracellular antibiotic resistance genes in airborne $PM_{2.5}$ for respiratory exposure in urban areas. *Environmental Science & Technology Letters*, *8*(2), 128–134.

Health Effects Institute. (2024). State of Global Air 2024, Boston, USA.

Ho, S. S. H., and Yu, J. Z. (2004). In-injection port thermal desorption and subsequent gas chromatography-mass spectrometric analysis of polycyclic aromatic hydrocarbons and n-alkanes in atmospheric aerosol samples. *Journal of Chromatography A*, *1059*(1-2), 121–129.

Honda, A., Okuda, T., Nagao, M., Miyasaka, N., Tanaka, M., and Takano, H. (2021). $PM_{2.5}$ collected using cyclonic separation causes stronger biological responses than that collected using a conventional filtration method. *Environmental Research*, *198*, 110490.

Hopke, P. K., Dai, Q., Li, L., and Feng, Y. (2020). Global review of recent source apportionments for airborne particulate matter. *Science of the Total Environment*, *740*, 140091.

Hou, T., Zhu, L., Wang, Y., and Peng, L. (2024). Oxidative stress is the pivot for $PM_{2.5}$-induced lung injury. *Food and Chemical Toxicology*, *184*, 114362.

Hsu, C. Y., Chi, K.-H., Wu, C.-D., Lin, S.-L., Hsu, W.-C., Tseng, C.-C., Chen, M.-J., and Chen, Y.-C. (2021). Integrated analysis of source-specific risks for $PM_{2.5}$-bound metals in urban, suburban, rural, and industrial areas. *Environmental Pollution*, *275*, 116652.

Hu, D., and Jiang, J. (2013). A study of smog issues and $PM_{2.5}$ pollutant control strategies in China. *Journal of Environmental Protection*, *4*(7), 746–752.

Hu, H., Jin, Q., and Kavan, P. (2014). A study of heavy metal pollution in China: Current status, pollution-control policies and countermeasures. *Sustainability*, *6*(9), 5820–5838.

Hu, X., Zhang, Y., Ding, Z., Wang, T., Lian, H., Sun, Y., and Wu, J. (2012). Bioaccessibility and health risk of arsenic and heavy metals (Cd, Co, Cr, Cu, Ni, Pb, Zn and Mn) in TSP and $PM_{2.5}$ in Nanjing, China. *Atmospheric Environment*, *57*, 146–152.

Huang, Q., Zhang, J., Peng, S., Tian, M., Chen, J., and Shen, H. (2014a). Effects of water soluble $PM_{2.5}$ extracts exposure on human lung epithelial cells (A549): a proteomic study. *Journal of Applied Toxicology*, *34*(6), 675–687.

Huang, R. J., Zhang, Y., Bozzetti, C., Ho, K. F., Cao, J. J., Han, Y., Daellenbach, K. R., Slowik, J. G., Platt, S. M., and Canonaco, F. (2014b). High secondary aerosol contribution to particulate pollution during haze events in China. *Nature*, *514*(7521), 218–222.

Hueglin, C., Gehrig, R., Baltensperger, U., Gysel, M., Monn, C., and Vonmont, H. (2005). Chemical characterisation of $PM_{2.5}$, PM_{10} and coarse particles at urban, near-city and rural sites in Switzerland. *Atmospheric Environment*, *39*(4), 637–651.

Husárová, S., Vaïtilingom, M., Deguillaume, L., Traikia, M., Vinatier, V., Sancelme, M., Amato, P., Matulová, M., and Delort, A.-M. (2011). Biotransformation of methanol and formaldehyde by bacteria isolated from clouds. Comparison with radical chemistry. *Atmospheric Environment*, *45*(33), 6093–6102.

Innocente, E., Squizzato, S., Visin, F., Facca, C., Rampazzo, G., Bertolini, V., Gandolfi, I., Franzetti, A., Ambrosini, R., and Bestetti, G. (2017). Influence of seasonality, air mass origin and particulate matter chemical composition on airborne bacterial community structure in the Po Valley, Italy. *Science of the Total Environment*, *593*, 677–687.

IQAir. (2019). World Air Quality Report.

Jaenicke, R. (2005). Abundance of cellular material and proteins in the atmosphere. *Science*, *308*(5718), 73–73.

Jahne, M. A., Rogers, S. W., Holsen, T. M., Grimberg, S. J., and Ramler, I. P. (2015). Emission and dispersion of bioaerosols from dairy manure application sites: human health risk assessment. *Environmental Science & Technology*, *49*(16), 9842–9849.

Jalava, P. I., Happo, M. S., Huttunen, K., Sillanpää, M., Hillamo, R., Salonen, R. O., and Hirvonen, M.-R. (2015). Chemical and microbial components of urban air PM cause seasonal variation of toxicological activity. *Environmental Toxicology and Pharmacology*, *40*(2), 375–387.

Jia, Y.-Y., Wang, Q., and Liu, T. (2017). Toxicity research of $PM_{2.5}$ compositions in vitro. *International Journal of Environmental Research and Public Health*, *14*(3), 232.

Jiang, W., Liang, P., Wang, B., Fang, J., Lang, J., Tian, G., Jiang, J., and Zhu, T. F. (2015). Optimized DNA extraction and metagenomic sequencing of airborne microbial communities. *Nature protocols*, *10*(5), 768–779.

Jiangmen Statistics Bureau. (2017). Statistical Communique of Jiangmen on the 2016 National Economic and Social Development (in Chinese). In: Retrieved from http://www.jiangmen.gov.cn/bmpd/jmstjj/zwgk/tjgbyfx/content/post_906092.html.

Jiangsu News Network. (2022). Nanjing: a trillion-yuan city on the path to catch-up. https://jsnews.jschina.com.cn/nj/a/202206/t20220627_3025405.shtml

Jin, L., Xie, J., Wong, C. K., Chan, S. K., Abbaszade, G. l., Schnelle-Kreis, J. r., Zimmermann, R., Li, J., Zhang, G., Fu, P., and Li, X. D. (2019). Contributions of city-specific fine particulate matter ($PM_{2.5}$) to differential *in vitro* oxidative stress and toxicity implications between Beijing and Guangzhou of China. *Environmental Science & Technology*, *53*(5), 2881–2891.

Juan, C. A., Pérez de la Lastra, J. M., Plou, F. J., and Pérez-Lebeña, E. (2021). The chemistry of reactive oxygen species (ROS) revisited: outlining their role in biological macromolecules (DNA, lipids and proteins) and induced pathologies. *International Journal of Molecular Sciences*, *22*(9), 4642.

Kannan, S., Misra, D. P., Dvonch, J. T., and Krishnakumar, A. (2007). Exposures to airborne particulate matter and adverse perinatal outcomes: a biologically plausible mechanistic framework for exploring potential. *Ciencia & saude coletiva*, *12*, 1591–1602.

Karimi, H., Nikaeen, M., Gholipour, S., Hatamzadeh, M., Hassanzadeh, A., and Hajizadeh, Y. (2020). $PM_{2.5}$-associated bacteria in ambient air: Is $PM_{2.5}$ exposure associated with the acquisition of community-acquired staphylococcal infections? *Journal of Environmental Health Science and Engineering*, *18*(2), 1007–1013.

Katsoyiannis, A., Sweetman, A. J., and Jones, K. C. (2011). PAH molecular diagnostic ratios applied to atmospheric sources: a critical evaluation using two decades of source inventory and air concentration data from the UK. *Environmental Science & Technology*, *45*(20), 8897–8906.

Kawanaka, Y., Tsuchiya, Y., Yun, S.-J., and Sakamoto, K. (2009). Size distributions of polycyclic aromatic hydrocarbons in the atmosphere and estimation of the contribution of ultrafine particles to their lung deposition. *Environmental Science & Technology*, *43*(17), 6851–6856.

Kim, J., Seo, M., Choi, J., and Na, M. (2022). MRA Toolbox v. 1.0: a web-based toolbox for predicting mixture toxicity of chemical substances in chemical products. *Scientific Reports*, *12*(1), 8880.

Kouassi, K. S., Billet, S., Garçon, G., Verdin, A., Diouf, A., Cazier, F., Djaman, J., Courcot, D., and Shirali, P. (2010). Oxidative damage induced in A549 cells by physically and chemically characterized air particulate matter ($PM_{2.5}$) collected in Abidjan, Côte d'Ivoire. *Journal of Applied Toxicology: An International Journal*, *30*(4), 310–320.

Kulmala, M., Asmi, A., Lappalainen, H., Baltensperger, U., Brenguier, J.-L., Facchini, M., Hansson, H.-C., Hov, Ø., O'Dowd, C., and Pöschl, U. (2011). General overview: European Integrated project on Aerosol Cloud Climate and Air Quality interactions (EUCAARI)–integrating aerosol research from nano to global scales. *Atmospheric Chemistry and Physics*, *11*(24), 13061–13143.

Lao, X. Q., Guo, C., Chang, L.-y., Bo, Y., Zhang, Z., Chuang, Y. C., Jiang, W. K., Lin, C., Tam, T., and Lau, A. K. (2019). Long-term exposure to ambient fine particulate matter ($PM_{2.5}$) and incident type 2 diabetes: a longitudinal cohort study. *Diabetologia*, *62*, 759–769.

Lee, J., Lilly, G. D., Doty, R. C., Podsiadlo, P., and Kotov, N. A. (2009). *In vitro* toxicity testing of nanoparticles in 3D cell culture. *Small*, *5*(10), 1213–1221.

Li, B., Ma, Y., Zhou, Y., and Chai, E. (2023). Research progress of different components of $PM_{2.5}$ and ischemic stroke. *Scientific Reports*, *13*(1), 15965.

Li, H., Wang, Q. g., Yang, M., Li, F., Wang, J., Sun, Y., Wang, C., Wu, H., and Qian, X. (2016). Chemical characterization and source apportionment of $PM_{2.5}$ aerosols in a megacity of Southeast China. *Atmospheric Research*, *181*, 288–299.

Li, J., Xu, X., Lv, J., Wu, Q., Ren, M., Cao, J., and Liu, P. (2020). Source apportionment and health risk quantification for heavy metal sources in soils near aluminum-plastic manufacturing facilities in northeast China. *Human and Ecological Risk Assessment: An International Journal*, *26*(8), 2225–2244.

Li, Y., Zhang, H., Li, A., Zhang, J., and Du, S. (2022). High time-resolved variations of proteins in $PM_{2.5}$ during haze pollution periods in Xi'an, China. *Environmental Pollution*, *305*, 119212.

Liao, H. T., Lee, C. L., Tsai, W. C., Yu, J. Z., Tsai, S. W., Chou, C. C., and Wu, C. F. (2021). Source apportionment of urban $PM_{2.5}$ using positive matrix factorization with vertically distributed measurements of trace elements and nonpolar organic compounds. *Atmospheric Pollution Research*, *12*(4), 200–207.

Liao, Q., Liu, C., Jin, Y., Hua, M., Zheng, L., Pan, Y., and Huang, S. (2011). On geochemical regionalization of soils in Jiangsu. *Journal of Geology*, *35*(3), 225–235.

Lim, E. Y., and Kim, G.-D. (2024). Particulate matter-induced emerging health effects associated with oxidative stress and inflammation. *Antioxidants*, *13*(10), 1256.

Lin, M., and Yu, J. Z. (2019). Dithiothreitol (DTT) concentration effect and its implications on the applicability of DTT assay to evaluate the oxidative potential of atmospheric aerosol samples. *Environmental Pollution*, *251*, 938–944.

Liu, H., Zhang, X., Zhang, H., Yao, X., Zhou, M., Wang, J., He, Z., Zhang, H., Lou, L., and Mao, W. (2018a). Effect of air pollution on the total bacteria and pathogenic bacteria in different sizes of particulate matter. *Environmental Pollution*, *233*, 483–493.

Liu, H., Zhang, Z., Wen, N., and Wang, C. (2018b). Determination and risk assessment of airborne endotoxin concentrations in a university campus. *Journal of aerosol science*, *115*, 146–157.

Liu, K., Hua, S., and Song, L. (2022). $PM_{2.5}$ exposure and asthma development: the key role of oxidative stress. *Oxidative Medicine and Cellular Longevity*, *2022*(1), 3618806.

Liu, L., Zhang, Y., Yang, Z., Luo, S., and Zhang, Y. (2021). Long-term exposure to fine particulate constituents and cardiovascular diseases in Chinese adults. *Journal of Hazardous Materials*, *416*, 126051.

Liu, X., Wu, W., Zou, H., Pan, C., Liu, M., and Li, H. (2025). Unveiling seasonal disparities in urban form: Exploring scale and intensity effects on $PM_{2.5}$ concentrations. *Urban Climate*, *59*, 102319.

Liu, Y., Dong, J., Xu, X., and Jiang, Y. (2020). $PM_{2.5}$ mass concentration variation in urban residential buildings during heating season in severe cold region of China: a case study in Harbin. *Science of the Total Environment*, *722*, 137945.

Longhin, E., Holme, J. A., Gutzkow, K. B., Arlt, V. M., Kucab, J. E., Camatini, M., and Gualtieri, M. (2013). Cell cycle alterations induced by urban $PM_{2.5}$ in bronchial epithelial cells: characterization of the process and possible mechanisms involved. *Particle and fibre toxicology*, *10*, 1–19.

Luo, W., Chen, H., Lei, A., Lu, J., and Hu, Z. (2014). Estimating cyanobacteria community dynamics and its relationship with environmental factors. *International Journal of Environmental Research and Public Health*, *11*(1), 1141–1160.

Lymperopoulou, D. S., Adams, R. I., and Lindow, S. E. (2016). Contribution of vegetation to the microbial composition of nearby outdoor air. *Applied and environmental microbiology*, *82*(13), 3822–3833.

Lyu, Y., Guo, H., Cheng, T., and Li, X. (2018). Particle size distributions of oxidative potential of lung-deposited particles: assessing contributions from quinones and water-soluble metals. *Environmental Science & Technology*, *52*(11), 6592–6600.

Ma, H., Li, J., Wan, C., Liang, Y., Zhang, X., Dong, G., Hu, L., Yang, B., Zeng, X., Su, T., Lu, S., Chen, S., Khorram, M. S., Sheng, G., Wang, X., Mai, B., Yu, Z., and Zhang, G. (2019). Inflammation Response of Water-Soluble Fractions in Atmospheric Fine Particulates: A Seasonal Observation in 10 Large Chinese Cities. *Environmental Science & Technology*, *53*(7), 3782–3790.

Maciejczyk, P., Zhong, M., Lippmann, M., and Chen, L. C. (2010). Oxidant generation capacity of source-apportioned $PM_{2.5}$. *Inhalation Toxicology*, *22*(sup2), 29–36.

Madsen, A. M., Uhrbrand, K., Kofoed, V. C., Fischer, T. K., and Frederiksen, M. W. (2023). A cohort study of wastewater treatment plant workers: association between levels of biomarkers of systemic inflammation and exposure to bacteria and fungi, and endotoxin as measured using two methods. *Water Research*, *231*, 119625.

Malm, W. C., Schichtel, B. A., Hand, J. L., and Collett Jr., J. L. (2017). Concurrent Temporal and Spatial Trends in Sulfate and Organic Mass Concentrations Measured in the IMPROVE Monitoring Program. *Journal of Geophysical Research: Atmospheres*, *122*(19), 10,462–410,476.

Manousakas, M., Papaefthymiou, H., Diapouli, E., Migliori, A., Karydas, A., Bogdanovic-Radovic, I., and Eleftheriadis, K. (2017). Assessment of $PM_{2.5}$ sources and their corresponding level of uncertainty in a coastal urban area using EPA PMF 5.0 enhanced diagnostics. *Science of the Total Environment*, *574*, 155–164.

Marcano, R., Rojo, M. Á., Cordoba-Diaz, D., and Garrosa, M. (2021). Pathological and therapeutic approach to endotoxin-secreting bacteria involved in periodontal disease. *Toxins*, *13*(8), 533.

Maron, P. A., Mougel, C., Lejon, D. P., Carvalho, E., Bizet, K., Marck, G., Cubito, N., Lemanceau, P., and Ranjard, L. (2006). Temporal variability of airborne bacterial community structure in an urban area. *Atmospheric Environment*, *40*(40), 8074–8080.

Matsui, E. C., Hansel, N. N., Aloe, C., Schiltz, A. M., Peng, R. D., Rabinovitch, N., Ong, M. J., Williams, D. A. L., Breysse, P. N., and Diette, G. B. (2013). Indoor pollutant exposures modify the effect of airborne endotoxin on asthma in urban children. *American journal of respiratory and critical care medicine*, *188*(10), 1210–1215.

Mooibroek, D., Schaap, M., Weijers, E., and Hoogerbrugge, R. (2011). Source apportionment and spatial variability of $PM_{2.5}$ using measurements at five sites in the Netherlands. *Atmospheric Environment*, *45*(25), 4180–4191.

Moretti, S., Smets, W., Hofman, J., Mubiana, K. V., Oerlemans, E., Vandenheuvel, D., Samson, R., Blust, R., and Lebeer, S. (2019). Human inflammatory response of endotoxin affected by particulate matter-bound transition metals. *Environmental Pollution*, *244*, 118–126.

Nadkarni, M. A., Martin, F. E., Jacques, N. A., and Hunter, N. (2002). Determination of bacterial load by real-time PCR using a broad-range (universal) probe and primers set. *Microbiology*, *148*(1), 257–266.

Nanjing Municipal Bureau of Statistics. (2020). *Nanjing municipal statistical bulletin of national economic and social development in 2019*. https://tjj.nanjing.gov.cn/bmfw/njsj/202201/t20220107_3256241.html

Nanjing Municipal Bureau Statistics. (2019). Nanjing Statistic Yearbook, Nanjing, China.

Nanjing Municipal Statistics Bureau. (2017). Nanjing statistical yearbook 2017 (in Chinese). In: Nanjing Press: Nanjing, China. Retrieved from http://221.226.86.104/file/2017/quxian/index.htm.

Nirmalkar, J., Lee, K., Ahn, J., Lee, J., and Song, M. (2023). Comparisons of spatial and temporal variations in $PM_{2.5}$-bound trace elements in urban and rural areas of South Korea, and associated potential health risks. *Atmosphere*, *14*(4), 753.

Norris, G., Duvall, R., Brown, S., Bai, S. (2014). EPA Positive Matrix Factorization (PMF) 5.0 fundamentals and User Guide Prepared for the US Environmental Protection Agency Office of Research and Development, Washington, DC. Inc., Petaluma.

O′ Sullivan, D., Murray, B. J., Ross, J. F., Whale, T. F., Price, H. C., Atkinson, J. D., Umo, N. S., and Webb, M. E. (2015). The relevance of nanoscale biological fragments for ice nucleation in clouds. *Scientific Reports*, *5*(1), 8082.

Oosthuizen, M. A., Wright, C. Y., Matooane, M., and Phala, N. (2015). Human health risk assessment of airborne metals to a potentially exposed community: a screening exercise. *Clean Air J.*, *25*(1), 51–57.

Pan, Y., Pan, X., Xiao, H., and Xiao, H. (2019). Structural characteristics and functional implications of $PM_{2.5}$ bacterial communities during fall in Beijing and Shanghai, China. *Frontiers in microbiology*, *10*, 2369.

Park, D. U., Yeom, J. K., Lee, W. J., and Lee, K. M. (2013). Assessment of the levels of airborne bacteria, gram-negative bacteria, and fungi in hospital lobbies. *International Journal of Environmental Research and Public Health*, *10*(2), 541–555.

Park, J., Park, E. H., Schauer, J. J., Yi, S.-M., and Heo, J. (2018). Reactive oxygen species (ROS) activity of ambient fine particles ($PM_{2.5}$) measured in Seoul, Korea. *Environment International*, *117*, 276–283.

Pavagadhi, S., Betha, R., Venkatesan, S., Balasubramanian, R., and Hande, M. P. (2013). Physicochemical and toxicological characteristics of urban aerosols during a recent Indonesian biomass burning episode. *Environmental Science and Pollution Research*, *20*, 2569–2578.

Peng, J., Yi, B., Wang, M., Tan, J., and Huang, Z. (2021). CRISPR/Cas9-mediated whole genomic wide knockout screening identifies specific genes associated with $PM_{2.5}$-induced mineral absorption in liver toxicity. *Frontiers in Bioengineering and Biotechnology*, *9*, 669434.

Perrone, M. G., Gualtieri, M., Ferrero, L., Porto, C. L., Udisti, R., Bolzacchini, E., and Camatini, M. (2010). Seasonal variations in chemical composition and in vitro biological effects of fine PM from Milan. *Chemosphere*, *78*(11), 1368–1377.

Ping, L., Wang, Y., Lu, Y., Lee, L.-C., and Liang, C. (2023). Tracing the sources of $PM_{2.5}$-related health burden in China. *Environmental Pollution*, *327*, 121544.

Pöhlker, C., Wiedemann, K. T., Sinha, B., Shiraiwa, M., Gunthe, S. S., Smith, M., Su, H., Artaxo, P., Chen, Q., and Cheng, Y. (2012). Biogenic potassium salt particles as seeds for secondary organic aerosol in the Amazon. *Science*, *337*(6098), 1075–1078.

Pun, V. C., Kazemiparkouhi, F., Manjourides, J., and Suh, H. H. (2017). Long-term $PM_{2.5}$ exposure and respiratory, cancer, and cardiovascular mortality in older US adults. *American journal of epidemiology*, *186*(8), 961–969.

Rabinovitch, N., Liu, A. H., Zhang, L., Rodes, C. E., Foarde, K., Dutton, S. J., Murphy, J. R., and Gelfand, E. W. (2005). Importance of the personal endotoxin cloud in school-age children with asthma. *Journal of Allergy and Clinical Immunology*, *116*(5), 1053–1057.

Rasuli, L., Dehghani, M. H., Aghaei, M., Mahvi, A. H., Mubarak, N. M., and Karri, R. R. (2022). Occurrence and fate of bacterial endotoxins in the environment (air, water, wastewater) and remediation technologies: An overview. *Chemosphere*, *303*, 135089.

Ravindra, K., Sokhi, R., and Van Grieken, R. (2008). Atmospheric polycyclic aromatic hydrocarbons: source attribution, emission factors and regulation. *Atmospheric Environment*, *42*(13), 2895–2921.

Reche, C., Moreno, T., Amato, F., Viana, M., Van Drooge, B. L., Chuang, H.-C., Bérubé, K., Jones, T., Alastuey, A., and Querol, X. (2012). A multidisciplinary approach to characterise exposure risk and toxicological effects of PM_{10} and $PM_{2.5}$ samples in urban environments. *Ecotoxicology and Environmental Safety*, *78*, 327–335.

Romano, S., Becagli, S., Lucarelli, F., Rispoli, G., and Perrone, M. (2020). Airborne bacteria structure and chemical composition relationships in winter and spring PM_{10} samples over southeastern Italy. *Science of the Total Environment*, *730*, 138899.

Ruiz, N., Kahne, D., and Silhavy, T. J. (2009). Transport of lipopolysaccharide across the cell envelope: the long road of discovery. *Nature Reviews Microbiology*, *7*(9), 677–683.

Russell, L. M. (2003). Aerosol organic-mass-to-organic-carbon ratio measurements. *Environmental Science & Technology*, *37*(13), 2982–2987.

Ryan, P. H., Bernstein, D. I., Lockey, J., Reponen, T., Levin, L., Grinshpun, S., Villareal, M., Khurana Hershey, G. K., Burkle, J., and LeMasters, G. (2009). Exposure to traffic-related particles and endotoxin during infancy is associated with wheezing at age 3 years. *American journal of respiratory and critical care medicine*, *180*(11), 1068–1075.

Ryou, H. G., Heo, J., and Kim, S. Y. (2018). Source apportionment of PM_{10} and $PM_{2.5}$ air pollution, and possible impacts of study characteristics in South Korea. *Environmental Pollution*, *240*, 963–972.

Salana, S., Yu, H., Dai, Z., Subramanian, P. G., Puthussery, J. V., Wang, Y., Singh, A., Pope, F. D., Leiva G, M. A., and Rastogi, N. (2024). Inter-continental variability in the relationship of oxidative potential and cytotoxicity with $PM_{2.5}$ mass. *Nature Communications*, *15*(1), 5263.

Samake, A., Uzu, G., Martins, J., Calas, A., Vince, E., Parat, S., and Jaffrezo, J. (2017). The unexpected role of bioaerosols in the Oxidative Potential of PM. *Scientific Reports*, *7*(1), 10978.

Sanchez de la Campa, A., García-Salamanca, A., Solano, J., de la Rosa, J., and Ramos, J.-L. (2013). Chemical and microbiological characterization of atmospheric particulate matter during an intense African dust event in Southern Spain. *Environmental Science & Technology*, *47*(8), 3630–3638.

Sandoval, S. S., and Silva, N. (2023). Review on generation and characterization of copper particles and copper composites prepared by mechanical milling on a lab-scale. *International Journal of Molecular Sciences*, *24*(9), 7933.

Santibáñez-Andrade, M., Quezada-Maldonado, E. M., Rivera-Pineda, A., Chirino, Y. I., García-Cuellar, C. M., and Sánchez-Pérez, Y. (2023). The road to malignant cell transformation after particulate matter exposure: from oxidative stress to genotoxicity. *International Journal of Molecular Sciences*, *24*(2), 1782.

Schaeffer, J. W., Reynolds, S., Magzamen, S., VanDyke, A., Gottel, N. R., Gilbert, J. A., Owens, S. M., Hampton-Marcell, J. T., and Volckens, J. (2017). Size, composition, and source profiles of inhalable bioaerosols from Colorado dairies. *Environmental Science & Technology*, *51*(11), 6430–6440.

She, Q., Peng, X., Xu, Q., Long, L., Wei, N., Liu, M., Jia, W., Zhou, T., Han, J., and Xiang, W. (2017). Air quality and its response to satellite-derived urban form in the Yangtze River Delta, China. *Ecological Indicators*, *75*, 297–306.

Shen, F., Niu, M., Chen, H., Zhang, T., Li, J., Tong, H., and Wu, Y. (2024). Nonlinear proinflammatory effect of short-term $PM_{2.5}$ exposure: A potential role of lipopolysaccharide. *Journal of Environmental Sciences*, *136*, 292–300.

Shen, F., Zheng, Y., Niu, M., Zhou, F., Wu, Y., Wang, J., Zhu, T., Wu, Y., Wu, Z., and Hu, M. (2019). Characteristics of biological particulate matters at urban and rural sites in the North China Plain. *Environmental Pollution*, *253*, 569–577.

Sheng, X., Ting, Y. P., and Pehkonen, S. O. (2008). The influence of ionic strength, nutrients and pH on bacterial adhesion to metals. *Journal of Colloid and Interface Science*, *321*(2), 256–264.

Siudek, P. (2020). Seasonal variability of trace elements in fine particulate matter ($PM_{2.5}$) in a coastal city of northern Poland–profile analysis and source identification. *Environmental Science: Processes & Impacts*, *22*(11), 2230–2243.

Smith, D. J., Jaffe, D. A., Birmele, M. N., Griffin, D. W., Schuerger, A. C., Hee, J., and Roberts, M. S. (2012). Free tropospheric transport of microorganisms from Asia to North America. *Microbial Ecology*, *64*, 973–985.

Song, H. S., Bang, W. G., Chung, N., Cho, Y. S., Kim, Y. S., and Cho, M. H. (2003). Effect of chelators and reductants on the mobilization of metals from ambient particulate matter. *Environmental Science & Technology*, *37*(16), 3531–3536.

Steiner, A. L., Brooks, S. D., Deng, C., Thornton, D. C., Pendleton, M. W., and Bryant, V. (2015). Pollen as atmospheric cloud condensation nuclei. *Geophysical research letters*, *42*(9), 3596–3602.

Sun, J., Yu, J., Shen, Z., Niu, X., Wang, D., Wang, X., Xu, H., Chuang, H. C., Cao, J., and Ho, K. F. (2021). Oxidative stress–inducing effects of various urban $PM_{2.5}$ road dust on human lung epithelial cells among 10 Chinese megacities. *Ecotoxicology and Environmental Safety*, *224*.

Survey, G. G. (2010). Multi-purposes Geochemical Survey: Pearl River Delta, Guangdong Province.

Taira, M., Sakakibara, K., Saeki, K., Ohira, S.-I., and Toda, K. (2020). Determination of oxoanions and water-soluble species of arsenic, selenium, antimony, vanadium, and chromium eluted in water from airborne fine particles ($PM_{2.5}$): effect of acid and transition metal content of particles on heavy metal elution. *Environmental Science: Processes & Impacts*, *22*(7), 1514–1524.

Tang, J. Y., McCarty, S., Glenn, E., Neale, P. A., Warne, M. S. J., and Escher, B. I. (2013). Mixture effects of organic micropollutants present in water: Towards the development of effect-based water quality trigger values for baseline toxicity. *Water Research*, *47*(10), 3300–3314.

Thai, P., Chen, Y., Dolganov, G., and Wu, R. (2005). Differential regulation of MUC5AC/Muc5ac and hCLCA-1/mGob-5 expression in airway epithelium. *American Journal of Respiratory Cell and Molecular Biology*, *33*(6), 523–530.

Thangavel, P., Park, D., and Lee, Y. C. (2022). Recent insights into particulate matter ($PM_{2.5}$)-mediated toxicity in humans: an overview. *International Journal of Environmental Research and Public Health*, *19*(12), 7511.

Thilsing, T., Madsen, A. M., Basinas, I., Schlünssen, V., Tendal, K., and Bælum, J. (2015). Dust, endotoxin, fungi, and bacteria exposure as determined by work task, season, and type of plant in a flower greenhouse. *Annals of Occupational Hygiene*, *59*(2), 142–157.

Tian, Y., Xiang, X., Wu, Y., Cao, Y., Song, J., Sun, K., Liu, H., and Hu, Y. (2017). Fine particulate air pollution and first hospital admissions for ischemic stroke in Beijing, China. *Scientific Reports*, *7*(1), 3897.

Tian, Y. Z., Shi, G. L., Huang Fu, Y. Q., Song, D. L., Liu, J. Y., Zhou, L. D., and Feng, Y. C. (2016). Seasonal and regional variations of source contributions for PM_{10} and $PM_{2.5}$ in urban environment. *Science of the Total Environment*, *557*, 697–704.

Torres-Ramos, Y. D., Montoya-Estrada, A., Guzman-Grenfell, A. M., Mancilla-Ramirez, J., Cardenas-Gonzalez, B., Blanco-Jimenez, S., Sepulveda-Sanchez, J. D., Ramirez-Venegas, A., and Hicks, J. J. (2011). Urban $PM_{2.5}$ induces ROS generation and RBC damage in COPD patients. *Front Biosci (Elite Ed)*, *3*, 808–817.

Traina, G., Bolzacchini, E., Bonini, M., Contini, D., Mantecca, P., Caimmi, S. M. E., and Licari, A. (2022). Role of air pollutants mediated oxidative stress in respiratory diseases. *Pediatric Allergy and Immunology*, *33*, 38–40.

USEPA. (2009). *Risk Assessment Guidance for Superfund. Volume 1. Human Health Evaluation Manual. Part F(Final)*. https://www.epa.gov/risk/risk-assessment-guidance-superfund-rags-part-f

USEPA. (2010). External Review Draft. Washington, DC: U.S. EPA Integrated Risk Information System; 2010. Development of a Relative Potency Factor (RPF) Approach for Polycyclic Aromatic Hydrocarbon (PAH) Mixtures.

USEPA. (2012). Sustainable Futures/P2 Framework Manual. Section 13: Quantitative Risk Assessment Calculations. In.

USEPA. (2018). Regional Screening Levels (RSLs) - Generic Tables (2018). In: US Environmental Protection Agency Washington, DC. Available at https://www.epa.gov/risk/regional-screening-levels-rsls-generic-tables.

Vaïtilingom, M., Amato, P., Sancelme, M., Laj, P., Leriche, M., and Delort, A.-M. (2010). Contribution of microbial activity to carbon chemistry in clouds. *Applied and environmental microbiology*, *76*(1), 23–29.

Vaïtilingom, M., Attard, E., Gaiani, N., Sancelme, M., Deguillaume, L., Flossmann, A. I., Amato, P., and Delort, A.-M. (2012). Long-term features of cloud microbiology at the puy de Dôme (France). *Atmospheric Environment*, *56*, 88–100.

Vaïtilingom, M., Deguillaume, L., Vinatier, V., Sancelme, M., Amato, P., Chaumerliac, N., and Delort, A.-M. (2013). Potential impact of microbial activity on the oxidant capacity and organic carbon budget in clouds. *Proceedings of the National Academy of Sciences*, *110*(2), 559–564.

Van der Gon, H. D., Hulskotte, J., Visschedijk, A., and Schaap, M. (2007). A revised estimate of copper emissions from road transport in UNECE-Europe and its impact on predicted copper concentrations. *Atmospheric Environment*, *41*(38), 8697–8710.

Viana, M., Kuhlbusch, T. A., Querol, X., Alastuey, A., Harrison, R. M., Hopke, P. K., Winiwarter, W., Vallius, M., Szidat, S., and Prévôt, A. S. (2008). Source apportionment of particulate matter in Europe: a review of methods and results. *Journal of aerosol science*, *39*(10), 827–849.

Villeneuve, D. L., Blankenship, A. L., and Giesy, J. P. (2000). Derivation and application of relative potency estimates based on *in vitro* bioassay results. *Environmental Toxicology and Chemistry*, *19*(11), 2835–2843.

Visser, M., Spaan, S., Arts, H., Smit, L., and Heederik, D. (2006). Influence of different cleaning practices on endotoxin exposure at sewage treatment plants. *The Annals of occupational hygiene*, *50*(7), 731–736.

Wang, G., Zhao, J., Jiang, R., and Song, W. (2015). Rat lung response to ozone and fine particulate matter ($PM_{2.5}$) exposures. *Environmental toxicology*, *30*(3), 343–356.

Wang, H., Cheng, M., Dsouza, M., Weisenhorn, P., Zheng, T., and Gilbert, J. A. (2018). Soil bacterial diversity is associated with human population density in urban greenspaces. *Environmental Science & Technology*, *52*(9), 5115–5124.

Wang, J., Li, S., Li, H., Qian, X., Li, X., Liu, X., Lu, H., Wang, C., and Sun, Y. (2017). Trace metals and magnetic particles in $PM_{2.5}$: Magnetic identification and its implications. *Scientific Reports*, *7*(1), 9865.

Wang, S., Liu, W., Li, J., Sun, H., Qian, Y., Ding, L., Ma, H., and Li, J. (2021a). Seasonal variation characteristics of bacteria and fungi in $PM_{2.5}$ in typical basin cities of Xi'an and Linfen, China. *Atmosphere*, *12*(7), 809.

Wang, X., Bi, X., Sheng, G., and Fu, J. (2006). Chemical composition and sources of PM_{10} and $PM_{2.5}$ aerosols in Guangzhou, China. *Environmental monitoring and Assessment*, *119*(1), 425–439.

Wang, Y., Qi, A., Wang, P., Tuo, X., Huang, Q., Zhang, Y., Xu, P., Zhang, T., Zhang, X., and Zhao, T. (2022). Temporal profiles, source analysis, and health risk assessments of parent polycyclic aromatic hydrocarbons (PPAHs) and their derivatives (NPAHs, OPAHs, ClPAHs, and BrPAHs) in $PM_{2.5}$ and $PM_{1.0}$ from the eastern coastal region of China: Urban coastal area versus coastal background area. *Chemosphere*, *292*, 133341.

Wang, Z., Liang, L., and Wang, X. (2021b). Spatiotemporal evolution of $PM_{2.5}$ concentrations in urban agglomerations of China. *Journal of Geographical Sciences*, *31*(6), 878–898.

Waters, C. N., Zalasiewicz, J., Summerhayes, C., Barnosky, A. D., Poirier, C., Gałuszka, A., Cearreta, A., Edgeworth, M., Ellis, E. C., and Ellis, M. (2016). The Anthropocene is functionally and stratigraphically distinct from the Holocene. *Science*, *351*(6269), aad2622.

Wierzbicka, A., Omelekhina, Y., Saber, A. T., Bloom, E., Gren, L., Poulsen, S. S., Strandberg, B., Pagels, J., and Jacobsen, N. R. (2022). Indoor $PM_{2.5}$ from occupied residences in Sweden caused higher inflammation in mice compared to outdoor $PM_{2.5}$. *Indoor Air*, *32*(12).

Wolf, J. C., and Segner, H. E. (2023). Hazards of current concentration-setting practices in environmental toxicology studies. *Critical Reviews in Toxicology*, *53*(5), 297–310.

Xia, L., and Gao, Y. (2011). Characterization of trace elements in $PM_{2.5}$ aerosols in the vicinity of highways in northeast New Jersey in the US east coast. *Atmospheric Pollution Research*, *2*(1), 34–44.

Xie, J., Jin, L., Cui, J., Luo, X., Li, J., Zhang, G., and Li, X. D. (2020). Health risk-oriented source apportionment of $PM_{2.5}$-associated trace metals. *Environmental Pollution*, *262*, 114655.

Xie, J., Jin, L., He, T., Chen, B., Luo, X., Feng, B., Huang, W., Li, J., Fu, P., and Li, X. (2018). Bacteria and antibiotic resistance genes (ARGs) in $PM_{2.5}$ from China: implications for human exposure. *Environmental Science & Technology*, *53*(2), 963–972.

Xie, M., Coons, T. L., Hemann, J. G., Dutton, S. J., Milford, J. B., Peel, J. L., Miller, S. L., Kim, S.-Y., Vedal, S., and Sheppard, L. (2012). Intra-urban spatial variability and uncertainty assessment of $PM_{2.5}$ sources based on carbonaceous species. *Atmospheric Environment*, *60*, 305–315.

Xu, F., Shi, X., Qiu, X., Jiang, X., Fang, Y., Wang, J., Hu, D., and Zhu, T. (2020). Investigation of the chemical components of ambient fine particulate matter ($PM_{2.5}$) associated with *in vitro* cellular responses to oxidative stress and inflammation. *Environment International*, *136*, 105475.

Xu, H., Xiao, Z., Chen, K., Tang, M., Zheng, N., Li, P., Yang, N., Yang, W., and Deng, X. (2019). Spatial and temporal distribution, chemical characteristics, and sources of ambient particulate matter in the Beijing-Tianjin-Hebei region. *Science of the Total Environment*, *658*, 280–293.

Yadav, A. K., Sahoo, S. K., Patra, A. C., Thakur, V. K., Dubey, J. S., Singh, S., Lenka, P., Jha, V., Kumar, A. V., and Shirin, S. (2022). Enrichment factor and chemical composition of size separated airborne particulate matter of Singrauli Coalfield, India. *Aerosol Science and Engineering*, *6*(4), 414–436.

Yan, R. H., Peng, X., Lin, W., He, L. Y., Wei, F. H., Tang, M. X., and Huang, X. F. (2022). Trends and challenges regarding the source-specific health risk of $PM_{2.5}$-bound metals in a Chinese megacity from 2014 to 2020. *Environmental Science & Technology*, *56*(11), 6996–7005.

Yan, Z., Ge, P., Lu, Z., Liu, X., Cao, M., Chen, W., and Chen, M. (2023). The cytotoxic effects of fine particulate matter ($PM_{2.5}$) from different sources at the air-liquid interface exposure on A549 cells. *Toxics*, *12*(1), 21.

Yang, L., Li, C., and Tang, X. (2020). The impact of $PM_{2.5}$ on the host defense of respiratory system. *Frontiers in Cell and Developmental Biology*, *8*, 91.

Yao, L., Zhao, X., Zhou, G.-J., Liang, R., Gou, T., Xia, B., Li, S., and Liu, C. (2020). Seasonal succession of phytoplankton functional groups and driving factors of cyanobacterial blooms in a subtropical reservoir in South China. *Water*, *12*(4), 1167.

Yoda, Y., Takagi, H., Wakamatsu, J., Ito, T., and Shima, M. (2019). Association of airborne endotoxin concentrations with pulmonary function and airway inflammation among students. *Environmental Epidemiology*, *3*, 456.

Yue, Y., Chen, H., Setyan, A., Elser, M., Dietrich, M., Li, J., Zhang, T., Zhang, X., Zheng, Y., and Wang, J. (2018). Size-resolved endotoxin and oxidative potential of ambient particles in Beijing and Zurich. *Environmental Science & Technology*, *52*(12), 6816–6824.

Yunker, M. B., Macdonald, R. W., Vingarzan, R., Mitchell, R. H., Goyette, D., and Sylvestre, S. (2002). PAHs in the Fraser River basin: a critical appraisal of PAH ratios as indicators of PAH source and composition. *Organic Geochemistry*, *33*(4), 489–515.

Zeng, L., Offor, F., Zhan, L., Lyu, X., Liang, Z., Zhang, L., Wang, J., Cheng, H., and Guo, H. (2019). Comparison of $PM_{2.5}$ pollution between an African city and an Asian metropolis. *Science of the Total Environment*, *696*, 134069.

Zhang, C., Tian, F., Zhang, M., Zhang, Z., Bai, M., Guo, G., Zheng, W., Wang, Q., Shi, Y., and Wang, L. (2019). Endotoxin contamination, a potentially important inflammation factor in water and wastewater: A review. *Science of the Total Environment*, *681*, 365–378.

Zhang, Q., Zhao, Z., Wu, Z., Niu, X., Zhang, Y., Wang, Q., Ho, S. S. H., Li, Z., and Shen, Z. (2024a). Toxicity source apportionment of fugitive dust $PM_{2.5}$-bound polycyclic aromatic hydrocarbons using multilayer perceptron neural network analysis in Guanzhong Plain urban agglomeration, China. *Journal of Hazardous Materials*, *468*, 133773.

Zhang, R., Jing, J., Tao, J., Hsu, S. C., Wang, G., Cao, J., Lee, C. S. L., Zhu, L., Chen, Z., and Zhao, Y. (2013). Chemical characterization and source apportionment of $PM_{2.5}$ in Beijing: seasonal perspective. *Atmospheric Chemistry and Physics*, *13*(14), 7053–7074.

Zhang, T., Yan, B., Henneman, L., Kinney, P., and Hopke, P. K. (2024b). Regulation-driven changes in $PM_{2.5}$ sources in China from 2013 to 2019, a critical review and trend analysis. *Science of the Total Environment*, 173091.

Zhang, X., Gao, H., Qi, A., Duan, S., Zhang, W., Zhang, Y., Huang, Q., Zhao, T., Han, G., and Wang, W. (2024c). Origins and health risk assessment of PAHs/APAHs/NPAHs/OPAHs in $PM_{2.5}$ at a background site in North China Plain: Implications for crude oil emissions. *Atmospheric Pollution Research*, *15*(5), 102081.

Zhang, Y.-L., and Cao, F. (2015). Fine particulate matter ($PM_{2.5}$) in China at a city level. *Scientific Reports*, *5*(1), 14884.

Zhao, Y., Liu, Y., Cui, L., Hou, J., Gao, F., Norback, D., and Sun, Y. (2024). Endotoxins in household dust in Northern China: associations with home environment factors and childhood asthma and allergies. *Atmosphere*, *15*(7), 759.

Zhen, Q., Deng, Y., Wang, Y., Wang, X., Zhang, H., Sun, X., and Ouyang, Z. (2017). Meteorological factors had more impact on airborne bacterial communities than air pollutants. *Science of the Total Environment*, *601*, 703–712.

Zheng, H., Zhao, B., Wang, S., Wang, T., Ding, D., Chang, X., Liu, K., Xing, J., Dong, Z., Aunan, K., Liu, T., Wu, X., Zhang, S., and Wu, Y. (2019). Transition in source contributions of $PM_{2.5}$ exposure and associated premature mortality in China during 2005–2015. *Environmental Internatinal*, *132*, 105111.

Zhou, Q., Chen, J., Zhang, J., Zhou, F., Zhao, J., Wei, X., Zheng, K., Wu, J., Li, B., and Pan, B. (2022). Toxicity and endocrine-disrupting potential of $PM_{2.5}$: Association with particulate polycyclic aromatic hydrocarbons, phthalate esters, and heavy metals. *Environmental Pollution*, *292*, 118349.

Zhou, S., Davy, P. K., Huang, M., Duan, J., Wang, X., Fan, Q., Chang, M., Liu, Y., Chen, W., and Xie, S. (2018). High-resolution sampling and analysis of ambient particulate matter in the Pearl River Delta region of southern China: source apportionment and health risk implications. *Atmospheric Chemistry and Physics*, *18*(3), 2049–2064.

Zou, Y., Jin, C., Su, Y., Li, J., and Zhu, B. (2016). Water soluble and insoluble components of urban $PM_{2.5}$ and their cytotoxic effects on epithelial cells (A549) *in vitro*. *Environmental Pollution*, *212*, 627–635.

Publications from the Research Project

1. **Wang, Y.,** Xie, J., Jin, L., Sun, X., Zhang, L., Yang, Q., Luo, X., Li, J., and Li, X. D. (2025). Beyond mass concentration: the critical role of chemical and biological compositions and sources in $PM_{2.5}$-induced toxicity in two Chinese megacities. *Environmental Pollution*, 127146.

2. Yang, Q., Xie, J., Zhang, Lu., Yu, J. Z., **Wang, Y.,** Li, X. D. (2025). Traffic-related $PM_{2.5}$ pollution in Hong Kong: component-specific and source-resolved health risks and cytotoxicity. *Environmental Pollution*, 126525.